University of Wisconsin Milwaukee
UWM Digital Commons

Theses and Dissertations

May 2022

Development of New Treatments for Asthma and Neuropathic Pain Based on ɣ-Aminobutyric Acid a Receptor (GABAAR) Ligands

Nicolas Mark Zahn
University of Wisconsin-Milwaukee

Follow this and additional works at: https://dc.uwm.edu/etd

 Part of the Allergy and Immunology Commons, Biochemistry Commons, and the Cell Biology Commons

Recommended Citation

Zahn, Nicolas Mark, "Development of New Treatments for Asthma and Neuropathic Pain Based on ɣ-Aminobutyric Acid a Receptor (GABAAR) Ligands" (2022). *Theses and Dissertations*. 2968.
https://dc.uwm.edu/etd/2968

This Dissertation is brought to you for free and open access by UWM Digital Commons. It has been accepted for inclusion in Theses and Dissertations by an authorized administrator of UWM Digital Commons. For more information, please contact scholarlycommunicationteam-group@uwm.edu.

DEVELOPMENT OF NEW TREATMENTS FOR ASTHMA AND NEUROPATHIC PAIN BASED ON ɣ-AMINOBUTYRIC ACID A RECEPTOR ($GABA_AR$) LIGANDS

by

Nicolas M. Zahn

A Dissertation Submitted in

Partial Fulfillment of the

Requirements for the Degree of

Doctor of Philosophy

in Chemistry

at

The University of Wisconsin – Milwaukee

May 2022

ABSTRACT

DEVELOPMENT OF NEW TREATMENT FOR ASTHMA AND NEUROPATHIC PAIN BASED ON ɣ-AMINOBUTYRIC ACID A RECEPTOR ($GABA_AR$) LIGANDS

by

Nicolas M. Zahn

The University of Wisconsin-Milwaukee, 2022
Under the Supervision of Professor Alexander (Leggy) Arnold

The γ-aminobutyric acid A receptor ($GABA_AR$) is a ligand-gated pentameric chloride channel consisting of several identified subunits: α1-6, β1-3, γ1-3, δ, ε, π, θ, ρ1-3.[1-2] Typical arrangement of subunits consists of two α subunits, two β subunits, and one γ subunit.[3] $GABA_ARs$ have two binding sites for the endogenous ligand γ-aminobutyric acid (GABA), between the α and β subunits. $GABA_ARs$ also have a binding site for positive allosteric modulators, such as benzodiazepines, between the α and γ subunits.[4-5]

Due to their ability to treat anxiety, epilepsy, insomnia, and muscle relaxation, benzodiazepines are widely prescribed pharmaceuticals.[6-7] Still, adverse effects result from benzodiazepine use, including but not limited to: sedation, impaired motor coordination, amnesia, tolerance, dependence, and severe withdrawal symptoms.[6, 8] Selectivity of benzodiazepines to specific $GABA_AR$ subtypes is currently well accepted drug discovery strategy.[8]

The rotarod assay has been used for over 70 years to quantify the neurological effects of muscle relaxants, convulsants, and central nervous system (CNS) depressants.[12] It is a reliable and sensitive *in vivo* sensorimotor assay that can detect neurological deficits such as sedation or impaired motor

coordination.[12] Additionally, an open field test can be performed in parallel to provide a more robust analysis of neurological deficits. The Arnold Group has used these assays to screen hundreds of novel subtype-selective imidazodiazepines to identify those without adverse CNS effects.

Imidazodiazepines demonstrating no adverse CNS effects were used to develop leads to treat asthma inflammation and neuropathic pain by targeting non-neuronal cells expressing a narrow subset of $GABA_AR$ subunits. [9-11] T-lymphocytes, alveolar macrophages, and eosinophils[17] all have been shown to express functional $GABA_ARs$ suggesting their role in the airway inflammatory response.[13–15] $CD4^+$ T-lymphocytes are of significant interest for their role in stimulating and coordinating the airway inflammatory immune response.[14] Here, we describe the relationship between imidazodiazepines targeting non-neuronal immune cells and the corresponding airway inflammatory response both *in vivo* and *in vitro*.

Airway hyperresponsiveness (AHR) was investigated in methacholine-challenged murine models *in vivo* using a non-invasive airway mechanics (NAM) plethysmograph. Methacholine, a cholinergic drug, acts on muscarinic receptors and causes narrowing of airways similar to asthma.[16] The NAM instrument measures pressure, volume, and frequency of respiration and combines these parameters into an sRaw value measured in cmH_2O*sec. Several novel imidazodiazepines were identified to have lower sRaw values in this model compared to commercially available asthma therapeutics. This trend was observed in studies of repeat dose and prophylactic dose for orally and nebulized delivered compounds, as well as for rescue inhalant studies. Lead compounds were also subject to *in vitro* experimentation.

$CD4^+$ T-cells have a well understood role in asthma and are responsible for perpetuating the inflammatory response by infiltrating airways and secreting inflammatory cytokines.[18] The cytokine release directs other cell types to mediate many of the clinical characteristics of asthma, including heightened IgE production, increased eosinophilia, and accelerated immune cell proliferation.[19] This complex inflammatory reaction can be classified into Th1 or Th2 responses. Th1 responses are

characterized by cytokines like interferon γ (IFNγ), interleukin-2 (IL-2), and lymphotoxin (LT), which promote the cell-mediated immune response.[20] The Th2 immune response is characterized by production of multiple cytokines: IL-4, IL-5, IL-10, and IL-13, among others.[20] To investigate the anti-inflammatory effects of $GABA_AR$ ligands, a protocol was developed to quantify the reduction of IL-5 and IL-13 production by primary activated $CD4^+$ T-cells isolated from female Swiss Webster splenocytes using rtPCR.

Functional γ-aminobutyric acid type A receptors ($GABA_ARs$) are well-characterized in neurons and have been discovered on glial cells. This includes α1, α3, and β1 subunits found on mouse microglia,[21] which have been reported to mediate immune signaling.[22] Previous anti-inflammatory studies with novel α2/α3-subtype $GABA_AR$ positive allosteric modulators have shown analgesic properties.[25,26] Taken together, these results suggest that novel imidazodiazepines are neuropathic pain lead compounds, reducing inflammation through targeting CNS microglia, and providing an analgesic effect. A murine formalin test was performed to investigate *in vivo* compound efficacy in reducing neuropathic pain.

© Copyright by Nicolas M. Zahn, 2022
All Rights Reserved

To

my parents,

my family,

and my friends.

TABLE OF CONTENTS

LIST OF FIGURES

LIST OF TABLES

LIST OF ABBREVIATIONS

AHR: Airway Hyperresponsiveness

ASM: Airway Smooth Muscle

ATP: Adenosine Triphosphate

Balb/c: Albino, Immunodeficient Mouse Strain

BALF: Bronchoalveolar Lavage Fluid

BCA: Bicinchoninic Acid

bp: Base Pair

BSA: Bovine Serum Albumin

BZD: Benzodiazepine

CFW: Swiss Webster Mouse Strain

CNS: Central Nervous System

CRAC: Calcium Release Activated Channel

DEX: Dexamethasone

DMSO: Dimethyl Sulfoxide

DNA: Deoxyribonucleic Acid

EC: Effective Concentration

ECS: Extracellular Solution

EE: Ethyl Ester

ELISA: Enzyme-Linked Immunosorbent Assay

eNOS: Epithelial Nitric Oxide Synthase

F: Frequency

FBS: Fetal Bovine Serum

GABA: γ-Aminobutyric Acid

$GABA_AR$: γ-Aminobutyric Acid Type A Receptor

GABA-T: γ-Aminobutyric Acid Transaminase

GAD: Glutamic Acid Decarboxylase

GAT: γ-Aminobutyric Acid Transporter

h: Hours

HIV: Human Immunodeficiency Virus

IACUC: Institutional Animal Care and Use Committee

IC: Inhibitory Concentration

ICS: Inhaled Corticosteroids

IFNγ: Interferon-γ

IL: Interleukin

iNOS: Inducible Nitric Oxide Synthase

IP: Intraperitoneal

KOR: κ Opioid Receptor

LABA: Long-Acting Beta adrenergic-Agonists

LPS: Lipopolysaccharide

MAPK: Mitogen-Activated Protein Kinase

MBP: Major Basic Protein

MIDD0301 – Milwaukee Institute for Drug Discovery Compound #0301

min: Minutes

ml: Milliliter

mg: Milligram

mRNA: Messenger Ribonucleic Acid

NAM: Non-Invasive Airway Mechanics

NIMH: National Institute of Mental Health

nNOS: Neuronal Nitric Oxide Synthase

NO: Nitric Oxide

NP: Neuropathic Pain

ns/n.s.: Not Significant

Ova: Ovalbumin

PEG: Polyethylene Glycol 400

PBR: Peripheral Benzodiazepine Receptor

PBS: Phosphate Buffered Saline

PDSP: Psychoactive Drug Screening Program

PHA: Phytohemagglutinin

PMA: Phorbol 12-Myristate 13-Acetate

PO: Oral Gavage

PSI: Pounds per Square Inch

RBC: Red Blood Cell

RNA: Ribonucleic Acid

RPM: Revolutions per Minute

RT-qPCR: Reverse Transcription Quantitative Polymerase Chain Reaction

sec: Seconds

SEM: Standard Error of the Mean

sRaw – Specific Airway Resistance

TNFβ: Tumor Necrosis Factor β

µl: Microliter

ug: Microgram

UWM: University of Wisconsin – Milwaukee

ACKNOWLEDGEMENTS

First, I would like to thank my advisor Dr. Leggy Arnold for accepting me into his research group, the numerous grant applications he has sent out to fund my research, and the countless hours spent advising me both in and out of the lab. I have developed skills that are directly attributed to his persistent encouragement and creating an environment that enables growth across multiple disciplines of research. Dr. Arnold, I will forever be grateful for how much you have helped me over the past 7+ years as a lab technician and graduate student. It is difficult to put into words the admiration and thankfulness I have for getting the opportunity to be one of your students. You have been absolutely pivotal helping me follow my dreams.

I would like to thank my committee members, Dr. Douglas Stafford, Dr. Nicholas Silvaggi, Dr. James Cook, Dr. Shama Mirza, and Dr. Douglas Steeber. Your knowledge and expertise have been critical in helping me develop the framework for my research. I also extend additional gratitude to Dr. Stafford for his guidance and contributions towards my research as a graduate student and my work within the MIDD.

To the past and present lab members, thank you for understanding and listening during conversations on topics both involved and uninvolved with our lab work. You have all been excellent resources of knowledge and have provided countless suggestions that have greatly benefitted my research. Furthermore, thank you for the friendships we've developed that will far surpass my time in graduate school.

Thank you to all of my personal friends that have listened to my research and conversations over the years. Jonathan Beyer, Tommy Grelecki, Dillon Wegner, Clay Letter, Tanner Blom, Rashell Landeros,

Tyler Nuthals, and Aleah Pfefferle, thank you for being my best friends and visiting me at UW-Milwaukee. I cherish every moment we have together and have profound admiration for all of you.

A special thanks goes to the Schultz family. Randy, Mouse, and Dano, thank you for everything. The weekends at the cabin, the countless sporting events we've watched and cheered for, the hundreds of meals you've cooked for me, and the conversations and laughter we've shared. You have brought me in and treated me like a son and for that you will always be family to me. Your support along my journey has helped me more than you can imagine.

Most importantly, thank you to my family. Emily, Justin, Haisley, and Oakley, your support and happiness has brought so much joy to my life. Adam, thank you for your wisdom and perspective that an older brother would provide. Mom and Dad, you have been my rock to lean on every step of the way. You've provided guidance, structure, and support far greater than I ever thought possible. When I have been discouraged, you have been there for me. You have been the greatest proponent to my education; this degree is just as much yours as it is mine. I am thankful to have such incredible parents.

Lastly, I would like to thank my late friend Tyler James Pfefferle. You showed belief in me years before I saw it in myself. When I left Seymour, you visited me more than anyone else. I will never forget your encouragement and I am forever thankful for the memories we've shared together. Losing a friend like you has taught me to love more and appreciate the moments I have with those I cherish most dearly. This thesis is dedicated in your honor.

CHAPTER 1

Introduction to the

γ-Aminobutyric Acid A Receptor

1.1 γ-Aminobutyric Acid (GABA)

1.1.1 Discovery of GABA

γ-Aminobutyric acid (GABA) was first discovered in the late 1800's as a plant and microbe component of the Krebs cycle.[27] It was not until the 1950's Eugene Roberts and Sam Frankel showed it was an amine that accumulates in very high concentrations in the brain, up to 1000x more than any other neurotransmitter.[28-29] In 1959, GABA (initially named Substance I) was found to inhibit crayfish neurons, confirming its function as an inhibitory neurotransmitter.[30] This discovery was widely questioned because GABA lacks rapid inactivation.[31-32] It was later proven that GABA hyperpolarizes neocortical neurons and that GABA inactivation occurred through rapid cellular uptake, reinforcing its classification as an inhibitory neurotransmitter.[33-34]

1.1.2 Formation of GABA

The GABA shunt (**Figure 1**) is the main pathway that forms GABA. α-ketoglutarate is first formed from succinic semialdehyde through the Krebs cycle. This relation to the Krebs cycle prompted hypotheses that GABA had a function in metabolism.[35] In the mitochondria, GABA-transaminase (GABA-T) converts α-ketoglutarate to glutamate.[36] Glutamate is then converted to GABA by glutamate decarboxylase (GAD), an enzyme located in the presynaptic terminals.[36] There are two types of GAD: 1) GAD_{65}, which is activated in demand for additional GABA needed for neurotransmission, and 2) GAD_{67}, which produces GABA independent from neurotransmission.[37]

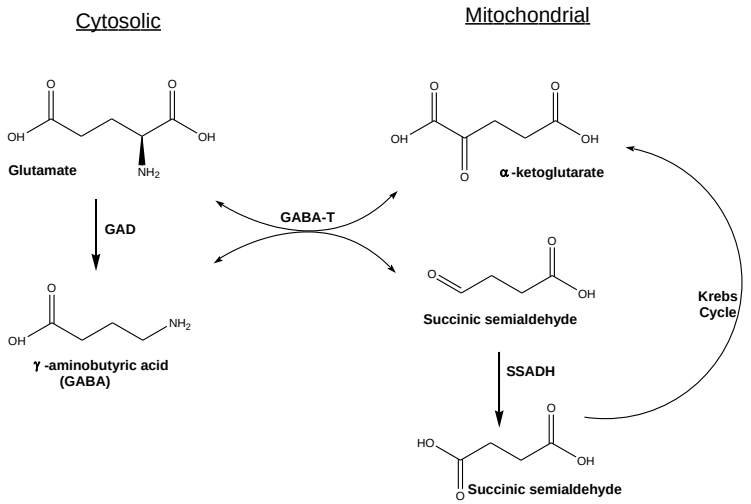

Figure 6. GABA Shunt Relating Cytosol and Mitochondria. *GABA-T: GABA α-oxoglutarate transaminase, GAD: glutamic acid decarboxylase, SSADH: succinic semialdehyde dehydrogenase.*[36]

Once presynaptic neurons are depolarized, GABA is released into the synaptic cleft. Once bound to receptors on the postsynaptic cell surface, GABA is uptaken by the GABA transporter (GAT) to prevent binding to nearby synapses[38] despite the internal GABA concentration being roughly 200 times greater than the external GABA concentration.[36] GABA is then reused by neurons or subsequently converted back to succinic semialdehyde by GABA-T and enters the Krebs cycle.[36] GABA can also be generated through glial uptake and converted through the Krebs cycle to form glutamine, which can then be converted to GABA.[36]

1.2 The γ-Aminobutyric Acid A Receptor ($GABA_AR$)

1.2.1 Discovery of the $GABA_AR$

After nearly three decades of research, the $GABA_AR$ structure was first proposed in 1990.[39] During that time, glycine, nicotinic acetylcholine, and $5HT_3$ neurotransmitter receptors were discovered that demonstrated sequence homology in the ligand-binding regions with the $GABA_AR$.[40] This group of receptors was named the Cys loop ligand-gated ion channel superfamily.[41] Approximations of GABA and other modulator binding were needed until the heteropentameric $GABA_AR$ structure was characterized

through high-resolution cryo-electron microscopy (cryo-EM), confirming the binding site of GABA and flumazenil, an allosteric modulator.[42-43]

1.2.2 The Structure of $GABA_AR$

$GABA_AR$ arrangements contain a heteropentameric membrane bound receptor consisting of 19 possible subunits (α1–6, β1–3, γ1–3, δ, ε, π, θ, ρ1-3).[44-45] The cryo-EM structure (**Figure 2**) elucidated by Zhu et al. in 2018 showed similar subunit structure with an extracellular domain containing a Cys loop and 10 β-strands within a β-sandwich, proceeded by four α-helices to form the membrane bound ion channel.[42]

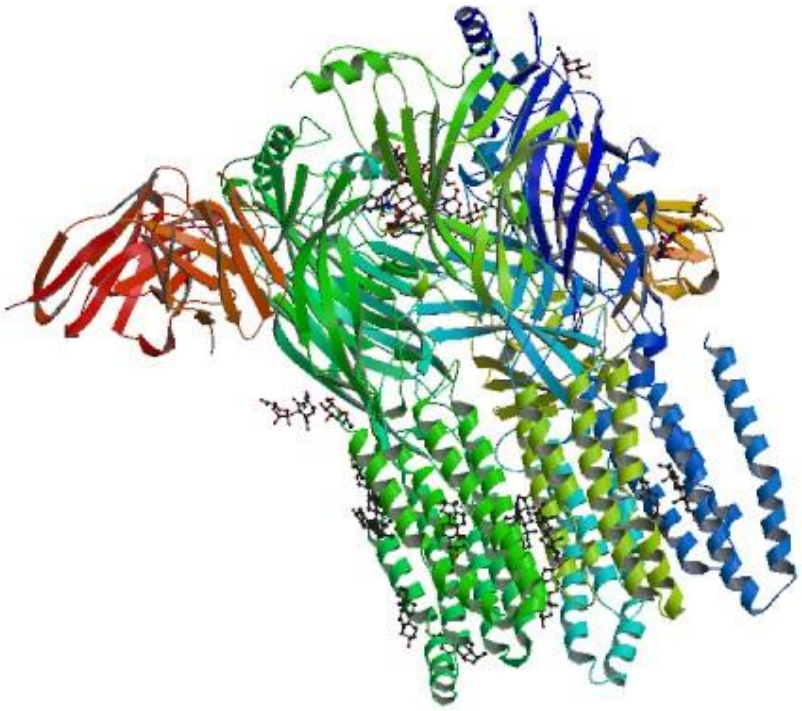

Figure 7. Cryo-electron microscopy structure of the $GABA_AR$. *First elucidated in 2018, the $GABA_AR$ is composed of α1, β2, and γ2 subunits with GABA and flumazenil bound as determined by Zhu et al.[42] In red and yellow are antibodies used for isolation of the protein. Accessed from the Protein Data Bank (PDB: 6D6U).*

Classical $GABA_ARs$ have two α, two β, and a tertiary γ or δ subunit.[46] Expression of these subunits is heterogeneous across cell and tissue types, and is discussed in **1.4** Distribution of GABAAR**$GABA_AR$ Distribution**.[47] The cryo-EM structure in **Figure 2** is an α1β2γ2 receptor, one of the most common $GABA_AR$

receptors found in the brain.[42] The receptor can be identified by monoclonal antibodies, which bind the extracellular domain of the α and β subunits seen in red and yellow (**Figure 3**).[42]

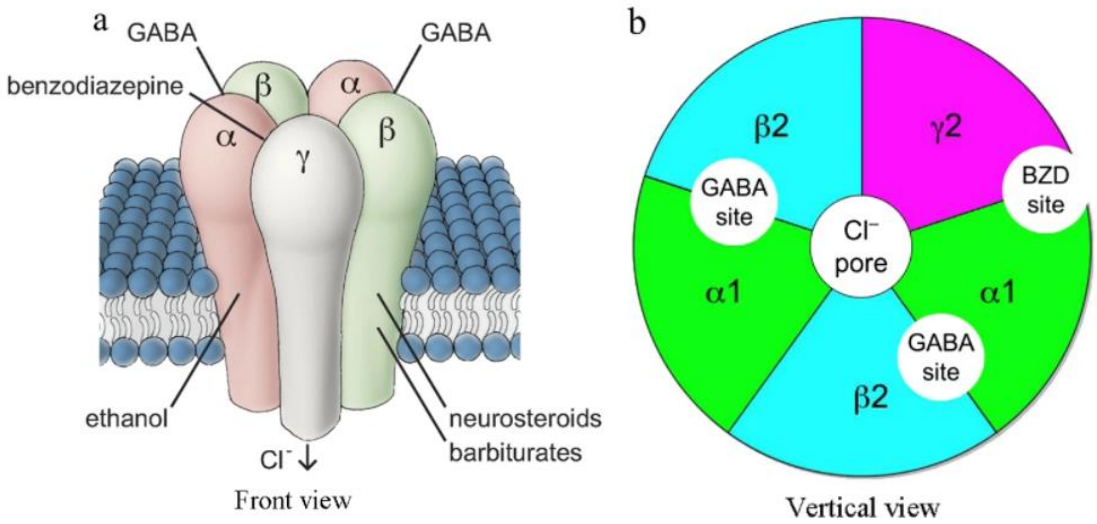

Figure 8. Structure of the GABA$_A$R. *a.) Lateral view, and b.) vertical view of a typical GABA$_A$R containing two α subunits, two β subunits, and one γ subunit, forming two extracellular binding sites between α and β subunits for the endogenous ligand GABA and one extracellular binding site between α and γ subunits for positive allosteric modulators such as benzodiazepines.*[48]

Due to the number of ligand binding sites on GABA$_A$Rs, it can be targeted by different ligands including GABA. The three main binding sites for existing ligands are the GABA site, the benzodiazepine site, and the chloride channel. Additional binding sites exists for allosteric modulators such as neurosteroids, barbiturates, and ethanol.[36,47]

There are two binding sites for the endogenous ligand GABA, located between α and β subunits.[36,47] GABA$_A$Rs contain a phenylalanine and three tyrosine residues that form an aromatic glove that binds the exposed nitrogen on GABA.[42] Once bound, the carboxylate group on GABA provides an additional interaction with a threonine group on the GABA$_A$R to further stabilize binding.[42]

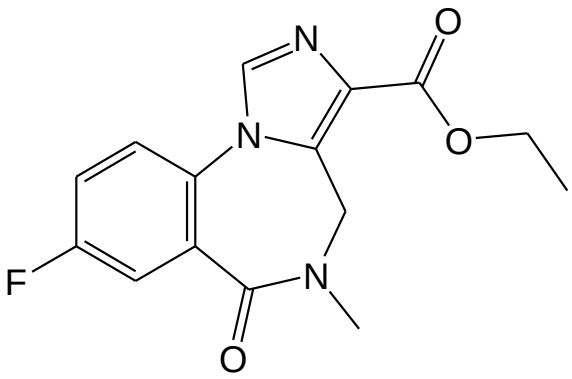

Figure 4. Structure of Flumazenil. *With a molecular weight of 303.3 g/mol, flumazenil is a competitive $GABA_AR$ antagonist and is used to treat benzodiazepine overdoses.*

Flumazenil contains a fluorine (**Figure 4**) that interacts with the α1 subunit and an ethyl ester that binds with the γ2 subunit.[42] Aromatic residues on both the alpha and gamma subunit form the benzodiazepine binding site. A phenylalanine, two tyrosines, two serines, and one threonine form half of the binding site situated on the alpha subunit, while a phenylalanine, one tyrosine, and one threonine the other half located on the gamma subunit. The fluorine on flumazenil hydrogen bonds to a histidine on the α1 subunit, a residue conserved through α1-3 and α5 subunits.[42] $GABA_ARs$ containing α4 and α6 subunits are diazepam insensitive, as these subunits contain arginine residues.[42]

1.3 $GABA_AR$ Modulation

1.3.1 The GABA Binding Site

Agonists

In addition to endogenous ligands, $GABA_ARs$ can be activated by synthetic agonists. Derived from the psychoactive mushroom *Amanita muscarina*, muscimol is a conformationally restrained isoxazole that behaves similarly to GABA due to similar structure.[49,50] Although its activity is subtype-independent, it has been shown to act as an agonist at α4-containing receptors.[50]

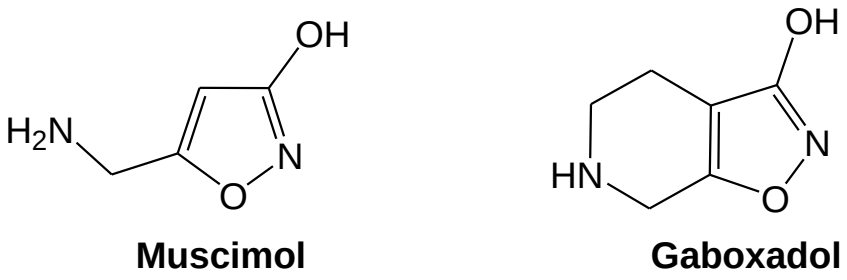

Figure 9. Structure of Muscimol and Gaboxadol. *Gaboxadol (4,5,6,7-tetrahydroisoxazolo(5,4-c)pyridine-3-ol (THIP)) targets the δ subunit of the $GABA_AR$ and was derived from muscimol (isoxazole) as a sleep aid but was later discontinued. Muscimol behaves similar to GABA due to structure similarity despite its confirmational rigidity. Gaboxadol is believed to belong to a separate class of agonists.*[53]

Gaboxadol, an agonist selective for the δ subunit, was developed from the muscimol structure as a sleep aid,[50] although it was discontinued after showing limited efficacy in addition to adverse side effects. [51,52] Termed a "super agonist," gaboxadol induces twice the response of GABA or muscimol at α4-containing receptors.[49] However, both GABA and muscimol binding is increased when diazepam is bound to the benzodiazepine site, while gaboxadol binding is unaltered. In addition, gaboxadol is less potent with EC_{50} values over 30 times higher than either GABA or muscimol.[49] Both of these factors support the notion that gaboxadol, despite its structural similarity, belongs to a different class of agonist.[53]

Antagonists

Gabazine (**Figure 6**) was first synthesized in 1986 after experiments were performed that investigated arylaminopyridazine derivatives of GABA.[56] It is a GABA binding site antagonist, as its effects were shown to be reversed by muscimol[28] in addition to mutational studies of the GABA binding site.[55]

Bicuculline (**Figure 10**) is an alkaloid that was first characterized in 1970 as the first $GABA_AR$ selective antagonist.[56] When the convulsant activities of bicuculline were evaluated, it was shown to have limited solubility and stability.[49, 56] Bicuculline salts such as bicuculline methiodide or methochloride were generate, although with limited success.[56] These salts are typically less selective and interact with other proteins resulting in cofounding results.[56] $GABA_AR$ subunit composition has little effect on the action of bicuculline, however α6-containing receptors are slightly less sensitive.[57]

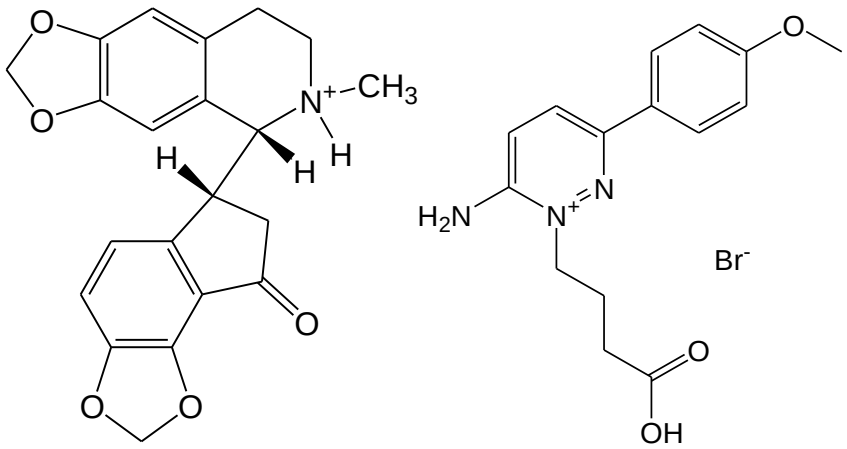

Figure 10. Structure of Bicuculline (Left) and Gabazine (Right). *Bicuculine is an alkaloid that was first characterized in 1970 as the first $GABA_AR$ selective antagonist, while gabazine is a GABA binding site antagonist.*[56]

Though gabazine and bicuculline have similar mechanisms of action, they interact with different residues of the GABA binding site.[56] In comparison, gabazine is more potent with an IC_{50} of 0.2 µM compared to 0.9 µM for bicuculline.[55]

1.3.2 The Chloride Channel

Antagonists

Isolated from moonseed plants, picrotoxin is a non-competitive antagonist of $GABA_AR$ with universal efficacy.[58,59] Although shown to be an equal mixture of picrotoxinin and picrotin (**Figure 7**), picrotoxinin is 30 times more potent than picrotin.[60] It is thought to bind within the chloride pore of $GABA_ARs$, interacting with a alpha helix bound in the cell membrane.[58] Mutational studies have shown picrotoxin binding in the V257 region of the α1 subunit.[61] Picrotoxin binding within the chloride channel is well known. The interactions are hypothesized on structurally similar nicotinic acetylcholine receptors, which are homopentameric in contrast to $GABA_ARs$ which are heteropentameric.[58]

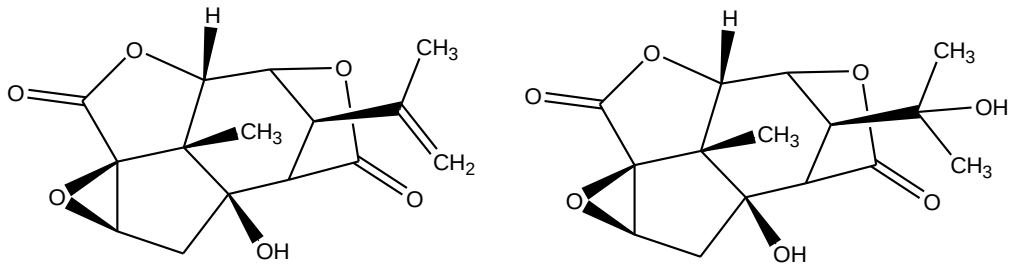

Figure 7. Structure of Picrotoxinin and Picrotin. *Isolated from moonseed plants, picrotoxin is an equal mixture of picrotoxinin and picrotin, however picrotoxinin is 30 times more potent than picrotin.*[60]

1.3.3 The Benzodiazepine Binding Site

Positive Allosteric Modulators

Benzodiazepines were discovered by molecular manipulation of benzheptoxdiazines, a class originally investigated for new dyestuffs, which are precursors to many dyes.[62] After failing their original purpose, benzodiazepines were investigated as tranquilizers. They were yet largely unexplored, were varied and easily transformed, and were a readily available compound that had similar structure to other biologically active ligands.[62]

Interestingly, no positive results were gained after years of trial and error. It was only during a final laboratory cleaning that one compound and its salt formation were thought to have been overlooked and was sent for biological testing. Results confirmed improved muscle relaxation and anticonvulsant activities when compared to chlorpromazine, the current standard drug at the time.[62] Once approved by the FDA, the first benzodiazepine, named Librium, was on the market.[62] Diazepam (trade name Valium®) was introduced three years later. [62] As benzodiazepine research soared, the structure-activity relationship of benzodiazepines and $GABA_AR$s began to unfold. In 1975, clonazepam entered the market closely followed by lorazepam in 1977.[62] Many of these drugs are still in use today, as alprazolam and clonazepam were the 23rd and 38th most prescribed drugs in 2018.

Knock-in mouse models have recently been developed, with specific residues mutated in α subunits,[64] to perform pharmacological and behavioral studies that link each α subtype to certain physiological effects. Anxiolysis and muscle relaxation can be achieved though targeting the α2 or α3 subunit-containing $GABA_AR$, while avoiding the α1 subunit-containing $GABA_AR$ can greatly reduce adverse effects such as unwanted amnesia or addiction.[64] Furthermore, many other clinically relevant effects can be achieved and are summarized in **Figure 8**.

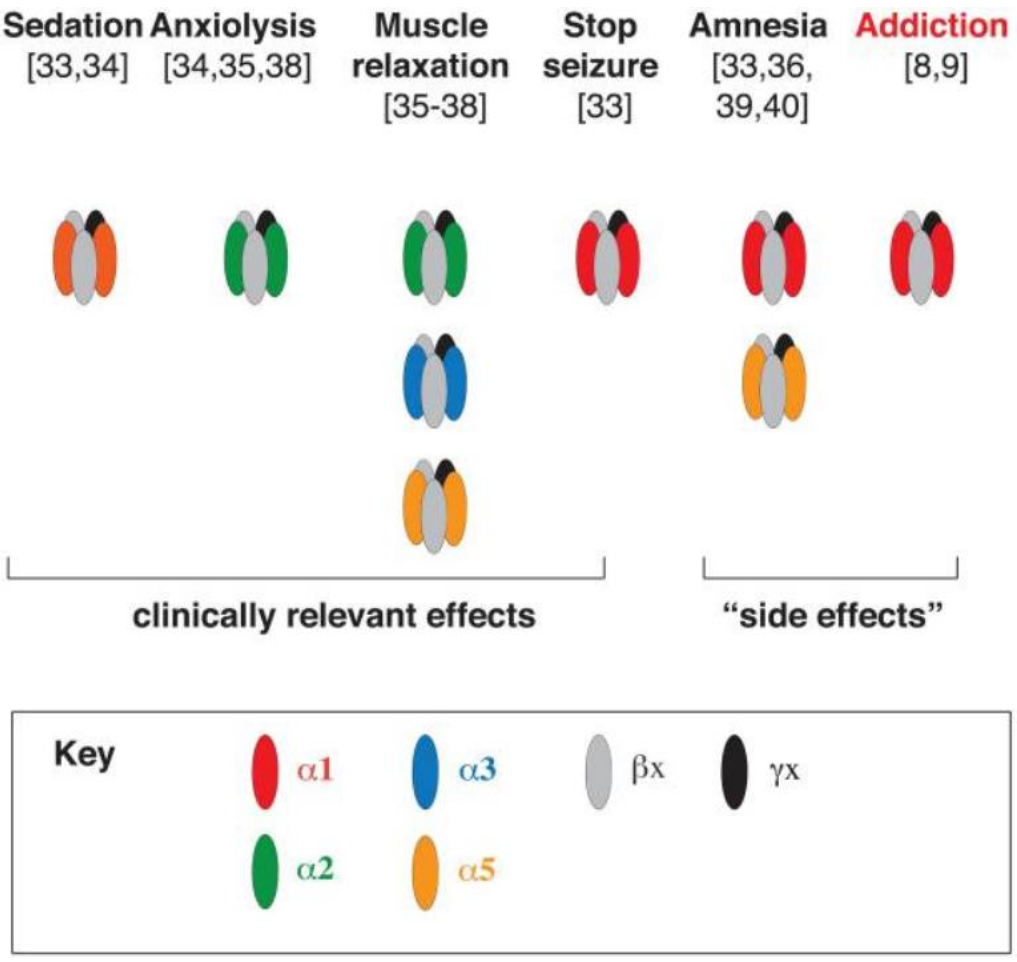

Figure 8. Benzodiazepine Pharmacology of Different Subtypes. *Knock-in mouse models show correlation between $GABA_AR$ subunits and pharmacological effects.*[64]

To achieve subtype-selectivity of novel benzodiazepines, Professor James Cook developed a pharmacophore model that guides synthesis towards compounds that selectively bind specific α subunit-containing $GABA_ARs$.[65] This successful model has generated subtype-selective imidazodiazepines

targeting numerous diseases ranging from central nervous system diseases such as depression,[66] schizophrenia,[67] and neuropathic pain[68] to pulmonary diseases such as asthma.[69-72] Biological results pertaining to novel imidazodiazepines used for asthma and neuropathic pain are discussed in the proceeding chapters.

Negative Allosteric Modulators

Flumazenil (**Error! Reference source not found.**) is an imidazodiazepine that antagonizes α1-3 and α5-containing $GABA_A$Rs. Flumazenil competes for the benzodiazepine binding site and is used to reverse benzodiazepine effects, such as diazepam-induced sedation.[73] Interestingly, flumazenil can also act as a weak partial agonist for α4/6-containing receptors.[74-75]

First reported as a behavioral alcohol antagonist, Ro15-4513 (**Figure 9**) is an analog of flumazenil that reverses ethanol-enhanced $GABA_A$R currents through α4/6 and δ-containing $GABA_A$Rs.[58] Flumazenil is not capable of blocking the effects of ethanol, as it is thought the long nitrogen tail of Ro15-4513 blocks ethanol binding at the δ subunit, whereas the analogous fluorine on flumazenil does not.[76]

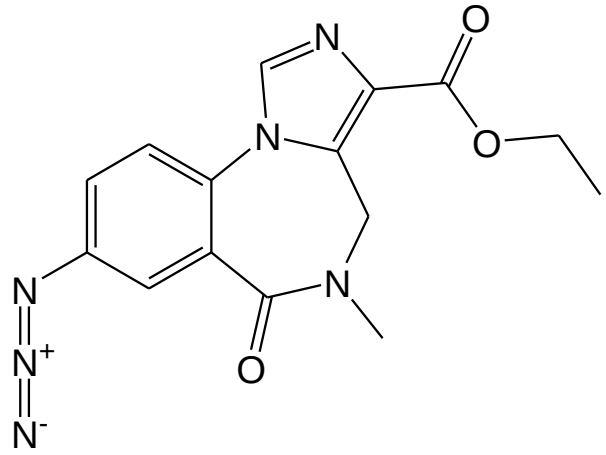

Figure 9. Structure of Ro15-4513. *Analogous to flumazenil, Ro15-4513 differentiates with the presence of a long nitrogen tail that is able to block ethanol binding at the δ subunit. Flumazenil exhibits a fluorine at this position that is not able to block ethanol binding.*[76]

1.4 Distribution of $GABA_AR$

$GABA_ARs$ have been known to be highly expressed in the brain and meditate inhibitory neurotransmission. More recently, $GABA_ARs$ have been discovered across peripheral tissues throughout the body. Endocrine tissues such as the testes have been shown to express $GABA_ARs$ in addition to GAD_{65} and GAD_{67} in mouse, hamster, rat, and human models.[80] Bone marrow stromal cells have also been shown to express receptors with alpha 1, beta 2/3, and epsilon – containing $GABA_AR$ subunits when responding to induction treatment.[84] $GABA_ARs$ are also present on immune cells such as lymphocytes and macrophages and in airway smooth muscle,[81-83] providing a target for ligands aimed to treat diseases associated with airway hyperresponsiveness.

Error! Reference source not found. contains human proteome information from the Human Protein Atlas (www.proteinatlas.org), and shows breakdown of protein expression by tissue, cell, pathology, and other cellular effects.[77-79] This project combines data from three individual projects: i.) The Human Protein Atlas, ii.) through Genotype-Tissue Expression, and iii.) The FANTOM5 project, normalizing the expression determined for each of these individual projects, combines it, and expresses it as normalized unitless expression of transcribed RNA. The procedure is complex and described at https://www.proteinatlas.org/about/assays+annotation.

Error! Reference source not found. also shows the distribution of alpha subunits throughout various tissue types. Expression of alpha subunits in the brain varies widely by region. For instance, the cerebral cortex has three times higher expression of α1-3 and α5 subunits than α4 subunits, and fifty times as high as α6 expression. However, α6 expression has been found to be highly concentrated in the cerebellum, where it has a concentrations ten times higher than any other alpha subunit. In contrast to the brain where normalized expression of alpha subunits is quite high (levels around ~96), peripheral tissues have much lower $GABA_AR$ expression, usually around normalized levels of ~1.

Table 1. Distribution of $GABA_AR$ Alpha Subunits in Human Tissues[77-79]

		$GABA_AR$ Subunit					
	Tissue Type	**α1**	**α2**	**α3**	**α4**	**α5**	**α6**
Brain	Olfactory Region	22	31	10.5		15.2	0
	Cerebral Cortex	58.6	52.6	30.1	16.1	52.6	1.6
	Hippocampal Formation	10.5	38.9	10.9	1.9	20.9	0
	Amygdala	8.5	38.5	7.7	2.7	12	0
	Basal Ganglia	21.9	34.4	15.2	8.9	48.2	0
	Hypothalamus	8.8	7.7	15.9	1.4	6	0
	Thalamus	0	7.1	1.1		2	0
	Midbrain	6.7	3.7	4.7	1	2.3	0
	Pons and Medulla	7.4	10.5	6.2		1	2.6
	Cerebellum	35.2	10.4	1.3	0.3	0.1	96.4
	Corpus Callosum	1.8	4.9	3.3		0.8	0
	Spinal Cord	1.3	6.9	2.1	0	0.3	0.7
Lung	Lung	1	1	0.7	0	0.8	0
Endocrine Tissues	Thyroid Gland	1	1.1	0.7	0	0.9	0
	Parathyroid Gland	1	0.9	0.6	0	0.7	0
	Adrenal Gland	2.6	1.3	0.7	0.1	0.8	0
	Pituitary Gland	0.1	0.6	0.9	0.2	0.1	0
Muscle Tissues	Heart Muscle	1	1	0.7	4	0.9	0
	Smooth Muscle	1	1.3	0.8	0	1.4	0
	Skeletal Muscle	1	1	0.8	0	0.7	0
Lymphoid Tissues	Thymus	0	0	0		1.3	0
	Appendix	1	1.4	0.6	0.1	0.8	0
	Spleen	1.1	2.3	0.7	0	0.8	0
	Lymph Node	1	1.4	0.7	0	0.8	0
	Tonsil	1.3	1.4	0.9	0	1.1	0
	Bone Marrow	1	1.2	0.7	0	0.8	0

ASM has been shown to express $GABA_AR$s containing α4 and α5 subunits in mammalian airways,[85] and both α4- and α5-selective $GABA_AR$ positive modulators relaxed pre-contracted ASM.[86-88] Even $GABA_AR$s containing α4 subunits are found in the membrane of various immune cells.[89-91] GABA (the natural ligand of the GABAAR) and muscimol (a full GABAAR agonist) have also been shown to elicit significant lymphocyte membrane currents and GABA decreased phytohemagglutinin-induced T-cell proliferation.[71]

Taken together, the peripheral GABAergic system represents a compelling new drug target for asthma in light of its influence on ASM relaxation, inflammatory modulation, and regulation of mucus hypersecretion. The well-established class of benzodiazepines can now be tailored to new targets and new diseases while maintaining the safety and efficacy of established pharmaceuticals. The following chapters herein aim to support the use of imidazodiazepines to target non-neuronal cell types in diseases like asthma and neuropathic pain.

CHAPTER 2

Safety Evaluation of MIDD0301

2.1 Introduction

Asthma is an expanding public health challenge with a patient population approaching 10% of the global population. Low-dose inhaled corticosteroid (with or without a long-acting β2-agonist) inhalers are the most common use of asthma treatment.[92] However, this disease responds poorly to corticosteroids in refractory asthma, prompting increased oral dosing that is linked to increased side effects. Furthermore, corticosteroids can be ineffective in steroid-tolerant disease.[93] Injectable biologics can efficaciously target inflammation in certain subsets of asthma patients, but high costs limit their use in only severe disease.[94–95] In contrast to these therapeutic treatments, MIDD0301 has been developed to target $GABA_AR$ on airway smooth muscle (ASM) and inflammatory cells, providing a novel asthma drug mechanism of action.[96]

MIDD0301 is an allosteric $GABA_AR$ agonist that has been shown to alleviate multiple symptoms of asthma in animal models after oral dosing.[96] The $GABA_AR$ is a membrane chloride ion channel that opens in the response to GABA. The receptor is a heteropentamer (comprised of subunits: α1–6, β1–3, γ1–3, δ, ε, π, θ, ρ1-3), and most often takes the form of two alpha, two beta, and one tertiary subunit.[97] During the last decades, the role of $GABA_ARs$ in the brain has been studied extensively and several drugs targeting this receptor are currently available to treat a variety of CNS indications.[98]

Recently, $GABA_AR$ subunits have been identified in many non-CNS cells (human protein atlas).[99] Importantly, $GABA_AR$ alpha subunits have been identified in several cell types associated with asthma such as airway epithelia cells, ASM, and airway leukocytes (such as $CD4^+$ T cells, and alveolar macrophages).[100–104] MIDD0301 was shown to relax constricted ASM and reduce airway hyperresponsiveness in an ovalbumin-induced murine model of asthma (MIDD0301 chemical structure and properties are summarized in **Figure 10**).[96] MIDD0301 has a half-life of almost 4 h in the lung and only 5% of the circulating amount of MIDD0301 was found in the brain.[105] In sensorimotor studies, no CNS effects were observed even up to oral doses of 1000 mg/kg. Importantly, MIDD0301 has excellent anti-

inflammatory properties leading to the reduction of eosinophil and macrophage numbers in the lungs of asthmatic mice.

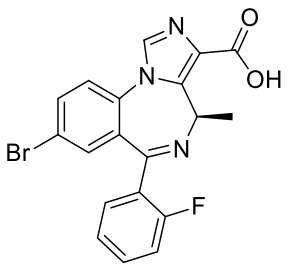

MIDD0301

Physical properties:

1. Aqueous solubility: 490 uM (Filtration assay)
2. clogP: 0.71 (Shake flask)
3. TPSA: 70.3 Å2 (MOE calculation)
4. Ligand efficiency: 0.27
5. Ligand lipophilicity efficiency: 2.63

***In vitro* activity:**

1. Binding affinity: 72 nM (Rat brain radioactive assay)
2. Efficacy/Potentiation (% at 100 nM, GABA(A)R subtypes)
   $\alpha_1\beta_3\gamma_2$: 208%, $\alpha_2\beta_3\gamma_2$: 211%, $\alpha_3\beta_3\gamma_2$: 200%
   $\alpha_4\beta_3\gamma_2$: 322%, $\alpha_5\beta_3\gamma_2$: 213% (patch clamp)
3. T cells Cl^- potentiation: 512 % @ 17 nM (patch clamp)
4. ASM relaxation at 25 uM: (less < 1 uM tissue)
   25% (15 min), 50% (45 min), tracheal rings (guinea pig)

***In vitro* safety pharmacology**

1. Viability kidney cells >82% at 400 uM
2. Viability liver cells >81% at 200 uM
3. Cardiotoxicity (hERG), 2.7% inhibition at 10 uM
4. NIH PDSP drug screen (48 receptors)-No hits
5. CYP3A4 inhibition, 12% inhibition at 50 uM

Figure 10. *Structure, physical properties, in vitro activity, and safety pharmacology of MIDD0301.*[96]

A change of $CD4^+$ T cell transmembrane current was observed in the presence of MIDD0301 (EC_{50} = 17 nM) and 20 mg/kg MIDD0301 (PO) was sufficient to reduce $CD4^+$ T cell numbers in the asthmatic mouse lung. Furthermore, reduction of specific pro-inflammatory cytokines, such as IL-17, IL-4, and TNFα, was observed in MIDD0301-treated asthmatic mice, confirming the immunoregulatory properties of MIDD0301.

International regulatory bodies require that investigational new drugs be evaluated for the potential to induce immunosuppression (e.g., FDA Guidance, Oct. 2002 and ICH Expert Working Group advises to carry out immunotoxicity studies in agreement with the European Union, Japan and US regulatations).[106] These studies are especially important for investigational drugs that are designed to reduce immune responsiveness or suspected to have immune suppression as a side effect. Importantly, these experiments are the first systematic evaluation of a drug specifically targeting the $GABA_AR$ on immune cells, showing that therapeutically relevant anti-inflammatory activity can be achieved without off-target systemic immune suppression. Here, in addition to anatomical and histological measures, we

followed ICH S8 guidelines to investigate systemic immune suppressive effects of MIDD0301 by quantifying T-cell dependent humoral immune responses to dinitrophenol (DNP) following immunization with dinitrophenyl-keyhole limpet hemocyanin (DNP-KLH).[107] Safety of MIDD0301 was initially shown by administering twice daily doses of up to 100 mg/kg in mice. No adverse effects were observed during five days of this treatment.[96] Here we report the pharmacological effects of MIDD0301 following 28-day repeat dosing with 100 mg/kg MIDD0301 twice daily. Numerous anatomic, hematologic, and immunologic measures were evaluated in male and female mice to uncover any immune-related toxicities.

2.2 Methods

2.2.1 Materials

Chemicals. MIDD0301 was synthesized using a published procedure.[109] Purity was of >98% as determined by HPLC. Identity was determined by ^{1}H-NMR, ^{13}C-NMR, and high-resolution mass spectrometry. Prednisone (>98% purity) was purchased from Sigma (P6254-1g). Skippy creamy peanut butter was used as vehicle for oral dosing.

Experimental animals. Eight- and six-week-old Swiss Webster male and female mice (Charles River Laboratory) were housed under specific pathogen-free conditions, under standard conditions of humidity, temperature, and a controlled 12 h light and dark cycle and ad libitum access to food and water. All animal experiments were in compliance with the University of Wisconsin−Milwaukee Institutional Animal Care and Use Committee (IACUC).

MIDD0301 and prednisone formulation and administration. Oral gavage: 0.2 ml of MIDD0301 in a 2% hydroxypropyl methylcellulose solution (Sigma-Aldrich, St. Louis, MO) and 2.5% polyethylene glycol (Sigma-Aldrich, St. Louis, MO) was administered by oral gavage with 20G gavage needles (Kent Scientific Corporation, Torrington CT) to a group of mice twice a day for 7 days. Oral administration: MIDD0301 was formulated in 100 mg of peanut butter at a dose of 100 mg/kg. Twice a day, mice were taken from their

cages and put in separate boxes that contained 100 mg of peanut butter or 100 mg of compound formulated peanut butter. The animals were left in the container during the feeding and returned 30 min later to their group cage. During that time all the peanut butter was consumed.

Immunogen preparation and administration: A 1 mg/ml DNP-KLH aqueous solution was prepared from solid DNP-KLH (Sigma, 324121-100 mg) and 7.5 ml of that solution added to 7.5 ml of a 40 mg/ml $Al(OH)_3$ suspension (Thermo, Imject Alum 77161). 100 µl of this solution (50 µg DNP-KLH and 2 mg $Al(OH)_3$) was injected IP on days 1 and 21 for immunization.

Necropsy. Mice were euthanized by carbon dioxide asphyxiation followed by cervical dislocation and blood withdrawn by cardiac puncture. Half of the blood was combined with EDTA for blood cell and platelet analysis. The other half was coagulated at room temperature and centrifuged for 10 min at 2,000 rpm for DNP specific IgG ELISA. After gross pathology, spleen and thymus were removed and fixed in 10% neutral buffered formalin overnight at 4°C, followed by three washes with water, and storage in 70% ethanol before sectioning. The small intestine was excised and rinsed with water using a syringe with a blunt needle. The clean intestine was washed with 7% (vol/vol) acetic acid/PBS solution and lumen rinsed using a syringe with a blunt needle. After 5 min, the Peyer's patches turned white and were readily counted by visual examination.

Hematology: EDTA-treated blood samples were analyzed with scil Vet ABC^{TM} Hematology Analyzer providing data on 13 hematology parameters.

Histology: General histology processing was performed by the Wisconsin Children's Research Institute including drying, embedding, slicing, and H&E staining. Representative sections were visualized by light microscopy at the indicated magnification.

Quantification of DNP IgG. DNP IgG was quantified by ELISA using DNP coated wells (Kamiya Biomedical Company #KT-672). Serum from non-immunized mice was diluted 1:10,000 and DNP-KLH-immunized mouse blood was diluted 1:100,000. The assay was performed following the manufacturer's instructions.

2.3 Results

Previous oral dosing of MIDD0301 in mice for pharmacodynamic studies was carried out by oral gavage using 2% hydroxypropyl methylcellulose and 2.5 % polyethylene glycol.[96] During studies of five-day duration, no significant average animal weight changes were observed. It was still necessary to perform a pilot study wherein a small group of mice were gavaged twice a day for seven days with vehicle to determine if this route would be suitable for longer-term studies. The study concluded that mice receiving vehicle gavage twice a day lost weight (28.2 ± 2.3 g) during the seven-day trial in comparison to non-treated animals (29.1 ± 2.3 g). Oral gavage is a preferred and precise route of administration, however, it has been reported that even when carried out by experienced personnel, respiratory complications, stomach distension, and inflammation due to small lacerations of the esophagus occur.[111] Furthermore, it has been shown that over time gavaged mice will show impaired weight gain due to reduced food intake.[112] Handling and restraining of animals during feeding further induces stress, which has been associated with decrease food intake.[113]

Based on these factors, we chose an oral administration protocol previously reported where glucose jelly was used to deliver the anti-obesity drug Rimonabant.[114] However, we decided to use peanut butter for better uniformity of the formulation. To initiate the study, two groups of mice were trained to consume 100 mg of peanut butter twice a day for one week. To ensure precise administration of peanut butter or peanut butter with 100 mg/kg MIDD0301 formulation, each mouse was placed individually in a small feeding container with 200 ± 20mg of peanut butter or peanut butter formulation. Mice were returned to group housing cages after consumption. A third group of mice was not treated nor placed into feeding containers. The body weights of mice over the course of the study are shown in **Figure 11**.

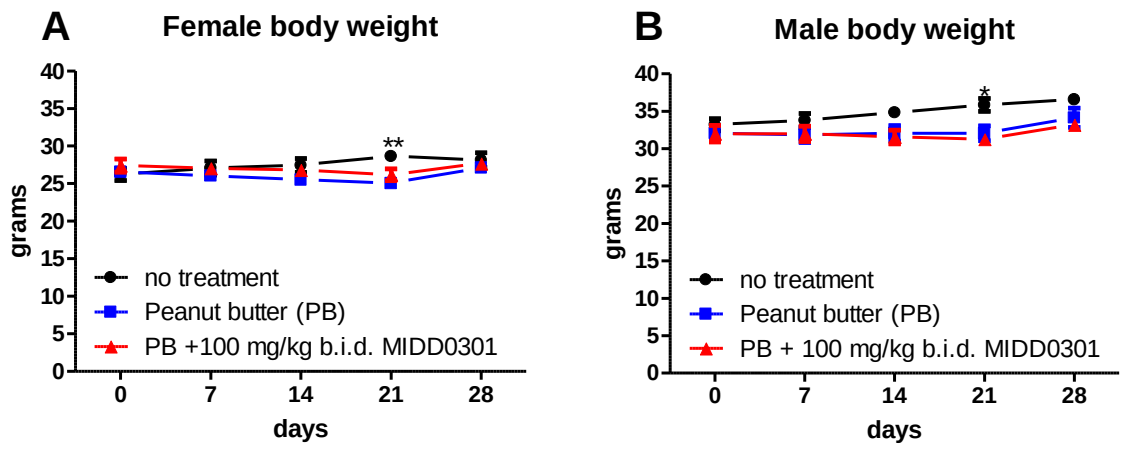

Figure 11. Average mouse body weights over the 28-day study*. In separate feeding containers, Swiss Webster male and female mice (8 weeks of age) consumed peanut butter or peanut butter + 100 mg/kg MIDD0301 twice a day. Mice in the "no treatment" group were not moved into feeding containers. Animals were weighed every week (mean ± SEM, n = 5). 2-way ANOVA was used for statistical analysis and indicated as * = p < 0.05 and ** = p < 0.01.*

The average starting weight of the 8-week-old female Swiss Webster mice was lower than the corresponding male group. Throughout the study, the average weights of MIDD0301-treated adult female and male mice were not significantly different from the peanut butter-only treated group. Interestingly, at day 21 both male and female mice receiving peanut butter (with or without MIDD0301) had average weights less than untreated control mice. However, all groups exhibited similar weights at the end of the study (28 days). The average Swiss Webster female weight after 12 weeks was 26 ± 2 grams and 35 ± 2 grams for males, which is in agreement with the average expected weight for this mouse strain.[115] No such differences or abnormalities were observed in any group during weight measurements, gastrointestinal distress, grooming behavior, and movement.

To determine the effect of MIDD0301 on systemic immune function, female and male 6-week-old Swiss Webster mice were immunized with 50 µg DNP-KLH in alum on days one and 21. Consumption of peanut butter formulated MIDD0301 (100 mg/kg, twice a day), peanut butter + prednisone (5 mg/kg/day), or peanut butter alone was carried out for 28 consecutive days. During that period, mice were weighted on days 14 and 28 (**Figure 12**).

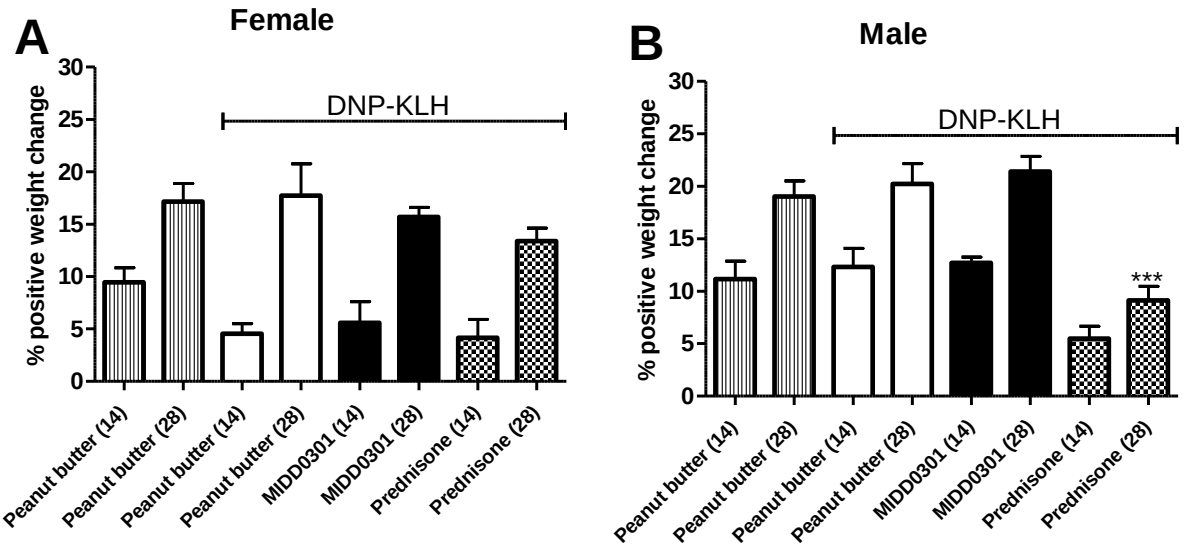

Figure 12. Effect of DNP-KLH immunization on average body weight*. In separate feeding containers, Swiss Webster female and male mice (6 weeks of age at the beginning of the study) consumed peanut butter, peanut butter + MIDD0301 (100 mg/kg, twice a day), or peanut butter + prednisone (5 mg/kg/day). Three groups were immunized with DNP-KLH on days 1 and 21. Animals were weighed on days (14) and (28). Data are expressed as mean ± SEM, n = 5. ANOVA was used for statistical analysis, *** = P < 0.001.*

As expected, the average weight of female mice increased for the non-immunized and DNP-KLH immunized control groups over the course of four weeks. No significant changes were observed between these two groups. Additionally, no significant changes were observed for the MIDD0301 (100 mg/kg, twice a day) and prednisone (5 mg/day) treated female mice in comparison to their corresponding peanut butter only control group. Consistent with the results for female mice, DNP-KLH immunization did not cause significant weight changes in male mice over the study duration, in comparison to the non-immunized mice. The average weight of male mice administered MIDD0301 (100 mg/kg, twice a day) was similar to the peanut butter only control group. However, DNP-KLH immunized male mice treated with prednisone (5 mg/kg/day) had significantly reduced average weight at the 28-day time point, in comparison to peanut butter only treated DNP-KLH immunized male mice.

Lymphoid organs and tissues, including thymus, spleen, and Peyer's patches were evaluated in all mouse groups after the 28-day MIDD0301 or prednisone treatment regimens. The results are presented in **Figure 13**.

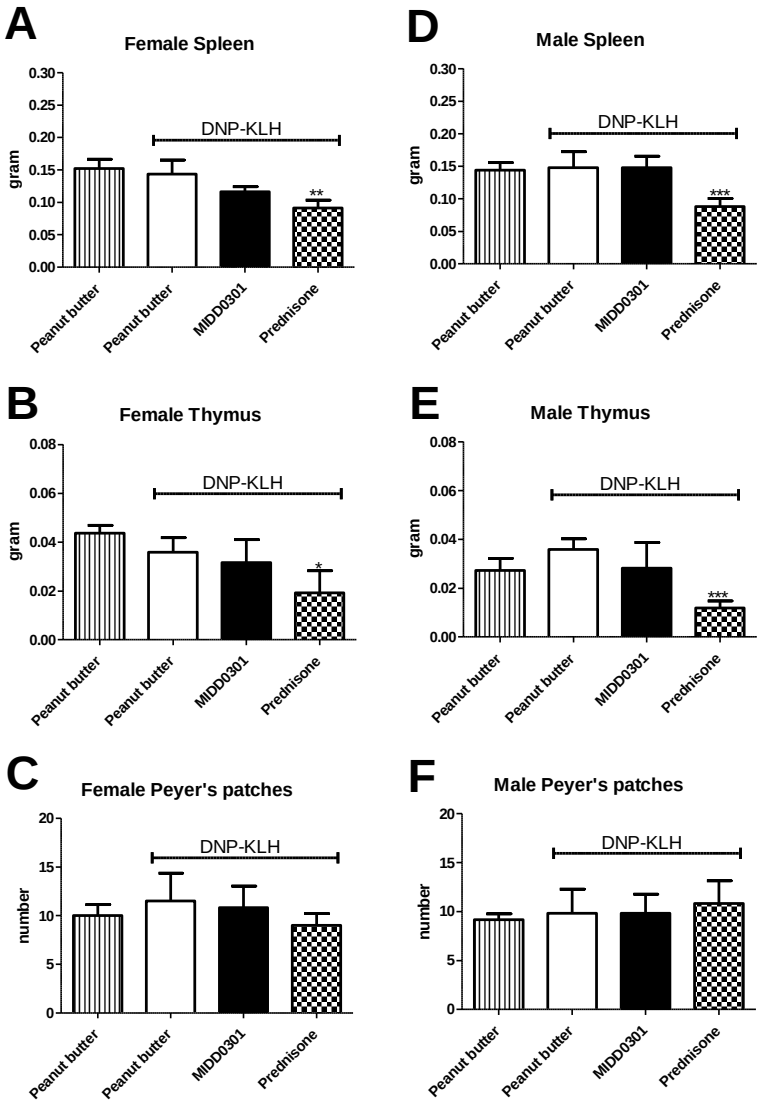

Figure 13. Evaluation of lymphoid organs and Peyer's patches in DNP-KLH immunized Swiss Webster mice after 28 days of treatment. *Mice were 6 weeks old at the beginning of the study.* ***A-C****) Female Swiss Webster mice consumed peanut butter, peanut butter + MIDD0301 (100 mg/kg, twice a day) or peanut butter + prednisone (5 mg/kg/day).* ***D-F)*** *Corresponding groups of male Swiss Webster mice were treated in the same fashion. After 28 days, organs were harvested and weighted and intestines dissected for Peyer's patch counting. Data are expressed as mean ± SEM, n = 5. ANOVA was used for statistical analysis: * = p < 0.05; ** = p < 0.01, and *** = p < 0.001.*

No significant differences were observed for spleen and thymus weights or Peyer's patch numbers between peanut butter fed DNP-KLH immunized and non-immunized animals (**Figure 13, A-F**). Spleen and thymus from DNP-KLH immunized MIDD0301 treated male and female mice had weights similar to corresponding DNP-KLH immunized mice given peanut butter alone. However, both male and female mice treated with 5 mg/kg/day prednisone had significantly smaller spleen and thymus weights in comparison to peanut butter only treated DNP-KLH immunized mice. The numbers of Peyer's patches were unchanged in all groups. Lymphoid organs were further evaluated for gross histological alterations by H&E staining. The images are shown in **Figure 14**.

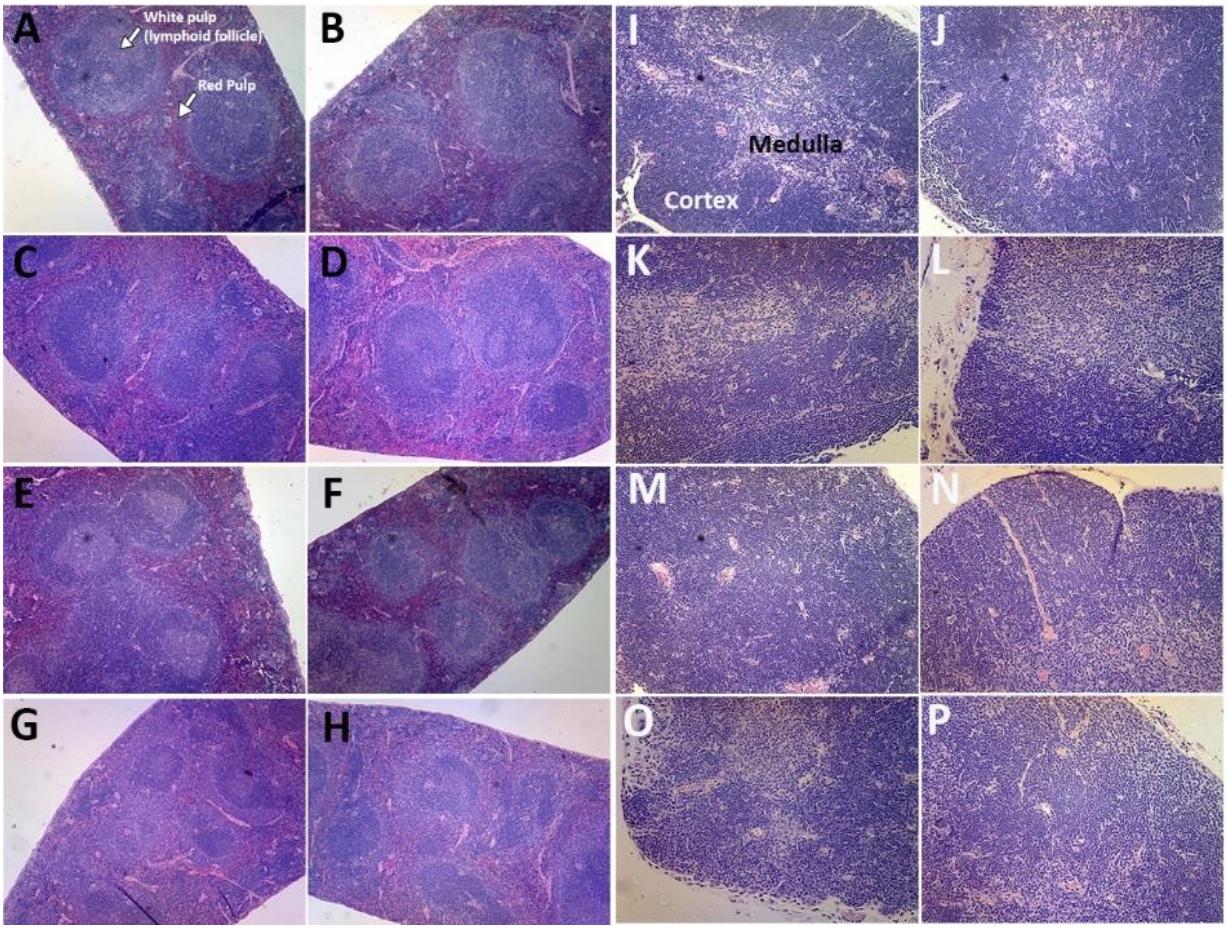

Figure 14. H&E stained sections of mouse spleens (A-H, 40x) and thymus (I-P, 100x). *A&I) male mice, peanut butter, B&J) female mice, peanut butter, C&K) male DNP-KLH-immunized mice, peanut butter, D&L) female DNP-KLH-immunized mice, peanut butter, E&M) male DNP-KLH-immunized mice, peanut butter + MIDD0301 (100 mg/kg) twice a day for 28 days, F&N) female DNP-KLH-immunized mice, peanut butter + MIDD0301 (100 mg/kg) twice a day for 28 days. G&O) male DNP-KLH-immunized mice, peanut butter + prednisone 5 mg/kg/day for 28 days, H&P) female DNP-KLH-immunized mice, peanut butter + prednisone 5 mg/kg/day for 28 days.*

H&E stained spleen sections reveal typical histological presence of white (lymphoid follicles) and red pulp in all mouse groups. The cellular arrangements of follicles show no remarkable differences among the groups, except for the prednisone-treated animals (**Figure 14, G and H**) that exhibited smaller and less uniform follicle size. Similar splenic changes have been reported in patients taking corticosteroids over a long period of time.[116] H&E staining also highlighted the lymphocyte-rich white pulp, with well-defined features of centrally located germinal centers and the surrounding marginal zone for all spleen sections. The thymus histology of all groups appeared unchanged following treatment. The medulla and cortex regions were well defined in all groups and the thymus cell density appeared unchanged in all groups. Overall, no significant changes in the spleen and thymus histology were observed after repeated MIDD0301 treatment. However, prednisone-treated animals did exhibit some alteration in spleen histology.

Blood was collected from mice after the 28-day treatment regime for hematologic evaluation. The evaluation is summarized in **Table 2.**

Mouse (Male)	Peanut butter[a]	Peanut butter[b]	MIDD0301[b]	Prednisone [b]
		DNP-KLH-immunization		
[c]WBC x10^3 (mm^3)	6.4 ± 0.7	6.2 ± 0.5	6.1 ± 0.7	5.8 ± 0.7
[d]RBC x10^6 (mm^3)	8.7 ± 0.2	8.1 ± 0.1	8.3 ± 0.2	8.0 ± 0.1
[e]HGB (g/dl)	14.9 ± 0.2	14.7 ± 0.2	15.1 ± 0.3	15.4 ± 0.2
[f]HCT (%)	45.1 ± 0.8	41.9 ± 0.3	43.3 ± 1.2	42.8 ± 0.3
[g]MCV (µm^3)	52.0 ± 0.8	51.8 ± 0.8	51.8 ± 0.4	53.4 ± 0.9
[h]MCH (pg)	17.2 ± 0.3	18.2 ± 0.4	18.2 ± 0.2	19.3 ± 0.3
[i]MCHC (g/dl)	33.1 ± 0.2	35.1 ± 0.4	35.0 ± 0.3	36.1 ± 0.2
[k]RDW (%)	15.0 ± 0.3	15.0 ± 0.4	15.0 ± 0.2	15.7 ± 0.7
[l]PLT x10^3 (mm^3)	986 ± 67	880 ± 40	903 ± 37	944 ± 27
[m]MPV (µm^3)	5.4 ± 0.1	5.3 ± 0.1	5.3 ± 0.1	5.4 ± 0.1
[n]DIFF (%)				
[o]LYM	55.0 ± 2.0	44.0 ± 2.9	50.0 ± 0.7	36.6 ± 2.4
[p]MON	10.5 ± 0.5	9.9 ± 0.3	9.4 ± 0.2	11.3 ± 0.3
[q]GRA	34.5 ± 2.1	46.1 ± 2.8	40.6 ± 0.7	52.1 ± 2.5
Mouse (Female)	Peanut butter[a]	Peanut butter[b]	MIDD0301[b]	Prednisone [b]
		DNP-KLH-immunization		
[c]WBC x10^3 (mm^3)	6.1 ± 0.2	6.5 ± 0.6	5.4 ± 0.7	7.4 ± 0.9

[d]RBC x10^6 (mm^3)	8.4 ± 0.1	7.5 ± 0.2	8.0 ± 0.1	7.8 ± 0.1
[e]HGB (g/dl)	14.6 ± 0.3	14.4 ± 0.2	14.2 ± 0.1	15.0 ± 0.2
[f]HCT (%)	43.4 ± 0.9	39.7 ± 0.8	41.6 ± 0.3	41.1 ± 0.5
[g]MCV (μm^3)	51.8 ± 0.6	53.4 ± 0.9	52.5 ± 0.9	52.6 ± 0.9
[h]MCH (pg)	17.3 ± 0.2	19.4 ± 0.6	18.3 ± 0.3	19.2 ± 0.4
[i]MCHC (g/dl)	33.6 ± 0.3	36.4 ± 0.6	35.0 ± 0.3	36.6 ± 0.4
[k]RDW (%)	14.5 ± 0.2	14.9 ± 0.3	15.2 ± 0.1	15.0 ± 0.4
[l]PLT x10^3 (mm^3)	840 ± 54	781 ± 39	789 ± 29	837 ± 39
[m]MPV (μm^3)	5.4 ± 0.1	5.5 ± 0.2	5.2 ± 0.1	5.3 ± 0.1
[n]DIFF (%)				
[o]LYM	53.8 ± 3.1	47.2 ± 1.4	54.7 ± 2.5	40.4 ± 1.9
[p]MON	10.8 ± 0.3	11.1 ± 0.7	11.0 ± 0.5	10.0 ± 0.7
[q]GRA	35.4 ± 3.4	41.7 ± 1.4	34.3 ± 2.6	49.6 ± 2.6

Table 2. Hematology parameters for non-immunized and DNP-KLH-immunized Swiss Webster mice after indicated treatment for 28 days. *The data are expressed as mean ± SEM, n = 5. [a]Non-immunized male and female Swiss Webster mice consumed peanut butter (100 mg/day, twice a day); [b]DNP-KLH immunized male and female Swiss Webster mice consumed peanut butter; peanut butter + 100 mg/kg MIDD0301 twice a day, or peanut butter + 5 mg/kg/day prednisone; [c]white blood cells; [d]red blood cells; [e]hemoglobin; [f]hematocrit; [g]mean corpuscular volume; [h]mean cell hemoglobin; [i]mean cell hemoglobin concentration; [k]red cell distribution width; [l]platelets; [m]mean platelet volume; [n]differential white blood cell count; [o]lymphocytes; [p]monocytes; [q]granulocytes; The data is expressed as mean ± SEM, n = 5. ANOVA was used for statistical analysis.*

Overall, no significant differences in hematology parameters were found among the four different treatment groups as determined by ANOVA analysis. However, differential lymphocyte values trended lower in the prednisone-treated male and female groups, whereas the differential granulocytes were the highest in these groups. An elevation of granulocytes is consistent with corticosteroid use in humans where granulocyte (particularly neutrophil) levels are known to increase.[117] Most importantly, male and female mice treated with MIDD0301 exhibited differential white blood cells counts similar to the control groups, which are in accord with previously reported hematology ranges for adult Swiss Webster mice.[118]

Three groups of female and male mice were immunized with DNP-KLH on days one and 21 of this study. To investigate the effect of MIDD0301 on a T-dependent humoral immune response, serum DNP IgG was measured by ELISA for all mice at day 28 (**Figure 15**).

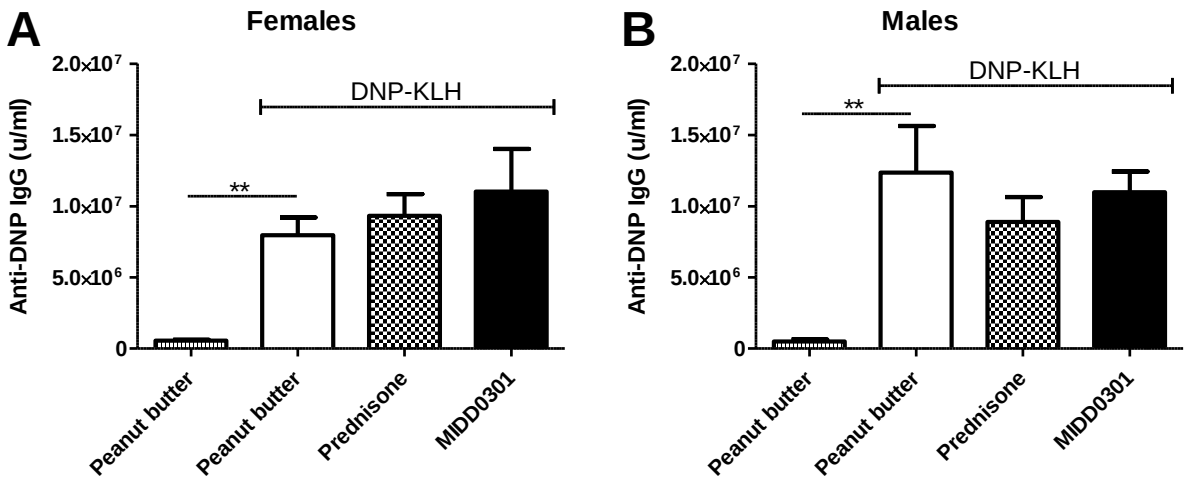

Figure 15. Quantification of mouse serum DNP IgG. Swiss Webster male and female mice consumed peanut butter, peanut butter + MIDD0301 (100 mg/kg, twice a day), or peanut butter + prednisone (5 mg/kg/day). *DNP-KLH immunization occurred on days 1 and 21 and DNP-specific IgG was quantified on day 28. Data are expressed as mean ± SEM, n = 5. ANOVA analysis was used for statistical analysis. ** = P < 0.01.*

As expected, DNP-KLH immunization significantly increased DNP-specific IgG in female and male mice (**Figure 15**). IgG levels were similar for all DNP-KLH-immunized mice, regardless of treatment. This confirmed repeat MIDD0301 dosing at 100 mg/kg twice a day did not impair systemic immune function as measured by a secondary antibody response to a classic T-dependent antigen.

2.4 Discussion

Immunotoxicity evaluations are a crucial part of preclinical studies for drug candidates before entering human trials. MIDD0301 is a small molecule that is effective in reducing airway constriction and airway inflammation and was first developed for the oral treatment of asthma. In an ovalbumin-induced murine model of asthma, administration of MIDD0301 was able to reduce the number of bronchoalveolar leukocytes, including eosinophils, macrophages, and $CD4^+$ T cells.[96] The mode of action of MIDD0301 is novel, targeting $GABA_A$Rs of leukocytes and ASM. It has been shown that both resting and activated T cells express different subtypes of $GABA_A$Rs;[120] thus selective $GABA_A$R targeting therapeutics can be anti-inflammatory without inducing general suppression of the immune system.

MIDD0301 modulates the transmembrane potential of T-cells, which may directly or indirectly reduce the release of intercellular calcium, as shown in presence of $GABA_AR$ ligand XHE-III-74 acid.[121] In turn, calcium homeostasis mediates the immune response of T cells.[122] To further understand the influence of MIDD0301 on systemic immunity, high doses of MIDD0301 (100 mg/kg) were administrated orally twice daily. Differential white cell counts demonstrated no changes in the number and ratio of lymphocytes, monocytes, and granulocytes in the blood of MIDD0301 treated compared to vehicle treated animals. Furthermore, lymphoid organs (spleen and thymus) and Peyer's patches were unchanged by treatment as determined by organ weight and histology. This is significant, as oral dosing of other anti-inflammatory agents like dexamethasone are known to induce severe apoptosis of intestinal lymphatic tissue and reduce the numbers of Peyer's patches.[123] These results are consistent with our observations, where prednisone treatment caused reduced spleen and thymus mass in both female and male mice. Female and male mice were immunized with DNP-KLH to determine if MIDD0301 caused systemic immune suppression. DNP-specific antibody quantification showed that oral dosing of MIDD0301 twice daily for 28 days did not diminish this T-dependent response.

Taken together, we have demonstrated that MIDD0301 induces no adverse immunotoxicological effects in mice at 100 mg/kg twice a day over a period of 28 days. The production of specific antibodies following DNP-KLH immunization was not diminished by MIDD0301, although in an ovalbumin-induced model of asthma, MIDD0301 reduced the number of lung leukocytes.[96] Accordingly, MIDD0301 acts as an anti-inflammatory agent that selectively reduces inflammation in the lung without compromising systemic immune function. Finally, these studies show that MIDD0301 is a safer alternative to prednisone, where 5 mg/kg/day prednisone (2.5% of the MIDD0301 dose) for 28 days in mice reduced spleen and thymus masses, altered spleen morphology, and reduced animal weight.

2.5 Conclusion

The study design employed oral administration of mice twice daily throughout the study period with 100 mg/kg MIDD0301 mixed in peanut butter. Compound dosing did not reveal signs of general toxicity as determined by animal weight, organ weight, or hematology. Peanut butter plus test drug (in addition to *ad libitum* standard rodent chow) did not affect weight gain in the adult mice, in contrast to weight loss in 5 mg/kg prednisone-treated mice. Spleen and thymus weights were unchanged in MIDD0301-treated mice, but prednisone significantly reduced the weight of those organs over the 28-day dosing. Similarly, no differences in spleen or thymus histology were observed following MIDD0301 treatment, but prednisone treatment induced morphological changes in the spleen. The number of small intestine Peyer's patches was not affected by MIDD0301 treatment, an important factor for orally administered drugs. Circulating lymphocyte, monocyte, and granulocyte numbers were unchanged in the MIDD0301-treated animals, whereas differential lymphocyte numbers were reduced in prednisone-treated animals. MIDD0301 treatment did not alter IgG antibody responses to dinitrophenol (DNP) following dinitrophenyl-keyhole limpet hemocyanin immunization, indicating that systemic humoral immune function was not affected. Taken together, these studies show that repeated daily administration of MIDD0301 is safe and not associated with adverse immunotoxicological effects in mice.

CHAPTER 3

Sensorimotor Investigations of New Drug Candidates

3.1 Rotarod Test Background

The most commonly prescribed class of drugs for the treatment of insomnia and anxiety are benzodiazepines.[124] Although they exhibit high efficacy, there are often unwanted effects that include but are not limited to: anxiety, smooth muscle relaxation, sedation, impaired motor coordination, seizures, and tolerance.[129–131] Despite the development of compounds that strictly target $GABA_aR$ subtypes that do not mediate these unwanted effects, it is still necessary to demonstrate this *in vivo*.[125]

The first scientists to investigate sensorimotor coordination and impairment using a rotarod device were N.W. Dunham and T.S. Miya in 1957.[126] Although quite rudimentary to the rotarod apparatuses of today, the function still remains as an initial screening assay to understand the pharmacological effect of a drug as it pertains to sensorimotor coordination. Mice are placed on a rod that can be set to specific acceleration and velocity, and time is recorded until they fall or the end of the experiment is reached. Depending on the breed, strain, and sex of the mice, training for an appropriate acceleration and velocity are determined prior to experimentation to avoid unnecessary physical activity that may contribute to false positives yet ensuring that affected mice will still fail the experiment.[127] The rod is placed at a height that dissuades mice from jumping off, yet avoids injury when they fall. This test gives insight to possible impaired neurological function, and is widely used to investigate drugs for the aforementioned unwanted effects.[126]

3.2 Instrumentation

The rotarod apparatus used to determine sensorimotor effects is the AccuRotor 4-Channel RotaRod (Omnitech Electronics, Inc., Columbus, OH). Velocity, acceleration, direction, and time are controlled appropriately depending on the breed, strain, and sex of mice. The bottom of each well

contains a touch-activated sensor that records the time when a mouse falls off the rod.[128] The RotaRod apparatus is shown in **Figure 16** below.

Figure 16. Mice performing on the RotaRod apparatus*. Each mouse has an individual compartment that contains a rotating rod roughly 20 cm above a touch-sensitive pad that will mark the time when a mouse falls off the rod. The height and size of the rotating rod dissuade mice from falling off the rod, yet avoid injury when they do fall.*

3.3 Protocol

3.3.1 Experimental

Six-week-old female Swiss Webster (CFW) mice were purchased from The Jackson Laboratory and allowed one week acclimation upon arrival. Mice were then trained to balance on the RotaRod apparatus for three minutes at a velocity between 15-18 rpm. Acceleration from initial velocity to maintained velocity was set at 15 sec. Training was complete once mice were able to remain on the rotating rod for

the full three minutes without a failure. A failure was defined as a mouse falling twice within the three-minute time period, as it was common for a mouse to fall once. To avoid false positives, it was established that a mouse falling twice was indicative of impaired sensorimotor coordination and the time of the failure recorded. Mice are simply placed back on the rotating rod after the first fall. Training typically took two to three weeks before mice were suitable for compound testing.

Compounds were delivered to trained mice via intraperitoneal (IP), subcutaneous (SC), or oral gavage (PO) administration. Volumes varied from 50 µl to 250 µl depending on compound solubility. IP and SC vehicle consisted of 10% DMSO (Fisher Scientific, D128-500), 40% propylene glycol (Spectrum, P1440), and 50% PBS (Hyclone, SH30256.01). Poor aqueous solubility was often an issue, so compounds were first dissolved in DMSO prior to propylene glycol and PBS addition. PO vehicle consisted of 2% polyethylene glycol and prepared 2.5% hydroxypropylmethyl cellulose (HPMC) solution. Compounds were first dissolved in polyethylene glycol with mortar and pestle, with addition of heat required for less soluble compounds. HPMC was then added and mixed to appropriate volume and concentration. All administrations used 1 ml syringes (BD, 309626), however 25G needles were used for IP and SC injections, while a blunt oral gavage needle was used for PO administration.

Mice were placed on the rod at 10, 30, and 60 min following compound delivery. The time of the second fall (a failure) was recorded if it occurred prior to 3 min. Data were graphed using GraphPad Prism 5.0. A Two-Way ANOVA comparing group means with Bonferroni Correlation was performed to express data as mean ± SEM (N = 10). $*(p<.05)$, $**$ $(p<.01)$, or $***$ $(p<0.001)$ significance was compared to vehicle-treated mice.

3.3.2 Results

Vehicle treated mice were used as negative control, with no observable sedation or motor coordination impairment on the rotarod regardless of type of administration. 5 mg/kg diazepam (IP) was typically used as positive control, as it induced severe motor impairment at 10 min, moderate impairment at the 30 min, and little to no impairment at the 60 min. All compounds of interest were delivered at 40 mg/kg via oral gavage (PO) unless otherwise noted.

All rotarod studies are graphed with statistics and reported in **Appendix RotaRod Graphs**. The majority of all compounds passed the rotarod test without demonstrating motor impairment or sedation in mouse models. These compounds were then subject to further *in vivo* and *in vitro* testing. Compounds (**Figure 17**) that demonstrated significant motor impairment or sedation compared to negative control vehicle and/or positive control diazepam-treated mice are reported in **Table 3**.

Key	
ns	No Significance
N/A	Not Available
PO	Oral Admin.
IP	Intraperitoneal Admin.
*	Significantly Higher
*	Significantly Lower

Compound	Dose	Significance vs. Vehicle (+ Control)					Significance vs. 5mg/kg IP Diazepam (- Control)				
		10min	30min	60min	120min	240min	10min	30min	60min	120min	240min
RJ-II-68	40mg/kg PO	***	ns	ns	N/A	N/A	ns	**	ns	N/A	N/A
MRS-II-57	40mg/kg PO	**	ns	ns	N/A	N/A	***	ns	ns	N/A	N/A
MRS-I-64	40mg/kg PO	***	ns	ns	N/A	N/A	ns	**	ns	N/A	N/A
KRM-II-81	100mg/kg PO	*	ns	ns	N/A	***	ns	*	ns	N/A	***
KRM-II-82	100mg/kg PO	*	*	**	N/A	ns	ns	ns	ns	N/A	ns
KRM-II-68	40mg/kg PO	***	***	***	N/A	N/A	ns	***	***	N/A	N/A
RJ-II-70	40mg/kg PO	***	***	ns	N/A	N/A	ns	ns	ns	N/A	N/A
RJ-II-71	40mg/kg PO	***	ns	ns	N/A	N/A	ns	ns	ns	N/A	N/A
8a	40mg/kg PO	***	**	ns	N/A	N/A	ns	ns	ns	N/A	N/A
8b	40mg/kg PO	***	***	ns	N/A	N/A	ns	ns	ns	N/A	N/A
FR-I-44	80mg/kg PO	***	***	*	N/A	N/A	ns	ns	ns	N/A	N/A
GL-I-43	40mg/kg PO	***	***	ns	N/A	N/A	*	ns	ns	N/A	N/A
RV-II-04	40mg/kg PO	***	***	***	N/A	N/A	*	ns	**	N/A	N/A
MP-III-23	40mg/kg PO	***	**	ns	N/A	N/A	ns	ns	ns	N/A	N/A
KPP-IV-09	100mg/kg PO	*	ns	ns	ns	ns	ns	ns	ns	ns	ns
KPP-III-96B	100mg/kg PO	*	*	*	N/A	*	ns	ns	ns	N/A	ns
KRM-II-08	10mg/kg IP	***	***	***	N/A	N/A	*	***	***	N/A	N/A
TA-I-12	10mg/kg IP	***	***	***	N/A	N/A	**	**	**	N/A	N/A
TA-I-16	10mg/kg IP	***	***	***	N/A	N/A	**	**	**	N/A	N/A

Table 3. Asthma and Pain Compounds Demonstrating Significant Motor Impairment Compared to Vehicle and Diazepam. *Trained female CFW mice (N≥10) were placed on the RotaRod at 10, 30, and 60 min after compound administration. Compounds near the top of the table were shown to have significantly better motor coordination compared to 5 mg/kg diazepam IP, while compounds near the bottom of the table had significantly worse motor coordination compared to 5 mg/kg diazepam IP.*

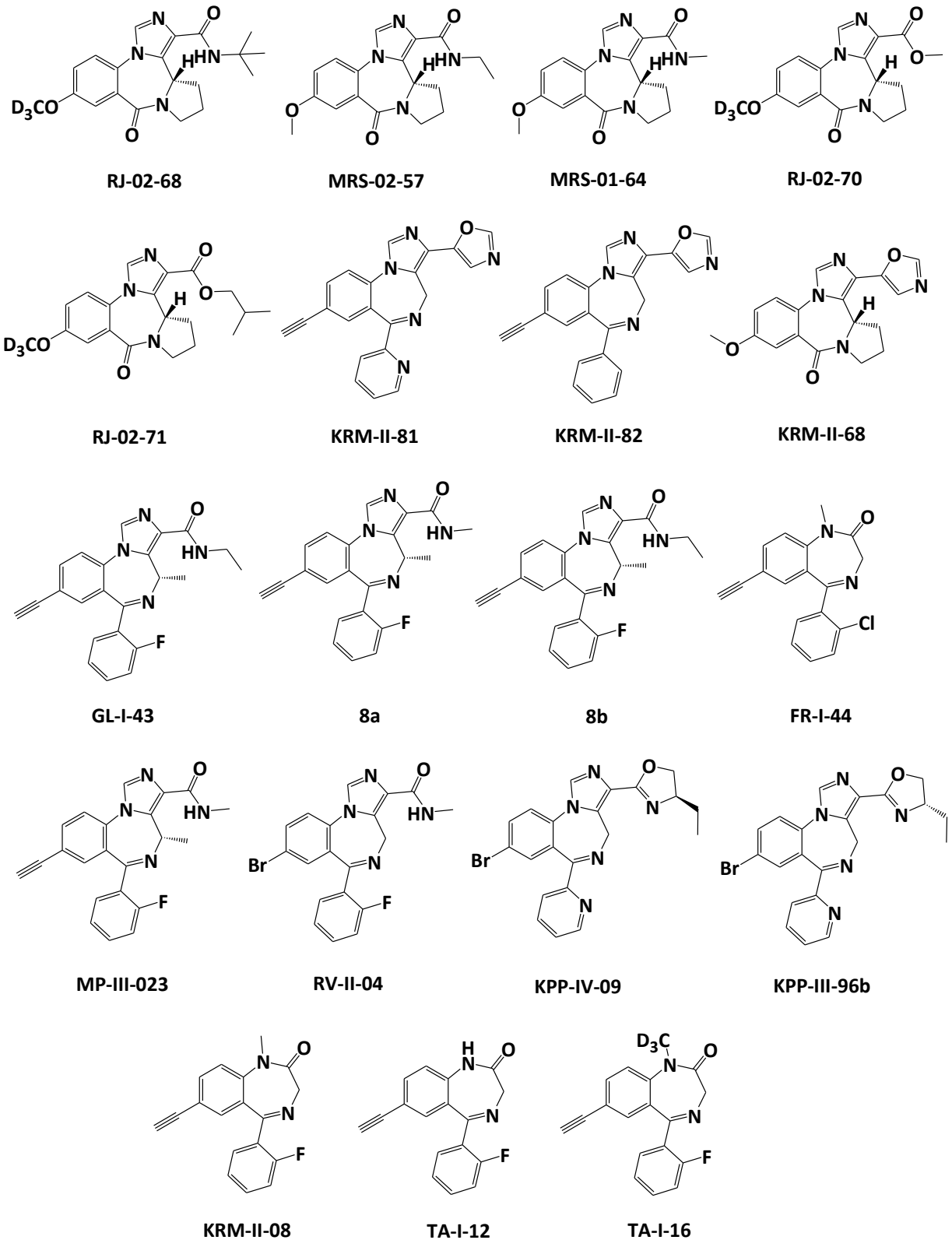

Figure 17. Structures of Asthma and Pain Compounds Demonstrating Significant Motor Impairment. *Asthma compounds RJ-02-68, MRS-02-57, MRS-01-64, RJ-02-70, and RJ-02-71 were found to cause motor impairment. Remaining compounds were designed to treat neuropathic pain and were also found to cause motor impairment.*

Figure 17 shows the structures of asthma compounds RJ-02-68, MRS-02-57, MRS-01-64, RJ-02-70, and RJ-02-71 along with other pain compounds that demonstrate significant sedation or motor impairment shown in **Table 3.**

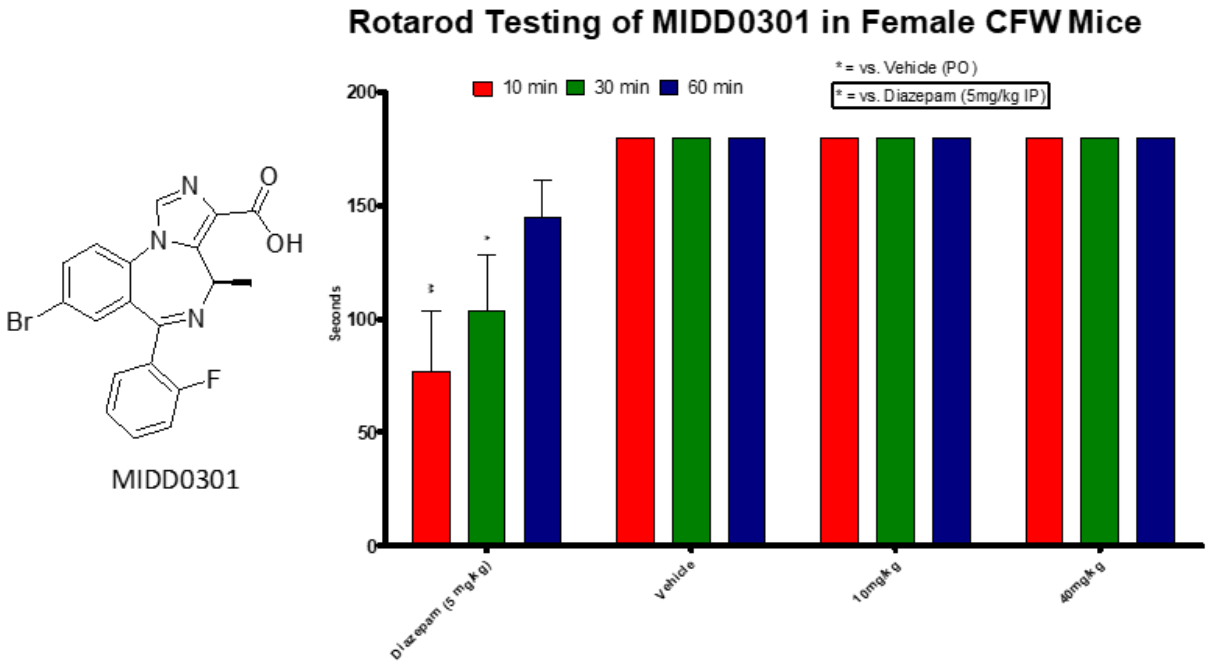

Figure 18. RotaRod Testing of Lead Asthma Drug Candidate MIDD0301. *Trained female CFW mice (N≥10) were placed on the RotaRod at 10, 30, and 60 min after compound administration. The rotarod was set at a constant rate of 18 rpm. Compounds were administered and compared to vehicle as negative control and diazepam as positive control.*

Lead compound MIDD0301 was shown to have no impaired motor coordination up to 40 mg/kg PO on the rotarod test. **Figure 18** was an important initial test amongst others confirming MIDD0301 to be a promising drug candidate.

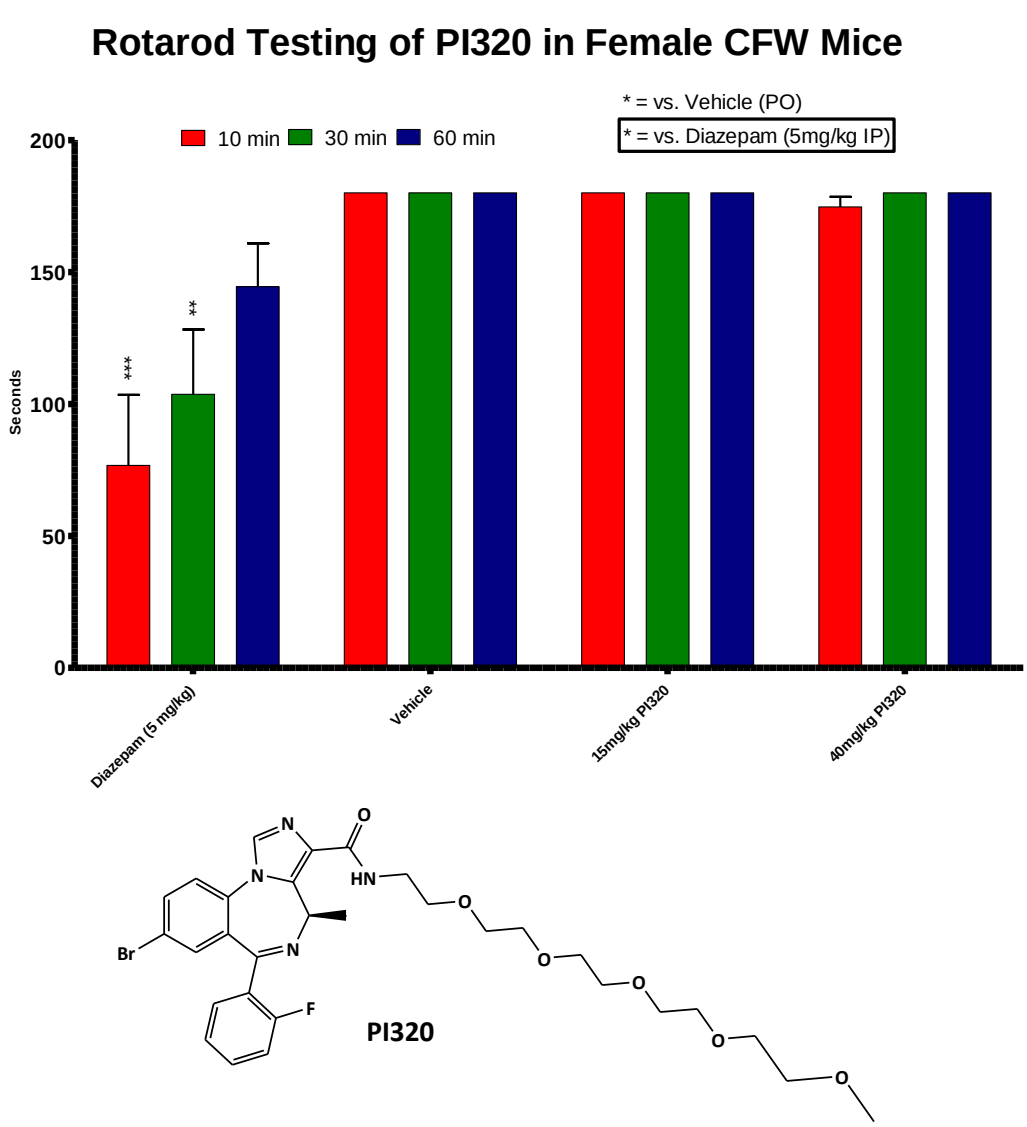

Figure 19. RotaRod Testing of MIDD0301 Analog PI320. *Trained female CFW mice (N≥10) were placed on the RotaRod at 10, 30, and 60 min after compound administration. The rotarod was set at a constant rate of 18 rpm. Compounds were administered and compared to vehicle as negative control and diazepam as positive control.*

PI320 was analyzed on the rotarod apparatus under similar conditions as MIDD0301 and is shown in **Figure 19**. PI320 has no impaired motor coordination up to 40 mg/kg PO on the rotarod test.

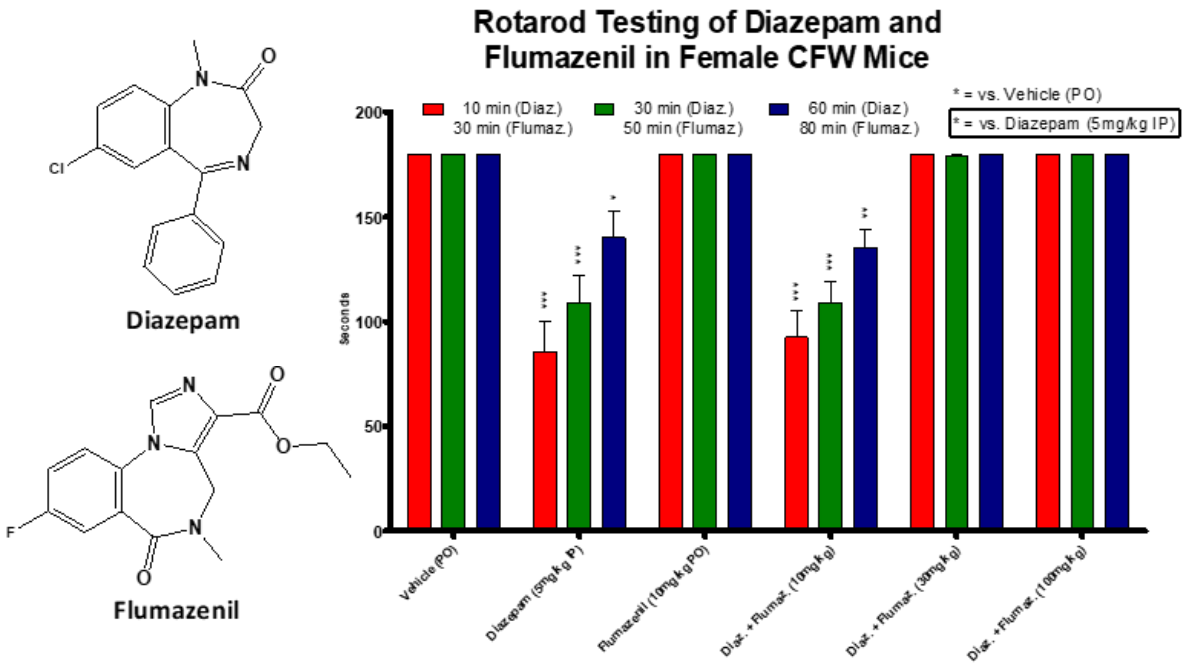

Figure 20. RotaRod Data Single Dose and Co-administration of Diazepam and Flumazenil. *Trained female CFW mice (N≥10) were placed on the RotaRod at 10, 30, and 60 min after diazepam administration, which corresponds to 30, 50, and 80 min after flumazenil administration. The rotarod was set at a constant rate of 18 rpm. Compounds were administered and compared to vehicle as negative control and diazepam as positive control.*

Investigating sensorimotor effects of diazepam (positive allosteric $GABA_aR$ modulator) and flumazenil (allosteric $GABA_aR$ antagonist) on the rotarod apparatus showed diazepam causing sedation and impaired motor coordination at 5 mg/kg (IP), while flumazenil showed no sedation or impaired motor coordination at 10 mg/kg (PO) **Figure 20.** We further observed no sedation or impaired motor coordination for the co-administration of diazepam 5 mg/kg (IP) and flumazenil 30 mg/kg (PO). Flumazenil (PO) was delivered 20 min prior to diazepam (IP) to match the T_{max} value of each compound. When delivered at concentrations greater than 30 mg/kg, flumazenil antagonized the sedative and impaired motor function normally observed with 5 mg/kg (IP) diazepam administration.

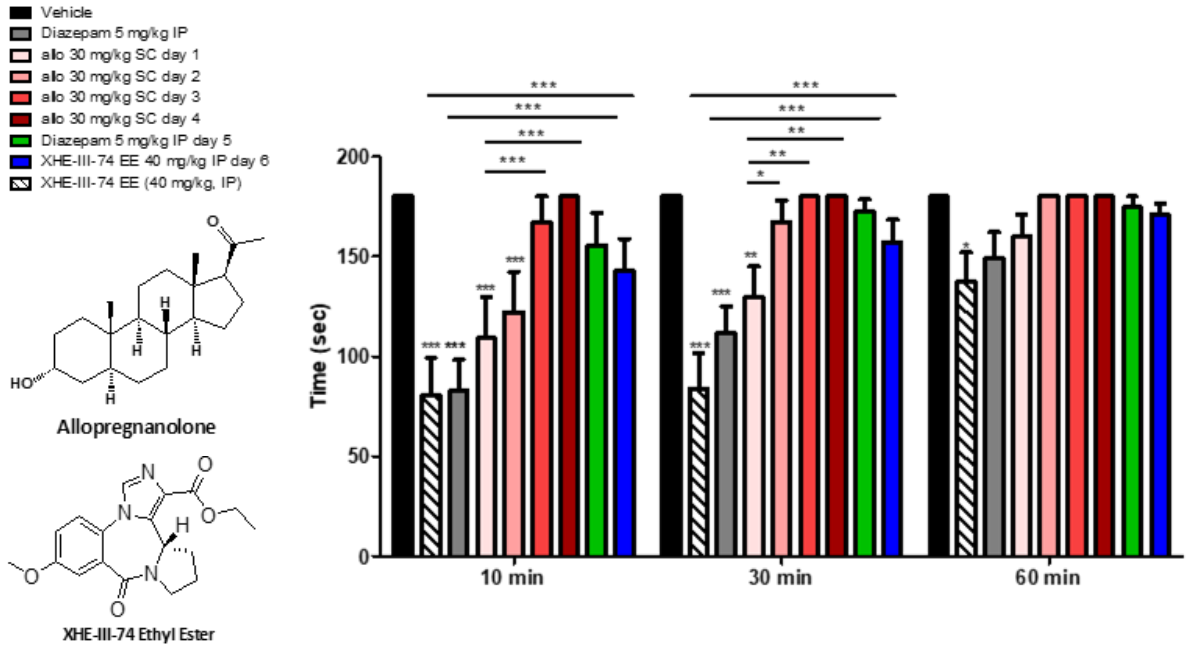

Figure 21. 5-Day RotaRod Experiment of Single Dose and Co-administration of Diazepam and XHE-III-74 EE Before and After Allopregnanolone Treatment*. Trained female CFW mice (N≥10) were placed on the RotaRod at 10, 30, and 60 min after compound administration. The rotarod was set at a constant rate of 18 rpm. Compounds were administered and compared to vehicle as negative control and diazepam as positive control.*

Figure 21 conveys a repeat dose study of allopregnanolone (ALLO) at 30 mg/kg (SC) for four days where mice showed significantly less sedation/motor impairment on days three and four compared to days one and two. No sedation/motor impairment was present on the last day of ALLO administration. After four days of ALLO administration, diazepam was administered on day five and showed significantly less sedation/motor impairment compared to the initial diazepam administration given as positive control. XHE-III-74EE, a compound known to target the α4 subunit and impair motor coordination once passing through the blood-brain-barrier (BBB), was administered on day six of the study. No motor impairment was observed. Repeat dosing of ALLO was shown to develop tolerance in female Swiss Webster mice to motor impairment not only for ALLO, but also for diazepam and XHE-III-74EE.

3.3.3 Discussion

The protocol implemented was able to screen compounds and identify the level of motor impairment or sedation in compound-treated mice across several time points. Compounds near the top of **Table 3** such as RJ-II-68, MRS-II-57, MRS-I-64, KRM-II-81, KRM-II-68, and GL-I-43 treated-mice were shown to cause significantly lower time spent on the rotarod compared to vehicle-treated mice, yet still demonstrated significantly less motor impairment when compared to diazepam-treated mice. Compounds near the bottom of **Table 3** such as RV-II-04, KRM-II-08, TA-I-12, and TA-I-16 were shown to have significantly higher motor impairment compared to both vehicle-treated and diazepam-treated mice. These compounds were no longer investigated for potential therapeutic effect due to such negative CNS effects and motor impairment.

Compounds causing motor impairment were then screened for common functional groups to investigate possible structure-activity relationships. Functional groups of potential asthma compounds at the R1 position (**Structure A**) that were amides showed the most motor impairment, followed by esters and thioesters. Compound with a carboxylic acid group showed no sedation or motor impairment in any compound tested. At the R2 position (**Structure A**), all compounds that demonstrated motor impairment had either methoxy or deuterated-methoxy groups. However, compounds that contained a hydroxyl or bromine group at the R2 position did not show motor impairment or sedation.

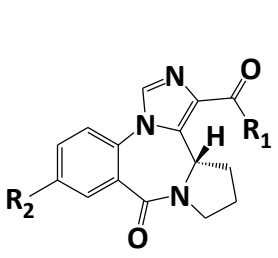

Structure A

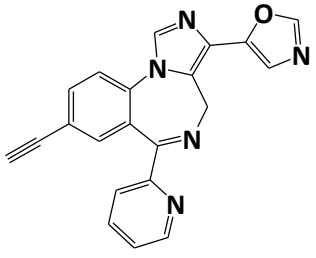

Structure B

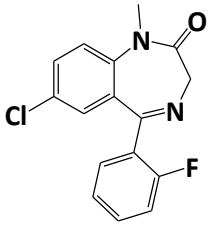

Structure C

Compounds developed to treat pain from **Figure 17** are represented in **Structure B**. Of the 11 compounds containing an oxazole at the 3-position, five were shown to cause significant motor

impairment. However, none of the 23 compounds tested that contain an oxadiazole at the 3-position were shown to cause motor impairment. At the 8-position, both ethynyl and bromine groups were found to cause impaired motor function whereas there was no impairment from compounds containing a chlorine at this position.

Traditional benzodiazepine structures lacking the imidazole top bearing a carboxylic acid, and/or oxazole groups and are represented in **Structure C**. These compounds (FR-I-44, KRM-II-08, TA-I-12, and TA-I-16) were considerably more sedating than other compounds and caused sedation or motor impairment (**Table 3**).

The majority of all compounds analyzed on the RotaRod apparatus showed no motor impairment or sedation and lead compounds were further pursued for cytotoxic, metabolic, and pharmacokinetic analysis.

3.4 Conclusion

The RotaRod assay is a robust experimental paradigm that is able to classify compounds based on sedation or impaired sensorimotor coordination. Studies involving co-administration can also be used to confirm site-specific binding. The data can provide further insight into the distribution of the compound into the brain. This information can be used for the justification of future pharmacokinetic analysis.

Compounds XHE-III-74EE, RJ-02-50, MIDD0301, and PI320 were identified as potential drug candidates due to their lack of adverse central nervous system effects.Compounds FR-I-44, KRM-II-08, TA-I-12, and TA-I-16 contained the traditional benzodiazepine structure and were shown cause much more sedation and impairment than the most sedating and motor-impairing imidazodiazepines.

The RotaRod assay is currently being performed by Michelle Meyer, a member of the Arnold Group. Slight changes such as method of administration, RotaRod acceleration rate, speed, and timing of

measurement have been made to the protocol to accommodate different breeds and experimentation requirements.

CHAPTER 4

Investigation of R/S MIDD0301 and PI320

4.1 Introduction

During acute asthma exacerbations, narrowing of airways caused by airway smooth muscle (ASM) contraction (bronchospasm) occurs rapidly in response to allergens, irritants, or other stimuli such as exercise, cold air, or anxiety. Rapid onset ASM relaxing agents (bronchodilators) currently provide immediate bronchospasm relief, while combinations of β-adrenergic receptor agonists (BAA), anticholinergic agents, leukotriene receptor antagonists, corticosteroids, and biologics are used to maintain airway function and control lung inflammation. Asthma is a heterogeneous disease with a spectrum of phenotypes and endotypes including paucigranulocytic, eosinophilic, neutrophilic, and mixed granulocytic inflammation,[132] which have variable responses or resistance to existing pharmacotherapy. In addition to other approaches, targeting gamma-butyric acid type A receptors ($GABA_AR$s) in the lung is a novel asthma drug strategy.[133] $GABA_AR$s are well-characterized ligand-gated chloride ion channels known for their expression on neurons and response to inhibitory neurotransmitter GABA and other ligands.[134] Recently, functional $GABA_AR$s have been identified on non-central nervous system (CNS) cell types, such as ASM[135] and inflammatory cells.[136] We have developed subtype selective $GABA_AR$ allosteric ligands that relax constricted rodent and human ASM *ex vivo*.[137–143] *In vivo* studies with orally dosed asthmatic mice demonstrated reduced inflammation and relaxation of methacholine-induced bronchospasm.[137–142]

GABA has been shown to be an important modulator in immune cells,[144] and is present in nanomolar concentrations in the blood.[145] Our group has demonstrated that nanomolar concentrations of $GABA_AR$ allosteric ligands and GABA are sufficient to change the transmembrane current of isolated mouse $CD4^+$ T cells.[23] Oral administration of allosteric $GABA_AR$ ligands reduced the number of lung inflammatory cells in ovalbumin-sensitized and challenged asthmatic mice. Cytokines, such as IL-17, IL-4, and TNFα, were also downregulated in the lungs.[24]

Respiratory diseases such as asthma and COPD are often treated with inhaled BAA and corticosteroids to achieve high concentrations locally in the lung with minimize systemic exposure. However, about 80−90% of an inhaled medication are likely to be swallowed.[146] Adverse systemic effects of BAA include increased heart rate, palpitation, vasodilation, and reflex tachycardia.[147] To prevent adverse systemic effects, antedrugs with limited systemic half-lives have been developed.[148] This strategy is also employed to reduce the adverse effects of inhaled corticosteroids,[149] which include adrenal atrophy, osteoporosis, steroid-induced myopathy, osteonecrosis, fluid retention, edema, hypertension, arrhythmias, dermatological, ophthalmologic, gastrointestinal, and neuropsychiatric effects.[150] In contrast, orally administered allosteric $GABA_AR$ modulator MIDD0301 reduces asthma symptoms[24] yet exhibits no observed systemic adverse effects following repeated dosing of 200 mg/kg for 28 days.[151] Comparatively, a 40-fold lower dose of prednisone caused weight loss and reduced the size of the spleen and thymus. Investigating repeat-inhaled nebulized doses of MIDD0301 showed bronchodilation at doses lower than single treatments. Cardiovascular, CNS, and respiratory toxicity studies have confirmed the safety of inhaled MIDD0301 at exposure 50-fold greater than its therapeutic dose.

Here it is shown that (R) and (S) enantiomers of MIDD0301, as well as PI320, rapidly reduce bronchoconstriction when delivered orally or by inhalation. The onset of action and effective doses were comparable to BAAs or corticosteroids in both allergen-induced murine asthma models and A/J mouse models.

4.2 Methods

4.2.1 Materials

Chemicals. MIDD0301 was synthesized using a published procedure.[162] Purity of >99% was determned by HPLC. Identity was determined by ^{1}H NMR, ^{13}C NMR, and high-resolution mass spectrometry. Albuterol,

montelukast, dexamethasone, fluticasone, and diazepam were purchased from MilliporeSigma (St. Louis, MO) and used without further purification.

Drug Formulation. For nebulization, a 3 mg/ml solution of MIDD0301 was prepared in PBS (137 mM NaCl, 2.7 mM KCl, 10 mM Na_2HPO_4, and 1.8 mM KH_2PO_4) or water and pH adjusted to 7.2 with NaOH. For other compound concentrations, this solution was diluted with water. For oral administration, MIDD0301, montelukast, and dexamethasone were suspended in polyethylene glycol (MilliporeSigma, St. Louis, MO) and diluted in a 2% aqueous solution of hydroxypropyl methylcellulose (MilliporeSigma, St. Louis, MO). The final polyethylene glycol concentration was 2.5%. Albuterol was dissolved in water for nebulized administration. Fluticasone and diazepam were dissolved in PBS with 0.17% Tween-80.

Experimental Animals. Male and female BALB/cJ, female A/J, and male C57/BL6J were purchased from Jackson Laboratory (Bar Harbor, ME), and female Swiss Webster mice were purchased from Charles River Laboratory (Wilmington, MA). Female C57/BL6-129S6 hybrid mice were obtained from a breeding colony at the University of Wisconsin-Milwaukee. The mice were offspring from C57BL/ 6J female and Scn1a± (37107-JAX, 129S6 background) male and tested negative for this mutation. Animals were housed in a pathogen-free and 12 h light and dark cycle environment. Animals had ad libitum access to food and water. UW-Milwaukee and Columbia University confirmed that all animal experiments were in compliance with Institutional Animal Care and Use Committees.

Measurement of sRaw Using the Buxco FinePointe Noninvasive Airway Mechanics (NAM) Instrument (DSI, St. Paul, MN). Mice were trained once a day for 5 days to become accustomed to the measuring chambers during nebulization and data acquisition. Instrument calibration was carried out before each experiment. A general protocol outline is under **4.2.2 Experimental Protocol** with individual study protocols described in **4.3 Results and Discussion**. Specific airway resistance (sRaw) was computed with FinePointe software using ventilation parameters recorded for the nasal and thoracic chambers. AHR

measurements are based on phase delay between the nasal and thoracic air flows. Compounds were nebulized as indicated for each experiment. Methacholine was dissolved in PBS and nebulized as indicated for each experiment. Nebulizers were calibrated for each measurement. Usually, nebulization occurred for 1 min followed by a 3 min data acquisition and a 1 min pause before the next methacholine nebulization. Data analysis was carried out with GraphPad Prism (GraphPad, San Diego, CA) using two-way ANOVA and Bonferroni posttest.

Ovalbumin (OVA) Sensitization and Challenge. Male C57BL/6 or male BALB/cJ mice were sensitized with intraperitoneal (IP) injections of 100 µl of a 0.9% NaCl aqueous solution with 0.5 mg/ml OVA (Sigma-Aldrich, St. Louis, MO) and 20 mg/ml alum (Inject Alum; 40 mg/ml, Thermo Scientific, Pierce, Rockford, IL) on days 0, 7, and 14. During days 22−27, mice were anesthetized with isoflurane and challenged daily with 1 mg/kg OVA intranasally. AHR measurements were conducted on day 28.

House Dust Mite (HDM) Sensitization. Eight-week-old male C57BL/6 mice were briefly anesthetized with isoflurane (Baxter, Deerfield, IL) and administered HDM antigen (30 µg dissolved in 25 µl of PBS; Greer Laboratories, Lenoir, NC) or PBS alone (nonsensitized controls) intranasally while spontaneously breathing once a day for 3 weeks.

LPS/INFγ Challenge. Eight-week-old female Swiss Webster or female BALB/c mice were anesthetized with a 100 µl IP injection of xylazine (2 mg/ml) and ketamine (10 mg/ml). Portions of 50 µl of a 0.1% bovine serum albumin solution containing 30 µg/ml mouse INFγ (R&D systems, Minneapolis, MN) and 1 µg of LPS (MilliporeSigma, St. Louis, MO) were administered intratracheally. AHR was determined 24 h after installation.

Rotarod. Groups of 10 female Swiss Webster mice were trained to maintain balance at a constant speed of 15 rpm on the rotarod apparatus (Omnitech Electronics Inc., Nova Scotia, Canada) for 3 min. MIDD0301

in PBS (3.2 mg/ml) was administered as an aerosol using a NAM chamber (DSI, St. Paul, MN). After 10, 30, and 60 min after each nebulization, mice were placed on the rotarod for 3 min. If a mouse fell before the 3 min was completed, it was placed again on the rod. If a mouse fell for the second time, the time of the fall was recorded. Data analysis was carried out with GraphPad Prism (GraphPad, San Diego, CA) using two-way ANOVA and Bonferroni posttest.

Blood Pressure Measurements. Mice were trained for 3 days before the measurement to stay calm in the heating chamber for 10 min with continuous blood pressure measurements. The measurements were performed at the same time each day in absolute silence, with no extraneous odors, and with the least possible handling. Systolic and diastolic blood pressures were measured by tail-cuff plethysmography (IITC Life Science Inc., Woodland Hills, CA). The heat chamber was set at 28−30 °C for optimal tail arterial dilation to allow the measurement of the pulsatile pressure. A tail cuff/sensor was inflated by the system to a maximum pressure of ∼250 mm/Hg, and systolic blood pressure and pulse were determined using the optical sensor. Animals were administered vehicle or MIDD0301 by oral gavage, and measurement occurred 1 h after administration. Ten repeated measurements were performed with each mouse with a group size of four. Data analysis was carried out with GraphPad Prism (GraphPad, San Diego, CA) using two-way ANOVA and Bonferroni posttest.

4.2.2 Experimental Protocol

Experimental protocols often vary depending on the strain of mouse. While A/J mice already exhibit the phenotype found in humans with asthma, other strains like Balb/c and Swiss Webster mice need to be exposed to allergens to develop airway hyperresponsiveness. The development of a formulation and route of administration needs to be determined for instillation, drug administration, and appropriate dose of anesthesia. Furthermore, strain and age of mice influence the methacholine concentrations required to illicit airway hyperresponsiveness. To best control these parameters, a general

outline is followed for all AHR trainings, administrations, intratracheal instillations, and AHR measurements (**Table 4)**.

During experimental planning, mice are ordered and typically take 5-10 days to arrive. Mice are allowed to acclimate to the new facility for one week, and AHR training begins on day 13. Training consists of restraining the mice in the chamber of the Buxco NAM instrument and recording sRaw and breathing frequency over a three-minute timeframe. Mice are usually split into three groups: Vehicle, Positive Control, and our lead compound of interest. The first group is given MIDD0301 once daily via gavage (PO) administration on days 16-20 of the study. Intratracheal instillation of the IFN-γ/LPS inoculum is performed on MIDD0301 mice in the afternoon on day 20. On day 21, approximately 12 h after intratracheal instillation, AHR measurements are performed over a period of 30 min. MIDD0301 mice are introduced to increasing concentrations of nebulized methacholine in PBS. The second group of mice is given a positive control (dexamethasone) once daily via intraperitoneal (IP) administration on days 19-21. On the afternoon of the 21st day, intratracheal administration is performed on the positive control mice. AHR measurements are taken on day 21, approximately 12 h after intratracheal instillation. The third group of mice is given a once daily oral gavage dose of vehicle on days 20-22 of the study. Intratracheal instillation is performed on day 22, and final AHR measurements for vehicle mice are taken on day 23.

Days		MIDD0301 Group		Dexamethasone Group		Vehicle Group	
1	Buy mice						
6th	Arrival						
13th	AHR training						
14th	AHR training						
15th	AHR training						
16th	AHR training	Oral dosing with MIDD					
17th	AHR training	Oral dosing with MIDD					
18th		Oral dosing with MIDD					
19th		Oral dosing with MIDD		IP dosing with Dex.			
20th		Oral dosing with MIDD	Intratracheal Instillation (afternoon)	IP dosing with Dex.		Oral dosing vehicle	
21st		Measure AHR (morning)		IP dosing with Dex.	Intratracheal Instillation (afternoon)	Oral dosing vehicle	
22nd				Measure AHR (morning)		Oral dosing vehicle	Intratracheal Instillation (afternoon)
23rd						Measure AHR (morning)	

Table 4. Schedule of AHR Training, Dosing, Intratracheal Instillation, and Measuring AHR. *Due to time and instrumental constraints, experiments need to be precisely scheduled over several days.*

4.2.3 Buxco Acclimation Training

Mice were placed individually into the Buxco chamber (**Figure 22**) with a collar to prevent movement, and a face plate with a rubber seal to prevent unwanted air flow. The restraint containing the restrained mice are then placed into the chamber of the NAM instrument, and the mice were given one min of acclimation to return to normal breathing levels. Measurements were taken for five min, followed by one min of relaxation before the mice were removed from the NAM instrument and Buxco chamber. Chambers were washed with alcohol wipes and soap water and dried before the next mouse was placed in the Buxco chamber. Data were transferred from FinePointe software (**Figure 23**) to Microsoft Excel, and graphed in GraphPad (GraphPad Software, San Diego, CA). Data from individual mice and groups of mice were graphed, and are shown in **Figure 24**.

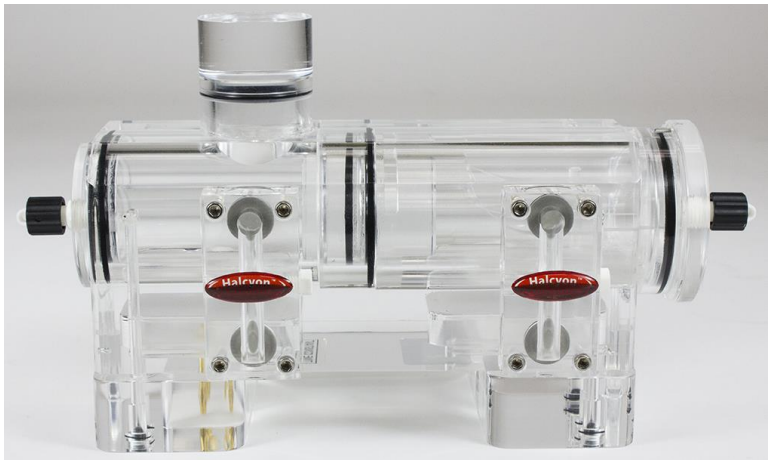

***Figure 22**. **Buxco Chamber.** The chamber is responsible for restraining mice and measuring specific airway resistance through a Noninvasive-Airway Mechanics (NAM) instrument.*

Figure 23. FinePointe Software. *sRaw, thoracic flow, nasal flow, and total volume of mice are recorded and averaged. Outliers are rejected during data recording.*

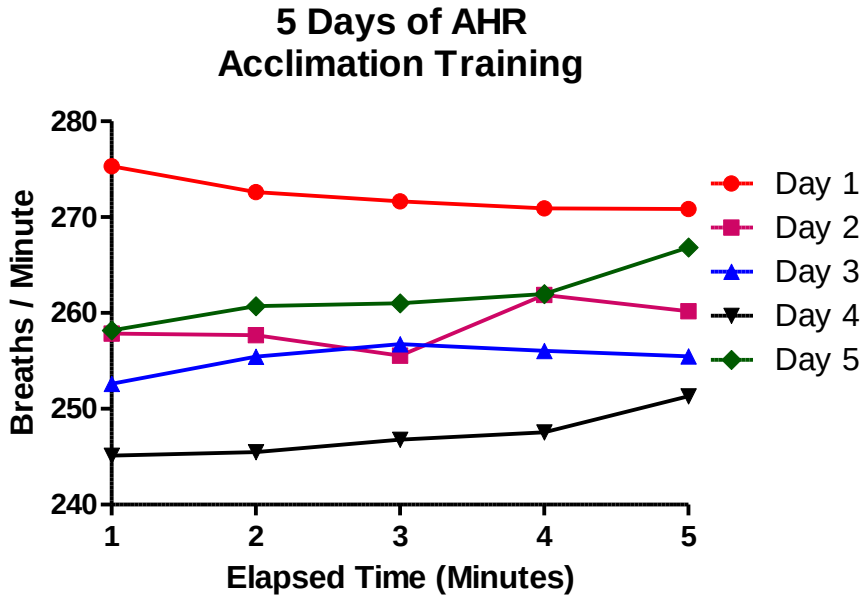

Figure 24. Breathing frequency. *Averages are taken in one-min intervals for all mice during five days of acclimation training. After one day of training, mice began to establish a baseline for breathing frequency.*

4.2.4 Anesthetization

During training, a mixture of 2 mg/ml xylazine and 10 mg/ml ketamine (1:5 ratio) was prepared in sterile PBS. 100 µl of this cocktail was administered to each mouse via IP injection. After roughly five min, the mice were observed for the effects of the anesthetic. The following signs were checked to confirm anesthesia:

- Breathing rate slowing down.

- When picked up by the neck, there is no forelimb stretching

- No response when hind limbs are stimulated.

If a mouse was exhibiting any of the above symptoms, a few min were allowed to pass before again confirming anesthesia. During training, several of the mice were unable to become sedated under the prepared concentrations of anesthesia. The ratio of xylazine : ketamine was then altered to 1:4, and all of the mice were fully anesthetized during the study. Mice were then placed on an angled wooden platform (**Figure 25**) by hanging its incisors on a mounted horizontal wire and were gently restrained with a piece of ribbon mounted to the angled wooden platform. Intratracheal instillation was then performed.

Figure 25. Angled Wooden Platform. *Mice hanging from their incisors on the angled wooden platform. Mice can be place prone or supine depending on preference and inoculation tools available.*

4.2.5 Inoculum Preparation

Inoculum solution should be prepared prior to anesthetization, as mice will be fully anesthetized for only a short period of time. Under sterile conditions, a 0.1% bovine serum albumin solution in phosphate buffer saline containing 30 µg/ml mouse INFγ (R&D systems, Minneapolis, MN) and 1 µg of LPS (MilliporeSigma, St. Louis, MO) was prepared and administered intratracheally.

4.2.6 Intratracheal Instillation of Inoculum

1. Fill a 1 ml syringe fitted with a sterile bent gavage needle with 50 µl of the inoculum solution. The syringe should be loaded with a 100 µl air pocket behind the inoculum. This ensures the formulation is adequately instilled into all parts of the lung and none resides in the trachea.

2. Place the anesthetized mouse onto the angled wooden platform with their incisors hooked on the hanging wire.

3. Turn on the laryngoscope and use the tip to gently pry open the mouth. Pull the tongue out and hold it to the side with a blunt end forceps. Care should be taken when pulling the tongue from the mouth and should be done gently so no tissue damages occur.

4. While the tongue is pulled to the side, guide the laryngoscope blade towards the back of the mouth. Keep the laryngoscope pressed down very gently at a 90° angle until you see and/or feel the opening of the trachea. Hold the laryngoscope in place so the tongue does not block the trachea.

5. With your other hand, take the 1 ml syringe containing the inoculum, fitted with bent intratracheal gavage needle and insert the needle into the trachea until the bend in the needle reaches the front incisors. This ensures the tip of the needle has passed the trachea and is in the lungs. Carefully push the plunger evenly as to avoid bubbling while delivering the inoculum. Gently remove the needle out of the trachea as soon as possible. (Mice will suffocate and die if the trachea is blocked for too long.) Hold the mouse upright for a few sec to allow inoculum to be inhaled into the lungs.

6. Remove the mouse from the platform and place it near a heating lamp. Do not leave mice under direct heat for extended periods of time. Anesthesia should wear off 30 - 45 min after the procedure (recovery time varies based on strains). Close observation of the mice should occur during this time to prevent mice from getting too hot or too cold, as it could lead to respiratory distress.

4.2.7 AHR Measurements

On days 21-23, AHR measurements were taken as shown in **Table 4**. Each group of mice followed the same AHR measurement protocol. Mice were placed in the restraint and into the chamber, and the chamber placed into the NAM instrument. Mice were administered 20 µl of nebulized PBS over one min. After nebulization, AHR was measured for three min, followed by one min of rest. This five-min sequence of measurements was repeated for each mouse four more times, with log scale concentrations of 1.56 mg/ml, 3.125 mg/ml, 6.25 mg/ml, and 12.5 mg/ml of nebulized methacholine in PBS. For this protocol, the total time spent for each mouse in the Buxco chamber on the NAM instrument was 25 min. The number of five-min sequences and concentrations of methacholine varying depending on the study. Data were transferred from DSI FinePointe software to Microsoft Excel and GraphPad for data analysis via a Two-Way ANOVA Bonferroni post-test comparing group means.

4.3 Results and Discussion

4.3.1 MIDD0301

The studies herein offer further characterization of (R) and (S) MIDD0301, as well as PI320 as an inhaled medication for rapid relief or oral medication of long-term relief of bronchospasm. The described pharmacological effects of nebulized MIDD0301 in murine lung inflammation induced by diverse allergens, bacterial, and viral mediators (and steroid resistant inflammation) support future clinical evaluation of MIDD0301 as a first-line drug for use across asthma inflammatory endotypes.

Despite the availability of several drugs for asthma symptom control, the disease progresses in many patients, prompting increased dosing, the use of drug combinations, or the use of stronger medications with greater risks of adverse effects. By safely targeting $GABA_A$Rs in the lung, MIDD0301 offers a novel mechanism of action and provides an important therapeutic alternative to existing drugs that are limited by safety liabilities, restricted efficacy, and drug tolerance.

We quantified the efficacy of MIDD0301 by its ability to reduce methacholine-induced airway hyperresponsiveness in mice using a whole-body plethysmograph. Following the protocol previously explained (**Table 4**) with the exception of instillation and the vehicle or drug (MIDD0301 or albuterol) being nebulized and the specific airway resistance (sRaw) recorded for 3 min. After acclimatization, methacholine (40 mg/ml, 20 µl) was nebulized for 1 min followed by 3 min of data acquisition and 1 min or recovery. This assembly was repeated five times, and average sRaw values for albuterol and MIDD0301 were recorded (**Figure 26A**).

sRaw increased with successive constant methacholine challenges in female C57BL/6J-129S6 hybrid mice from 1.5 to 2.5 cmH2O*sec. Experiments with female C57BL/ 6J mice resulted in constant sRaw values at methacholine concentrations up to 60 mg/ml (data not shown). Nebulized MIDD0301 (3 mg/kg) significantly reduced sRaw of C57BL/6J-129S6 mice during the fourth and fifth methacholine challenges and was more effective than 7.2 mg/kg albuterol at these challenges. Albuterol (7.2 mg/kg) and MIDD0301 (1 mg/kg) were similarly effective in reducing sRaw during the fifth methacholine challenge, reflecting greater potency of MIDD0301 in reducing methacholine-induced airway constriction compared to nebulized albuterol in normal, spontaneously breathing mice without lung inflammation.

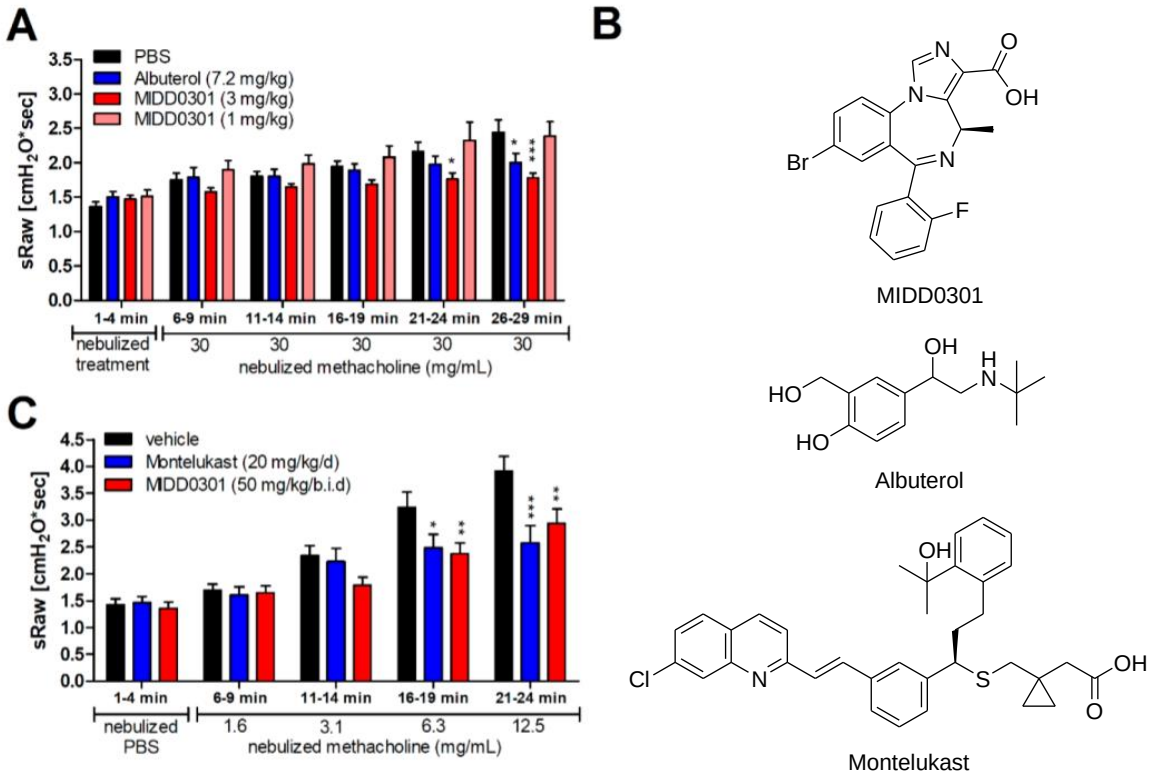

Figure 26. Pharmacological activity of MIDD0301 in allergen-induced asthmatic mice. *(A) Female C57BL/6J-129S6 hybrid mice were challenged intranasally with 1 mg/kg ovalbumin for five consecutive days (n = 11). Specific airway resistance (sRaw) was measured using a NAM instrument after a single nebulized dose of vehicle or vehicle plus drug, followed by nebulized methacholine challenge. (B) Structures of MIDD0301, albuterol, and montelukast. (C) Male BALB/c mice were sensitized (days 0, 7, and 14) and challenged intranasally (days 22–27) with OVA (n = 14). Drugs were administered orally for 5 days during the intranasal OVA challenge. Specific airway resistance (sRaw) was measured using a NAM instrument after nebulized methacholine challenges. Data are shown as means ± SEM. *, **, and *** indicate p < 0.05, p < 0.01, and p < 0.001 significance between vehicle- and drug-treated animals for each individual methacholine challenge determined by two-way ANOVA.*

Next, we investigated the pharmacological activity of MIDD0301 using mouse asthma models where lung inflammation was induced by ovalbumin (OVA) oral sensitization and challenge. Data collected using OVA-sensitized C57BL/6J-129S6 hybrid mice comparing MIDD0301 and albuterol are presented as sRaw in **Figure 26A**. **Figure 26B** shows the structures of drugs administered. Evaluation of oral asthma drug montelukast and MIDD0301 using the OVA model in BALB/cJ mice is depicted in **Figure 26C** and **Figure 26C Protocol**.

OVA-sensitized C57BL/6J-129S6 hybrid mice pretreated with nebulized vehicle exhibited sRaw values increasing from 1.4 to 2.4 cmH_2O*sec during a course of five sequential challenges of 30 mg/ml methacholine (**Figure 26A**). Prophylactic dosing of 3 mg/kg MIDD0301 significantly reduced sRaw at both

the fourth and fifth methacholine challenge points and gave responses greater than 7.2 mg/ml nebulized albuterol. The lower dose of 1.0 mg/kg MIDD0301 was not effective in reducing sRaw at any of the albuterol challenges.

In comparison to OVA sensitization, HDM allergen sensitization caused greater influx of eosinophils and neutrophils in the BALF, higher levels of IL-4 and IL-10, and increased subepithelial collagen in C57BL/6 mice.[152] Our collaborators (Emala Group, Columbia University) challenged C57BL/6J mice daily with intranasally administered HDM for 3 weeks, which resulted in a significant increase of lung resistance as measure by the forced oscillation method. The absolute airway resistance of HDM-challenged and MIDD0301-treated mice was comparable to the naïve C57BL/6J mice for the last two methacholine doses,[152] mirroring results found in both the OVA-sensitized C57BL/6J-129S6 hybrid mouse model and the OVA model in Balb/cJ mice.

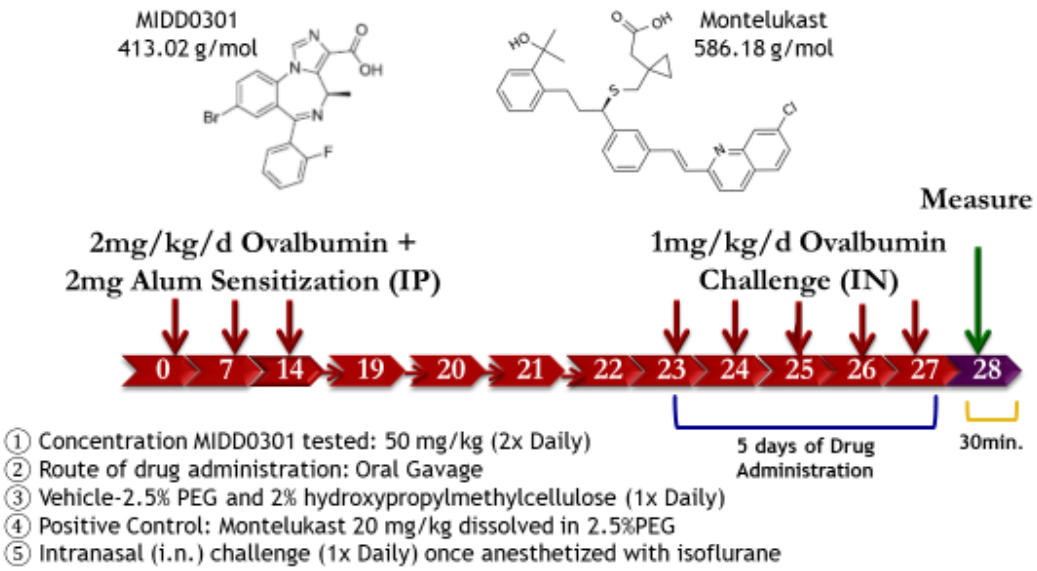

Figure 26C Protocol. *Ovalbumin and alum sensitization via IP administration occurred on days 0, 7, and 14. Intranasal ovalbumin challenge and MIDD0301 administration occurred on days 23 to 27, with AHR recordings occurring on day 28. Animals are often sacrificed at the completion of day 28 to harvest tissue samples for pharmacokinetic analysis.*

It has been reported that OVA sensitization results in more robust AHR in BALB/c compared to C57BL/6 mice; conversely, peribronchial eosinophilia was more pronounced in the C57BL/6 compared to BALB/c mice.[153] We used the BALB/c model to compare AHR following oral treatment with either leukotriene receptor antagonist montelukast or MIDD0301. Here, we observed a change of sRaw from 1.5 to 3.8 cmH2O*sec during graded methacholine challenges in vehicle-treated mice. Treatment with montelukast (20 mg/kg/day) for five consecutive days significantly reduced AHR at the 6.25 and 12.5 mg/ml methacholine challenges (**Figure 26C**). MIDD0301 treatment (50 mg/kg/b.i.d.) over the same 5-day period caused a similar significant reduction of sRaw. We previously reported the characterization of alleviated lung inflammation (inflammatory cell numbers and cytokine levels) in this model after repeated oral dosing of MIDD0301.[24]

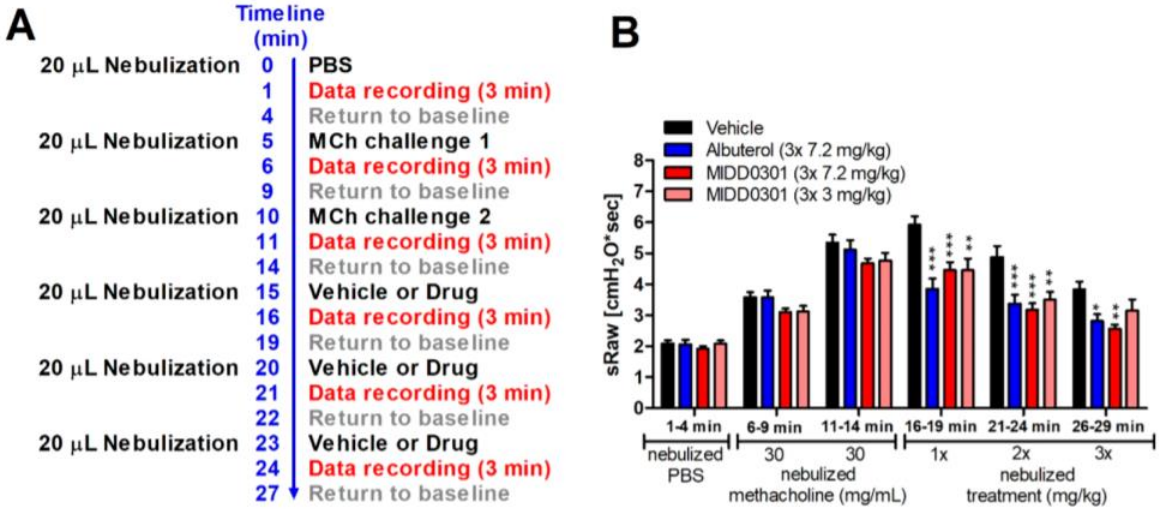

Figure 27. Acute relief of methacholine-induced bronchospasm with MIDD0301 or albuterol treatment. *(A) Protocol to determine AHR using the NAM instrument. (B) sRaw was measured using female A/J mice first challenged with methacholine followed by treatment with nebulized vehicle or indicated drug. Data are depicted as means ± SEM of n = 10. *, **, and *** indicate p < 0.05, p < 0.01, and p < 0.001 significance between vehicle- and drug-treated animals using two-way ANOVA.*

The relief of acute bronchospasm by inhaled drug treatment (in contrast to the previous prophylactic study design) was investigated with A/J mice, which display pronounced AHR to methacholine challenge in the absence of lung inflammation induced by allergen.[154] In the treatment

study design outlined in **Figure 27**, animals were challenged first with nebulized methacholine followed by nebulized treatment with MIDD0301 or albuterol.

After two nebulized methacholine (30 mg/ml, 20 µl) challenges, sRaw reached 5.4 cmH_2O*sec. Subsequent nebulized vehicle treatments resulted in sRaw values ranging from 5.8 to 3.9 cmH_2O*sec, which were all significantly elevated from the sRaw at the initial vehicle administration. Thus, elevated AHR persisted for at least 15 min after the methacholine challenge. Mailhot-Larouche et al. reported bronchoconstriction for at least 10 min after methacholine challenge in BALB/c mice.[155] The first application of albuterol (7.2 mg/kg) reduced AHR, confirming its activity as a fast-acting bronchodilator. Further AHR reductions were observed during the subsequent second and third doses. MIDD0301 (7.2 mg/kg) also reduced AHR during all three doses similar to albuterol. Although these compounds mediate their pharmacological effect through different receptors, G-protein-coupled receptor BAA versus ion-channel $GABA_AR$, their onset of action is similar. Relaxation of ASM *ex vivo* by MIDD0301 was observed at least 15 min following administration.[24] In a similar assay, the reported onset of action of long-acting BAA salmeterol was 19.5 min, whereas albuterol reduced bronchoconstriction as quickly as 1.8 min.[156] Herein, we demonstrated *in vivo* that MIDD0301 and albuterol relaxed constricted airway smooth muscle within 3 min. 3 mg/kg MIDD0301 was sufficient to reduce AHR during the first and second doses after the methacholine challenge. Taken together, these data support the use of MIDD0301 as a fast-acting bronchospasm reliever that quickly reverses bronchoconstriction induced by methacholine and retains effectiveness upon repeated nebulized administrations.

Steroid resistant asthma is often associated with elevated levels of IFNγ and is consistent with a neutrophilic and eosinophilic disease endotype.[157] The underlying pathogenic mechanism could be microbial lung infection leading to asthma, which is controlled poorly with steroids due to impaired nuclear translocation of the liganded glucocorticoid receptor in pulmonary macrophages.[158] Intratracheal

installation of INFγ and bacterial lipopolysaccharide (LPS) was used to model microbial infection and induced severe, acute lung inflammation, which was less responsive to oral steroid treatment.[159] We thus evaluated the pharmacological effect of nebulized and oral MIDD0301 in the INFγ/LPS lung inflammation model in comparison to albuterol and two steroids, inhaled fluticasone and oral dexamethasone. The results are summarized in **Figure 28**.

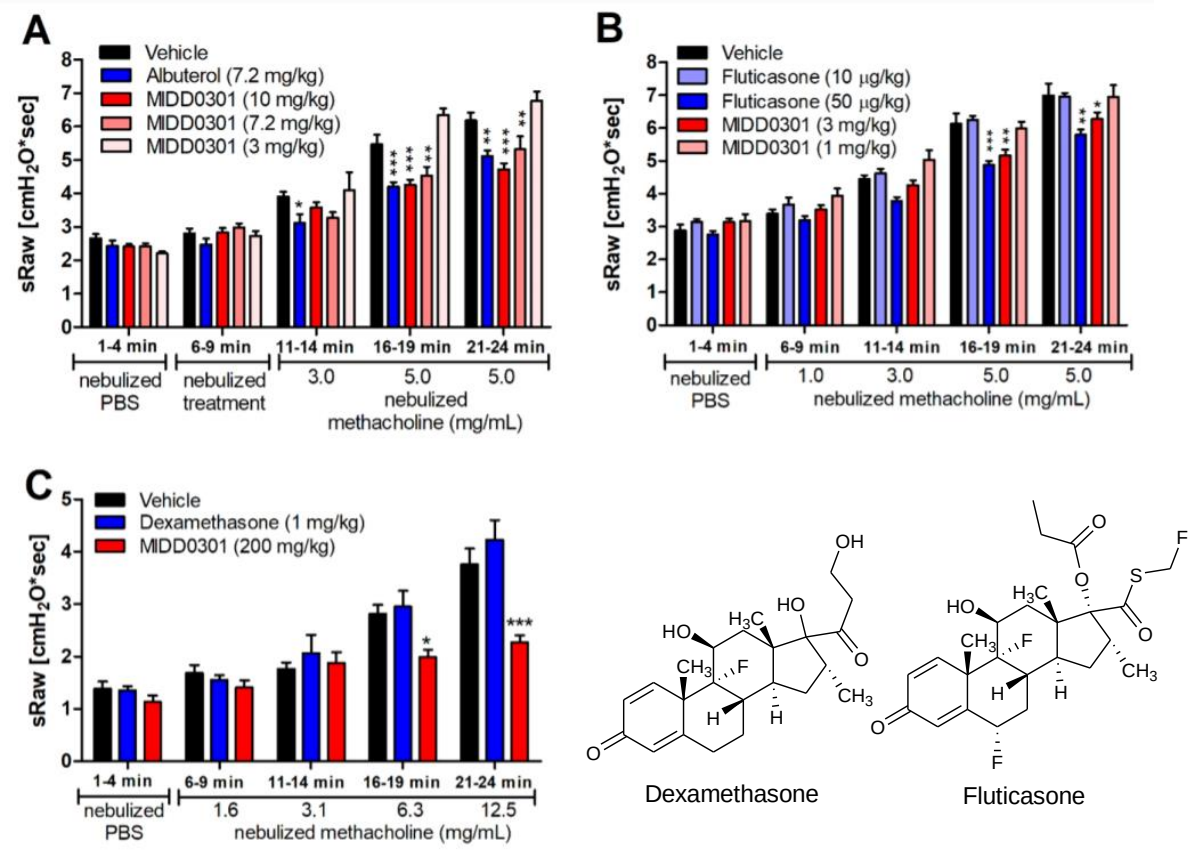

Figure 28. Pharmacological effect of MIDD0301 in a steroid resistant asthma model. *(A) Female Swiss Webster mice were challenged intratracheally with LPS and INFγ 1 day before the measurement. sRaw was measured repeatedly after nebulization of vehicle, followed by drug in vehicle and nebulized methacholine using the NAM instrument. (B) Nebulized fluticasone and MIDD0301 were administered to female Swiss Webster mice daily for 3 days followed by intratracheal instillation of LPS and INFγ on the second to last day. One h after the last administration of vehicle or drug, mice were exposed to nebulized PBS and graded doses of methacholine each followed by sRaw measurements. (C) Dexamethasone was administered orally for three consecutive days and MIDD0301 for five consecutive days to female BALB/c mice followed by intratracheal administration of LPS and INFγ on the second to last day. One h after the last administration of vehicle or drug in vehicle on the last day, mice were exposed to nebulized PBS followed by doses of methacholine. Data are depicted as means ± SEM of n = 10. *, **, and *** indicate p < 0.05, p < 0.01, and p < 0.001 significance between vehicle- and drug-treated groups determined by two-way ANOVA.*

Twenty-four h after intratracheal installation of LPS and INFγ, Swiss Webster mice were treated with graded doses of methacholine, resulting in a sRaw of 6.0 cmH_2O*sec after the third administration.

Our adaptation of the model reported by Li et al.[159] employs female Swiss Webster instead of BALB/c mice, which enabled us to use lower doses of nebulized methacholine and spontaneously breathing animals instead of the forced oscillation technique. Nebulization of 7.2 mg/kg albuterol significantly reduced AHR at all methacholine challenges (**Figure 28A**). Three different doses of nebulized MIDD0301 were administered. At the higher 10 and 7.2 mg/kg MIDD0301 doses, reduction of sRaw occurred at the second and third methacholine challenges. The 3 mg/kg MIDD0301 dose was ineffective at all three methacholine challenges. Thus, for severe LPS- and INFγ-induced lung inflammation, nebulized MIDD0301 and albuterol demonstrated similar reduction of AHR.

Next, MIDD0301 was compared to the corticosteroid fluticasone using repeated nebulized administration for 3 days (**Figure 28B**). The recommended human daily dose of fluticasone ranges between 176 and 440 μg for adults (70 kg), corresponding to 2.5−6.2 μg/kg. Fluticasone at 10 μg/kg did not reduce sRaw in the INFγ/LPS model. To observe a fluticasone effect in this model, we raised the dose to 50 μg/kg, which was able to significantly reduce AHR after repeated nebulized administrations at the third and fourth methacholine challenges. It was reported that similar high doses were needed to reduce AHR in mice infected with *Mycoplasma pneumoniae*.[160] By comparison, MIDD0301 reduced AHR after repeated doses of 3 mg/kg at the fourth and fifth methacholine challenges. A single nebulization of MIDD0301 just before the methacholine challenge did not reduce AHR (**Figure 28A**), which reflects an inadequate time to develop pronounced anti-inflammatory effects from repeated daily dosing with MIDD0301. A nebulized repeated dose of 1 mg/kg MIDD0301, on the other hand, was not adequate to improve the LPS/INFγ-induced lung inflammation.

Li et al. stated that orally administered dexamethasone did not reduce AHR in the LPS/INFγ lung inflammation model,[159] which prompted the investigation of the efficacy of orally administered MIDD0301. Female BALB/c mice were used for this study, which exhibit a different range of sRaw values

in response to methacholine than female Swiss Webster mice. Starting with 1.6 mg/ml methacholine and increasing the challenge to 12.5 mg/ml resulted in a sRaw change from 1.4 to 3.8 cmH_2O*sec (**Figure 28C**). Consistent with the work of others, oral dexamethasone at 1 mg/kg/d for 3 days did not reduce methacholine-induced AHR. Higher glucocorticoid doses were avoided because of observed toxicity of orally administered prednisone in our previous study.[151] In contrast, 200 mg/kg/d MIDD0301 resulted in lower sRaw values at the third and fourth methacholine challenges. Thus, orally administered MIDD0301 significantly reduced AHR resulting from severe lung inflammation induced by LPS and INFγ.

To correlate the nebulized exposure of MIDD0301 using a NAM chamber to the amount of MIDD0301 that reaches the lungs, a pharmacokinetic study was conducted to quantify tissue concentrations over 2 h. Female Swiss Webster mice were administered 20 µl of nebulized 7.5 mM MIDD0301 (pH 7.5) while in the NAM instrument. Groups of four were sacrificed at 5, 10, 20, 30, 40, 60, and 120 min after compound administration. Due to time constraints as well as only having two available nebulizers on the NAM instrument, it was crucial to develop a protocol outlining exact time of nebulization and respective sacrifice time (**Figure 29**). Specific timeframes needed to be considered for loading the mice into the NAM restraint, loading the restraint into the NAM chamber, nebulization time, removing mouse from chamber and restraint, transport across the animal facility to the sacrifice room, CO_2 asphyxiation and cervical dislocation, and harvesting of tissue samples. Cardiac puncture for blood draw needs to immediately follow cervical dislocation and correspond to the exact time allocated for each respective group. Drawn blood was immediately mixed with heparin, stored in cryo vials, and placed on dry ice.

Figure 29. Protocol for Drug Administration, Sacrificing, and Harvesting Samples for PK Analysis. *To minimize time, mice needed to be administered drug formulation (Red), sacrificed (light blue), and samples harvested according to established times. Shown is the protocol for the t = 5 min nebulization. Once a mouse was being perfused of blood, the next mouse was loaded into the NAM instrument for drug nebulization.*

Due to blood often covering lung and brain samples during extraction, it was important to perfuse blood before organ harvesting as trace amounts of compound and analytes in blood may show up in analysis of other samples. An established protocol by Gage et. al was followed.[176] Tissue and organ harvesting would proceed with removal of sternum, anterior chest cavity, and thymus to expose the heart and ascending aorta. Under a surgical microscope, an incision (>5 mm) was made at the apex of the left ventricle and a 30G perfusion probe was inserted and guided into the left ventricle with a suture (**Figure 30**). The probe was gently guided into the ascending aorta until it was visible. The suture was then clamped to prevent backflow. A gravity-assisted pump containing 0.9% NaCl in PBS solution was then opened to a flow rate of 1 ml/min and careful observation was made to ensure the PBS solution was filling and

expanding the ascending aorta. The right atrium was then cut open to drain perfused blood. After roughly 15 min, no visible blood was exiting the right atrium and kidney color was changed from deep red to a tan color, indicating adequate perfusion of blood. Harvesting of organ samples followed and were placed in cryo vials on dry ice. At the completion of organ harvesting, blood and tissue samples were stored in liquid nitrogen for pharmacokinetic analysis via HPLC/MS.

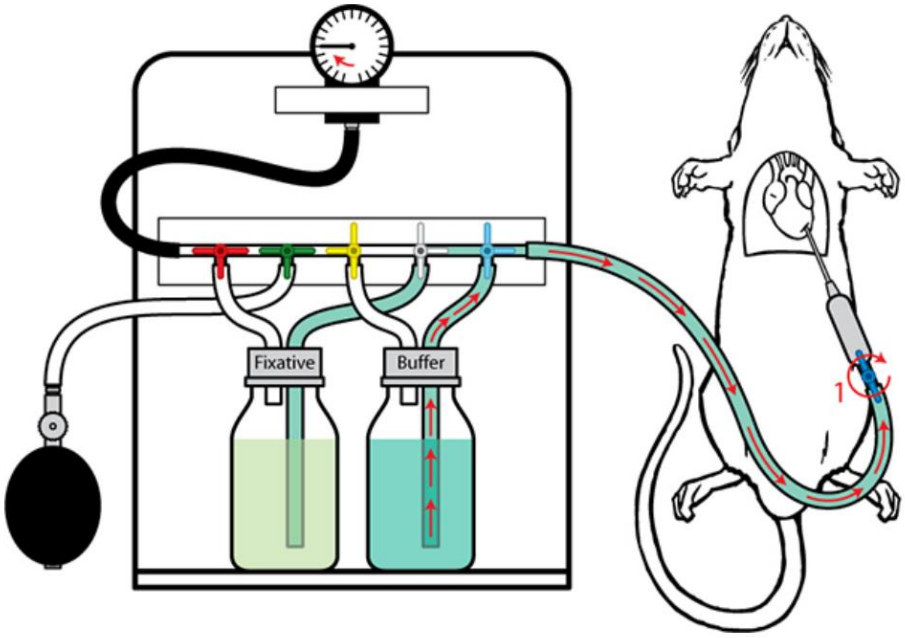

Figure 30. Whole Animal Perfusion Fixation for Rodents. *After sacrificing and cardiac puncture, mice were perfused of blood to reduce cross-contamination of other tissue samples. Perfusion was complete when blood was no longer visible in the right atrium exit incision and kidney color changed from deep red to a pale brown color.*

At t = 0 min, 0.06% of the nebulized MIDD0301 was found in lung. The half-life of MIDD0301 in lung was 5.2 min. MIDD0301 has a binding affinity of 72 nM for the GABAAR; thus, therapeutic concentrations for receptor activation were maintained at this level for at least 25 min. In addition, MIDD0301 blood concentration and to a lesser degree its lung concentration increased at 60 min, suggestive of intestinal absorption of ingested drug. As pointed out in **4.1 Introduction**, about 80−90% of inhaled medication is likely to be swallowed.[146] In contrast to the lung, the concentration of MIDD0301 in blood increased marginally, indicating intestinal uptake and metabolism before entering the blood

circulation. Similar ratios between lung and blood concentrations were observed for nebulized MIDD0301 administration using a flexiVent respiratory system, with a reported brain concentration of less than 3% of the lung concentration.[141]

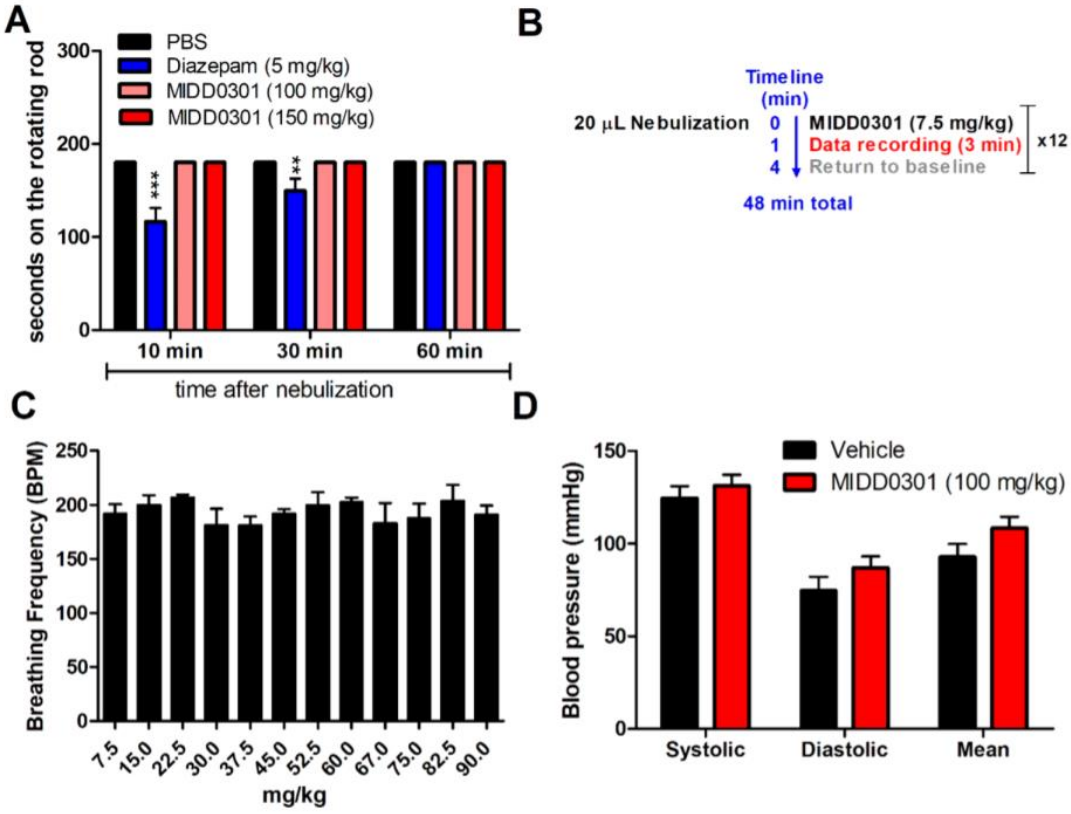

Figure 31. Safety evaluation of nebulized MIDD0301 in mice. *(A) Sensorimotor coordination: Compounds were formulated as described in the Materials and Methods section and nebulized at indicated doses using the NAM instrument. After removal from the nebulization chamber, female Swiss Webster mice were tested on a rotarod at 15 rpm for 3 min at 10, 30, and 60 min. The time of fall was recorded if occurring prior to 3 min. Data are expressed as means ± SEM (n = 10). (B) Protocol to determine the respiratory safety of repeated nebulized MIDD0301 dosing using the NAM instrument. (C) Four C57BL/6 mice were subjected to the protocol described in part B and breathing frequencies measured over 3 min after each MIDD0301 nebulization. Data are depicted as means ± SD. (D) Systolic and diastolic blood pressures were measured with a noninvasive tail cuff plethysmograph 1 h after oral MIDD0301 administration. Ten measurements were performed for each female Swiss Webster mouse in groups of four. ** ($p < 0.01$) and *** ($p < 0.001$) values were determined by two-way ANOVA.*

To confirm minimal brain distribution of MIDD0301 with the absence of CNS effects, mice that received nebulized MIDD0301 were studied for possible sensorimotor impairment using the RotaRod instrument (**Figure 31A**). Female Swiss Webster mice were trained to balance on a rotating rod for 3 min and tested 10, 30, and 60 min after nebulization of MIDD0301 or positive control compound diazepam, a

$GABA_AR$ ligand that is known to achieve high brain concentrations. The lack of central activity, specifically in the medulla, was demonstrated with measurements of breathing frequencies after repeated nebulization with MIDD0301 (**Figure 31C**). Cardiovascular safety was investigated usibg blood pressure measurements after oral administration of MIDD0301 (**Figure 31D**).

MIDD0301, at nebulized doses of 100 and 150 mg/kg, did not cause sensorimotor impairment (**Figure 31A**). In contrast, nebulized diazepam at 5 mg/kg exhibited significant CNS effects. These results are in agreement with studies performed for orally administrated MIDD0301 and diazepam.[24] Interestingly, a recent clinical study with inhaled diazepam confirmed bronchodilation for patients with asthma.[161] The authors proposed that diazepam acted on the peripheral nervous system regulating the airway smooth muscle tone rather than directly relaxing contracted airway smooth muscle, which has been demonstrated for MIDD0301 using *ex vivo* human lung tissue.[141] To show that bronchodilation by MIDD0301 is limited to constricted airways (e.g., in the presence of methacholine or caused by lung inflammation), naïve mice were treated with nebulized MIDD0301 followed by airway measurements using a whole-body plethysmograph (**Figure 31C**). Breathing frequencies did not change over a period of 48 min, with a combined dose of 90 mg/kg. Cardiovascular safety of MIDD0301 was shown *in vivo* at a dose of 100 mg/kg using a noninvasive tail-cuff plethysmograph (**Figure 31D**). Blood pressure values obtained for MIDD0301 were not statistically different from vehicle controls. These results are consistent with earlier published findings on the inability of MIDD0301 to interact with the Kv11.1 potassium ion channel (hERG).[151]

4.3.2 PI320

Next, we determined the *in vivo* activity of PI320 in relaxing airway smooth muscle. Mouse inflammatory AHR was induced with INFγ and LPS via intratracheal installation (**Figure 32**). Elevated levels of IFNγ in the lung were observed in neutrophilic asthma patients who responded poorly to steroid treatment.[165] One contributing factor was the impaired nuclear translocation of the liganded

glucocorticoid receptor in pulmonary macrophages.[166] LPS models a microbial infection leading to a macrophage-mediated inflammatory response.[167]

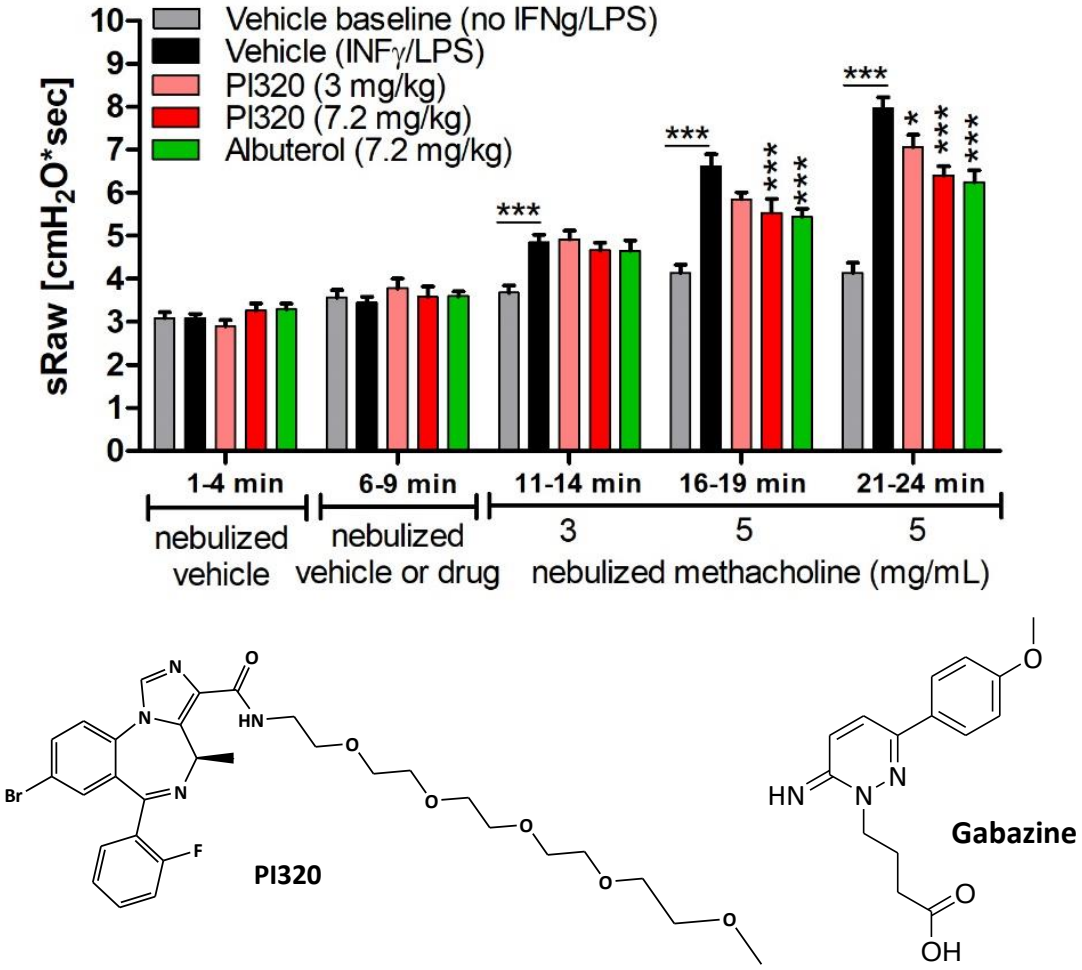

Figure 32. Pharmacological effect of PI320 in a steroid resistant asthma model. *Female Swiss Webster mice received an intratracheal solution of LPS and INFγ one day before the measurement. sRaw was measured repeatedly after nebulization of vehicle, followed by drug in vehicle and nebulized methacholine using a NAM instrument. Data are depicted as means ± SEM of n = 10. * and *** indicate p < 0.05 and p < 0.001 significance between vehicle and drug treated groups determined by 2-way ANOVA with Bonferroni correlation.*

The intratracheal installation of INFγ/LPS markedly increased the sRaw value (**Figure 32, black bar**). After the first nebulized methacholine challenge (3 mg/ml, 20 µl), the sRaw increased from 3.7 to 4.8 cmH_2O*sec. Further methacholine challenges increased the sRaw to 8.0 cmH_2O*sec. Animals that received nebulized albuterol (7.2 mg/kg) prior to the methacholine challenge, showed reductions of AHR for the second and third methacholine administrations. Similar results were observed for PI320 at the

same dose. PI320 also reduced AHR for the third methacholine challenge at 3 mg/kg and therefore performed better than MIDD0301, which showed no efficacy in this model at 3 mg/kg.[164] The precise measurement of lung function parameters such as airway resistance and elastance alternatively can be conducted using an invasive forced oscillation technique.[165] Collaborators using a flexiVent apparatus showed 1.5 mg/kg of MIDD0301 was sufficient to reduce airway resistance.[164] Future studies will be performed to quantify the dose-dependent changes of airway resistance for PI320.

Further investigations with PI320 were conducted with A/J mice that display severe AHR to methacholine without a pre-existing allergic state due their unique genetic profile.[168]

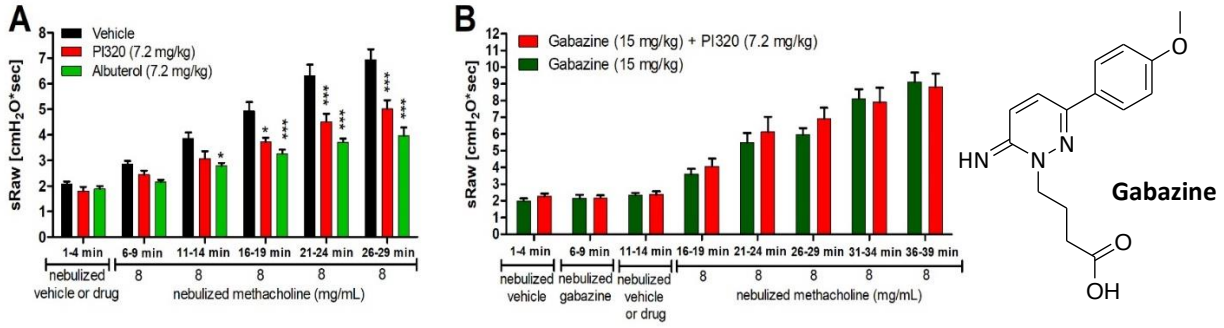

Figure 33. Airway smooth muscle relaxation in female A/J mice. *A) sRaw was measured after nebulized vehicle or PI320 treatment (7.2 mg/kg) followed by repeated treatment with nebulized methacholine. B) sRaw was measured after nebulized $GABA_A$ receptor antagonist gabazine (15 mg/kg) or gabazine followed by PI320 (7.2 mg/kg) and repeated nebulized methacholine applications. Data are depicted as means ± SEM of n = 10. * and *** indicate $p < 0.05$ and $p < 0.001$ significance between vehicle and drug treated animals using a 2-way ANOVA with Bonferroni correlation.*

The repeated nebulized administration of methacholine induced severe AHR resulting in sRaw values of more than 7.0 cmH_2O*sec after five applications (**Figure 33A**). The nebulized administration of albuterol (7.2 mg/kg) prior to the methacholine challenge reduced AHR for the second and subsequent methacholine applications. Similar effects were observed for nebulized 7.2 mg/kg PI320 for the third and subsequent methacholine applications. The reduction of AHR by PI320 was not statically different from albuterol and could be reversed by $GABA_A$ receptor antagonist gabazine (**Figure 33B**). The nebulized application of gabazine (15 mg/kg) increased the sRaw from 7.0 cmH_2O*sec to 9.1 cmH_2O*sec for the last methacholine application, which is consistent with the previously reported increase of contractile force

of acetylcholine-contracted guinea pig tracheal rings.[169] Other studies with gabazine included the reversal of PI320 analog SH-053-2'F-R-CH_3 induced negative membrane potential and bradykinin-induced $[Ca^{2+}]_i$ of ASM.[42]

4.3.3 R and S MIDD0301

Next, we investigated the ability of MIDD0301 and MIDD0301S to reduce AHR using two different murine models (**Figure 34**).

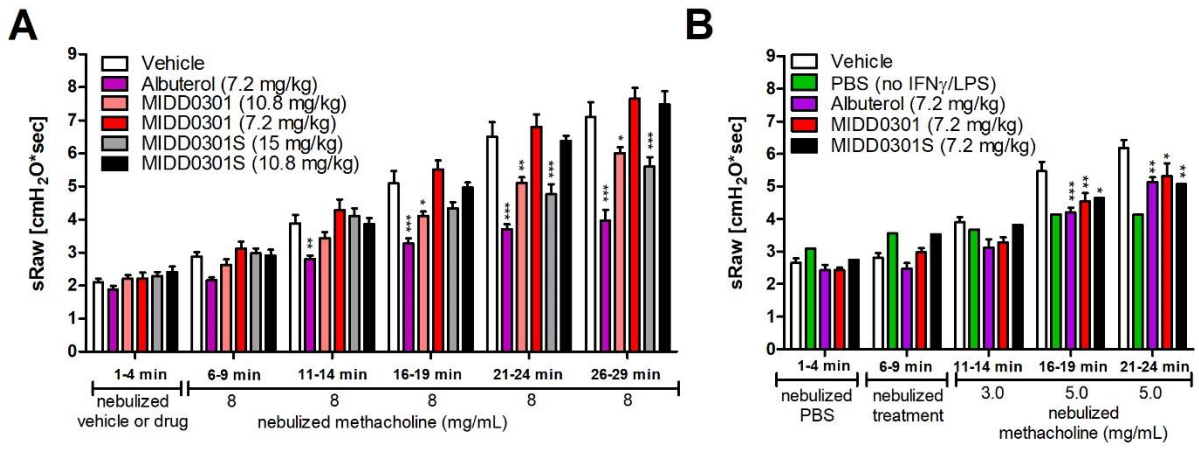

Figure 34. Pharmacological effect of nebulized MIDD0301 and MIDD0301S. *A) Female A/J mice received nebulized treatment followed by nebulized methacholine challenges. Specific airway resistance (sRaw) values were recorded for 3 min and depicted as means ± SEM (n = 10). B) Female Swiss Webster mice were challenged intratracheally with LPS and INFγ one day before the measurement. sRaw was measured repeatedly for 3 min after nebulized vehicle or nebulized treatment followed by nebulized methacholine. Data are depicted as means ± SEM (n = 10). *, ** and *** indicate p < 0.05, p < 0.01, and p < 0.001 significance, respectively, between vehicle and drug treated groups as determined by 2-way ANOVA repeated measures with Bonferroni correlation.*

A/J mice display pronounced AHR in response to inhaled methacholine in the absence of allergen induced lung inflammation.[171] Following nebulized drug treatment, methacholine (8 mg/ml, 20 µl) was nebulized five times, resulting in an average specific airway resistance (sRaw) of 7.1 cmH_2O*sec after the fifth methacholine dose (**Figure 34A**). Nebulized albuterol significantly alleviated AHR at the second through fifth methacholine administrations. Significant reductions of AHR were observed with 10.8 mg/kg MIDD0301 pre-treatment at the last three methacholine challenges. However, MIDD0301 was not effective at 7.2 mg/kg. MIDD0301S appeared to reduce AHR at 10.8 mg/kg but significant AHR reduction

was achieved only at the final two methacholine challenges using 15 mg/kg nebulized pre-treatment. In this model, MIDD0301 is slightly more effective than MIDD0301S at 10.8 mg/kg at the fourth and fifth methacholine challenges.

In a second mouse AHR model, animals received an intratracheal installation of IFNγ and LPS one day before treatment with a single dose of 7.2 mg/kg albuterol, MIDD0301, or MIDD0301S, followed by AHR measurement **(Figure 34B**). Animals given a sham intratracheal installation with PBS (i.e., no IFNγ/LPS) exhibited baseline AHR (sRaw = 3 - 4 cmH_2O*sec) at the sequential methacholine challenges. All three test compounds significantly reduced AHR compared to vehicle treatment at the last two methacholine challenges. There was no significant difference between the efficacy of MIDD0301 and MIDD0301S at any methacholine challenge in this study.

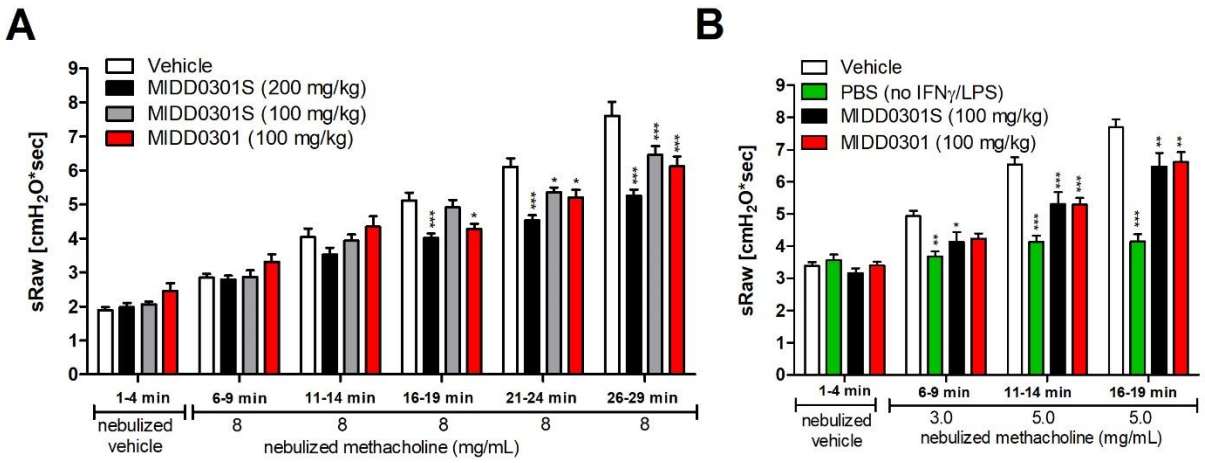

Figure 35. Pharmacological effect of orally administered MIDD0301 and MIDD0301S. *A) Female A/J mice received orally administered compounds for three days followed by nebulized methacholine challenges. Specific airway resistance (sRaw) values were recorded for 3 min and depicted as means ± SEM (n = 10). B) Female Swiss Webster mice received compounds via oral gavage for three days followed by intratracheal instillation of LPS and INFγ on the second to last day. Forty min after the last oral administration of vehicle or drug, mice were given nebulized vehicle (PBS) followed by graded doses of methacholine. Data are depicted as means ± SEM (n = 10). *, **, and *** indicate $p < 0.05$, $p < 0.01$, and $p < 0.001$ significance, respectively, between vehicle and drug treated groups determined by 2-way ANOVA repeated measures with Bonferroni correlation.*

Next, the pharmacological effect of orally administered MIDD0301 and MIDD0301S was compared. No observable adverse effects were found in A/J mice during the three-day treatment with either compound or dose. MIDD0301S at 200 mg/kg/day resulted in significantly reduced sRaw values at

the third, fourth, and fifth methacholine challenges (**Figure 35A**). At 100 mg/kg/day, MIDD0301S and MIDD0301 reduced AHR at the fourth and fifth methacholine challenges. MIDD0301 was further able to reduce sRaw at 100 mg/kg/day at the third methacholine challenge. Together, the reductions of AHR with 100 mg/kg/day MIDD0301S were not statistically different from MIDD0301 for all nebulized methacholine challenges. Similar results were observed using the steroid resistant IFNγ and LPS mouse asthma model (**Figure 35B**). A 100 mg/kg/day oral dose of MIDD0301S for three days prior to the AHR measurement resulted in significantly reduced sRaw at all methacholine challenges. MIDD0301 reduced AHR at the second and third methacholine challenges. The sRaw effects from MIDD0301S and MIDD0301 treatment were not statically different from each other.

The brain concentration (non-perfused) of MIDD0301 following oral dosing is approximately 5% of the blood concentration.[24] Correspondingly, no adverse CNS effects were observed following 100 mg/kg b.i.d. repeated daily dosing or a single 1,000 mg/kg bolus dose.[151] The safety of orally dosed MIDD0301 and MIDD0301S at 500 mg/kg was evaluated using the rotarod test (**Chapter 3.1**) to assess sensorimotor coordination and motor learning and behavioral changes by measuring open field (**Chapter 4.4**) movements (**Figure 13**).

4.4 Open Field Test Background

In addition to the RotaRod test, the open field test offers insight to the behavior of mice.[173] First developed to be used on a swine irradiation project at Iowa State university in 1967, the open field test has been adapted to investigate behavior across several species, ranging from humans to mice.[173–175] The object of the test is to record the total overall movement of an animal. Comparisons may then be drawn between drug-treated groups and control groups by identifying differences or similarities in overall and average rate of movement. To perform this experiment in mice, an 8” x 12” mouse cage (Thoren Caging Systems, Inc.) was used and mice were allowed to acclimate to the cage. Recordings were performed under controlled sound, lighting, and temperature.

4.5 Instrumentation

The open field test was recorded using an iPhone 8 (Apple Inc.) attached to an O-ring stand and placed directly above the mouse cage to ensure the entirety of the cage and mouse movement was recorded. A dark, quiet room along with background white noise was required to prevent any distractions in the mice that would interfere with the study. After recordings, files were converted and compiled with x.Vid-1.3.6-20191204.exe, VLC Media Player, and EthoWatcher (VirtualDub) software to remove background and obtain higher resolution in mouse movement. GraphPad Prism 5.0 was used for data analysis.

4.6 Protocol

4.6.1 Experimental

Six-week-old female Swiss Webster (CFW) mice were purchased from The Jackson Laboratory and were allowed one week acclimation upon arrival. After acclimation, individual mice were placed into the container and recorded for 90 sec for three consecutive days to identify normal baseline behavior and

movement. After three days of recording baseline behavior, mice were prepared to begin compound experimentation.

Mice were dosed with compound by either oral gavage (PO) or intraperitoneally (IP). At T_{max} after compound administration, mice were placed into the container for recording. After 90 sec of recording, mice were removed from the cage and placed back into their respective containers. Data recording consisted of 60 sec, with the first 15 sec and last 15 sec of the 90 sec recording period omitted to ensure the mouse was not exhibiting abnormal behavior due to being moved containers, as well as omitting any possible recording interference of the hand placing the mouse into the container. 60 sec of data for each mouse was then transferred to x.Vid-1.3.6-20191204.exe and VLC Media Player for video compression and improving resolution. EthoWatcher (VirtualDub) software was then used to quantify total mouse movement. However, the first few attempts of analysis were unsuccessful due to video recording and software issues. Former Arnold Group member Brandon Mikulsky made several changes to the protocol as well as developing a program that can be followed for successful data conversion and compilation (**Appendix D**).

4.6.2 Improved Experimental

In constructing the setup for the improved protocol, a clear mouse cage contrasted with a black background was used to reduce reflections being picked up in EthoWatcher. The only light source was indirect and provided by a lamp (Phillips, 80W Soft White) facing the wall. The goal was to avoid shadows and create an even distribution of light while providing sufficient amount of light for the camera. A white noise machine was placed nearby to reduce external noises.

At 15 min after injection, each mouse performed the open-field test. The camera was concretely placed on a stand with a top-down view. First, each video started with audio confirmation of the mouse being recorded. Five sec into video recording (with no mouse in the enclosure), the mouse was placed in the center. The mouse was recorded until the 2-min mark. At that point, the mouse was removed and the

procedure was repeated for each mouse in the group. The group sizes were reduced in size so each mouse was recorded at the same time after drug administration.

The video file was then converted from iPhone to the correct file type for Ethowatcher (**Appendix**). The video was also converted into black and white and with high contrast so the white mouse fur was the most visible object in the video. Each video was then processed through Ethowatcher. The data produced from each video was then compiled and graphed (**Figure 36**).

4.7 Results and Discussion

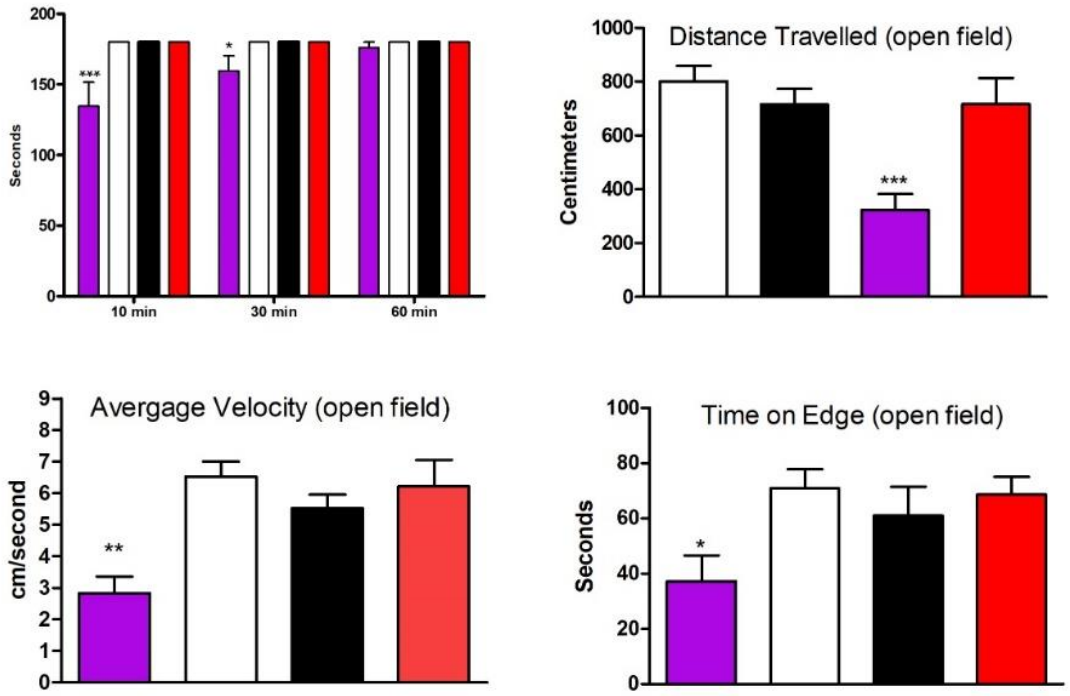

Figure 36. Safety evaluation of MIDD0301 and MIDD0301S in mice. ■ *Diazepam (8 mg/kg),* □ *vehicle,* ■ *MIDD0301S (500 mg/kg),* ■ *MIDD0301 (500 mg/kg); (A) Sensorimotor coordination: Trained female Swiss Webster mice received orally administrated drug and were monitored on a 15 rpm rotarod apparatus for 3 min at 10, 30, and 60 min. The time of fall was recorded if occurring prior to 3 min. Data are expressed as means ± SEM (n = 12), (B-D) Mouse movements in an unfamiliar cage were recorded 20 min after oral administration of compound. Data were recorded for two min. The edge area was defined as 2 inches from each side. Data are expressed as means ± SEM (n = 12). *, **, and *** indicate p < 0.05, p < 0.01, and p < 0.001 significance, respectively, between vehicle and drug treated groups determined by 2-way ANOVA with Bonferroni correlation.*

Neither MIDD0301 nor MIDD0301S dosed orally at 500 mg/kg caused any adverse sensorimotor effects (impairment of motor function) as measured by rotarod **(Figure 36**). In contrast, diazepam at 8 mg/kg caused significant impairment at 10 and 30 min after oral dosing, which dissipated after 60 min. Next, possible adverse CNS effects were evaluated using the open field test, which is a common paradigm to evaluate locomotion, anxiety-like behavior, exploratory behavior, and activity levels in rodents. Here, mouse movements in the open field apparatus were video recorded 20 min after oral drug dosing. Diazepam at 8 mg/kg resulted in significant reductions in distance travelled, average velocity, and resident time close to the edge of the cage. Conversely, MIDD0301 and MIDD0301S at 500 mg/kg did not cause any significant changes in any of the measured movement parameters when compared to vehicle treated mice. These data are consistent with previous results showing limited CNS distribution of MIDD0301 and the corresponding absence of sensorimotor or other behavioral effects (of either enantiomer) attributable to binding to $GABA_A$Rs expressed in the brain.

Once the protocol and methods were defined, the open field test was performed by Brandon Mikulsky and is currently being performed by Michelle Meyer. To streamline data analysis, several changes were made to the protocol by Michelle Meyer and former Arnold Group members Dylan Hoffman and Brandon Mikulsky. New containers and recording devices, as well as altering the EthoWatch software program to identify the mouse were utilized to garner more accurate representation of mouse movement and behavior.

With the adjustments to refine the protocol, the Open Field Test is a valuable assay that gives insight into compounds that do not exhibit excitatory or inhibitory sensorimotor coordination in mice. The data also provides a crude understanding of the brain metabolism and elimination of compounds prior to investigating their full pharmacokinetic profiles.

4.8 Conclusion

It can be concluded that (R) and (S) MIDD0301 and PI320 are potent bronchodilators that are effective in relieving methacholine-induced AHR in diverse animal models. The therapeutic value of these nebulized and orally administered compounds were demonstrated for lung inflammation induced by allergens and infectious mediators, which correspond to major disease pathways underlying human bronchoconstrictive disorders including asthma. These compounds represent first-in-class drugs based on a fundamentally novel asthma mechanism of action for the treatment of inflammatory respiratory diseases, namely, targeting $GABA_AR$ in the lung. Furthermore, when run in parallel, the RotaRod and oOpen field tests provided robust analysis of sensorimotor coordination, sedation, cognitive behavior, or overall movement in mice delivered these lead compounds. This approach can uncover safety and efficacy liabilities of existing drugs, and unlike current treatments, MIDD0301 is effective in reducing airway constriction and lung inflammation when administered by oral and inhaled routes.

CHAPTER 5

Identification of New

Anti-Inflammatory Compounds

5.1 Introduction

The three main hallmarks of asthma include lung inflammation, bronchoconstriction, and increased mucus production.[177] The most abundant types of immune cells that play a role in this pathophysiology are mast cells, B-cells, neutrophils, epithelial cells, eosinophils, macrophages, and T-lymphocytes.[177]

There are two main classes of T-lymphocytes: $CD4^+$ helper cells (T-helper cells), and $CD8^+$ cytotoxic cells, which are characterized based on their surface expression of CD4 or CD8, which form co-receptors with the T cell receptor to promote T-cell coactivation.[178,179] Antigen activation of the T-cell receptor (TCR) initiates several pathways and stimulates calcium to be released from intracellular stores, further promoting calcium entry through membrane bound store-operated calcium channels.[180] The foundation for the majority of inflammatory process mediated by T-cells is this increase in intracellular calcium. This includes short term stabilizing of antigen presentation, and inducing pathways that lead to genetic changes such as induction of cytokine transcription.[180]

It has been shown that $CD8^+$ cells are responsible for cytotoxicity and have a lesser understood role in asthma pathogenesis.[181] Although $CD8^+$ cells have been shown to suppress asthma phenotypes such as antigen specific IgE production, other studies have shown $CD8^+$ cells increase inflammation and airway hyperresponsiveness.[182]

Conversely, $CD4^+$ T-cells have a better understood role in asthma and are responsible for perpetuating the inflammatory response by infiltrating airways and secreting inflammatory cytokine mediators.[181] This cytokine release directs other cell types to mediate many of the clinical characteristics of asthma, including heightened IgE production by B-cells, increased blood eosinophilia, and immune cell proliferation (**Figure 37**).[183] This complex inflammatory reaction can classified into Th1 and Th2 responses. Th1 responses are characterized by cytokines like interferon γ (IFNγ), interleukin-2 (IL-2), and lymphotoxin (LT), which promote the cell-mediated immune response.[184] The Th2 immune response is characterized

by production of multiple cytokines: IL-4, IL-5, IL-10, and IL-13, among others.[184] This response promotes robust antibody responses and eosinophil activation.[8] Recent literature suggests asthma to be an imbalance between Th1 and Th2 responses.[185] There is overwhelming evidence that Th2 cytokines are the primary class of cytokines that lead to asthma pathology. However, Th1 cytokines such as IL-2, are present in bronchoalveolar lavage fluid (BALF) and serum in those experiencing asthmatic exacerbations.[186]

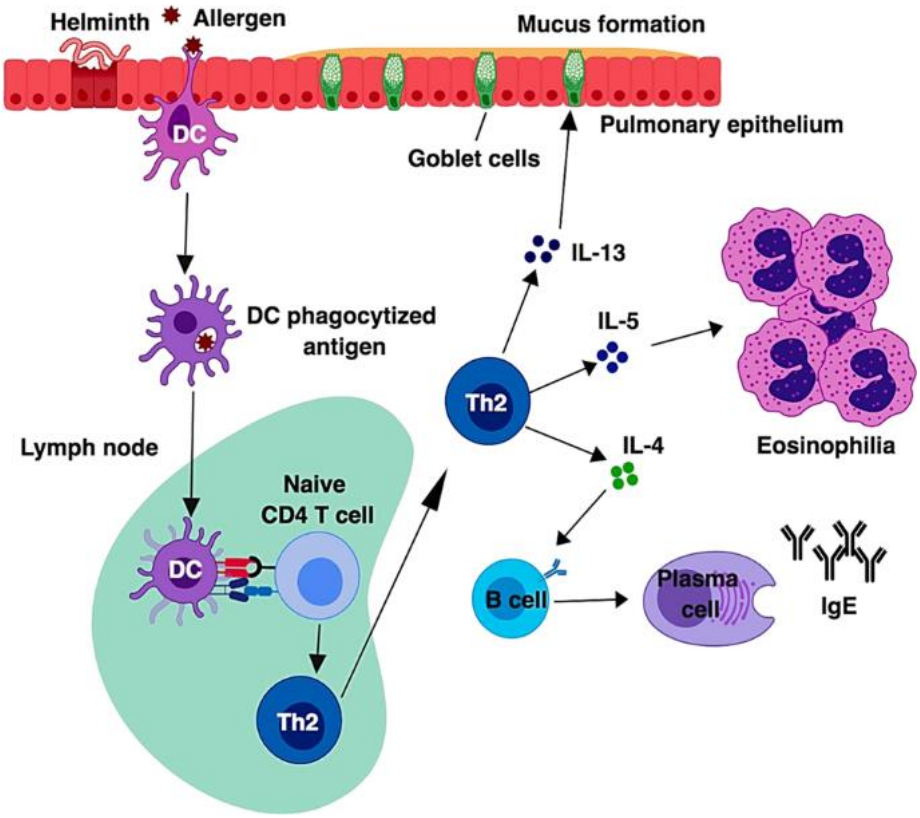

Figure 37. Th2 Cell-Mediated Inflammation.[197] *Dendritic antigen-presenting cells bind to naïve CD4 T-cells through CD4 and TCR coactivation causing an inflammatory response by infiltrating the airway and secreting inflammatory mediators like IL-4, IL-5, and IL-13 cytokines. This cytokine release directs other cell types that mediate asthma, including increased blood eosinophilia, heightened IgE production by B-cells, and immune cell proliferation.*[183]

Upon activation by an antigen, Th2 cytokine producing T-cells recruit eosinophils through IL-5 (**Figure 37**).[187] This recruitment directs eosinophils from the bone marrow through the blood and to the lung tissues.[187] Although atopy is correlated with excessive eosinophilia in the lung, there is a significant range of blood eosinophil concentrations among asthmatics.[189] During the asthmatic allergic response,

matured eosinophils migrate from bone marrow to the lung tissue, become stimulated, and consequently release several cytotoxic mediators in a process known as degranulation.[187,188] These mediators include eosinophil peroxidase and Major Basic Protein (MBP), both which have been shown to cause airway hyperresponsiveness (AHR).[187,188] MBP also triggers mast cells and basophils, initiating the release of histamine which leads to bronchial hyperreactivity.[188] Eosinophils also produce additional cytokines such as IL-13, which stimulates mucus production from goblet cells.[188]

Another key immune cell type involved in the asthmatic response are macrophages. There are three major classes of macrophage in the lung: i.) sputum-derived bronchial macrophages, ii.) interstitial macrophages in the interstitium, and iii.) alveolar macrophages in the alveoli lumen.[190] Depending on their role in the inflammatory process, these classes of macrophages can be characterized as either M1 or M2. M1 macrophages respond to intracellular pathogens and can be polarized by IFNγ and lipopolysaccharide (LPS). M2 macrophages phagocytose foreign pathogens and apoptotic cells and are polarized by IL-4 and IL-13.[190] M1 macrophages are thought to be more active in non-eosinophilic asthma, however it is still unclear which is more prevalent in asthmatics.[190]

Macrophages play an important role in propagating the inflammatory response.[190, 191] To promote this response, macrophages produce a multitude of factors that affect numerous other cell types. In asthmatics, alveolar macrophages increase NO production compared to healthy counterparts.[190] The regulation of T-lymphocyte proliferation is due to the upregulated nitric oxide synthase dependent pathway. Thus, excess NO can reduce the production of inflammatory cytokines from alveolar macrophages as a coping mechanism.[190] Nevertheless, excess NO causes vasodilation, increase in mucus secretion, and recruitment of eosinophils, which leads to cell injury, airway remodeling, and eventual steroid resistance.[191,192] Increased levels of exhaled NO are associated with accelerated decline in lung function in severe asthmatics.[192]

$GABA_AR$s have been recently characterized on many cell types related to asthma, including immune cells such as lymphocytes and macrophages in airway smooth muscle.[193-195] Lymphocytes have shown reduced proliferation in the presence of $GABA_AR$ agonists, supporting the notion that targeting $GABA_AR$s on macrophages could produce an anti-inflammatory effect.[194] Peritoneal macrophages also have reduced levels of cytokine production when treated with GABA, an effect that is reversed by the $GABA_AR$ channel blocker picrotoxin.[195] $GABA_AR$-mediated signaling has also proven essential in macrophage differentiation.[196]

To investigate the effect $GABA_AR$ ligand binding has on immune cells, a protocol was developed to quantify the production of IL-5 and IL-13 from negatively-selected $CD4^+$ T-cells isolated from female Swiss Webster splenocytes via rtPCR.

5.2 Methods

5.2.1 Materials

RBC Lysis Buffer (with ammonium chloride, sodium bicarbonate, and EDTA)

QIAshredder Kit (Qiagen Strasse #79654, Hilden, Germany)

RNeasy Mini Kit (Qiagen Strasse #74104, Hilden, Germany)

Affymetrix eBioscience MagniSort Magnet

MagniSort Negative Selections Beads B (Invitrogen #4332206, San Diego, CA)

MagniSort Mouse CD4 T Cell Enrichment Antibody Cocktail (Invitrogen #4338775, San Diego, CA)

TAE (50X) Tris-Acetate-EDTA Buffer (Boston BioProducts #A6R6S, Ashland, MA)

SYBR Safe DNA Gel Stain (Invitrogen #2080069, Carlsbad, CA)

One-Step SYBR Green Master Mix (2X) (Quantabio #66156026)

Quantifast SYBR Green RT-PCR Master Mix, 2X (Qiagen #163014623, Hilden, Germany)

Calcium Ionophore A23187 (Sigma #059M4000V)

Phorbol 12-myristate 13-acetate (Sigma #MKCG6946)

Mouse GAPDH Stellato Primers (IDT #282311543) (Product Data in Appendix: Primers)

Mouse IL-13 Huang Primers (IDT #282311546) (Product Data in Appendix: Primers)

β-Actin Primers (Product Data in Appendix: Primers)

Molecular Biology Agarose (Bio Rad #161-3101, Hercules, CA

RPMI 1640, 1X Media (Corning #10-040-CV, Manassas, VA) + 10% FBS, 1% Pen/Strep, 0.1% β-Mercaptoethanol

TECAN Infinite M1000 Instrument (Grödig, Austria)

Gel Electrophoresis Kit (Bio Rad, Hercules, CA)

PowerEase500 Gel Electrophoresis Power Kit (Invitrogen, San Diego, CA)

96-Well TwinTec Eppendorf PCR Plate (Millipore Sigma)

Eppendorf Mastercycler pro PCR System (Millipore Sigma)

Experimental Animals. Female Swiss Webster mice were purchased from Jackson Laboratory (Bar Harbor, ME). Animals were housed in a pathogen-free and 12 h light and dark cycle environment under standard humidity conditions. Animals had ad libitum access to food and water. UW-Milwaukee and Columbia University confirmed that all animal experiments were in compliance with Institutional Animal Care and Use Committees.

5.2.2 Experimental Protocol

Sacrificing & Tissue Harvesting. Mice were sacrificed by CO_2 asphyxiation, cervical dislocation, and cardiac puncture. To obtain enough splenocytes, three mice were sacrificed. Spleens were extracted and immediately stored in PBS on dry ice. Samples were then transferred from the animal facility to the lab for culturing.

Splenocyte Culturing. In a sterile biohood, spleens and PBS were poured into a petri dish. Spleens were cut into small pieces with a scalpel and smashed with the plunger of a syringe to disintegrate (**Figure 38**).

Mixture was then transferred with auto-pipet and disposed through a 0.22 µM filter on top of 50 ml conical vial. After centrifugation at 1600 rpm for 10 min, the supernatant was aspirated off and the pellet was resuspended in 2 ml of pre-warmed RBC lysis buffer. Cells were incubated at 37 °C for 2 min while gently mixing with pipet. After 2 min, 28 ml of PBS was added to stop lysis. Cells were then centrifuged at 1600 rpm for 10 min, and supernatant was removed. The splenocyte pellet was then reconstituted in 2 ml of isolation buffer containing PBS (Ca^{2+} and Mg^{2+} free) with 0.1% BSA and 2 mM EDTA. Cells were counted on a hemocytometer via live/dead stain with trypan blue. Cells were then diluted to $5x10^7$ cells/ml in isolation buffer and stored in 500 µl aliquots in 15 ml conical vials.

CD4 T-Cell Isolation. 500 µl of isolation buffer was added to each 15 ml conical vial containing $5x10^7$ cells/ml to yield ~1 ml. 100 µl of heat-inactivated FBS and 100 µl of Enrichment Antibody Mix (IgG in 0.1% BSA/PBS w/ 0.02% Sodium Azide) was added to each 15 ml conical vial. Each solution was gently mixed with pipet and incubated for 20 min at 4 °C. After 20 min, cells were washed with 4 ml of isolation buffer. Mixing was performed by inverting the tubes several times, and cells were centrifuged at 350 xg for 8 min at 4 °C. During centrifugation, dynabeads were washed according to the following protocol:

i. Vortex/Mix Dynabeads storage vial for 30 s.

ii. Transfer 500 µl Dynabeads to a glass tube.

iii. Add 1 ml isolation buffer to glass tube and gently mix.

iv. Place glass tube in magnet for 1 min and discard supernatant.

v. Remove tube from magnet and resuspend washed Dynabeads in 500 µl Isolation Buffer.

After centrifugation, the supernatant was aspirated off and each 15 ml conical vial containing cells were resuspended in 500 µl of isolation buffer. 50 µl of pre-washed dynabeads were added to each 500 µl solution containing cells in isolation buffer. The mixture was incubated for 15 min at room temperature with gentle mixing. After incubation, 2 ml of isolation buffer was added to each mixture and gently mixed with the pipet to avoid foaming or bubble formation. Each solution of cells and isolation buffer (roughly

2.5 ml) were transferred into individual glass tubes. Each tube was placed in the magnet for 2 min and the supernatant containing untouched naïve $CD4^+$ T-cells gently poured off (**Figure 38**). 2 ml of isolation buffer was added to the same glass tube and the process of placing in a magnet and pouring off untouched naïve $CD4^+$ T-cells repeated for all glass vials containing cells, isolation buffer, and dynabeads. All untouched naïve $CD4^+$ T-cells in solution were combined in a 50 ml conical vial.

CD4+ T-Cell Activation. Naïve $CD4^+$ T-cells were reconstituted in 18 ml RPMI1640 media containing β-ME, FBA, and Pen/Strep. Cells were mixed by gentle pipetting. 3 ml of RPMI1640 and cells were pipetted into three wells in a 6-well plate and labeled as Non-Activated (N/A). 2 µg/ml PMA/Ionomycin solution was used for cell activation and added to the remaining ~9 ml of RPMI1640 and cells and mixed with pipet. 3 ml was added to the remaining 3 wells in the plate and labeled Activated (Act.). Cells in 6-well plate were covered and incubated at 37 °C for three h to allow activation. The plate was gently shaken every 1 h to stimulate activation.

RNA isolation from Activated and Non-Activated $CD4^+$ T-Cells. Activated cells were pipetted into a labeled 15 ml conical vial and non-activated cells pipetted into a separate labeled vial. Cells were centrifuged for 3 min at 1000 rpm. After centrifugation, the supernatant was carefully removed by pipet. RLT/β-ME solution was prepared by adding 10 µl β-ME to 2 ml RLT solution. 350 µl RLT/β-ME solution was added to each pellet (both Act. and N/A) and gently mixed with pipet. Cell suspensions were then transferred to cell shredder vials and centrifuged at 10,000 rpm for 2 min. After centrifugation, 350 µl of 70% EtOH was added to each vial and mixed carefully. The 700 µl solution was then loaded into RNeasy columns and centrifuged for 15 sec at 10,000 rpm. RNA was captured on filter during centrifugation, and flow-through was discarded. 700 µl RWI Buffer was then added to the RNeasy columns and centrifuge for 15 sec at 10,000rpm. The flow-through was discarded. Next, 500 µl RPE Buffer was added to RNeasy columns and centrifuged for 15 sec at 10,000rpm. The flow-through was discarded. The last buffer application consisted of adding 500 µl RPE Buffer and centrifuging for 2 min at 10,000 rpm. The flow-

through was then discarded. RNA was eluted off RNeasy column filter by adding 50 µl of RNase-free water and centrifuging for 1 min at 10,000 rpm. The flow-through (containing RNA) was pipetted back onto filter and centrifuged again for 1 min at 10,000 rpm. In a 384-well plate (Eppendorf), 4 µl of each solution (Act. and N/A) were individually added in quadruplicate to separate wells containing 16 µl RNase-Free water. Samples were analyzed with a TECAN plate reader at absorbance readings of 260 nm and 280 nm. Absolute values of average RNA concentration were compared to RNase-free water (as negative control) and multiplied by path length factor to find RNA concentration in ng/ul. RNA was stored at -80 °C until rtPCR analysis.

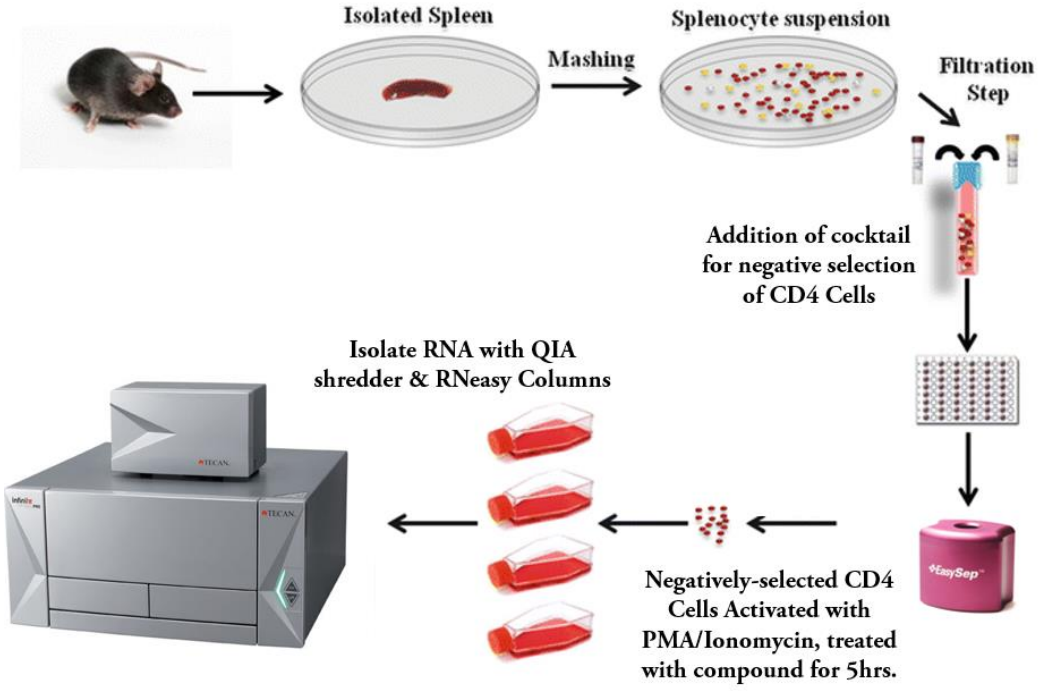

Figure 38. Diagram of Mouse Sacrificing to Total RNA Quantification. *Mice were sacrificed and spleens were isolated. Spleens were mashed and mixed with RBC lysis buffer. $CD4^+$ T cells were isolated through negative selection with MagniSort Dynabeads, and placed in RPMI1640 media. Half of the cells were activated with PMA/Ionomycin while the other half remained nonactivated. Compounds of interest were administered to select activated wells and allowed to incubate. Total RNA was quantified in nonactivated, activated, and activated + compound cells on a TECAN instrument.*

Real-Time Polymerase Chain Reaction. Total number of vials containing solution were equal to half the number of primers used. To each vial the following solution was prepared: 33 µl DNase-free water, 5 µl of

each matching forward and reverse primers (IL-5, IL-13, and housekeeping gene GAPDH), 2 µl RT Quantifast (qScript), and 50 µl SYBR dye. Each of these solutions were gently mixed with pipet and 18 µl aliquoted into four consecutive wells in a 96-well TwinTec Eppendorf plate. Based on the concentrations of total RNA of ~100ng/µl, it was determined that 7.6 µl of RNA solution would be diluted in 34.4 µl DNase-free water for both activated and non-activated samples. 2 µl of diluted RNA was added to each appropriate well while avoiding bubbles during pipetting. A rtPCR TwinTec Eppendorf screen cover was placed over the plate and the plate briefly centrifuged to remove all bubbles. The plate was then carefully transferred to the rtPCR Thermocycler instrument (Eppendorf). The thermocycler instrument filter was set at 520 nm for the SYBR green probe. Method times, temperatures, and cycle numbers are shown in **Figure 39**.

Preparing RNA Gel. 2 ml of 50x TAE Buffer was added to 98 ml deionized water. 2 g agarose was added, mixed, and microwave in 30 sec intervals until dissolved. Once cooled to 60 °C, 10 µl SYBR safe green dye was added to the solution. The gel was poured into an even tray and the well block placed into the gel. Once cooled off to room temperature, the well block was carefully removed from the gel. The gel was then removed from the tray and placed into the electrophoresis chamber. TAE buffer was then poured into the electrophoresis chamber up to the fill line (roughly 150 ml).

Running RNA Gel. To prepare PCR amplicons for gel electrophoresis, 3.5 µl of 6x dye was added to each well containing RNA in the 96-well Twin-Tec PCR plate. Into the first and last wells, 8 µl Low Density DNA ladder was added. GAPDH, IL5, and IL13 were then added to the remaining wells. The gel was ran at 145 V, 80 mA, and 10.0 W for 45 min.

5.3 Results and Discussion

The goal of the first experiment was to develop a successful protocol. Exceptions to the protocol under **Methods** include the cells incubating at 37 °C overnight (~20 h), as well as the cells not being

activated with PMA/Ionomycin. TECAN readings were taken at 260 nm and showed a total RNA concentration of 92.7 ng/µl after comparing vs negative control and multiplying by path length factor (PLF). RNA was stored in stock solution at -80 °C.

Sample preparation for rtPCR occurred at room temperature with careful attention to appropriate mixing, as well as reducing bubble formation and overall contamination. 7.5 µl RNA stock was added to 34 µl RNase-free water. Stock solutions were then prepared for each individual primer (β-Actin, IL-5, and IL-13) containing RNase-free water, 5 µl of each forward and reverse primer, RT Quantifast qScript, and SYBR Green dye. 18 µl of each stock solution was then pipetted into wells of the PCR plate in quadruplicate, and 2 µl of diluted RNA solution carefully added to each well. A PCR coverslip was carefully placed over the plate and the plate was centrifuged at 800 rpm for 20 sec. After centrifugation, the plate was placed in the Eppendorf Mastercycler pro PCR System and the Method was created (**Figure 39**).

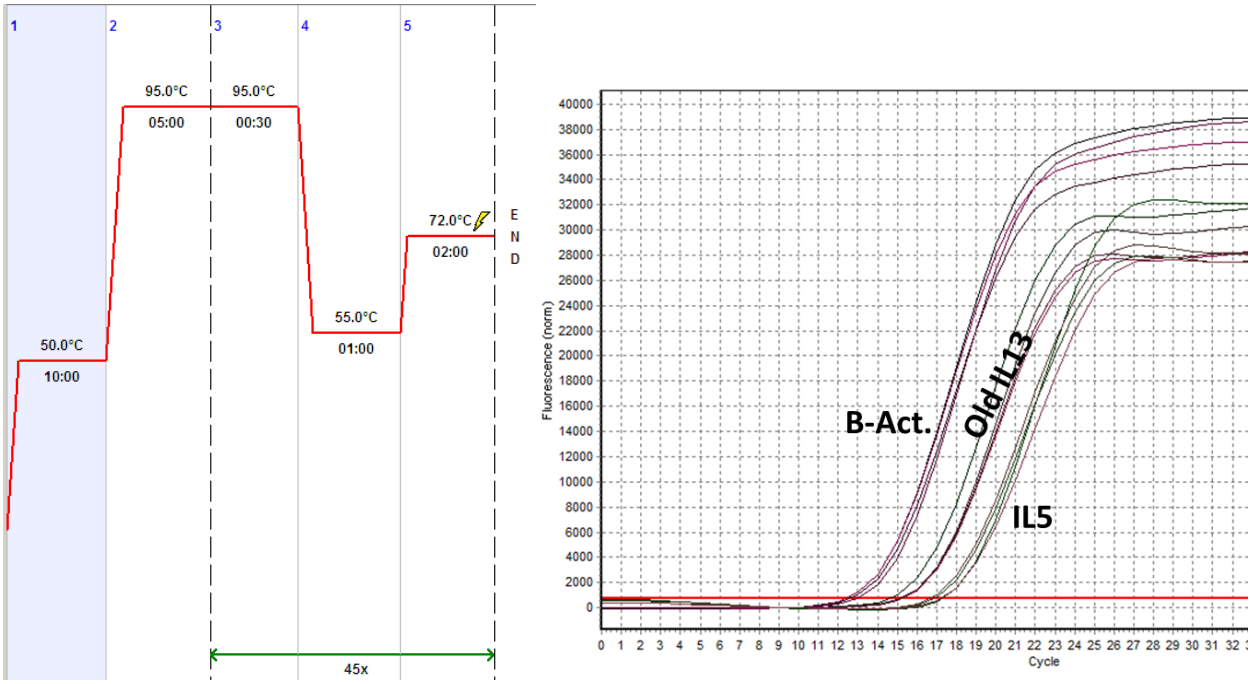

Figure 39. Initial Method and rtPCR Amplification Plot. *The samples were first held at 50 °C for 10 min, followed by 95 °C for 5 min for denaturation. Then, 45 cycles were performed of 95 °C for 30 sec, 55 °C for 1 min, 72 °C for 2 min. β-Actin had Ct values of ~13, IL-13 had Ct values of ~15, and IL-5 had values of ~17.*

Amplification for all sample wells had Ct values between 12.5 and 17.5 A larger variance in the IL-13 primer Ct values prompted a change to use a different IL-13 primer. Additionally, GAPDH a widely-used housekeeping gene,[198] was chosen for future experiments.

A 2% agarose RNA gel was then prepared and β-Actin, IL-13, and IL-5 were dyed in the PCR plate wells. The DNA ladder and the dyed, amplified PCR fragments were then loaded into respective wells of the gel. Gel electrophoresis was run at 125 V and 80 mA for 40 min. Product bands are shown in **Figure 40**.

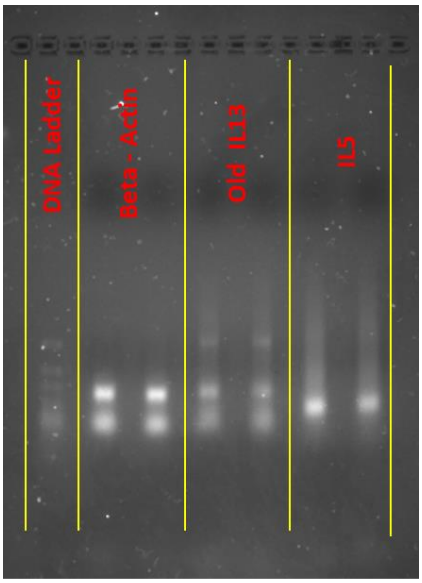

Figure 40. 2% Agarose Gel Confirming Presence of β-Actin, IL-13, and IL-5*. Gel electrophoresis was run at 125 V and 80 mA for 40 min.*

The IL-13 primer used was shown to have tailing and presence of other products, further confirming the need to use a different IL-13 primer. The experiment was then repeated under identical conditions with the exception of a different IL-13 primer and housekeeping gene (**Figure 41**). The same stock RNA was used (92.7 ng/µl).

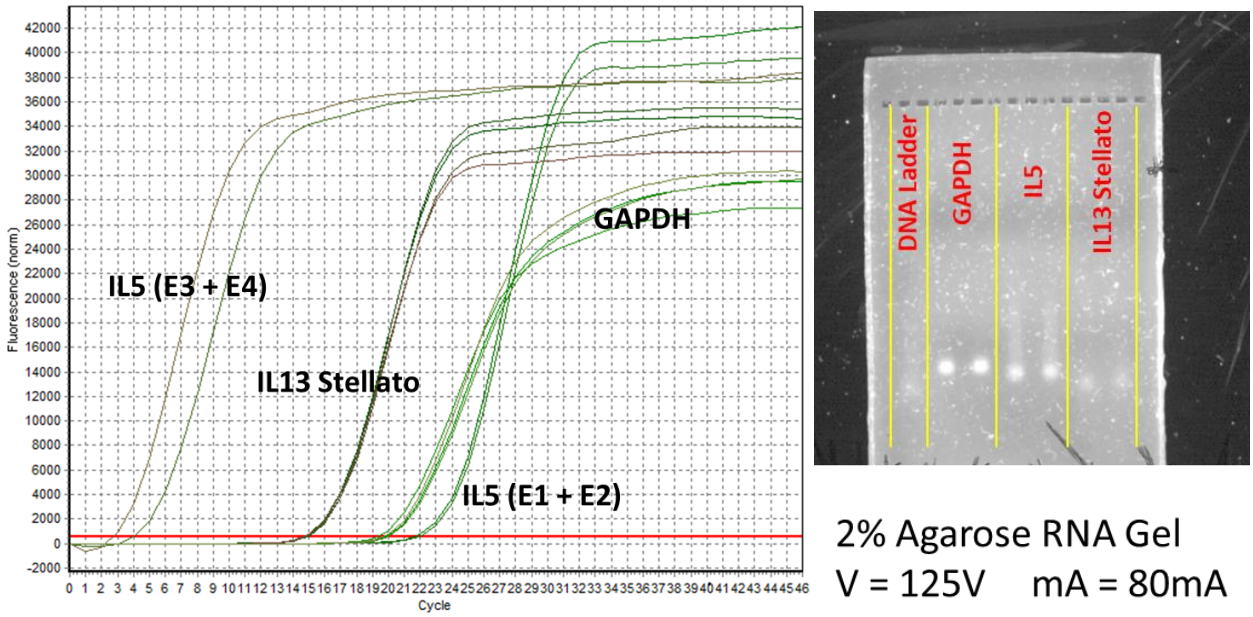

Figure 41. Second rtPCR Experiment with New Primers and RNA Gel Electrophoresis. *GAPDH was shown to amplify with small variance between samples and also presence was confirmed with gel electrophoresis. IL-13 Stellato did not have Ct values close to GAPDH and also showed poor band presence during gel electrophoresis, so it was no longer considered.*

The new IL-13 Stellato primer showed amplification with little variance, however, a cycle threshold number within closer proximity to the housekeeping gene was preferred. GAPDH showed adequate amplification with little variance and was chosen as the housekeeping gene for future experiments. The RNA gel was run under identical conditions as the first experiment, and showed presence of GAPDH and IL-5, however IL-13 Stellato had little visibility of band presence indicating poor or low amplification of IL-13 (**Figure 41**). The early amplification of two IL-5 wells were determined to likely be contaminated and were not cause for concern.

Using the same RNA stock solution and under identical conditions, a third rtPCR experiment was performed to identify an IL-13 primer with cycle threshold values similar to GAPDH. IL-13 Huang and IL-13 Emerson were compared to GAPDH and are shown in **Figure 42**.

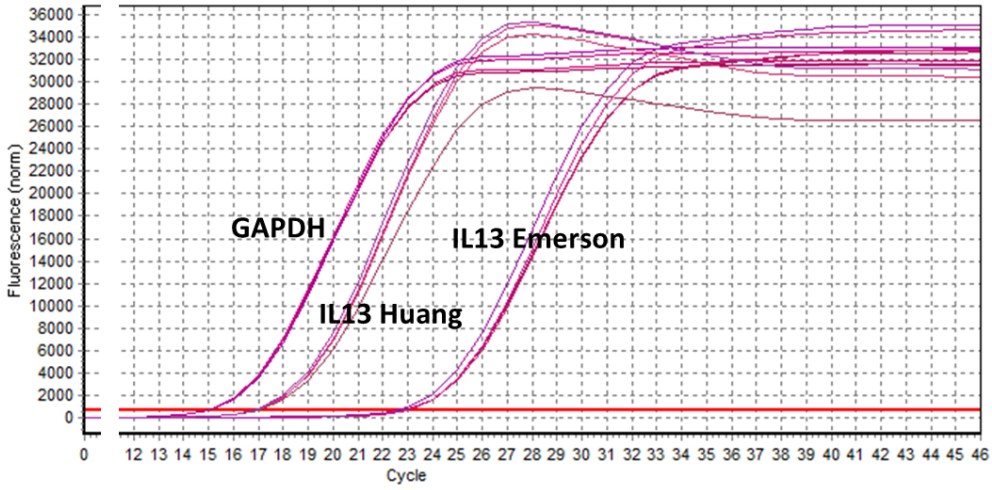

Figure 42. Comparison of IL-13 Primers to Housekeeping Gene GAPDH. *IL-13 Huang and IL-13 Emerson were analyzed under rtPCR. IL-13 Huang was chosen as the preferrable primer due to closer proximity to GAPDH as well as still having low intra-sample variance.*

IL-13 Huang showed close proximity to the cycle threshold of GAPDH while having low intra-sample variance (**Figure 42**). It was chosen for future experimentation.

The entire experiment was then repeated to replenish stores of RNA stock solution. The protocol in **Methods** was followed with the exception of $CD4^+$ T-cells being activated with PMA/ionomycin for 5 h (previous activation was for 20 h). A shorter activation/incubation time was chosen to try to increase total RNA yield. Results from the TECAN were successful, as activated cells had a concentration of 131 ng/µl and non-activated cells had a concentration of 143 ng/µl. GAPDH, IL-5, and IL-13 Huang were then analyzed by rtPCR in both Activated and non-activated RNA stock solutions.

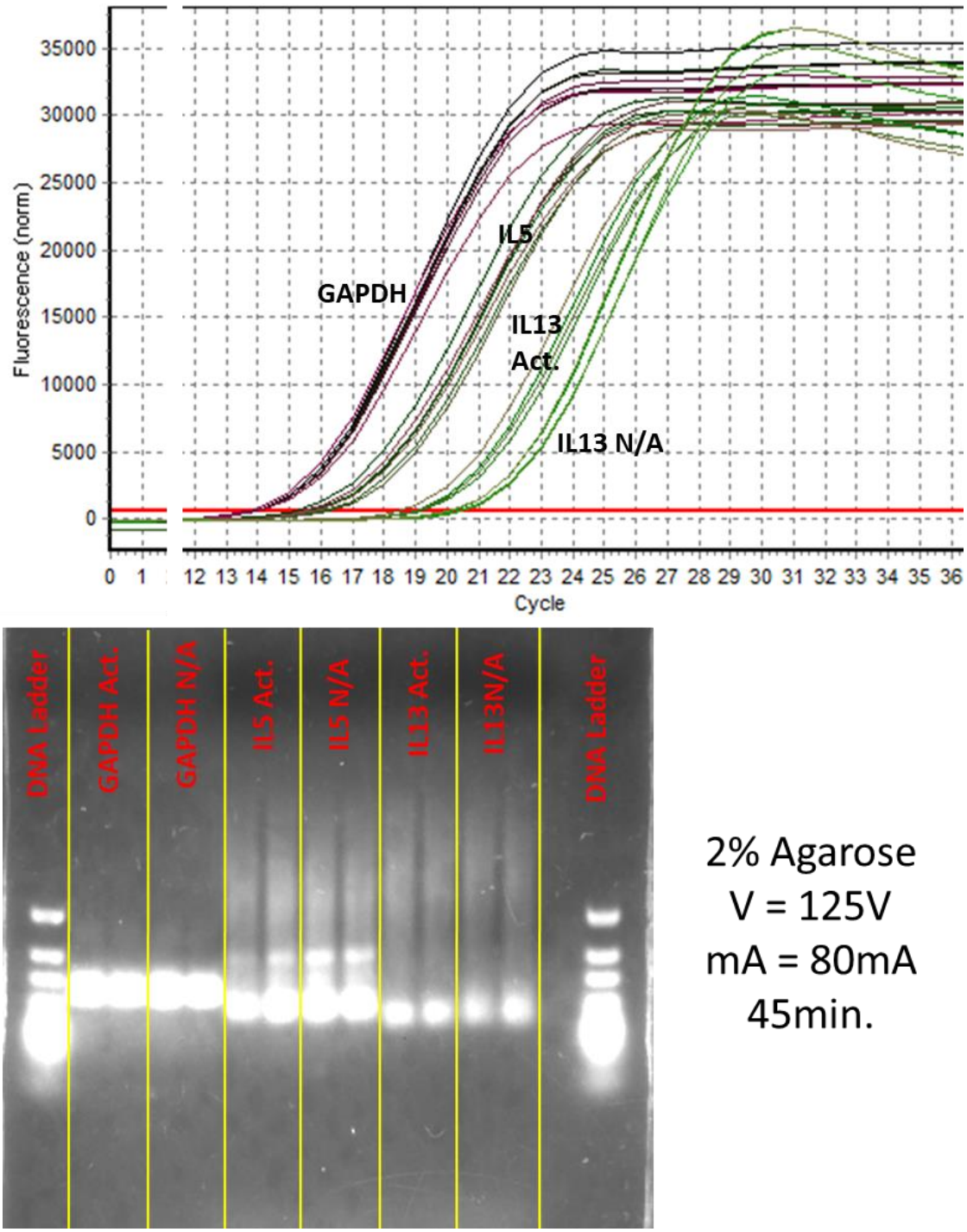

Figure 43. rtPCR Plot Comparing Cycle Thresholds for Different Primers in both Activated and Non-Activated RNA. *GAPDH was the first primer to show amplification, followed by IL-5 and IL-13. Gel electrophoresis showed band presence for all primers in both activated and non-activated RNA.*

Cycle thresholds for all samples were between 14 and 21 and still showed good separation between primers for easy identification (**Figure 43**). Furthermore, IL-13 Huang showed separation

between the activated and non-activated RNA, whereas GAPDH and IL-5 did not. Gel electrophoresis showed bright bands for all samples, hinting towards undesired RNA likely being amplified in addition to the genes of interest.

The complete experiment was then repeated with several changes in the protocol in an attempt to reduce unwanted DNA binding. Four mice were sacrificed and had their spleens removed and stored in pre-warmed PBS. The protocol for $CD4^+$ T-cell isolation was then performed at room temperature to preserve live cells. Unfortunately, this produced a more viscous solution than previously observed and caused MagniSort Dynabeads function to be inhibited. A total of five passes through the magnet were required to remove any visible presence of Dynabeads (**Figure 44**).

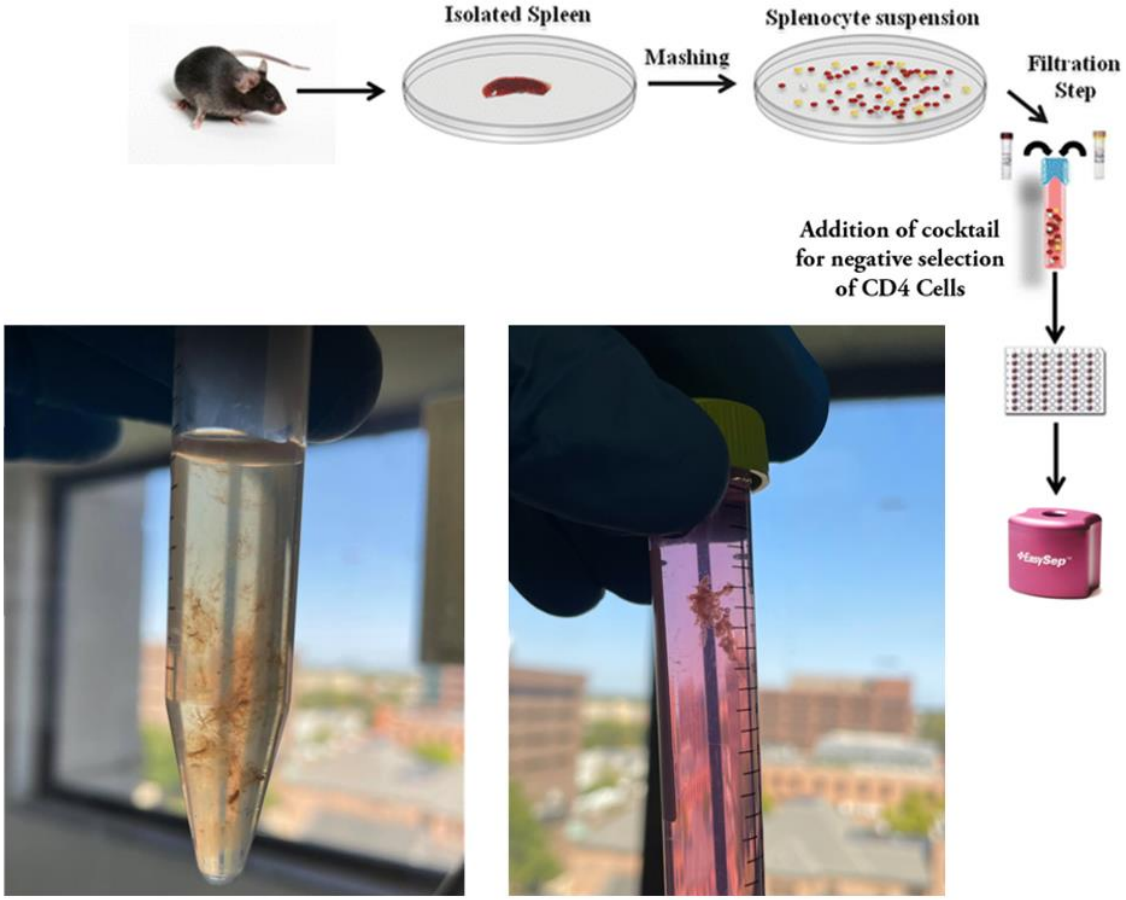

Figure 44. Dynabeads Presence when Protocol is ran at Room Temperature. *Five total passes through the magnet were required to eliminate visible Dynabeads from the isolated $CD4^+$ T-cells. After reconstitution in RPMI1640 + 10% FBS, 1% Pen/Strep, 0.1% β-Mercaptoethanol. a visible aggregate formed.*

After visible Dynabeads were removed from solution, the isolated $CD4^+$ T-cells were reconstituted in RPMI1640 + 10% FBS, 1% Pen/Strep, 0.1% β-Mercaptoethanol. A noticeable aggregate immediately formed (**Figure 44**). The aggregate was broken up by pipetting and one-third of the total solution was placed equally into the first two wells of a six-well plate and labeled N/A. A new formulation of 50 ng/ml PMA and 10 µg/ml ionomycin was prepared and added to the remaining 2/3 of solution and mixed with pipetting. Half of the remaining solution was then placed into two empty wells of the six-well plate and labeled Act. The remaining activated solution was treated with 30 µM GL-IV-03, mixed with pipet, and transferred equally into the last two empty wells and labeled Act. + GL-IV-03. Cells were incubated for one h to try to preserve live cells.

RNA was then isolated according to the protocol in **Methods**. Total RNA from this protocol was 95.4 ng/µl for non-activated, 71.6 ng/µl for activated, and 75.6 ng/µl for activated + GL-IV-03. Similar concentrations to the first experiment enabled the same volumes for rtPCR sample preparation as previous experiments. Results are shown in **Figure 45**.

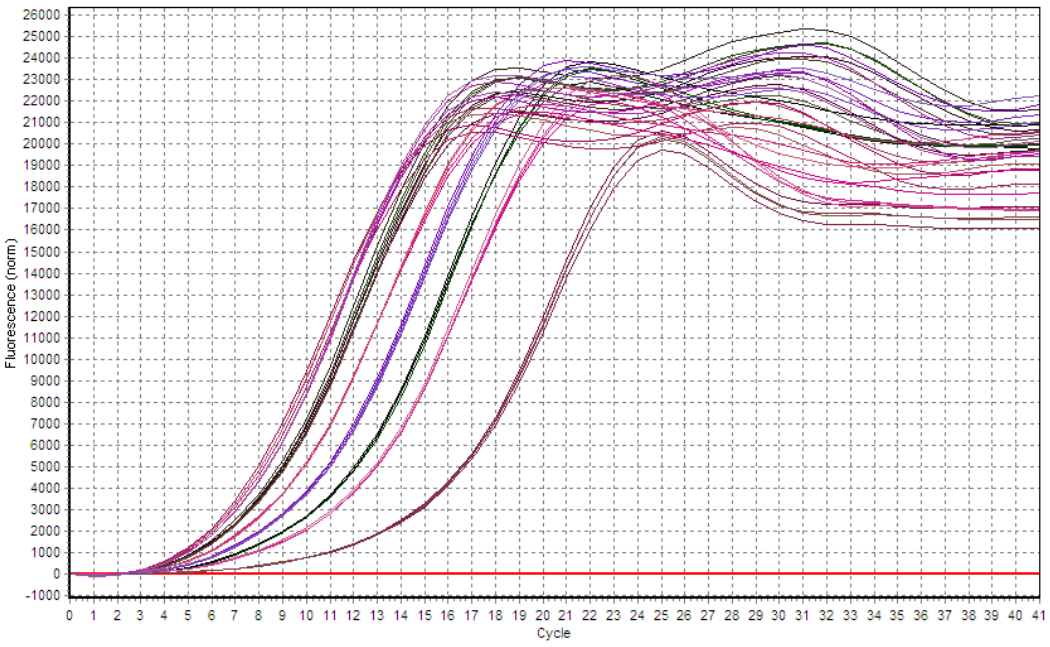

Figure 45. rtPCR Plot of Activated and Non-activated cells Using Updated Protocol. *Results show immediate overamplification, suggesting errors in rtPCR sample preparation.*

Results show immediate amplification and very low cycle threshold numbers. At first this was thought to be due to the formation of the unknown Dynabead aggregate during $CD4^+$ T-cell isolation, however, RNA isolation with the QIAshredder and RNeasy (Qiagen) kits would have removed these impurities when we found RNA concentrations from ~70-95 ng/µl. Due to these total RNA concentrations being similar to previous experiments, it was inferred that these low cycle threshold values were either due to the sample preparation prior to total RNA quantification or during rtPCR preparation.

To see if the immediate amplification was due to sample preparation for rtPCR, a known 96 ng/µl activated and 347 ng/µl non-activated stock RNA solution was provided by Dr. Alexander Arnold. The same protocol for rtPCR sample preparation was used and the same method was used on the thermocycler instrument (**Figure 46**).

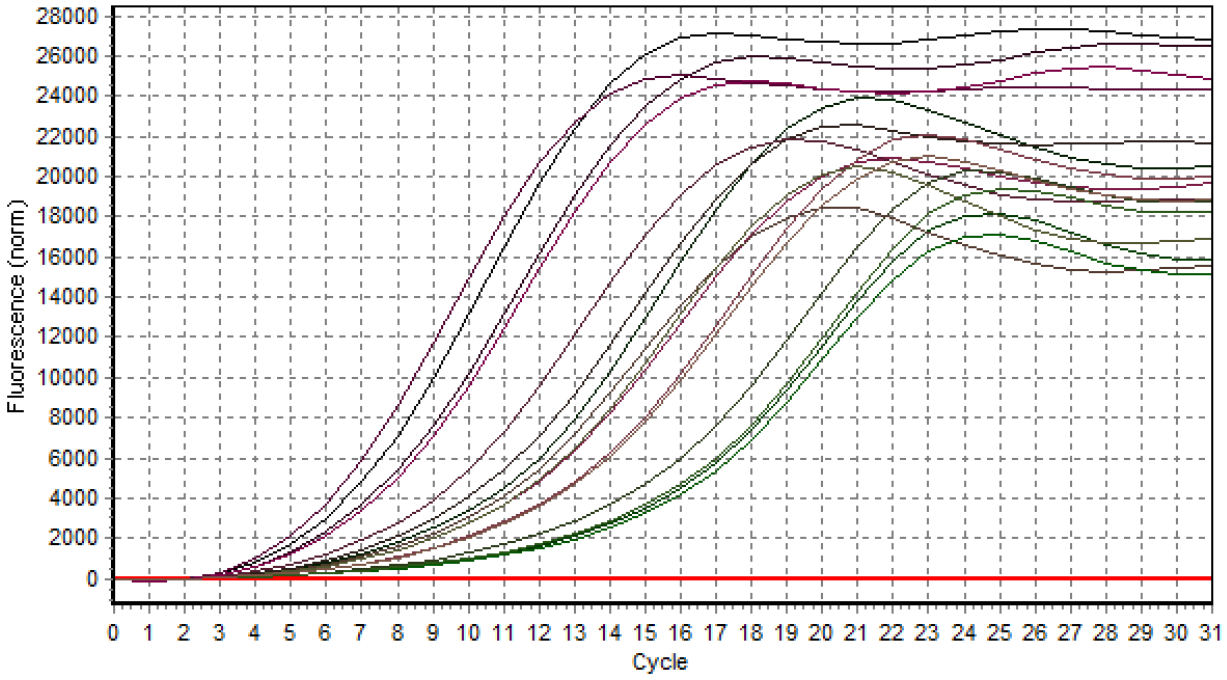

Figure 46. rtPCR Plot Showing Immediate Amplification. *When performing the rtPCR sample preparation with RNA isolated from Dr. Alexander Arnold, the same overamplification was observed suggesting errors in the rtPCR sample preparation protocol as opposed to sample preparation and isolation of RNA.*

Amplification was immediate before the instrument was able to report cycle threshold values, confirming that the rtPCR sample preparation protocol needed to be adjusted. In addition to immediate

amplification, there was also large intragroup variance. Troubleshooting included checking appropriate concentrations of primers, SYBR Green Dye, and reverse transcriptase. Furthermore, some SYBR Mix solutions begin to lose function when a cycle temperature goes below 60 °C.

During troubleshooting, other students in the UW-Milwaukee chemistry department also reported similar errors when using the rtPCR instrument. Immediate amplification along with large intragroup variance was occurring for RNA samples isolated from mouse ear and mammalian cells, suggesting an error may be occurring due to instrumental malfunction. However, this notion was quickly dismissed after instrumental maintenance still showed immediate amplification. Future studies will involve the optimization of the rtPCR sample preparation protocol with focus on lowering the primer concentration 2.5x, as it is thought the high primer concentration may be the cause of immediate amplification during rtPCR.

5.4 Conclusion

With adjustments to the initial protocol, this method can be used to quantify mediators that propagate the Th2-mediated inflammatory response. Preliminary results showed reduced IL-5 and IL-13 production in nonactivated $CD4^+$ T-cells compared to activated $CD4^+$ T-cells, demonstrating an efficacious model to be used for future studies. Although only IL-5 and IL-13 have been quantified using this protocol so far, other cytokines involved in the Th2-mediated inflammatory response can be quantified in the future, such as IL-4, IL-10, and TSLP. Arnold Group member Michelle Meyer is currently investigating levels of TSLP in atopic dermatitis mouse models using a similar protocol for sample preparation. Additionally, this protocol can be altered at the points of T-cell isolation and activation to identify Th1-mediated cells that contribute to other types of inflammation.

CHAPTER 6

INVESTIGATION OF GL-IV-03

FOR NEUROPATHIC PAIN

6.1 Formalin Test Introduction

Neuropathic Pain (NP) is a type of chronic pain that is difficult to treat and occurs in roughly 7% of the United States population.[202] This chronic pain can arise without overt stimulation of associated peripheral sensory endings and is commonly associated with diabetic neuropathy, HIV infection, post-herpetic neuralgia, and chemotherapy treatment for cancer.[203] Despite their controversial use, opioids are currently one of the leading NP therapeutic choices.[204] Other types of treatment include tricyclic antidepressants, serotonin-norepinephrine reuptake inhibitors, and anti-epileptics, which are often followed by second-line opioids and topical drugs or stronger third-line opioids.[204] It is not uncommon for patients to report minimal benefit from these drugs, as less than one-fourth of patients experiencing significant pain relief with these options.[205]

The first line of defense in the central nervous system (CNS) are microglia, the resident macrophages. The role of microglia in the CNS immune system has been implicated in many neuro-inflammatory diseases such as Alzheimer's disease, Parkinson's disease, multiple sclerosis, and neuropathic pain.[206] During inflammation, high amounts of NO are released into the spinal cord, which sensitizes the neurons and reduces firing thresholds, leading to increased neuronal firing and pain sensation.[207] It has been shown NO plays a role in pain, direct injection of NO causes pain, and NOS inhibitors have proven analgesic.[207]

Functional γ-aminobutyric acid type A receptors ($GABA_AR$) are well-characterized in neurons and have been discovered on glial cells. Currently, only α1, α3, and β1 subunits have been described in mouse microglia.[208] However, it has been established that $GABA_AR$ in microglia can mediate immune suppressive signaling.[209] Previous anti-inflammatory studies with novel α2/α3-subtype $GABA_AR$ positive allosteric modulators have shown that these compounds are capable of reducing alveolar macrophage populations,[23,24] as well as demonstrating analgesic properties.[212,26] Taken together, these results suggest

these novel imidazodiazepines are capable of mediating neuropathic pain by reducing inflammation through targeting CNS microglia as well as providing analgesic effect.

To investigate the *in vivo* effect of mediated neuropathic pain, a formalin test was performed in mouse models. The formalin test involves injecting formalin into the paw of a mouse and recording behavior during the biphasic pain response (1-5 min and 20-60 min).[214] The injection provides both mechanical (injection needle) and chemical (formalin causing increased NO and glutamate release) noxious stimuli for triggering two main types of nociceptors: i.) Aδ Nociceptors: myelinated fibers responsible for sharp, acute, localized pain,[217] and representative of Phase I, and ii.) C Nociceptors: unmyelinated fibers responsible for slower, poorly localized, "burning" or "throbbing" inflammatory-mediated pain,[217] and representative of Phase II. Stimulated nociceptors propagate the pain signal through sensory fibers of the dorsal horn by release of Substance P, which activates propagation of the second order neuron in the opposing lateral spinothalamic tract.[218] Once the nerve signal reaches the thalamus, it is relayed to the somatosensory cortex via a third order neuron that defines location and discrimination of pain source (i.e., mouse addressing the injected hind paw).[218]

6.2 Methods

6.2.1 Materials

Chemicals. GL-IV-03 and MP-IV-010 were synthesized using a published procedure.[215] Purity of >99% was determined by HPLC. Identity was determined by ^{1}H-NMR, ^{13}C-NMR, and high-resolution mass spectrometry. Ketoprofen was purchased from MilliporeSigma (St. Louis, MO) and used without further purification.

Drug Formulation. For oral administration, GL-IV-03, MP-IV-010, and ketoprofen were suspended in polyethylene glycol (MilliporeSigma, St. Louis, MO) and diluted in a 2% aqueous solution of hydroxypropyl methylcellulose (MilliporeSigma, St. Louis, MO). The final polyethylene glycol concentration was 2.5%. 1%

Formalin (MilliporeSigma, St. Louis, MO) was prepared in 0.9% NaCl in PBS. All reagents were prepared fresh each day with the exception of 2% aqueous solution of hydroxypropyl methylcellulose.

Experimental Animals. Male C57/BL6J mice were purchased from Jackson Laboratory (Bar Harbor, ME). Animals were housed in a pathogen-free and 12 h light and dark cycle environment under standard humidity conditions. Animals had ad libitum access to food and water. UW-Milwaukee and Columbia University confirmed that all animal experiments were in compliance with Institutional Animal Care and Use Committees.

Preparation of Compound in Vehicle Solution:

Reagents were prepared fresh each day with the exception of 2% hydroxypropyl methylcellulose (HPMC). All four groups were administered 200 µl of vehicle, ketoprofen, or test compound formulations via oral gavage (PO) once daily for five days. The first and second groups received the vehicle solution of 2.5% polyethylene glycol (PEG) in 2% HPMC. The third group received 30 mg/kg of ketoprofen (a commonly prescribed non-steroidal anti-inflammatory drug for treating neuropathic pain) in vehicle solution. 10 mg/kg GL-IV-03 in vehicle solution was delivered to the fourth group. Compounds were first mixed with PEG400 and ground with mortar and pestle until solution became a paste. 2% HPMC was then added to the paste and ground to obtain a suspension. Vials containing drug formulations were held in hand and gently shaken between drug formulation and drug administration to ensure compounds did not become insoluble during the administrations.

Preparation of Formalin Solution:

A 10% formalin solution was diluted 1:10 in 0.9% NaCl solution, yielding a 1% formalin solution for injections. 20 µl injections for four mice required 100 µl (20 µl excess) of 1% formalin solution. 30G x 1/2” Hypodermic BD Needles were used for administration.

6.2.2 Experimental Protocol

Four male C57BL/6 mice were weighed, numbered, and observed for any abnormalities, in which case they were excluded from the experiment. Mice were acclimated in the mouse restraint apparatus (**Figure 47**) for one min, followed by 10 min acclimation in an empty mouse cage (observation chamber) for two days prior to the first day of the experiment. The observation chamber set up was the same as the open field set up and described in **Chapter 4.4**. Due to time required for recovery from hind-paw injections, the study took place over several weeks.

Figure 47. Picture of Mouse Restraint*. Mice were loaded into the chamber tail first with their right hind-paw sticking out of the restraint. The nose cap was then slid into the restraint to prevent excessive movement yet not harm the mouse. 20 µl of 1% formalin solutions was delivered via intraplanar injection to the right hind-paw.*

For the first and second groups, only vehicle solution was administered for five days with the second group also receiving 1% formalin hind-paw injections on the fifth day. While the mouse was in the mouse restraint apparatus, 1% formalin solution was administered to the right hind paw via intraplantar injection just prior to T_{max} of test compound. Control of hind paw, precision of injection site, and rate of administration were crucial in reducing stress on the mice.

Immediately after the hind paw injection, mice were removed and placed into the observation chamber for 5 min to measure Phase I behavior, representing acute peripheral pain mediated by direct

activation of nociceptors. Five min after the hind paw injection, mice were placed back in their home cage for a 15 min quiescent period. Precisely 20 min following hind-paw injection, mice were placed back into the observation chamber for 10 min to measure Phase II behavior, representative of an inflammatory and/or neurogenic response. The Dubuisson and Dennis Model[216] was used to classify Phase I and Phase II behavior into four categories, numbered 0 through 3. Mice were marked 0 for normal behavior, 1 for limping or light resting of injected paw, 2 for noticeable elevation of injected paw, and 3 for licking and biting the injected paw in addition to the previous behaviors.

To conserve time, mice were injected at alternating intervals of 10 and 35 min to ensure vehicle/compound injection time, 1% formalin solution hind-paw injection, Phase I recording, and Phase II recording did not interfere with each other. Time spent participating in behavior during Phase I and Phase II was recorded on a timer and used to calculate a pain score for each mouse.[216]

Pain Score *= Σ(Respective Categorized Behavior x Duration of Behavior) / 300 sec*

Formalin-administered hind paw was observed daily for two weeks following treatment. Swelling and redness persisted up to 40 min after injection. Occasional bruising would last up to 3 days after formalin treatment. After four days, formalin treatment of hind paw was unnoticeable in appearance or behavior of mice.

After initial experimentation, it was determined that several parameters needed to be changed. The pain scores of formalin injected mice were not statistically different compared to non-formalin injected mice for Phases I or II. Difficulty distinguishing between each numbered behavior was of key concern. Furthermore, it was determined that the T_{max} of the compound needed to coincide with the timepoint of the pain response, not the timepoint of the 1% formalin hind-paw injection.

6.2.3 Improved Experimental

To improve model efficacy, the following changes were made to the experimental protocol. Formalin concentration was doubled from 1% to 2% to elicit a stronger pain response in non-treated mice when compared to baseline. Phase I and Phase II were recorded 20 min earlier to match T_{max} of GL-IV-03, and Phase II reduced from 10 min to five min. Behaviors of 0 (no attention to hind paw) vs. 3 (full attention to pain in injected hind paw) were of sole focus during Phase I and Phase II to better distinguish hind paw attention. Mice were observed for both Phase I and Phase II, with behavioral recordings (0 or 3) every 10 sec for the full five min. Total time spent in each behavior was then averaged for all mice, and pain scores were compared between non-formalin vehicle -treated (Group 1), formalin + vehicle -treated (Group 2), formalin + ketoprofen -treated (Group 3), and formalin + GL-IV-03 -treated (Group 4) mice. Number of mice in each group was also increased (N = 12).

After observing no adverse effects in mice four days after formalin treatment, it was confirmed that the same trained mice could be given injections in alternating hind paws once per week, for a maximum of four weeks (two injections to each hind paw). Mice were sacrificed at the completion of the study.

6.3 Results and Discussion

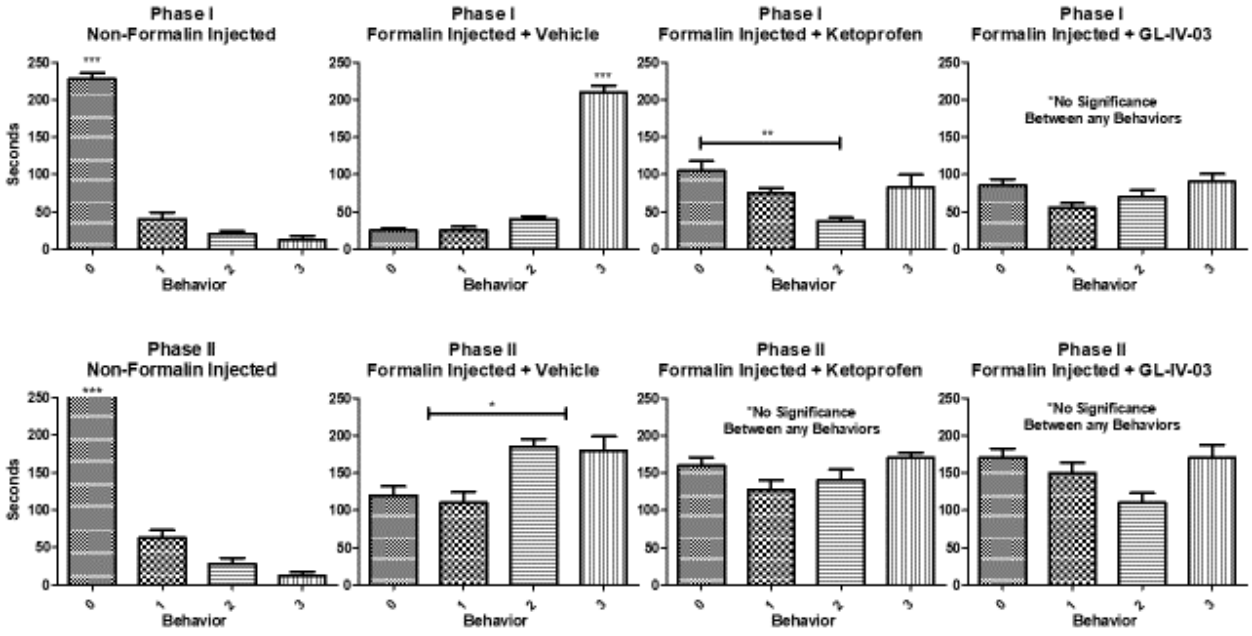

Figure 48. Comparing Classified Pain-Score Behaviors of Different Drug Administrations within Groups. *Mice were considered to have behavioral pain-score ratings of 0, 1, 2, or 3. Mice were split into groups of non-formalin injected, formalin-injected + vehicle, formalin-injected + ketoprofen, and formalin-injected + GL-IV-03. Data are expressed as means ± SEM (n = 4). *, **, and *** indicate p < 0.05, p < 0.01, and p < 0.001 significance, respectively, between vehicle and drug treated groups determined by one-way ANOVA with Bonferroni correlation.*

Figure 48 data are shown using the initial experimental protocol. Non-formalin injected mice delivered vehicle predominantly exhibited behavior scores of 0 during both Phase I and II. Formalin injected mice delivered vehicle showed significant pain scores for Phase I (***) and II (*). In formalin injected mice delivered 30 mg/kg ketoprofen, significance was only found between behaviors 0 and 2 for Phase I. This significance was considered an anomaly due to behavior 1 and 3 not being significantly different than behavior 0. No significance was found between behaviors in formalin injected mice delivered 10 mg/kg GL-IV-03.

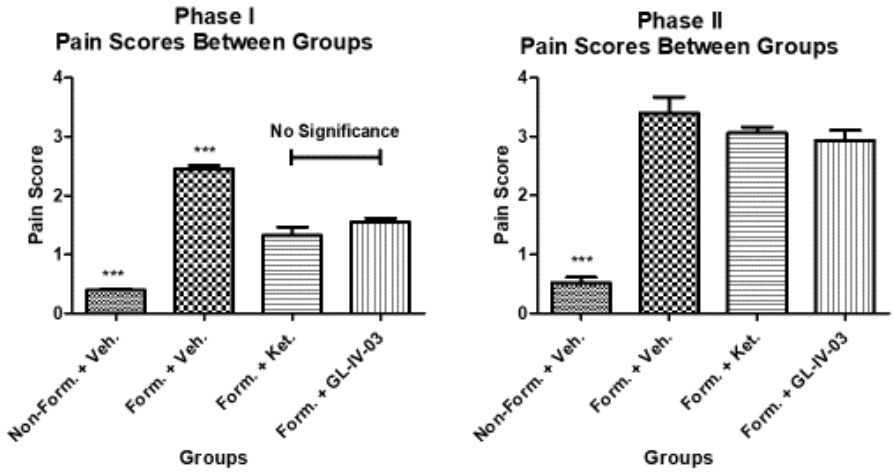

Figure 49. Comparing Classified Pain-Score Behaviors of Different Drug Administrations Between Groups. *Mice were considered to have pain-score behavioral ratings of 0, 1, 2, or 3. Mice were split into groups of non-formalin injected, formalin-injected + Vehicle, formalin-injected + ketoprofen, and formalin-injected + GL-IV-03. Data are expressed as means ± SEM (n = 4). *, **, and *** indicate $p < 0.05$, $p < 0.01$, and $p < 0.001$ significance, respectively, between vehicle and drug treated groups determined by one-way ANOVA with Bonferroni correlation.*

Comparing Phase I pain scores between groups showed a significant difference between the four groups in **Figure 49**. No difference was found in Phase II pain scores comparing formalin-injected + vehicle administered vs. formalin-injected + ketoprofen and formalin-injected + GL-IV-03 groups. Although significance was found between the non-formalin injected + vehicle vs. formalin-injected + vehicle groups for Phase II, the lack of difference between drug treatment vs. vehicle treatment prompted protocol changes previously mentioned in **6.2.3 Improved Experimental**. Furthermore, mice that did not receive formalin hind-paw injections exhibited a non-zero pain score under the initial Experimental Protocol, whereas they should not exhibit any value of pain score.

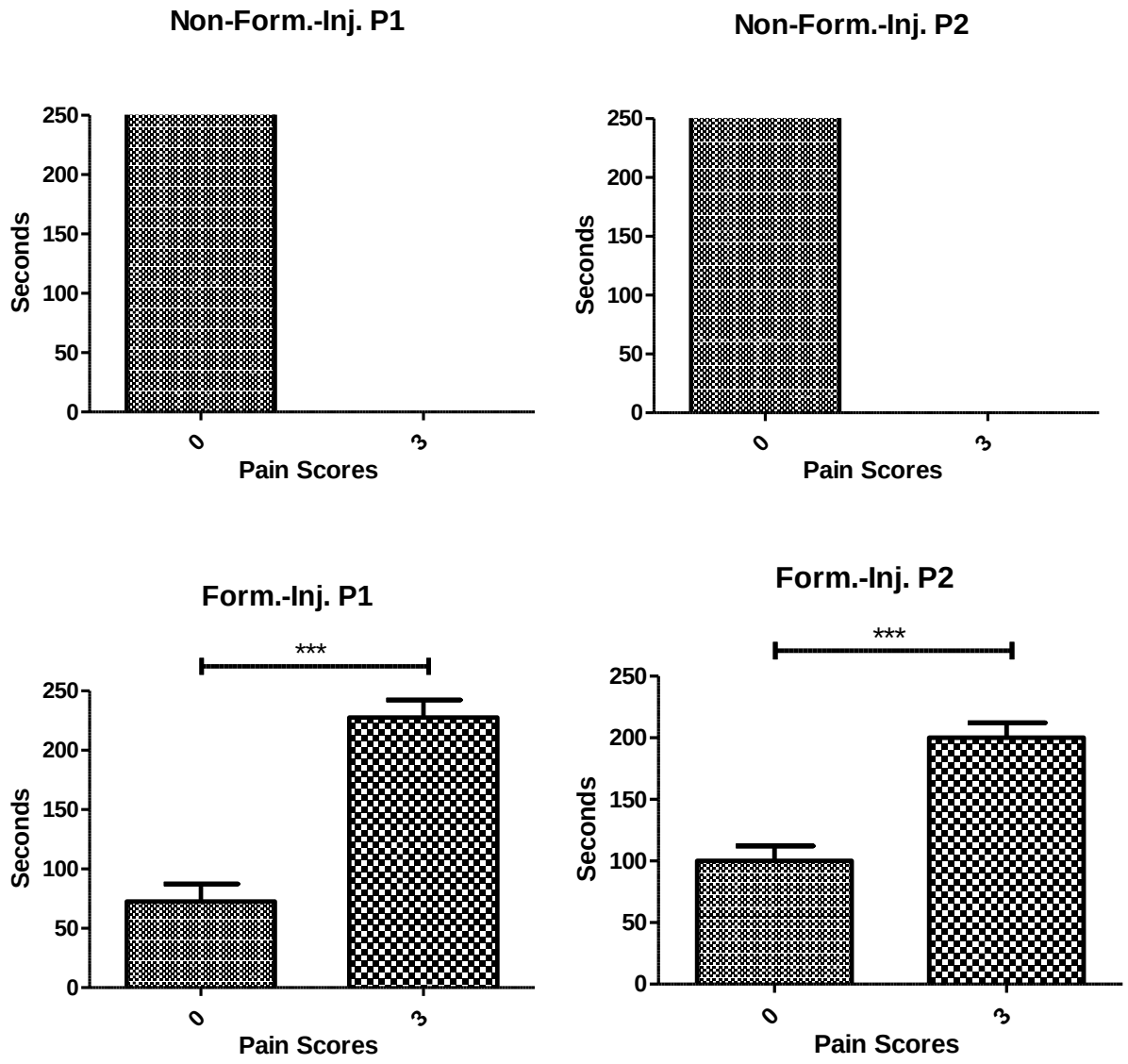

Figure 50. Comparing Classified Pain-Score Behaviors of Non-Formalin Injected and Formalin-Injected Mice under Improved Experimental. *Mice were considered to have behavioral pain-score ratings of 0 or 3. Mice were split into groups of Non-formalin injected + Vehicle and formalin-injected + Vehicle. Data are expressed as means ± SEM (n = 12). *, **, and *** indicate p < 0.05, p < 0.01, and p < 0.001 significance, respectively, between groups determined by one-way unpaired t-test comparing group means. Statistics were not calculated for Non-Formalin injected mice due to no observed recordings of pain score rating of 3.*

The improved experimental allowed easier classification between Behavioral Pain Scores**. Figure 50** shows behavioral pain scores of zero at all timepoints during Phase I and II for all mice that received no formalin hind-paw + vehicle administration. Mice that received formalin injections and vehicle administration exhibited a behavioral pain score of 3 over 75% of the time in Phase I and over two-thirds of the time in Phase II.

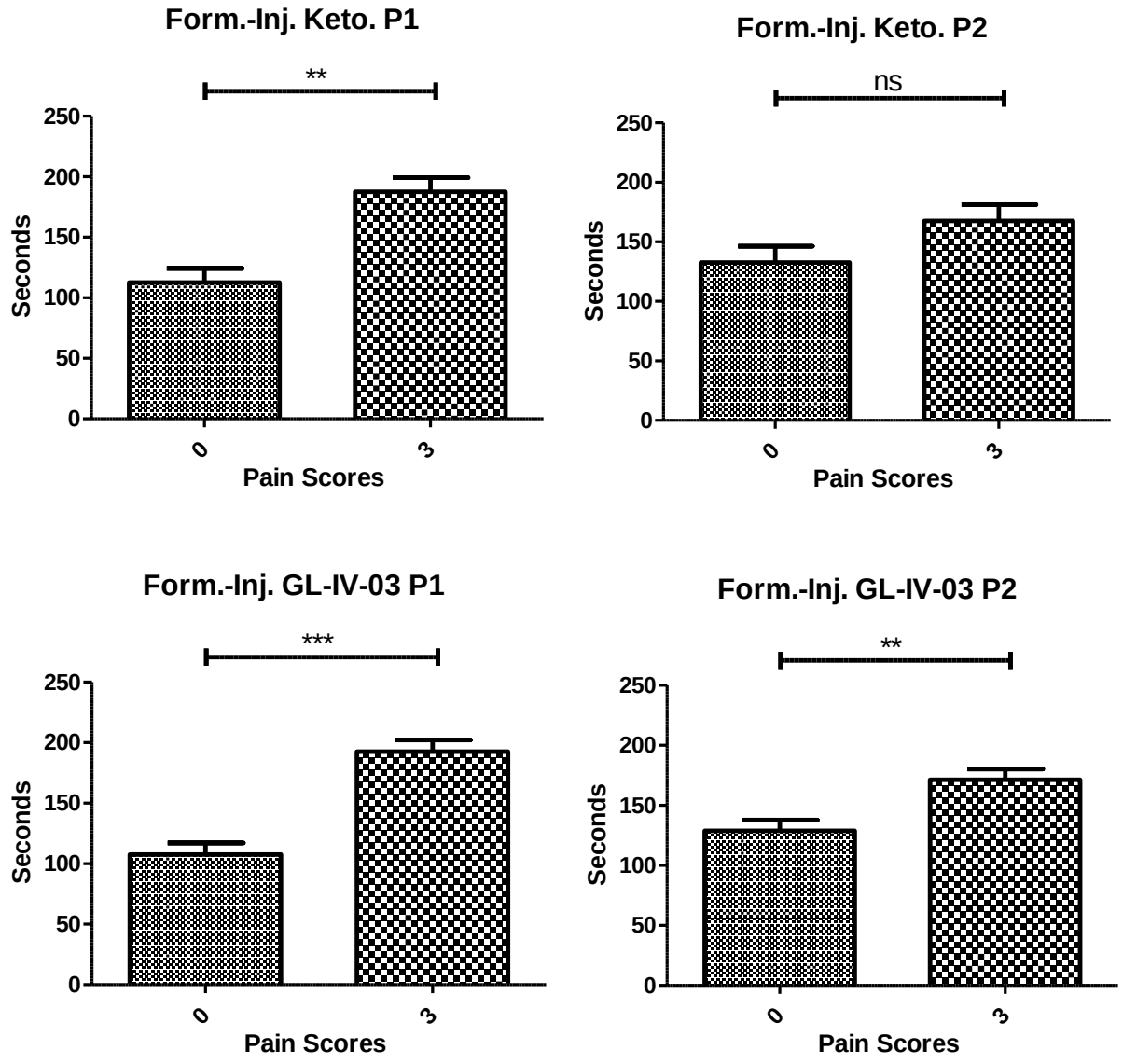

Figure 51. Comparing Classified Pain-Score Behaviors of Formalin Injected and Drug-Administered Mice under Improved Experimental. *Mice were considered to have behavioral pain-score ratings of 0 or 3. Mice were split into groups of formalin-injected + ketoprofen formalin-injected + GL-IV-03. Data are expressed as means ± SEM (n = 12). *, **, and *** indicate $p < 0.05$, $p < 0.01$, and $p < 0.001$ significance, respectively, between groups determined by one-way unpaired t-test comparing group means.*

Figure 51 shows sec spent exhibiting Behavioral Pain Scores of Phase I and II for mice that received formalin hind-paw + ketoprofen or GL-IV-03 administration. Mice that received formalin injections and ketoprofen administration exhibited a Behavioral Pain Score of 3 about 60% of the time in Phase I and roughly 55% of the time in Phase II. Statistical difference was observed between ketoprofen treated and GL-IV-03 treated mice for both Phase I and Phase II.

The antinociceptive effect of GL-IV-03 in the formalin test was then compared with the sensorimotor effect observed in the RotaRod test. Licking and biting of the injured hind paw as a demonstration of nociception was evaluated in comparison to the uninjured contralateral paw. The amount of time attending to this behavior during a five min interval for each treatment is presented in **Figure 52A**. Sensorimotor impairment and sedation were investigated between Phase I and Phase II with mice trained on the RotaRod, as licking and biting can also be representative of sedation or motor inhibition. The amount of time that mice remained balanced on the rod after intraperitoneal (IP) and oral (PO) treatment with GL-IV-03 and MP-IV-010 is summarized in **Figure 52B** and **Figure 52C.**

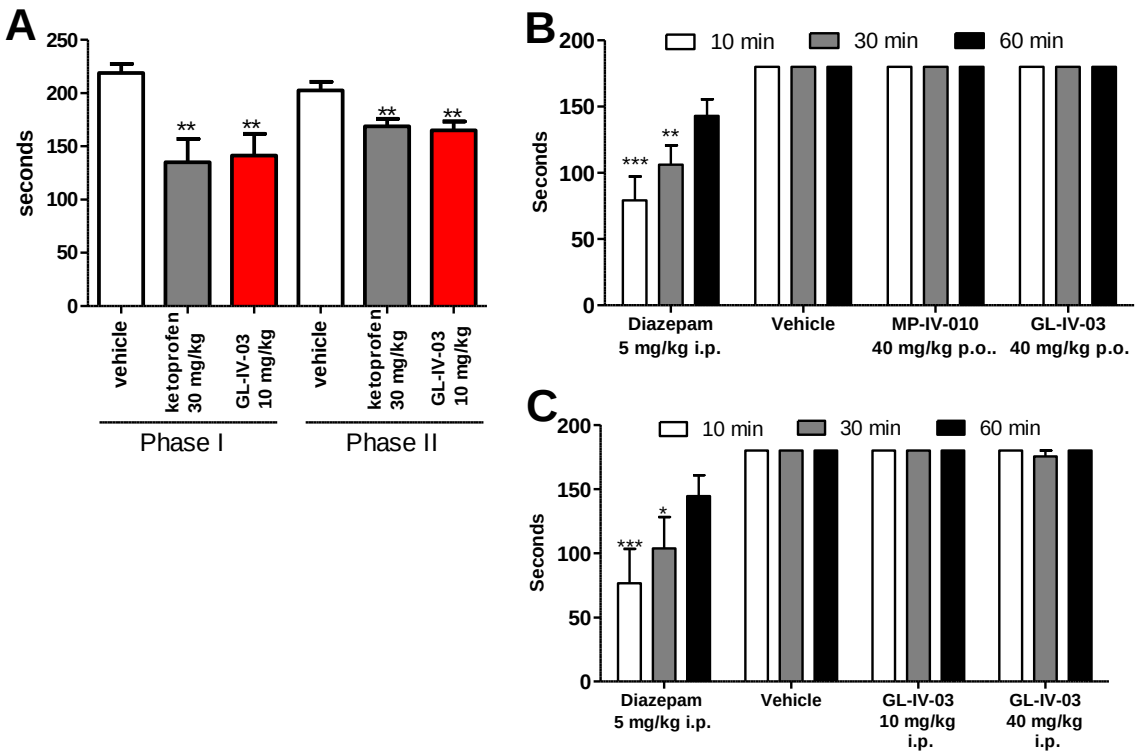

Figure 52. In vivo evaluation of MP-IV-010 and GL-IV-03. *A) Formalin test: Swiss Webster mice were treated orally four days in advance with indicated compounds and doses before the injection of 2% formalin in the right hind paw. Mice were evaluated during the first 5 min (phase 1) and after 20 min (phase 2) for 5 min in 5 sec intervals. Licking and biting the right hind paw during a 5 sec interval was noted and combined as total time addressing the injected paw. Data is given as mean with SEM (n = 12). ** indicate p < 0.01 (unpaired t-test); B) and C) Sensorimotor coordination: Swiss Webster mice were tested on a rotarod at 15 rpm for 3 min at 10, 30, and 60 min following compound treatment at indicated dose and administration. The time of fall was recorded if it occurred prior to 3 min. Data are expressed as mean ± SEM (n = 10). *, (p < 0.05), ** (p < 0.01) or *** (p < 0.001) significance compared to vehicle-treated mice (2 way ANOVA).*

GL-IV-03 exhibited antinociceptive effects in both acute pain (Phase I) and inflammation-mediated pain (Phase II) when administered orally at 10 mg/kg (**Figure 52A**). The effect was similar to non-steroidal anti-inflammatory drug ketoprofen at 30 mg/kg. Both GL-IV-03 and MP-IV-010 - administered PO at 4-fold the effective dose in the formalin test did not cause any sensorimotor deficits as measured on the RotaRod (**Figure 52B**). Furthermore, intraperitoneal (IP) injections of GL-IV-03 at 10 and 40 mg/kg did not influence the ability of mice to balance on a rotating rod for three min (**Figure 52C**). In contrast to diazepam, a benzodiazepine with high affinity for α1β2/3γ2 and other GABAAR subtypes, was sedating at 5 mg/kg IP.

6.4 Conclusion

The formalin test has been shown to be a reliable method to determine behavioral pain-score response in mouse models.[216] Allocating two different phases after hind-paw injection gives insight to the general type of neuropathic pain mediation. Phase I behavior represents acute peripheral pain mediated by direct activation of nociceptors while Phase II behavior represents an inflammatory and/or neurogenic response. Aligning the T_{max} of orally-delivered compounds with the elicited hind-paw pain response and timing of Phase I and II offers important insight as to neuropathic pain reducing properties of lead compounds. Furthermore, performing the RotaRod test between Phase I and Phase II provides information as to whether biting and scratching of the hind paw is due to the elicited pain response or due to sedation or impaired motor coordination.

Although simple in nature, the formalin test is typically a long term study as it requires periods of recovery and limited number of hind-paw injections for each mouse. Furthermore, mice can develop permanent damage after repeated hind-paw injections which may misrepresent behavioral pain-scores. Future experimentation of lead compounds aiming to treat neuropathic pain will utilize the changes described in the Improved Experimental.

Compound GL-IV-03 offers exciting potential as a drug candidate to treat both acute peripheral pain and inflammatory pain while not causing sedation or impaired motor coordination. At 10 mg/kg, GL-IV-03 showed similar potential for neuropathic pain treatment compared to 30 mg/kg ketoprofen in both Phase I and Phase II. It is expected that an increase in GL-IV-03 concentration would yield significantly lower behavioral pain-scores when compared to 30 mg/kg ketoprofen.

6.5 Nerve Ligation Test Background

Neuropathic pain commonly manifests from allodynia, a pain stimulus that does not normally illicit pain, and/or from hyperalgesia, an increase in pain from a stimulus that normally invokes pain.[213] Although the distribution of pain can extend beyond innervation, allodynia and hyperalgesia are typically localized to the site of pain stimulus and involve the corresponding nerve innervations.[68] The underlying mechanisms of allodynia and hyperalgesia contributing to NP are still unclear, however NP is thought to be driven by functional changes in directly injured Aδ- and C-fiber nociceptors as well as changes in fibers that lie adjacent to the injured neurons.[170–172] Injured neurons undergo degeneration, and recruit inflammatory processes around adjacent fibers.[70,96]

It has been shown that lumbar 4 (L4) spinal nerve ligation (SNL) in mice induced persistent hyperalgesia 4–10 days following injury.[137] To investigate this effect, a nerve ligation test protocol was developed for mice based on the widely-used nerve ligation Chung model used in rats.[210] Roughly 98% of sciatic nerve axons arise from the L4 and L5 nerves in rats,[138] whereas mouse sciatic nerve axons arise from the L3 and L4 nerves with a small (< 20%) contribution from the L5 nerve.[110] Occasionally, mice will have an L6 vertebrae, however nerve innervation has been shown to remain the same in these mice (**Figure 53**).[138] Thus, ligation of L3 – L5 nerves (Pudendal, Sural, and Tibial nerves) in mice was required for experimentation comparing ipsilateral vs. contralateral hind-paw reflex in groups of mice delivered either sham ligation, ligation, or ligation + drug administration.

To perform the nerve ligation test in mice, several weeks of training were required on newly sacrificed mice. Training consisted of correctly palpating the femur, making a small 5 mm incision parallel to and 1.5 mm posterior to the femur, separating muscles close to femur to expose sciatic nerve, using a suture to make a surgical knot around the isolated nerve, and guiding nerve, muscle fiber, and skin tissue back into location. The incision was then closed with a suture and surgical knot. Key steps of the nerve ligation surgery in live mice are shown in **Figure 54**.

In live mice, several steps also need to take place to preserve live tissue. Mice would be placed on heat pads once anesthetized and would have eyes and exposed nerves continually lubricated with saline solution. Clotting agents would also be readily available to prevent excessive blood loss. Experimentation would not begin until after three days post-surgery to allow diminished nerve hypersensitivity.

6.6 Methods

Experimental Animals. Male C57/BL6J mice were purchased from Jackson Laboratory (Bar Harbor, ME). Animals were housed in a pathogen-free and 12 h light and dark cycle environment under standard humidity conditions. Animals had ad libitum access to food and water. UW-Milwaukee and Columbia University confirmed that all animal experiments were in compliance with Institutional Animal Care and Use Committees.

Spinal nerve ligation. Paraspinal muscles around L3-S1 nerves were bluntly dissected and the L5 transverse process was carefully removed to expose the ventral ramus of the L3 – L5 spinal nerves. The spinal nerves were tightly ligated with silk suture (6-0; Look, Surgical Specialties Corporation, Reading, PA) and transected distal to the ligation. In sham ligated mice, the L5 transverse process was exposed but not removed and the spinal nerves were not touched.

Behavioral testing. In live mice, the radiant heat paw withdrawal test or the Von Frey test can be used to assess hypersensitivity. Mice are allowed to freely move on a caged floor surrounded by a plexiglass chamber. For the radiant heat paw withdrawal test, heat is applied to the plantar hind paw and reaction time is recorded. The Von Frey test involves a probe measuring the force applied to the planter hind paw before the mouse reacts to the stimulus. Ipsilateral and contralateral sides are tested in alternation and 4–5 measurements are obtained for each paw at each time point. Paw withdrawal/reaction latencies are assessed at T_{max} of compound of interest.

6.7 Results and Discussion

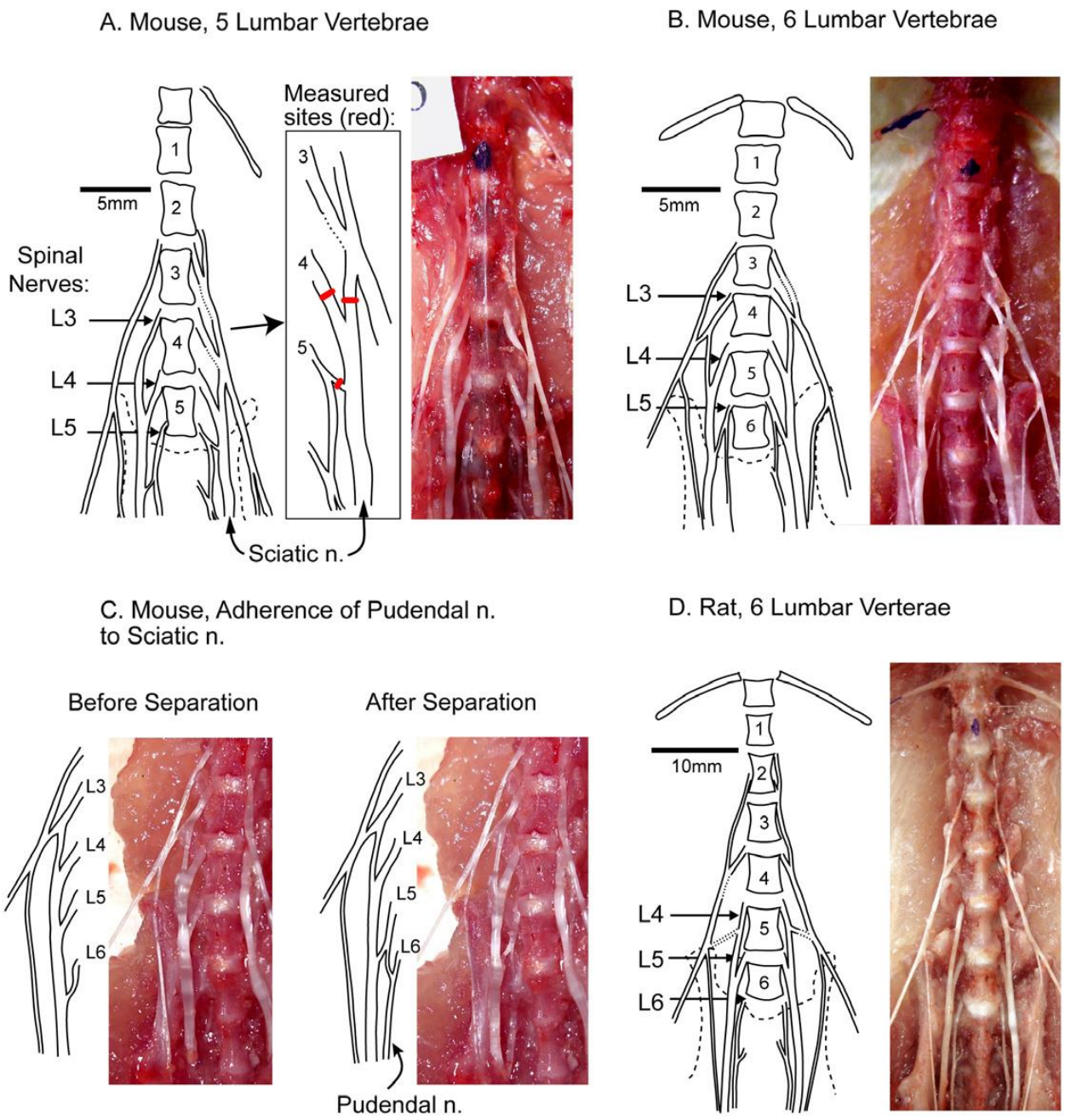

Figure 53. Posterior View of Sciatic Nerve Innervation of Mice and Rats*. Sciatic nerves in mice typically innervate from L3 – L5 vertebrae. The pudendal, sural, and tibial nerves all require isolation and ligation for complete distal transection of the sciatic nerve. Adaptations to the nerve ligation Chung model in rats was used to perform nerve ligation in mice.*[138]

Training consisted of performing the nerve ligation surgery on the sciatic nerve before advancing to ligation of other nerves. As a guide, **Figure 53** was used as well as adaptations to the nerve ligation Chung model.[210]

Figure 54. Sciatic Nerve Ligation Surgery in Mice*. The right leg of anesthetized mice is shaved and disinfected. A 5 mm parallel incision is made 1.5 mm posterior to the femur (**Top Left, Top Middle**). Muscles close to femur were separated (**Top Right**) to expose sciatic nerve (**Bottom Left**). A white suture was tied into a surgical knot around the isolated nerve (**Bottom Middle**). The nerve, muscle fiber, and skin tissue were guided back into original location. The incision was then closed with a suture and surgical knot (**Bottom Right**). Pictures from the Javid Bambad ARAS Medical Group.[69]*

Successful ligation of the sciatic nerve proved to be difficult in newly sacrificed mice even after four weeks of training. **Figure 54** diagrams the process of a sciatic nerve ligation in a live mouse (ARAS Medical Group).

6.8 Conclusion

At the completion of training, it was determined that the nerve ligation test would not be further pursued in live mice. Several factors contributed to this decision, including but not restricted to: limited skill identifying and uncovering all nerves innervating the sciatic nerve, difficulty performing successful nerve ligations without inflicting unnecessary nerve and muscle tissue damage, and most importantly, IACUC concerns regarding a ~50% survival rate post-surgery as reported from collaborators at the Medical College of Wisconsin.

However, with experienced personnel, the nerve ligation test is a valuable model to express allodynia and hyperalgesia in live mice. Comparing sham ligation, ligation, and ligation + drug administration provides insight as to the effect a lead compound may have in the treatment of neuropathic pain. Furthermore, this test in parallel with the formalin test offers a more complete understanding of the underlying mechanisms that may contribute to neuropathic pain.

REFERENCES

1. Richter, L.; de Graaf, C.; Sieghart, W.; Varagic, Z.; Morzinger, M.; de Esch, I. J.; Ecker, G. F.; Ernst, M., Diazepam-bound GABAA receptor models identify new benzodiazepine binding-site ligands. *Nature chemical biology* **2012**, *8* (5), 455-64.
2. Olsen, R. W.; Sieghart, W., GABA A receptors: subtypes provide diversity of function and pharmacology. *Neuropharmacology* **2009**, *56* (1), 141-8.
3. Olsen, R. W.; Sieghart, W., International Union of Pharmacology. LXX. Subtypes of gamma-aminobutyric acid(A) receptors: classification on the basis of subunit composition, pharmacology, and function. Update. *Pharmacological reviews* **2008**, *60* (3), 243-60.
4. Siegel, G. J., *Basic neurochemistry : molecular, cellular, and medical aspects*. 6th ed.; Lippincott Williams & Wilkins: Philadelphia, **1999**; p xxi, 1183.
5. Sieghart, W., Structure and pharmacology of gamma-aminobutyric acidA receptor subtypes. *Pharmacological reviews* **1995**, *47* (2), 181-234.
6. Griffin, C. E., 3rd; Kaye, A. M.; Bueno, F. R.; Kaye, A. D., Benzodiazepine pharmacology and central nervous system-mediated effects. *The Ochsner journal* **2013**, *13* (2), 214-23.
7. Donaldson, M.; Gizzarelli, G.; Chanpong, B., Oral sedation: a primer on anxiolysis for the adult patient. *Anesthesia progress* **2007**, *54* (3), 118-28; quiz 129.
8. Tan, K. R.; Rudolph, U.; Luscher, C., Hooked on benzodiazepines: GABAA receptor subtypes and addiction. *Trends in neurosciences* **2011**, *34* (4), 188-97.
9. Yocum, G. T.; Turner, D. L.; Danielsson, J.; Barajas, M. B.; Zhang, Y.; Xu, D.; Harrison, N. L.; Homanics, G. E.; Farber, D. L.; Emala, C. W., GABAA receptor alpha4-subunit knockout enhances lung inflammation and airway reactivity in a murine asthma model. *American journal of physiology. Lung cellular and molecular physiology* **2017**, *313* (2), L406-L415.
10. Mizuta, K.; Xu, D.; Pan, Y.; Comas, G.; Sonett, J. R.; Zhang, Y.; Panettieri, R. A., Jr.; Yang, J.; Emala, C. W., Sr., GABAA receptors are expressed and facilitate relaxation in airway smooth muscle. *American journal of physiology. Lung cellular and molecular physiology* **2008**, *294* (6), L1206-16.
11. Lee, M.; Schwab, C.; McGeer, P. L., Astrocytes are GABAergic cells that modulate microglial activity. *Glia* **2011**, *59* (1), 152-65.
12. Dunham, N. W.; Miya, T. S., A note on a simple apparatus for detecting neurological deficit in rats and mice. *Journal of the American Pharmaceutical Association. American Pharmaceutical Association* **1957,** *46* (3), 208-9.
13. Kudo, M.; Ishigatsubo, Y.; Aoki, I., Pathology of asthma. *Frontiers in microbiology* **2013**, *4*, 263.
14. Dionisio, L.; Jose De Rosa, M.; Bouzat, C.; Esandi Mdel, C., An intrinsic GABAergic system in human lymphocytes. *Neuropharmacology* **2011**, *60* (2-3), 513-9.
15. Reyes-Garcia, M. G.; Hernandez-Hernandez, F.; Hernandez-Tellez, B.; Garcia-Tamayo, F., GABA (A) receptor subunits RNA expression in mice peritoneal macrophages modulate their IL-6/IL-12 production. *Journal of neuroimmunology* **2007**, *188* (1-2), 64-8.
16. Cockcroft DW. Methacholine Challenge Testing in the Diagnosis of Asthma. Chest. **2020** Aug;158(2):433-434. doi: 10.1016/j.chest.2020.04.034. PMID: 32768054.
17. Nieman AN, Li G, Zahn NM, Mian MY, Mikulsky BN, Hoffman DA, Wilcox TM, Kehoe AS, Luecke IW, Poe MM, Alvarez-Carbonell D, Cook JM, Stafford DC, Arnold LA. Targeting Nitric Oxide Production in Microglia with Novel Imidazodiazepines for Nonsedative Pain Treatment. ACS Chem Neurosci. **2020** Jul

1;11(13):2019-2030. doi: 10.1021/acschemneuro.0c00324. Epub 2020 Jun 18. PMID: 32511908; PMCID: PMC7380323.
18. Koretzky, G. A., Multiple roles of CD4 and CD8 in T cell activation. *Journal of immunology* **2010,** *185* (5), 2643-4.
19. Maslan, J.; Mims, J. W., What is asthma? Pathophysiology, demographics, and health care costs. *Otolaryngologic clinics of North America* **2014,** *47* (1), 13-22.
20. Romagnani, S., T-cell subsets (Th1 versus Th2). *Annals of allergy, asthma & immunology : official publication of the American College of Allergy, Asthma, & Immunology* **2000,** *85* (1), 9-18; quiz 18, 21.
21. Lee, M.; Schwab, C.; McGeer, P. L., Astrocytes are GABAergic cells that modulate microglial activity. *Glia* **2011,** *59* (1), 152-65.
22. Wu, C.; Qin, X.; Du, H.; Li, N.; Ren, W.; Peng, Y., The immunological function of GABAergic system. *Frontiers in bioscience* **2017,** *22*, 1162-1172.
23. Forkuo, G. S.; Nieman, A. N.; Yuan, N. Y.; Kodali, R.; Yu, O. B.; Zahn, N. M.; Jahan, R.; Li, G.; Stephen, M. R.; Guthrie, M. L.; Poe, M. M.; Hartzler, B. D.; Harris, T. W.; Yocum, G. T.; Emala, C. W.; Steeber, D. A.; Stafford, D. C.; Cook, J. M.; Arnold, L. A., Alleviation of Multiple Asthmatic Pathologic Features with Orally Available and Subtype Selective GABAA Receptor Modulators. *Molecular pharmaceutics* **2017,** *14* (6), 2088-2098.
24. Forkuo, G. S.; Nieman, A. N.; Kodali, R.; Zahn, N. M.; Li, G.; Rashid Roni, M. S.; Stephen, M. R.; Harris, T. W.; Jahan, R.; Guthrie, M. L.; Yu, O. B.; Fisher, J. L.; Yocum, G. T.; Emala, C. W.; Steeber, D. A.; Stafford, D. C.; Cook, J. M.; Arnold, L. A., A Novel Orally Available Asthma Drug Candidate That Reduces Smooth Muscle Constriction and Inflammation by Targeting GABAA Receptors in the Lung. *Molecular pharmaceutics* **2018**.
25. Di Lio, A.; Benke, D.; Besson, M.; Desmeules, J.; Daali, Y.; Wang, Z. J.; Edwankar, R.; Cook, J. M.; Zeilhofer, H. U., HZ166, a novel GABAA receptor subtype-selective benzodiazepine site ligand, is antihyperalgesic in mouse models of inflammatory and neuropathic pain. *Neuropharmacology* **2011,** *60* (4), 626-32.
26. Lewter, L. A.; Fisher, J. L.; Siemian, J. N.; Methuku, K. R.; Poe, M. M.; Cook, J. M.; Li, J. X., Antinociceptive Effects of a Novel alpha2/alpha3-Subtype Selective GABAA Receptor Positive Allosteric Modulator. *ACS chemical neuroscience* **2017,** *8* (6), 1305-1312.
27. Cooper, J. R.; Bloom, F. E.; Roth, R. H., *The biochemical basis of neuropharmacology*. 8th ed.; Oxford University Press: Oxford ; New York, **2003**; p vii, 405.
28. Spiering, M. J., The discovery of GABA in the brain. *The Journal of biological chemistry* **2018,** *293* (49), 19159-19160.
29. Roberts, E.; Frankel, S., gamma-Aminobutyric acid in brain: its formation from glutamic acid. *The Journal of biological chemistry* **1950,** *187* (1), 55-63.
30. W.G. Van der Kloot; J. Robbins (**1959**). The effects of GABA and picrotoxin on the junctional potential and contraction of crayfish muscle. Experientia. 15: 36.
31. Edwards, D. H.; Heitler, W. J.; Krasne, F. B., Fifty years of a command neuron: the neurobiology of escape behavior in the crayfish. *Trends in neurosciences* **1999,** *22* (4), 153-61.
32. Hayashi, T., Inhibition and excitation due to gamma-aminobutyric acid in the central nervous system. *Nature* **1958,** *182* (4642), 1076-7.
33. Iversen, L. L.; Neal, M. J., The uptake of [3H]GABA by slices of rat cerebral cortex. *Journal of neurochemistry* **1968,** *15* (10), 1141-9.
34. Krnjevic, K.; Schwartz, S., The action of gamma-aminobutyric acid on cortical neurones. *Experimental brain research* **1967,** *3* (4), 320-36.
35. Cooper, J. R.; Bloom, F. E.; Roth, R. H., *The biochemical basis of neuropharmacology*. 8th ed.; Oxford University Press: Oxford ; New York, **2003**; p vii, 405 p.

36. Siegel, G. J., *Basic neurochemistry : molecular, cellular, and medical aspects*. 6th ed.; Lippincott Williams & Wilkins: Philadelphia, **1999**; p xxi, 1183.
37. Fenalti, G.; Law, R. H.; Buckle, A. M.; Langendorf, C.; Tuck, K.; Rosado, C. J.; Faux, N. G.; Mahmood, K.; Hampe, C. S.; Banga, J. P.; Wilce, M.; Schmidberger, J.; Rossjohn, J.; El-Kabbani, O.; Pike, R. N.; Smith, A. I.; Mackay, I. R.; Rowley, M. J.; Whisstock, J. C., GABA production by glutamic acid decarboxylase is regulated by a dynamic catalytic loop. *Nature structural & molecular biology* **2007,** *14* (4), 280-6.
38. Jin, X. T.; Galvan, A.; Wichmann, T.; Smith, Y., Localization and Function of GABA Transporters GAT-1 and GAT-3 in the Basal Ganglia. *Frontiers in systems neuroscience* **2011,** *5*, 63.
39. Olsen, R. W., Tobin, A. J., Molecular biology of $GABA_A$ receptors. *FASEB journal : official publication of the Federation of American Societies for Experimental Biology* **1990,** *4*, 1469-1480.
40. Bowery, N. G.; Smart, T. G., GABA and glycine as neurotransmitters: a brief history. *British journal of pharmacology* **2006,** *147 Suppl 1*, S109-19.
41. Schofield, P. R.; Darlison, M. G.; Fujita, N.; Burt, D. R.; Stephenson, F. A.; Rodriguez, H.; Rhee, L. M.; Ramachandran, J.; Reale, V.; Glencorse, T. A.; et al., Sequence and functional expression of the GABA A receptor shows a ligand-gated receptor super-family. *Nature* **1987,** *328* (6127), 221-7.
42. Zhu, S.; Noviello, C. M.; Teng, J.; Walsh, R. M., Jr.; Kim, J. J.; Hibbs, R. E., Structure of a human synaptic GABAA receptor. *Nature* **2018,** *559* (7712), 67-72.
43. Miller, P. S.; Aricescu, A. R., Crystal structure of a human GABAA receptor. *Nature* **2014,** *512* (7514), 270-5.
44. Richter, L.; de Graaf, C.; Sieghart, W.; Varagic, Z.; Morzinger, M.; de Esch, I. J.; Ecker, G. F.; Ernst, M., Diazepam-bound GABAA receptor models identify new benzodiazepine binding-site ligands. *Nature chemical biology* **2012,** *8* (5), 455-64.
45. Olsen, R. W.; Sieghart, W., GABA A receptors: subtypes provide diversity of function and pharmacology. *Neuropharmacology* **2009,** *56* (1), 141-8.
46. Olsen, R. W.; Sieghart, W., International Union of Pharmacology. LXX. Subtypes of gamma-aminobutyric acid(A) receptors: classification on the basis of subunit composition, pharmacology, and function. Update. *Pharmacological reviews* **2008,** *60* (3), 243-60.
47. Sieghart, W.; Savic, M. M., International Union of Basic and Clinical Pharmacology. CVI: GABAA Receptor Subtype- and Function-selective Ligands: Key Issues in Translation to Humans. *Pharmacological reviews* **2018,** *70* (4), 836-878.
48. Chen, X., van Gerven, J., Cohen, A. *et al.* Human pharmacology of positive GABA-A subtype-selective receptor modulators for the treatment of anxiety. *Acta Pharmacol Sin* 40**,** 571–582 (**2019**). https://doi.org/10.1038/s41401-018-0185-5
49. Krall, J., Balle, T., Krogsgaard-Larsen, N., Sorensen, T., Frolund, B., Chapter 8 - $GABA_A$ Receptor Partial Agonists and Antagonists: Structure, Binding Mode, and Pharmacology. In *Diversity and functions of GABA receptors : a tribute to Hanns Möhler, Part A*, Rudolph, U., Ed. Els: **2015**; pp 201-227.
50. Johnston, G. A., Muscimol as an ionotropic GABA receptor agonist. *Neurochemical research* **2014,** *39* (10), 1942-7.
51. Wafford, K. A.; Ebert, B., Gaboxadol--a new awakening in sleep. *Current opinion in pharmacology* **2006,** *6* (1), 30-6.
52. Lankford, D. A.; Corser, B. C.; Zheng, Y. P.; Li, Z.; Snavely, D. B.; Lines, C. R.; Deacon, S., Effect of gaboxadol on sleep in adult and elderly patients with primary insomnia: results from two randomized, placebo-controlled, 30-night polysomnography studies. *Sleep* **2008,** *31* (10), 1359-70.
53. Skerritt, J. H.; Johnston, G. A., Diazepam stimulates the binding of GABA and muscimol but not THIP to rat brain membranes. *Neuroscience letters* **1983,** *38* (3), 315-20.
54. Massey, S. C.; Linn, D. M.; Kittila, C. A.; Mirza, W., Contributions of GABAA receptors and GABAC receptors to acetylcholine release and directional selectivity in the rabbit retina. *Visual neuroscience* **1997,** *14* (5), 939-48.

55. Ueno, S.; Bracamontes, J.; Zorumski, C.; Weiss, D. S.; Steinbach, J. H., Bicuculline and gabazine are allosteric inhibitors of channel opening of the GABAA receptor. *The Journal of neuroscience : the official journal of the Society for Neuroscience* **1997,** *17* (2), 625-34.
56. Johnston, G. A., Advantages of an antagonist: bicuculline and other GABA antagonists. *British journal of pharmacology* **2013,** *169* (2), 328-36.
57. Krishek, B. J.; Moss, S. J.; Smart, T. G., A functional comparison of the antagonists bicuculline and picrotoxin at recombinant GABAA receptors. *Neuropharmacology* **1996,** *35* (9-10), 1289-98.
58. Olsen, R. W., Picrotoxin-like channel blockers of GABAA receptors. *Proceedings of the National Academy of Sciences of the United States of America* **2006,** *103* (16), 6081-2.
59. Olsen, R. W., GABAA receptor: Positive and negative allosteric modulators. *Neuropharmacology* **2018,** *136* (Pt A), 10-22.
60. Wang, D. S.; Buckinx, R.; Lecorronc, H.; Mangin, J. M.; Rigo, J. M.; Legendre, P., Mechanisms for picrotoxinin and picrotin blocks of alpha2 homomeric glycine receptors. *The Journal of biological chemistry* **2007,** *282* (22), 16016-35.
61. Xu, M.; Covey, D. F.; Akabas, M. H., Interaction of picrotoxin with GABAA receptor channel-lining residues probed in cysteine mutants. *Biophysical journal* **1995,** *69* (5), 1858-67.
62. Sternbach, L. H., The benzodiazepine story. *Journal of medicinal chemistry* **1979,** *22* (1), 1-7.
63. Fuentes, A. V.; Pineda, M. D.; Venkata, K. C. N., Comprehension of Top 200 Prescribed Drugs in the US as a Resource for Pharmacy Teaching, Training and Practice. *Pharmacy* **2018,** *6* (2).
64. Tan, K. R.; Rudolph, U.; Luscher, C., Hooked on benzodiazepines: GABAA receptor subtypes and addiction. *Trends in neurosciences* **2011,** *34* (4), 188-97.
65. Clayton, T.; Chen, J. L.; Ernst, M.; Richter, L.; Cromer, B. A.; Morton, C. J.; Ng, H.; Kaczorowski, C. C.; Helmstetter, F. J.; Furtmuller, R.; Ecker, G.; Parker, M. W.; Sieghart, W.; Cook, J. M., An updated unified pharmacophore model of the benzodiazepine binding site on gamma-aminobutyric acid(a) receptors: correlation with comparative models. *Current medicinal chemistry* **2007,** *14* (26), 2755-75.
66. Prevot, T. D.; Li, G.; Vidojevic, A.; Misquitta, K. A.; Fee, C.; Santrac, A.; Knutson, D. E.; Stephen, M. R.; Kodali, R.; Zahn, N. M.; Arnold, L. A.; Scholze, P.; Fisher, J. L.; Markovic, B. D.; Banasr, M.; Cook, J. M.; Savic, M.; Sibille, E., Novel Benzodiazepine-Like Ligands with Various Anxiolytic, Antidepressant, or Pro-Cognitive Profiles. *Molecular neuropsychiatry* **2019,** *5* (2), 84-97.
67. Gill, K. M.; Lodge, D. J.; Cook, J. M.; Aras, S.; Grace, A. A., A novel alpha5GABA(A)R-positive allosteric modulator reverses hyperactivation of the dopamine system in the MAM model of schizophrenia. *Neuropsychopharmacology : official publication of the American College of Neuropsychopharmacology* **2011,** *36* (9), 1903-11.
68. Jensen TS, Finnerup NB. Allodynia and hyperalgesia in neuropathic pain: clinical manifestations and mechanisms. Lancet Neurol **2014**; 13:924-35
69. Bambad, J.; et. al., ARAS Medical Group. **2021** https://www.youtube.com/watch?v=UjdmdQ4Of_k&t=260s
70. Sugiura S, Lahav R, Han J, Kou SY, Banner LR, de Pablo F, Patterson PH. Leukaemia inhibitory factor is required for normal inflammatory responses to injury in the peripheral and central nervous systems in vivo and is chemotactic for macrophages in vitro. Eur J Neurosci **2000**; 12:457–466. [PubMed: 10712626]
71. Forkuo, G. S.; Guthrie, M. L.; Yuan, N. Y.; Nieman, A. N.; Kodali, R.; Jahan, R.; Stephen, M. R.; Yocum, G. T.; Treven, M.; Poe, M. M.; Li, G.; Yu, O. B.; Hartzler, B. D.; Zahn, N. M.; Ernst, M.; Emala, C. W.; Stafford, D. C.; Cook, J. M.; Arnold, L. A., Development of GABAA Receptor Subtype-Selective Imidazobenzodiazepines as Novel Asthma Treatments. *Molecular pharmaceutics* **2016,** *13* (6), 2026-38.
72. Jahan, R.; Stephen, M. R.; Forkuo, G. S.; Kodali, R.; Guthrie, M. L.; Nieman, A. N.; Yuan, N. Y.; Zahn, N. M.; Poe, M. M.; Li, G.; Yu, O. B.; Yocum, G. T.; Emala, C. W.; Stafford, D. C.; Cook, J. M.; Arnold, L. A., Optimization of substituted imidazobenzodiazepines as novel asthma treatments. *European journal of medicinal chemistry* **2017,** *126*, 550-560.

73. Whitwam, J. G.; Amrein, R., Pharmacology of flumazenil. *Acta anaesthesiologica Scandinavica. Supplementum* **1995,** *108*, 3-14.
74. Hadingham, K. L.; Garrett, E. M.; Wafford, K. A.; Bain, C.; Heavens, R. P.; Sirinathsinghji, D. J.; Whiting, P. J., Cloning of cDNAs encoding the human gamma-aminobutyric acid type A receptor alpha 6 subunit and characterization of the pharmacology of alpha 6-containing receptors. *Molecular pharmacology* **1996,** *49* (2), 253-9.
75. Clayton, T.; Poe, M. M.; Rallapalli, S.; Biawat, P.; Savic, M. M.; Rowlett, J. K.; Gallos, G.; Emala, C. W.; Kaczorowski, C. C.; Stafford, D. C.; Arnold, L. A.; Cook, J. M., A Review of the Updated Pharmacophore for the Alpha 5 GABA(A) Benzodiazepine Receptor Model. *International journal of medicinal chemistry* **2015,** *2015*, 430248.
76. Hanchar, H. J.; Chutsrinopkun, P.; Meera, P.; Supavilai, P.; Sieghart, W.; Wallner, M.; Olsen, R. W., Ethanol potently and competitively inhibits binding of the alcohol antagonist Ro15-4513 to alpha4/6beta3delta GABAA receptors. *Proceedings of the National Academy of Sciences of the United States of America* **2006,** *103* (22), 8546-51.
77. Uhlen, M.; Zhang, C.; Lee, S.; Sjostedt, E.; Fagerberg, L.; Bidkhori, G.; Benfeitas, R.; Arif, M.; Liu, Z.; Edfors, F.; Sanli, K.; von Feilitzen, K.; Oksvold, P.; Lundberg, E.; Hober, S.; Nilsson, P.; Mattsson, J.; Schwenk, J. M.; Brunnstrom, H.; Glimelius, B.; Sjoblom, T.; Edqvist, P. H.; Djureinovic, D.; Micke, P.; Lindskog, C.; Mardinoglu, A.; Ponten, F., A pathology atlas of the human cancer transcriptome. *Science* **2017,** *357* (6352).
78. Uhlen, M.; Fagerberg, L.; Hallstrom, B. M.; Lindskog, C.; Oksvold, P.; Mardinoglu, A.; Sivertsson, A.; Kampf, C.; Sjostedt, E.; Asplund, A.; Olsson, I.; Edlund, K.; Lundberg, E.; Navani, S.; Szigyarto, C. A.; Odeberg, J.; Djureinovic, D.; Takanen, J. O.; Hober, S.; Alm, T.; Edqvist, P. H.; Berling, H.; Tegel, H.; Mulder, J.; Rockberg, J.; Nilsson, P.; Schwenk, J. M.; Hamsten, M.; von Feilitzen, K.; Forsberg, M.; Persson, L.; Johansson, F.; Zwahlen, M.; von Heijne, G.; Nielsen, J.; Ponten, F., Proteomics. Tissue-based map of the human proteome. *Science* **2015,** *347* (6220), 1260419.
79. Thul, P. J.; Akesson, L.; Wiking, M.; Mahdessian, D.; Geladaki, A.; Ait Blal, H.; Alm, T.; Asplund, A.; Bjork, L.; Breckels, L. M.; Backstrom, A.; Danielsson, F.; Fagerberg, L.; Fall, J.; Gatto, L.; Gnann, C.; Hober, S.; Hjelmare, M.; Johansson, F.; Lee, S.; Lindskog, C.; Mulder, J.; Mulvey, C. M.; Nilsson, P.; Oksvold, P.; Rockberg, J.; Schutten, R.; Schwenk, J. M.; Sivertsson, A.; Sjostedt, E.; Skogs, M.; Stadler, C.; Sullivan, D. P.; Tegel, H.; Winsnes, C.; Zhang, C.; Zwahlen, M.; Mardinoglu, A.; Ponten, F.; von Feilitzen, K.; Lilley, K. S.; Uhlen, M.; Lundberg, E., A subcellular map of the human proteome. *Science* **2017,** *356* (6340).
80. Geigerseder C, Doepner R, Thalhammer A, Frungieri MB, Gamel-Didelon K, Calandra RS, Köhn FM, Mayerhofer A. Evidence for a GABAergic system in rodent and human testis: local GABA production and GABA receptors. Neuroendocrinology. **2003** May;77(5):314-23. doi: 10.1159/000070897. PMID: 12806177.
81. Gallos, G.; Yim, P.; Chang, S.; Zhang, Y.; Xu, D.; Cook, J. M.; Gerthoffer, W. T.; Emala, C. W., Sr., Targeting the restricted alpha-subunit repertoire of airway smooth muscle GABAA receptors augments airway smooth muscle relaxation. *American journal of physiology. Lung cellular and molecular physiology* **2012,** *302* (2), L248-56.
82. Dionisio, L.; Jose De Rosa, M.; Bouzat, C.; Esandi Mdel, C., An intrinsic GABAergic system in human lymphocytes. *Neuropharmacology* **2011,** *60* (2-3), 513-9.
83. Reyes-Garcia, M. G.; Hernandez-Hernandez, F.; Hernandez-Tellez, B.; Garcia-Tamayo, F., GABA (A) receptor subunits RNA expression in mice peritoneal macrophages modulate their IL-6/IL-12 production. *Journal of neuroimmunology* **2007,** *188* (1-2), 64-8.
84. Marcoli M, Candiani S, Tonachini L, Monticone M, Mastrogiacomo M, Ottonello A, Cervetto C, Paluzzi P, Maura G, Pestarino M, Cancedda R, Castagnola P. In vitro modulation of gamma amino butyric acid (GABA) receptor expression by bone marrow stromal cells. Pharmacol Res. 2008 May;57(5):374-82. doi: 10.1016/j.phrs.2008.03.012. Epub **2008** Apr 8. PMID: 18467116.

85. Mizuta K, Xu D, Pan Y, Comas G, Sonett JR, Zhang Y, Panettieri RA Jr, Yang J, Emala CW Sr. GABAA receptors are expressed and facilitate relaxation in airway smooth muscle. Am J Physiol Lung Cell Mol Physiol. **2008**; 294(6):L1206–16. [PubMed: 18408071]
86. Yocum GT, Gallos G, Zhang Y, Jahan R, Stephen MR, Varagic Z, Puthenkalam R, Ernst M, Cook JM, Emala CW. Targeting the gamma-Aminobutyric Acid A Receptor alpha4 Subunit in Airway Smooth Muscle to Alleviate Bronchoconstriction. Am J Respir Cell Mol Biol. **2016**; 54(4):546– 53. [PubMed: 26405827]
87. Gallos G, Yocum GT, Siviski ME, Yim PD, Fu XW, Poe MM, Cook JM, Harrison N, Perez-Zoghbi J, Emala CW Sr. Selective targeting of the alpha5-subunit of GABAA receptors relaxes airway smooth muscle and inhibits cellular calcium handling. Am J Physiol Lung Cell Mol Physiol. **2015**; 308(9):L931–42. [PubMed: 25659897]
88. Gallos G, Yim P, Chang S, Zhang Y, Xu D, Cook JM, Gerthoffer WT, Emala CW Sr. Targeting the restricted alpha-subunit repertoire of airway smooth muscle GABAA receptors augments airway smooth muscle relaxation. Am J Physiol Lung Cell Mol Physiol. **2012**; 302(2):L248–56. [PubMed: 21949156]
89. Alam S, Laughton DL, Walding A, Wolstenholme AJ. Human peripheral blood mononuclear cells express GABAA receptor subunits. Molecular immunology. **2006**; 43(9):1432–42. [PubMed: 16213022]
90. Bjurstrom H, Wang J, Ericsson I, Bengtsson M, Liu Y, Kurnar-Mendu S, Issazadeh-Navikas S, Birnir B. GABA, a natural immunomodulator of T lymphocytes. J Neuroimmunol. **2008**; 205(1-2): 44–50. [PubMed: 18954912]
91. Wheeler DW, Thompson AJ, Corletto F, Reckless J, Loke JCT, Lapaque N, Grant AJ, Mastroeni P, Grainger DJ, Padgett CL, O'Brien JA, Miller NGA, Trowsdale J, Lummis SCR, Menon DK, Beech JS. Anaesthetic Impairment of Immune Function Is Mediated via GABA(A) Receptors. PloS one. **2011**; 6(2)
92. Myers TR. Guidelines for asthma management: a review and comparison of 5 current guidelines. Respir Care. **2008**;53:751-67; discussion 67-9.
93. Raundhal M, Morse C, Khare A, Oriss TB, Milosevic J, Trudeau J, et al. High IFN-gamma and low SLPI mark severe asthma in mice and humans. The Journal of clinical investigation. **2015**;125:3037-50.
94. Schumann C, Kropf C, Wibmer T, Rudiger S, Stoiber KM, Thielen A, et al. Omalizumab in patients with severe asthma: the XCLUSIVE study. The clinical respiratory journal. **2012**;6:215-27.
95. Abonia JP, Putnam PE. Mepolizumab in eosinophilic disorders. Expert review of clinical immunology. **2011**;7:411-7.
96. Moalem G, Tracey DJ. Immune and inflammatory mechanisms in neuropathic pain. Brain Res Rev **2006**; 51:240–264. [PubMed: 16388853]
97. Olsen RW, Sieghart W. GABA(A) receptors: Subtypes provide diversity of function and pharmacology. Neuropharmacology. **2009**;56:141-8.
98. Sieghart W. Chapter Three - Allosteric Modulation of GABAA Receptors via Multiple Drug-Binding Sites. Adv Pharmacol. **2015**;72:53-96.
99. https://wwwproteinatlasorg/ENSG00000187730-GABRD/tissue.
100. Fu XW, Wood K, Spindel ER. Prenatal nicotine exposure increases GABA signaling and mucin expression in airway epithelium. Am J Respir Cell Mol Biol. **2011**;44:222-9.
101. Xiang YY, Wang SH, Liu MY, Hirota JA, Li JX, Ju W, et al. A GABAergic system in airway epithelium is essential for mucus overproduction in asthma. Nature Medicine. **2007**;13:862-7.
102. Gallos G, Yim P, Chang S, Zhang Y, Xu D, Cook JM, et al. Targeting the restricted alpha-subunit repertoire of airway smooth muscle GABAA receptors augments airway smooth muscle relaxation. American journal of physiology Lung cellular and molecular physiology. **2012**;302:248-56.
103. Yocum GT, Turner DL, Danielsson J, Barajas MB, Zhang Y, Xu D, et al. GABAA receptor alpha4-subunit knockout enhances lung inflammation and airway reactivity in a murine asthma model. American journal of physiology Lung cellular and molecular physiology. **2017**;313:L406-L15.

104. Sanders RD, Grover V, Goulding J, Godlee A, Gurney S, Snelgrove R, et al. Immune cell expression of GABAA receptors and the effects of diazepam on influenza infection. J Neuroimmunol. **2015**; 282: 97-103.
105. Yocum GT, Perez-Zoghbi JF, Danielsson J, Kuforiji AS, Zhang Y, Li G, et al. A Novel GABAA Receptor Ligand MIDD0301 with Limited Blood-Brain Barrier Penetration Relaxes Airway Smooth Muscle Ex Vivo and In Vivo. American journal of physiology Lung cellular and molecular physiology. **2018**.
106. http://wwwichorg/products/guidelines/safety/safety-single/article/immunotoxicity-studies-for-human-pharmaceuticalshtml.
107. Kojima F, Frolov A, Matnani R, Woodward JG, Crofford LJ. Reduced T cell-dependent humoral immune response in microsomal prostaglandin E synthase-1 null mice is mediated by nonhematopoietic cells. J Immunol. **2013**;191:4979-88.
108. Tveden-Nyborg P, Bergmann TK, Lykkesfeldt J. Basic & Clinical Pharmacology & Toxicology Policy for Experimental and Clinical studies. Basic Clin Pharmacol Toxicol. **2018**;123:233-5.
109. Arnold LA, Stafford D, Cook CM, Emala CW, Forkuo GS, Jahan R, et al. GABA(A) receptor modulators and methods to control airway hyperresponsiveness and inflammation in asthma. WO2018/035246 A1. **2018**.
110. Swett JE, Torigoe Y, Elie VR, Bourassa CM, Miller PG. Sensory neurons of the rat sciatic nerve. Exp Neurol **1991**; 114:82–103. [PubMed: 1915738].
111. Brown AP, Dinger N, Levine BS. Stress produced by gavage administration in the rat. Contemporary topics in laboratory animal science. **2000**;39:17-21.
112. de Meijer VE, Le HD, Meisel JA, Puder M. Repetitive orogastric gavage affects the phenotype of diet-induced obese mice. Physiology & behavior. **2010**;100:387-93.
113. Balcombe JP, Barnard ND, Sandusky C. Laboratory routines cause animal stress. Contemporary topics in laboratory animal science. **2004**;43:42-51.
114. Zhang L, Lee NJ, Nguyen AD, Enriquez RF, Riepler SJ, Stehrer B, et al. Additive actions of the cannabinoid and neuropeptide Y systems on adiposity and lipid oxidation. Diabetes, obesity & metabolism. **2010**;12:591-603.
115. CFW (Swiss Webster mice) strain code: 024 Charles River description.
116. Hassan NM, Neiman RS. The pathology of the spleen in steroid-treated immune thrombocytopenic purpura. American journal of clinical pathology. **1985**;84:433-8.
117. Dale DC, Fauci AS, Guerry DI, Wolff SM. Comparison of agents producing a neutrophilic leukocytosis in man. Hydrocortisone, prednisone, endotoxin, and etiocholanolone. The Journal of clinical investigation. **1975**;56:808-13.
118. Serfilippi LM, Pallman DR, Russell B. Serum clinical chemistry and hematology reference values in outbred stocks of albino mice from three commonly used vendors and two inbred strains of albino mice. Contemporary topics in laboratory animal science. **2003**;42:46-52.
119. Meneton P, Ichikawa I, Inagami T, Schnermann J. Renal physiology of the mouse. American journal of physiology Renal physiology. **2000**;278:F339-51.
120. Bjurstom H, Wang J, Ericsson I, Bengtsson M, Liu Y, Kumar-Mendu S, et al. GABA, a natural immunomodulator of T lymphocytes. J Neuroimmunol. **2008**;205:44-50.
121. Forkuo GS, Guthrie ML, Yuan NY, Nieman AN, Kodali R, Jahan R, et al. Development of GABAA Receptor Subtype-Selective Imidazobenzodiazepines as Novel Asthma Treatments. Mol Pharm. **2016**;13:2026-38.
122. Monaco S, Jahraus B, Samstag Y, Bading H. Nuclear calcium is required for human T cell activation. J Cell Biol. **2016**;215:231-43.
123. Ruiz-Santana S, Lopez A, Torres S, Rey A, Losada A, Latasa L, et al. Prevention of dexamethasone-induced lymphocytic apoptosis in the intestine and in Peyer patches by enteral nutrition. Jpen-Parenter Enter. **2001**;25:338-45.

124. Donaldson, M.; Gizzarelli, G.; Chanpong, B., Oral sedation: a primer on anxiolysis for the adult patient. *Anesthesia progress* **2007,** *54* (3), 118-28; quiz 129.
125. Tan, K. R.; Rudolph, U.; Luscher, C., Hooked on benzodiazepines: GABAA receptor subtypes and addiction. *Trends in neurosciences* **2011,** *34* (4), 188-97.
126. Dunham, N. W.; Miya, T. S., A note on a simple apparatus for detecting neurological deficit in rats and mice. *Journal of the American Pharmaceutical Association. American Pharmaceutical Association* **1957,** *46* (3), 208-9.
127. Brooks, S. P.; Dunnett, S. B., Tests to assess motor phenotype in mice: a user's guide. *Nature reviews. Neuroscience* **2009,** *10* (7), 519-29.
128. OmniTech Electronics, I. Multi (Four Animal) Accelerating RotaRod. (accessed August **2019**).
129. Djouhri L, Koutsikou S, Fang X, McMullan S, Lawson SN. Spontaneous pain, both neuropathic and inflammatory, is related to frequency of spontaneous firing in intact C-fiber nociceptors. J Neurosci **2006**; 26:1281–1292. [PubMed: 16436616]
130. Mizuta, K.; Xu, D.; Pan, Y.; Comas, G.; Sonett, J. R.; Zhang, Y.; Panettieri, R. A., Jr.; Yang, J.; Emala, C. W., Sr., GABAA receptors are expressed and facilitate relaxation in airway smooth muscle. *American journal of physiology. Lung cellular and molecular physiology* **2008,** *294* (6), L1206-16.
131. Lee, M.; Schwab, C.; McGeer, P. L., Astrocytes are GABAergic cells that modulate microglial activity. *Glia* **2011,** *59* (1), 152-65.
132. Svenningsen, S., and Nair, P. (**2017**) Asthma Endotypes and an Overview of Targeted Therapy for Asthma. Front. Med. 4, 158.
133. Gross, N. J., and Barnes, P. J. (**2017**) New Therapies for Asthma and Chronic Obstructive Pulmonary Disease. Am. J. Respir. Crit. Care Med. 195, 159−166.
134. Sieghart, W., and Savic, M. M. (**2018**) International Union of Basic and Clinical Pharmacology. CVI: GABAA Receptor Subtype and Function-selective Ligands: Key Issues in Translation to Humans. Pharmacol. Rev. 70, 836−878.
135. Gallos, G., Yim, P., Chang, S., Zhang, Y., Xu, D., Cook, J. M., Gerthoffer, W. T., and Emala, C. W., Sr. (2012) Targeting the restricted alpha-subunit repertoire of airway smooth muscle GABAA receptors augments airway smooth muscle relaxation. Am. J. Physiol Lung Cell Mol. Physiol 302, L248−L256.
136. Prud'homme, G. J., Glinka, Y., and Wang, Q. (**2015**) Immunological GABAergic interactions and therapeutic applications in autoimmune diseases. Autoimmun. Rev. 14, 1048−1056.
137. Vilceanu D, Honore P, Hogan QH, Stucky CL. Spinal nerve ligation in mouse upregulates TRPV1 heat function in injured IB4-positive nociceptors. J Pain. 2010 Jun;11(6):588-99. doi: 10.1016/j.jpain.2009.09.018. Epub **2009** Dec 16. PMID: 20015699; PMCID: PMC2879455.
138. Rigaud M, Gemes G, Barabas ME, Chernoff DI, Abram SE, Stucky CL, Hogan QH. Species and strain differences in rodent sciatic nerve anatomy: implications for studies of neuropathic pain. Pain **2008**; 136:188–201. [PubMed: 18316160]
139. Liu CN, Wall PD, Ben-Dor E, Michaelis M, Amir R, Devor M. Tactile allodynia in the absence of C-fiber activation: altered firing properties of DRG neurons following spinal nerve injury. Pain **2000**; 85:503–521. [PubMed: 10781925]
140. Forkuo, G. S., Guthrie, M. L., Yuan, N. Y., Nieman, A. N., Kodali, R., Jahan, R., Stephen, M. R., Yocum, G. T., Treven, M., Poe, M. M., Li, G., Yu, O. B., Hartzler, B. D., Zahn, N. M., Ernst, M., Emala, C. W., Stafford, D. C., Cook, J. M., and Arnold, L. A. (**2016**) Development of GABAA Receptor Subtype-Selective Imidazobenzodiazepines as Novel Asthma Treatments. Mol. Pharmaceutics 13, 2026−2038.
141. Yocum, G. T., Perez-Zoghbi, J. F., Danielsson, J., Kuforiji, A. S., Zhang, Y., Li, G., Rashid Roni, M. S., Kodali, R., Stafford, D. C., Arnold, L. A., Cook, J. M., and Emala, C. W., Sr. (**2019**) A novel GABAA receptor ligand MIDD0301 with limited blood-brain barrier penetration relaxes airway smooth muscle ex vivo and in vivo. Am. J. Physiol Lung Cell Mol. Physiol 316, L385−L390.

142. Yocum, G. T., Gallos, G., Zhang, Y., Jahan, R., Stephen, M. R., Varagic, Z., Puthenkalam, R., Ernst, M., Cook, J. M., and Emala, C. W. (**2016**) Targeting the gamma-Aminobutyric Acid A Receptor alpha4 Subunit in Airway Smooth Muscle to Alleviate Bronchoconstriction. Am. J. Respir. Cell Mol. Biol. 54, 546−553.
143. Gallos, G., Yocum, G. T., Siviski, M. E., Yim, P. D., Fu, X. W., Poe, M. M., Cook, J. M., Harrison, N., Perez-Zoghbi, J., and Emala, C. W., Sr. (**2015**) Selective targeting of the alpha5-subunit of GABAA receptors relaxes airway smooth muscle and inhibits cellular calcium handling. Am. J. Physiol Lung Cell Mol. Physiol 308, L931−942.
144. Jin, Z., Mendu, S. K., and Birnir, B. (**2013**) GABA is an effective immunomodulatory molecule. Amino Acids 45, 87−94.
145. Yi, R., Zhao, S., Kong, N., Zhang, J., Loganathan, D., Merette, S., and Morrissey, B. (**2017**) Quantitation of gamma-aminobutyric acid in equine plasma by hydrophilic interaction liquid chromatography with tandem mass spectrometry. J. Sep Sci. 40, 3239−3247.
146. Bennett, J. A., Harrison, T. W., and Tattersfield, A. E. (**1999**) The contribution of the swallowed fraction of an inhaled dose of salmeterol to it systemic effects. Eur. Respir. J. 13, 445−448.
147. Cazzola, M., Page, C. P., Rogliani, P., and Matera, M. G. (**2013**) beta2-agonist therapy in lung disease. Am. J. Respir. Crit. Care Med. 187, 690−696.
148. Procopiou, P. A., Barrett, V. J., Bevan, N. J., Biggadike, K., Box, P. C., Butchers, P. R., Coe, D. M., Conroy, R., Emmons, A., Ford, A. J., Holmes, D. S., Horsley, H., Kerr, F., Li-Kwai-Cheung, A. M., Looker, B. E., Mann, I. S., McLay, I. M., Morrison, V. S., Mutch, P. J., Smith, C. E., and Tomlin, P. (**2010**) Synthesis and structure-activity relationships of long-acting beta2 adrenergic receptor agonists incorporating metabolic inactivation: an antedrug approach. J. Med. Chem. 53, 4522−4530.
149. Khan, M. O., and Lee, H. J. (**2008**) Synthesis and pharmacology of anti-inflammatory steroidal antedrugs. Chem. Rev. 108, 5131−5145.
150. Yasir, M., Goyal, A., Bansal, P., and Sonthalia, S. (**2020**) Corticosteroid Adverse Effects, In StatPearls; Treasure Island (FL).
151. Zahn, N. M., Huber, A. T., Mikulsky, B. N., Stepanski, M. E., Kehoe, A. S., Li, G., Schussman, M., Rashid Roni, M. S., Kodali, R., Cook, J. M., Stafford, D. C., Steeber, D. A., and Arnold, L. A. (**2019**) MIDD0301 - A first-in-class anti-inflammatory asthma drug targets GABAA receptors without causing systemic immune suppression. Basic Clin. Pharmacol. Toxicol. 125, 75−84.
152. Doras, C., Petak, F., Bayat, S., Baudat, A., Von Garnier, C., Eigenmann, P., and Habre, W. (**2018**) Lung responses in murine models of experimental asthma: Value of house dust mite over ovalbumin sensitization. Respir. Physiol. Neurobiol. 247, 43−51.
153. Gueders, M. M., Paulissen, G., Crahay, C., Quesada-Calvo, F., Hacha, J., Van Hove, C., Tournoy, K., Louis, R., Foidart, J. M., Noel, A., and Cataldo, D. D. (**2009**) Mouse models of asthma: a comparison ACS Pharmacology & Translational Science pubs.acs.org/ptsci Article https://dx.doi.org/10.1021/acsptsci.0c00180 ACS Pharmacol. Transl. Sci. XXXX, XXX, XXX−XXX I between C57BL/6 and BALB/c strains regarding bronchial responsiveness, inflammation, and cytokine production. Inflammation Res. 58, 845−854.
154. Cozzi, E., Ackerman, K. G., Lundequist, A., Drazen, J. M., Boyce, J. A., and Beier, D. R. (**2011**) The naive airway hyperresponsiveness of the A/J. mouse is Kit-mediated. Proc. Natl. Acad. Sci. U. S. A. 108, 12787−12792.
155. Mailhot-Larouche, S., Deschenes, L., Gazzola, M., Lortie, K., Henry, C., Brook, B. S., Morissette, M. C., and Bosse, Y. (**2018**) Repeated airway constrictions in mice do not alter respiratory function. J. Appl. Physiol. 124, 1483−1490.
156. Ball, D. I., Brittain, R. T., Coleman, R. A., Denyer, L. H., Jack, D., Johnson, M., Lunts, L. H., Nials, A. T., Sheldrick, K. E., and Skidmore, I. F. (**1991**) Salmeterol, a novel, long-acting beta 2-adrenoceptor agonist: characterization of pharmacological activity in vitro and in vivo. Br. J. Pharmacol. 104, 665−671.

157. ten Hacken, N. H., Oosterhoff, Y., Kauffman, H. F., Guevarra, L., Satoh, T., Tollerud, D. J., and Postma, D. S. (**1998**) Elevated serum interferon-gamma in atopic asthma correlates with increased airways responsiveness and circadian peak expiratory flow variation. Eur. Respir. J. 11, 312−316.
158. Chang, P. J., Michaeloudes, C., Zhu, J., Shaikh, N., Baker, J., Chung, K. F., and Bhavsar, P. K. (**2015**) Impaired nuclear translocation of the glucocorticoid receptor in corticosteroid insensitive airway smooth muscle in severe asthma. Am. J. Respir. Crit. Care Med. 191, 54−62.
159. Li, J. J., Wang, W., Baines, K. J., Bowden, N. A., Hansbro, P. M., Gibson, P. G., Kumar, R. K., Foster, P. S., and Yang, M. (**2010**) IL-27/IFN-gamma induce MyD88-dependent steroid-resistant airway hyperresponsiveness by inhibiting glucocorticoid signaling in macrophages. J. Immunol. 185, 4401−4409.
160. Chu, H. W., Campbell, J. A., Rino, J. G., Harbeck, R. J., and Martin, R. J. (**2004**) Inhaled fluticasone propionate reduces concentration of Mycoplasma pneumoniae, inflammation, and bronchial hyperresponsiveness in lungs of mice. J. Infect. Dis. 189, 1119−1127.
161. Miric, M., Ristic, S., Joksimovic, B. N., Medenica, S., Racic, M., Ristic, S., Joksimovic, V. R., and Skipina, M. (**2016**) Reversion of methacholine induced bronchoconstriction with inhaled diazepam in patients with asthma. Rev. Med. Chile 144, 434−441.
162. Knutson, D. E., Roni, R., Mian, Y., Cook, J. M., Stafford, D. C., and Arnold, L. A. (**2020**) Improved scale-up synthesis and purification of clinical asthma candidate MIDD0301. Org. Process Res. Dev. 24, 1467−1476.
163. Robichaud, A., Fereydoonzad, L., and Schuessler, T. F. (**2015**) Delivered dose estimate to standardize airway hyperresponsiveness assessment in mice. Am. J. Physiol Lung Cell Mol. Physiol 308, L837− 846.
164. Zahn, N. M.; Mikulsky, B. N.; Roni, M. S. R.; Yocum, G. T.; Mian, M. Y.; Knutson, D. E.; Cook, J. M.; Emala, C. W.; Stafford, D. C.; Arnold, L. A. Nebulized MIDD0301 Reduces Airway Hyperresponsiveness in Moderate and Severe Murine Asthma Models. *ACS Pharmacol Transl Sci* **2020**, *3* (6), 1381-1390. DOI: 10.1021/acsptsci.0c00180.
165. ten Hacken, N. H.; Oosterhoff, Y.; Kauffman, H. F.; Guevarra, L.; Satoh, T.; Tollerud, D. J.; Postma, D. S. Elevated serum interferon-gamma in atopic asthma correlates with increased airways responsiveness and circadian peak expiratory flow variation. *Eur Respir J* **1998**, *11* (2), 312-316. DOI: 10.1183/09031936.98.11020312.
166. Chang, P. J.; Michaeloudes, C.; Zhu, J.; Shaikh, N.; Baker, J.; Chung, K. F.; Bhavsar, P. K. Impaired nuclear translocation of the glucocorticoid receptor in corticosteroid-insensitive airway smooth muscle in severe asthma. *Am J Respir Crit Care Med* **2015**, *191* (1), 54-62. DOI: 10.1164/rccm.201402-0314OC.
167. Li, J. J.; Wang, W.; Baines, K. J.; Bowden, N. A.; Hansbro, P. M.; Gibson, P. G.; Kumar, R. K.; Foster, P. S.; Yang, M. IL-27/IFN-gamma induce MyD88-dependent steroid-resistant airway hyperresponsiveness by inhibiting glucocorticoid signaling in macrophages. *J Immunol* **2010**, *185* (7), 4401-4409. DOI: 10.4049/jimmunol.1001039.
168. Cozzi, E.; Ackerman, K. G.; Lundequist, A.; Drazen, J. M.; Boyce, J. A.; Beier, D. R. The naive airway hyperresponsiveness of the A/J mouse is Kit-mediated. *Proc Natl Acad Sci U S A* **2011**, *108* (31), 12787-12792. DOI: 10.1073/pnas.1106582108.
169. Gallos, G.; Gleason, N. R.; Virag, L.; Zhang, Y.; Mizuta, K.; Whittington, R. A.; Emala, C. W. Endogenous gamma-aminobutyric acid modulates tonic guinea pig airway tone and propofol-induced airway smooth muscle relaxation. *Anesthesiology* **2009**, *110* (4), 748-758. DOI: 10.1097/aln.0b013e31819c44e1.
170. Wu G, Ringkamp M, Hartke TV, Murinson BB, Campbell JN, Griffin JW, Meyer RA. Early onset of spontaneous activity in uninjured C-fiber nociceptors after injury to neighboring nerve fibers. J Neurosci **2001**; 21:RC140. [PubMed: 11306646]

171. Liu CN, Wall PD, Ben-Dor E, Michaelis M, Amir R, Devor M. Tactile allodynia in the absence of C-fiber activation: altered firing properties of DRG neurons following spinal nerve injury. Pain **2000**; 85:503–521. [PubMed: 10781925]
172. Campbell JN, Meyer RA. Mechanisms of neuropathic pain. Neuron **2006**; 52:77–92. [PubMed: 17015228]
173. Beilharz, R.G.; Cox, D.F. Genetic Analysis of Open Field Behavior in Swine. *Journal of Animal Science*. **1967**, Volume 26, Issue 5 (988–990).
174. Kraeuter, A.K.; Guest PC, Sarnyai, Z. The Open Field Test for Measuring Locomotor Activity and Anxiety-Like Behavior. *Methods Mol Biol*. **2019**, 1916:99-103.
175. Gromer, D.; Kiser, D.P.; Pauli, P. Thigmotaxis in a Virtual Human Open Field Test. *Scientific Reports*. **2021**, 11 (1), 6670.
176. Gage, G.; Kipke, D.; Shain, W. Whole Animal Perfusion Fixation for Rodents. *Neuroscience*. **2012**, doi: 10.3791/3564.
177. Kudo, M.; Ishigatsubo, Y.; Aoki, I., Pathology of asthma. *Frontiers in microbiology* **2013,** *4*, 263.
178. Abbas, A. K.; Lichtman, A. H.; Pillai, S., *Cellular and molecular immunology*. 7th ed.; Elsevier/Saunders: Philadelphia, **2012**; p x, 545 p.
179. Miceli, M. C.; Parnes, J. R., The roles of CD4 and CD8 in T cell activation. *Seminars in immunology* **1991,** *3* (3), 133-41.
180. Lewis, R. S., Calcium signaling mechanisms in T lymphocytes. *Annual review of immunology* **2001,** *19*, 497-521.
181. Koretzky, G. A., Multiple roles of CD4 and CD8 in T cell activation. *Journal of immunology* **2010,** *185* (5), 2643-4.
182. Betts, R. J.; Kemeny, D. M., CD8+ T cells in asthma: friend or foe? *Pharmacology & therapeutics* **2009,** *121* (2), 123-31.
183. Maslan, J.; Mims, J. W., What is asthma? Pathophysiology, demographics, and health care costs. *Otolaryngologic clinics of North America* **2014,** *47* (1), 13-22.
184. Romagnani, S., T-cell subsets (Th1 versus Th2). *Annals of allergy, asthma & immunology : official publication of the American College of Allergy, Asthma, & Immunology* **2000,** *85* (1), 9-18; quiz 18, 21.
185. Kidd, P., Th1/Th2 balance: the hypothesis, its limitations, and implications for health and disease. *Alternative medicine review : a journal of clinical therapeutic* **2003,** *8* (3), 223-46.
186. Larche, M.; Robinson, D. S.; Kay, A. B., The role of T lymphocytes in the pathogenesis of asthma. *The Journal of allergy and clinical immunology* **2003,** *111* (3), 450-63; quiz 464.
187. Possa, S. S.; Leick, E. A.; Prado, C. M.; Martins, M. A.; Tiberio, I. F., Eosinophilic inflammation in allergic asthma. *Frontiers in pharmacology* **2013,** *4*, 46.
188. McBrien, C. N.; Menzies-Gow, A., The Biology of Eosinophils and Their Role in Asthma. *Frontiers in medicine* **2017,** *4*, 93.
189. Mathur, S. K.; Fichtinger, P. S.; Evans, M. D.; Schwantes, E. A.; Jarjour, N. N., Variability of blood eosinophil count as an asthma biomarker. *Annals of allergy, asthma & immunology : official publication of the American College of Allergy, Asthma, & Immunology* **2016,** *117* (5), 551-553.
190. Balhara, J.; Gounni, A. S., The alveolar macrophages in asthma: a double-edged sword. *Mucosal immunology* **2012,** *5* (6), 605-9.
191. Prado, C. M.; Martins, M. A.; Tiberio, I. F., Nitric oxide in asthma physiopathology. *ISRN allergy* **2011,** *2011*, 832560.
192. van Veen, I. H.; Ten Brinke, A.; Sterk, P. J.; Sont, J. K.; Gauw, S. A.; Rabe, K. F.; Bel, E. H., Exhaled nitric oxide predicts lung function decline in difficult-to-treat asthma. *The European respiratory journal* **2008,** *32* (2), 344-9.
193. Gallos, G.; Yim, P.; Chang, S.; Zhang, Y.; Xu, D.; Cook, J. M.; Gerthoffer, W. T.; Emala, C. W., Sr., Targeting the restricted alpha-subunit repertoire of airway smooth muscle GABAA receptors augments

airway smooth muscle relaxation. *American journal of physiology. Lung cellular and molecular physiology* **2012,** *302* (2), L248-56.
194. Dionisio, L.; Jose De Rosa, M.; Bouzat, C.; Esandi Mdel, C., An intrinsic GABAergic system in human lymphocytes. *Neuropharmacology* **2011,** *60* (2-3), 513-9.
195. Reyes-Garcia, M. G.; Hernandez-Hernandez, F.; Hernandez-Tellez, B.; Garcia-Tamayo, F., GABA (A) receptor subunits RNA expression in mice peritoneal macrophages modulate their IL-6/IL-12 production. *Journal of neuroimmunology* **2007,** *188* (1-2), 64-8.
196. Januzi, L.; Poirier, J. W.; Maksoud, M. J. E.; Xiang, Y. Y.; Veldhuizen, R. A. W.; Gill, S. E.; Cregan, S. P.; Zhang, H.; Dekaban, G. A.; Lu, W. Y., Autocrine GABA signaling distinctively regulates phenotypic activation of mouse pulmonary macrophages. *Cellular immunology* **2018,** *332*, 7-23.
197. Gurram, R.K., Zhu, J. Orchestration between ILC2s and Th2 cells in shaping type 2 immune responses. *Cell Mol Immunol* 16**,** 225–235 (**2019**). https://doi.org/10.1038/s41423-019-0210-8
198. Radonić A, Thulke S, Mackay IM, Landt O, Siegert W, Nitsche A. Guideline to reference gene selection for quantitative real-time PCR. Biochem Biophys Res Commun. **2004** Jan 23;313(4):856-62. doi: 10.1016/j.bbrc.2003.11.177. PMID: 14706621.
199. Coordinate Regulation of GATA-3 and Th2 Cytokine Gene Expression by the RNA-Binding Protein HuR Cristiana Stellato,*,1 Matthew M. Gubin,†,‡,1 Joseph D. Magee,† Xi Fang,* Jinshui Fan,* Danielle M. Tartar,‡ Jing Chen,†,x Garrett M. Dahm,†,‡ Robert Calaluce,† Francesca Mori,{ Glenn A. Jackson,x Vincenzo Casolaro,‖ Craig L. Franklin,‡,x and Ulus Atasoy Journal of immunology **2011.**
200. 11-4 and 11-13 Production in Differentiated T Helper Type 2 Cells Is Not 11-4 Dependent. Hua Huang,'* Jane Hu-Li,* Hangjiong Chen,* S. Z. Ben-Sasson,+ and William E. Paul2* The Journal of Immunology, **1997**, 159: 3731-3738.
201. Claire L. Emson, Sarah E. Bell, Alison Jones, William Wisden, Andrew N.J. McKenzie Interleukin (IL)-4–independent Induction of Immunoglobulin (Ig)E, and Perturbation of T Cell Development in Transgenic Mice Expressing IL-13 JEM **1998**
202. Hedegaard, H.; Warner, M.; Minino, A. M., Drug Overdose Deaths in the United States, 1999-2016. *NCHS data brief* **2017,** (294), 1-8.
203. van Hecke, O.; Austin, S. K.; Khan, R. A.; Smith, B. H.; Torrance, N., Neuropathic pain in the general population: a systematic review of epidemiological studies. *Pain* **2014,** *155* (4), 654-62.
204. Colloca, L.; Ludman, T.; Bouhassira, D.; Baron, R.; Dickenson, A. H.; Yarnitsky, D.; Freeman, R.; Truini, A.; Attal, N.; Finnerup, N. B.; Eccleston, C.; Kalso, E.; Bennett, D. L.; Dworkin, R. H.; Raja, S. N., Neuropathic pain. *Nature reviews. Disease primers* **2017,** *3*, 17002.
205. Nightingale, S., The neuropathic pain market. *Nature reviews. Drug discovery* **2012,** *11* (2), 101-2.
206. Salter, M. W.; Stevens, B., Microglia emerge as central players in brain disease. *Nature medicine* **2017,** *23* (9), 1018-1027.
207. Levy, D.; Zochodne, D. W., NO pain: potential roles of nitric oxide in neuropathic pain. *Pain practice : the official journal of World Institute of Pain* **2004,** *4* (1), 11-8.
208. Lee, M.; Schwab, C.; McGeer, P. L., Astrocytes are GABAergic cells that modulate microglial activity. *Glia* **2011,** *59* (1), 152-65.
209. Wu, C.; Qin, X.; Du, H.; Li, N.; Ren, W.; Peng, Y., The immunological function of GABAergic system. *Frontiers in bioscience* **2017,** *22*, 1162-1172.
210. Kim SH, Chung JM. An experimental model for peripheral neuropathy produced by segmental spinal nerve ligation in the rat. Pain **1992**; 50:355–363. [PubMed: 1333581]
211. Sukhotinsky I, Ben-Dor E, Raber P, Devor M. Key role of the dorsal root ganglion in neuropathic tactile hypersensibility. Eur J Pain **2004**; 8:135–143. [PubMed: 14987623]
212. Di Lio, A.; Benke, D.; Besson, M.; Desmeules, J.; Daali, Y.; Wang, Z. J.; Edwankar, R.; Cook, J. M.; Zeilhofer, H. U., HZ166, a novel GABAA receptor subtype-selective benzodiazepine site ligand, is

antihyperalgesic in mouse models of inflammatory and neuropathic pain. *Neuropharmacology* **2011,** *60* (4), 626-32.
213. Haanpää M, Attal N, Backonja M, Baron R, Bennett M, Bouhassira D, Cruccu G, Hansson P, Haythornthwaite JA, Iannetti GD, Jensen TS, Kauppila T, Nurmikko TJ, Rice AS, Rowbotham M, Serra J, Sommer C, Smith BH, Treede RD. NeuPSIG guidelines on neuropathic pain assessment. Pain **2001**; 152:14-27.
214. F.V. Abbott, K.B. Franklin, R.F. Westbrook, The formalin test: scoring properties of the first and second phases of the pain response in rats, Pain, 60 (1995) 91-102.
215. Li, G., Nieman, A. N., Mian, M. Y., Zahn, N. M., Mikulsky, B. N., Poe, M. M., Methuku, K. R., Liu, Y., Cook, J. M., Stafford, D. C., & Arnold, L. A. (**2020)**. A Structure-Activity Relationship Comparison of Imidazodiazepines Binding at Kappa, Mu, and Delta Opioid Receptors and the $GABA_A$ Receptor. *Molecules (Basel, Switzerland)*, *25*(17), 3864. https://doi.org/10.3390/molecules25173864
216. Dubuisson D, Dennis SG. The formalin test: a quantitative study of the analgesic effects of morphine, meperidine, and brain stem stimulation in rats and cats. Pain. **1977** Dec;4(2):161-174. doi: 10.1016/0304-3959(77)90130-0. PMID: 564014.
217. Dubuc, Bruno. Ascending Pain Pathways. *The Brain From Top to Bottom*. https://thebrain.mcgill.ca /flash/d/d_03/d 03_cl/d_03_cl_dou/d_03_cl_dou.html. **2002**.
218. Graefe S, Mohiuddin SS. *Biochemistry, Substance P.* **2022** Jan-. Available from: https://www.ncbi.nlm.nih. gov/books/NBK554583/

APPENDICES

Appendix A – Asthma Compound Structures

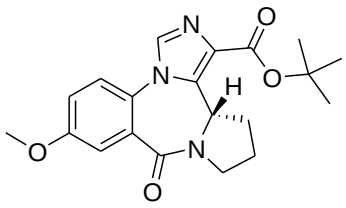

XHE-III-74

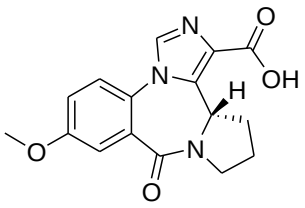

XHE-III-74 Acid

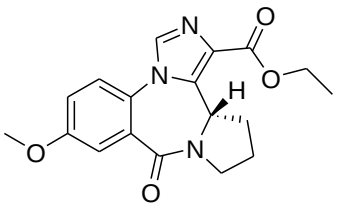

XHE-III-74 Ethyl Ester

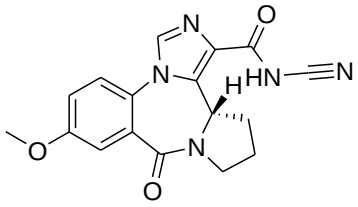

MRS-III-90

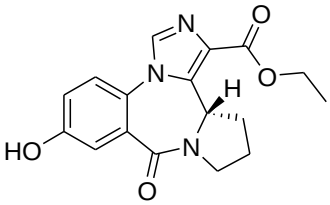

RJ-02-50

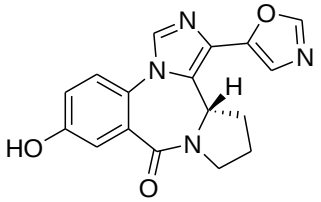

RJ-03-30

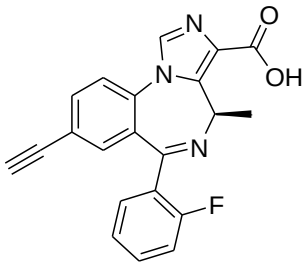

SH-053-2'F-R-CH_3 Acid

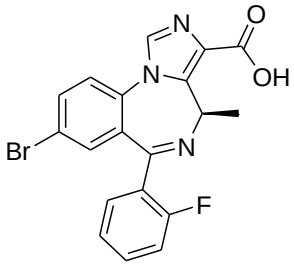

MIDD0301

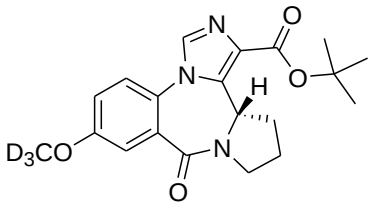

RJ-02-52

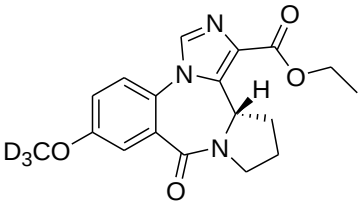

RJ-02-46

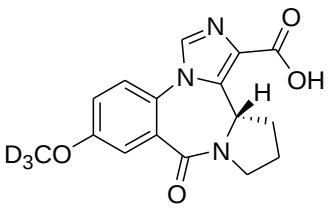

RJ-02-66

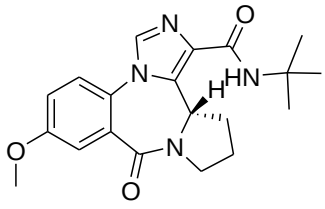

MRS-01-74

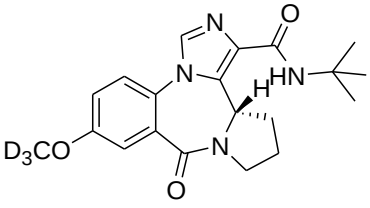

RJ-02-68

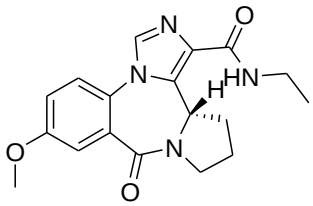

MRS-02-57

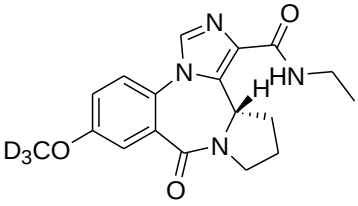

RJ-02-89

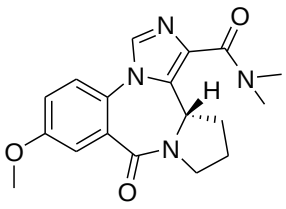
MRS-01-66

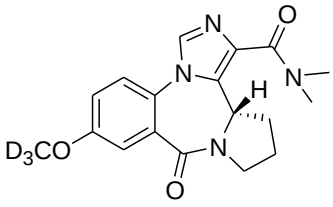
RJ-02-91

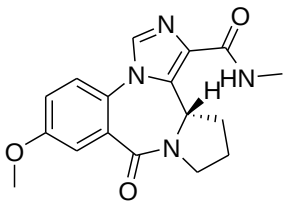
MRS-01-64

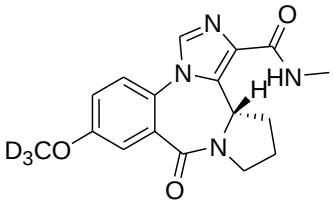
RJ-02-92

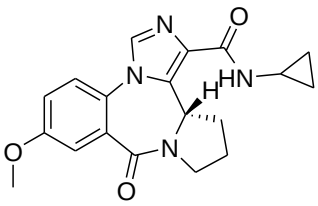
MRS-01-52

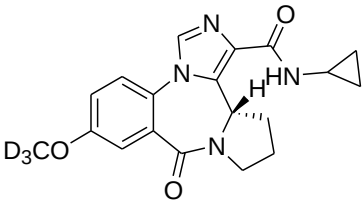
RJ-02-72

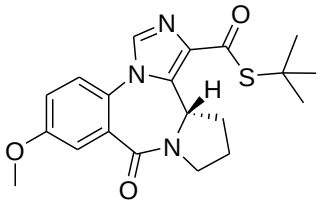
MRS-01-73

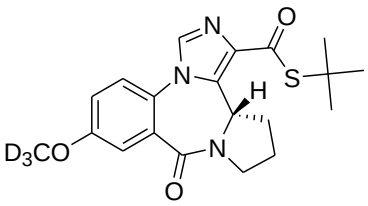
RJ-02-69

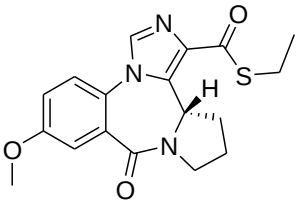
MRS-01-67

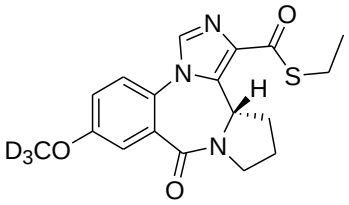
RJ-02-90

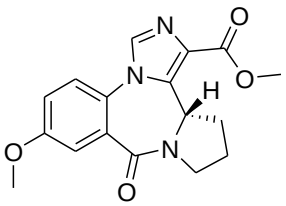
MRS-01-68

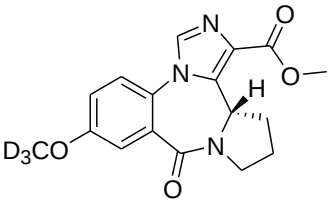
RJ-02-70

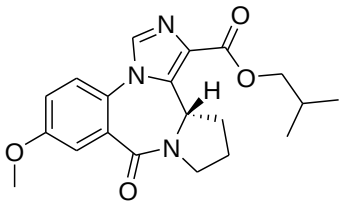
RJ-01-46

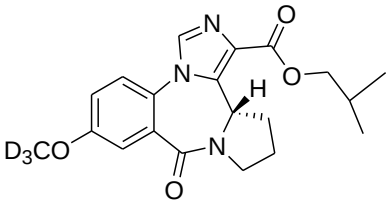
RJ-02-71

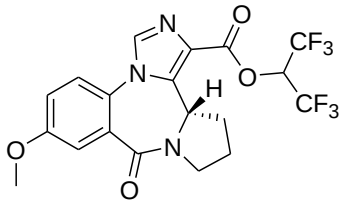
MRS-01-53

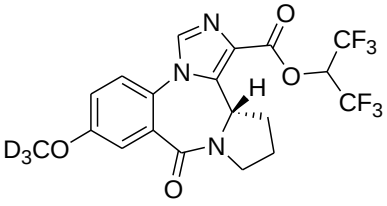
RJ-02-93

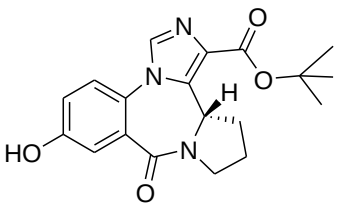
RJ-02-67

Appendix B – Pain Compound Structures

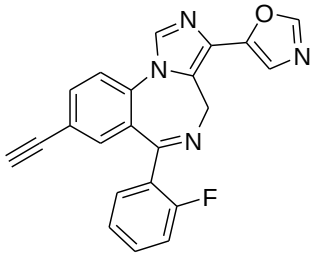

KRM-II-18B

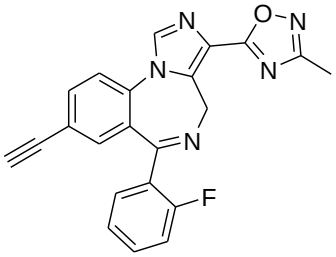

GL-III-23

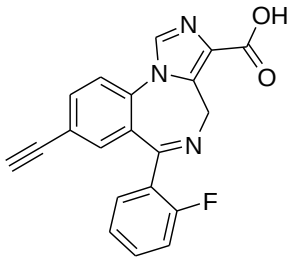

GL-III-79

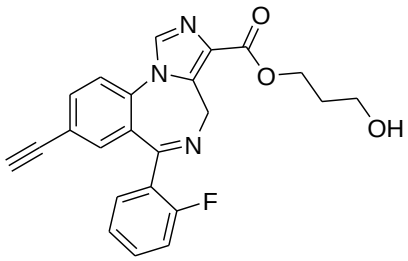

GL-II-80

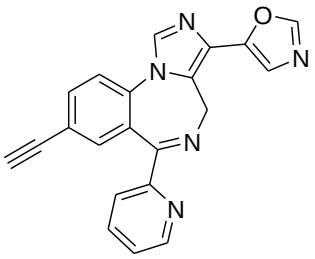

KRM-II-81

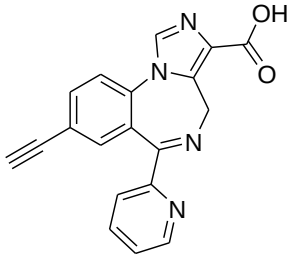

GL-III-13

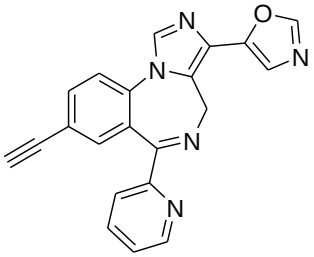

KRM-II-81

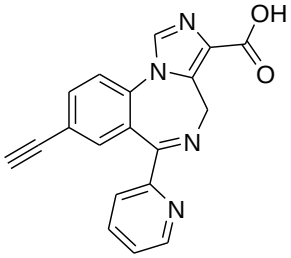

GL-III-13

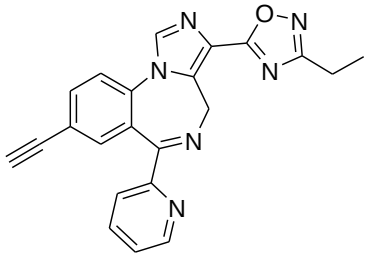

MP-III-80

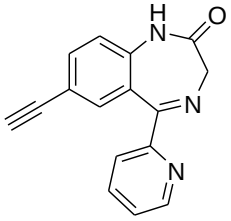

GL-III-58

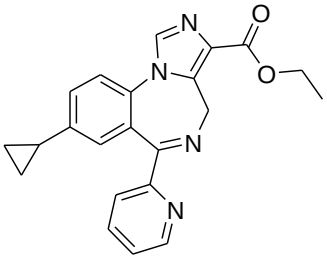

GL-IV-05

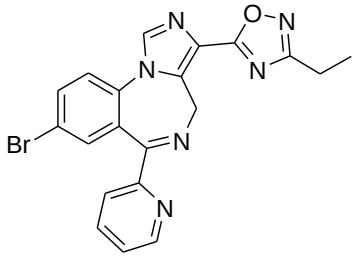

GL-III-99

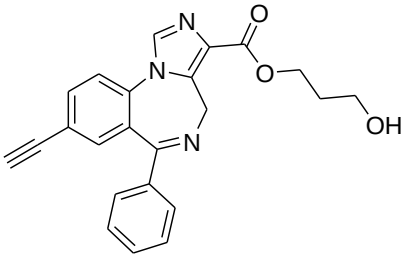

GL-I-48

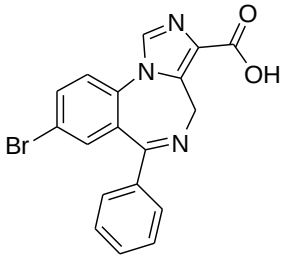

GL-I-50

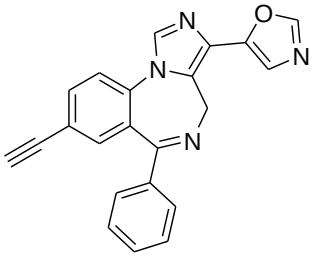

KRM-II-82

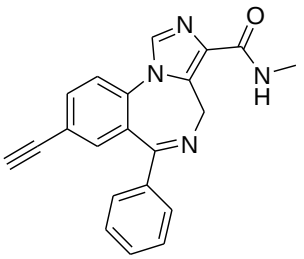

YT-III-31

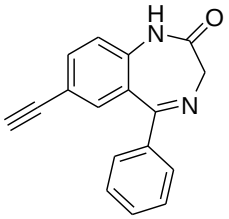

GL-III-59

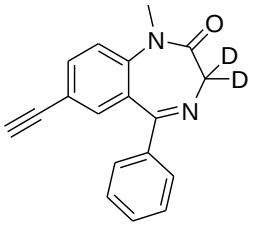

D2-QH-II-66

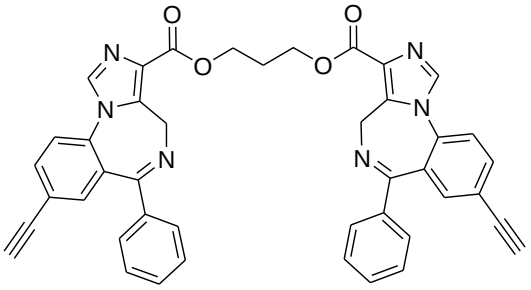

DMH-D-053

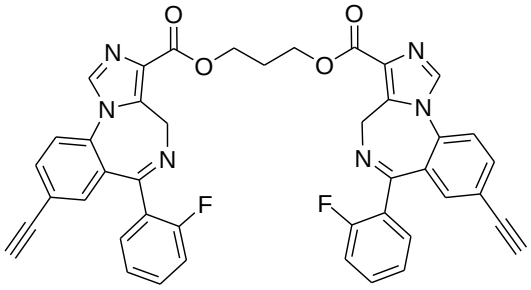

YT-III-271

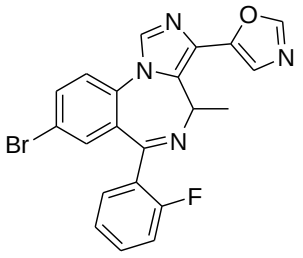

GL-III-76A

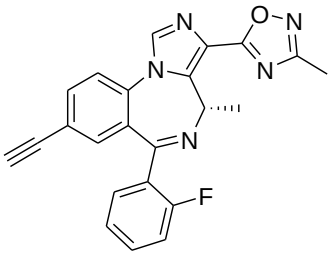

GL-I-65

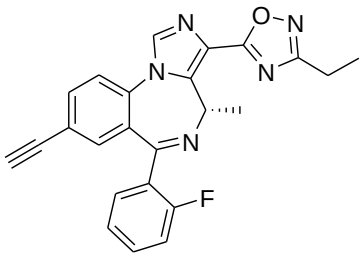

GL-I-66

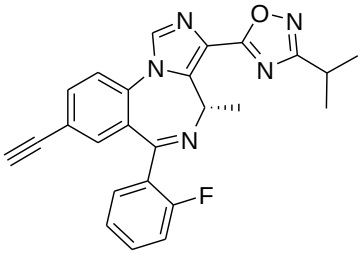

GL-I-81

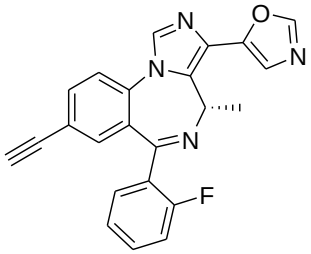

GL-III-78

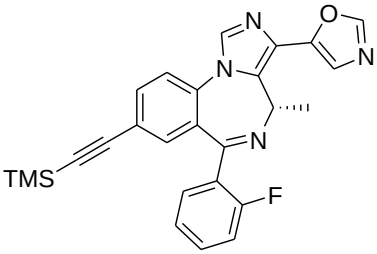

GL-III-77

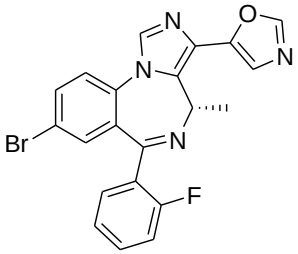

GL-III-76

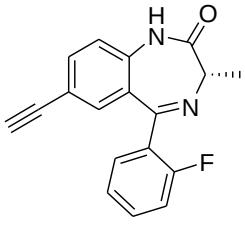

GL-I-64

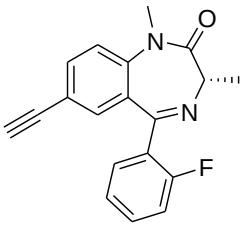

GL-III-24

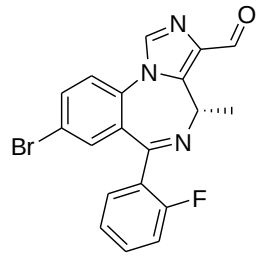
GL-III-75

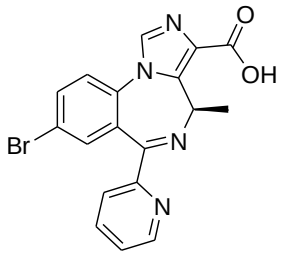
GL-II-51

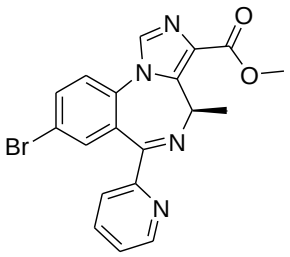
GL-II-32

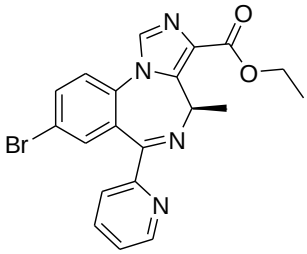
GL-II-06

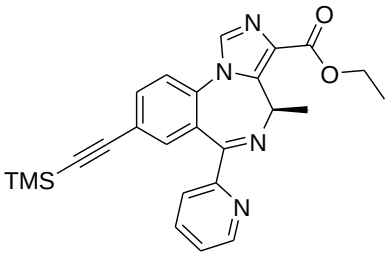
GL-II-18

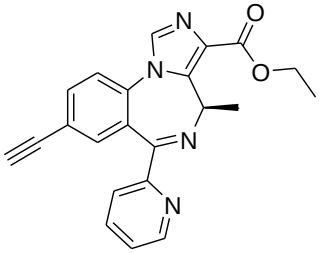
GL-II-19
SH-053-2'N-R-CH3

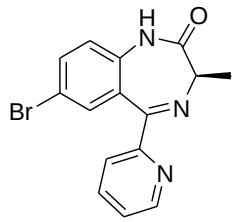
GL-II-05

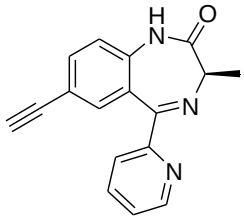
GL-III-27

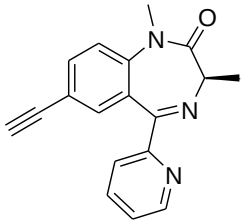
GL-II-61

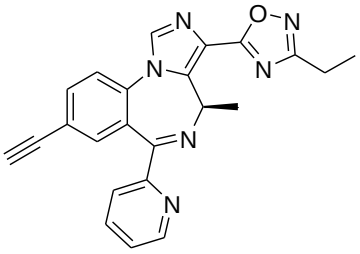
GL-III-97

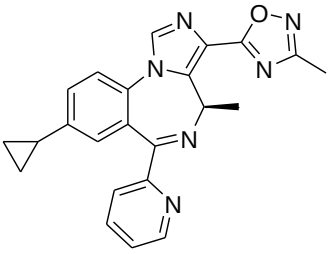
GL-III-64

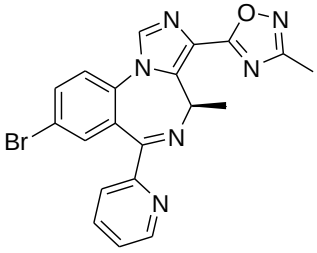
GL-II-54

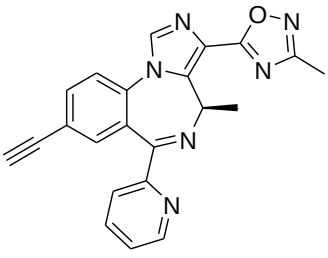
GL-II-33

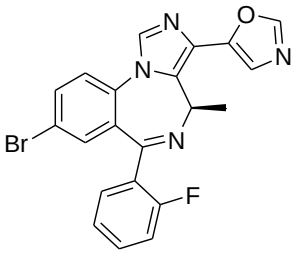
GL-III-36

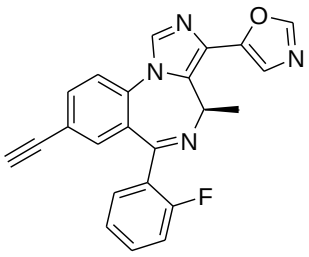
GL-III-73

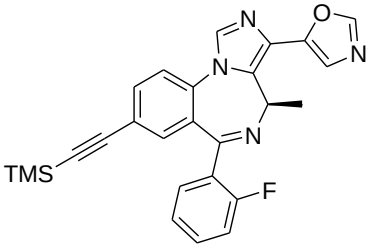

GL-III-72

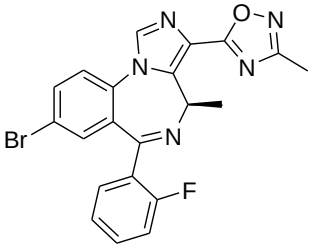

GL-III-60

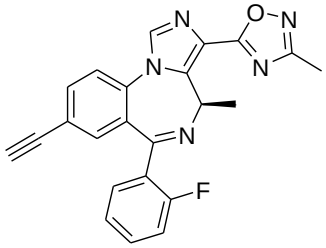

MP-IV-004

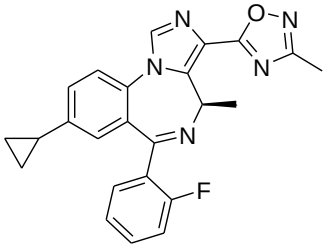

GL-III-63

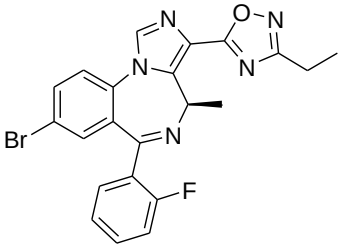

GL-III-98

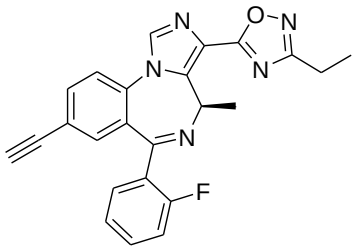

MP-IV-005

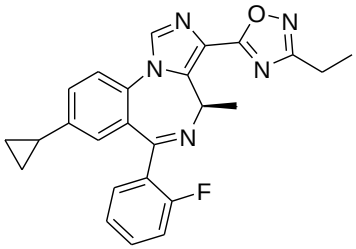

GL-IV-03

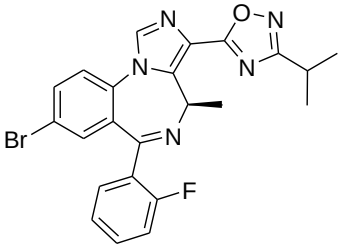

GL-IV-01

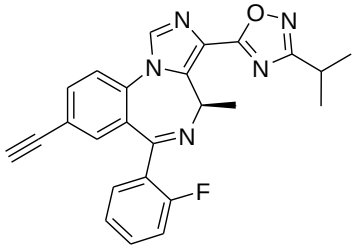

MP-IV-010

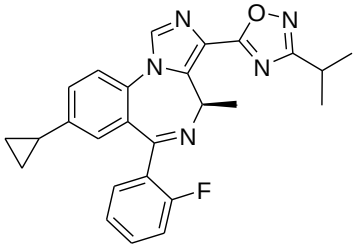

GL-IV-04

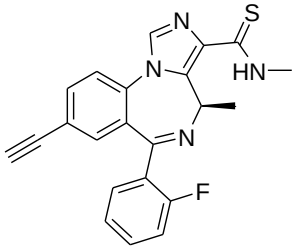

GL-III-84

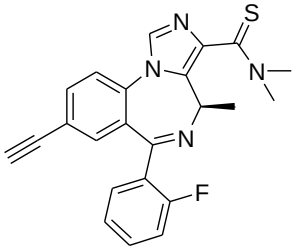

GL-III-85

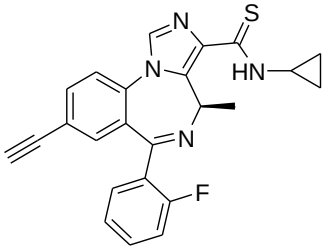

GL-III-87

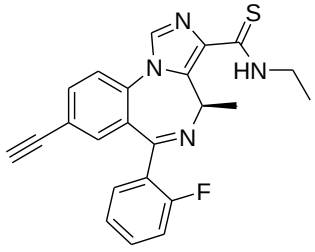

GL-III-86

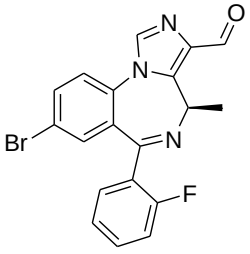

GL-III-35

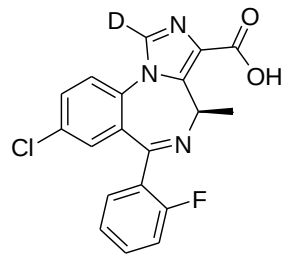

D1-GL-III-54

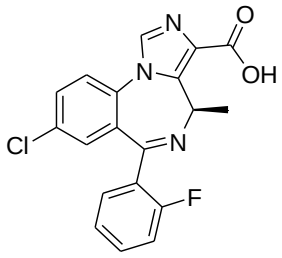

GL-III-54

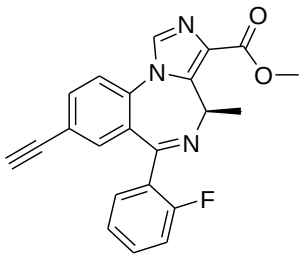

MP-III-004

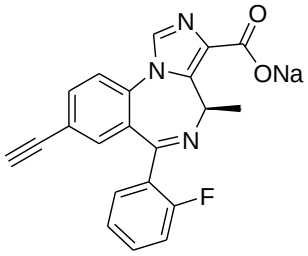

GL-IV-17

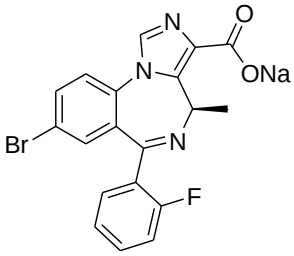

GL-IV-18

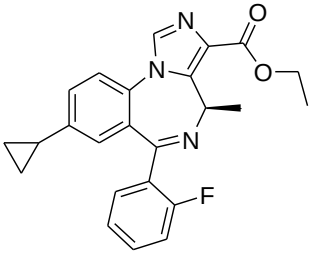

GL-III-42

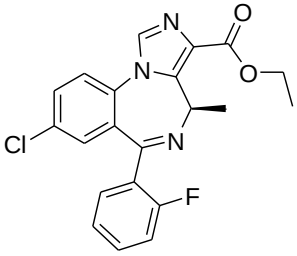

GL-III-53

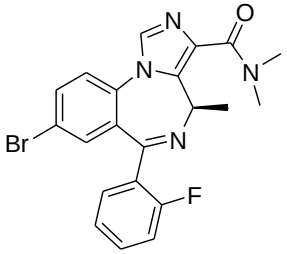

GL-III-69

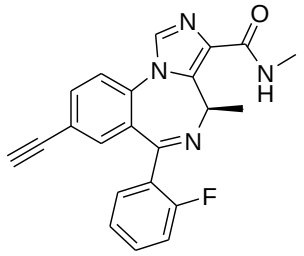

MP-III-022

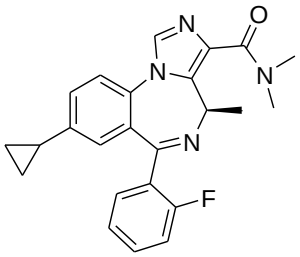

GL-III-70

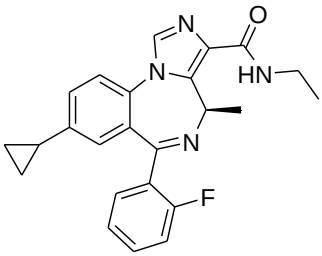

GL-III-68

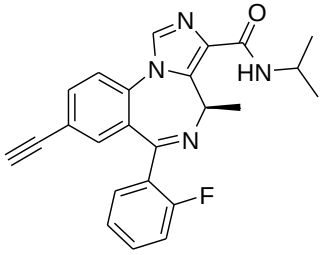

GL-III-66

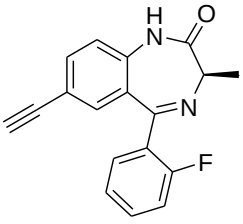

GL-I-62

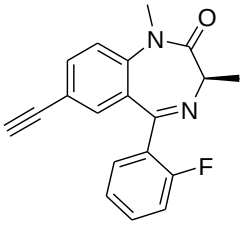

GL-III-25

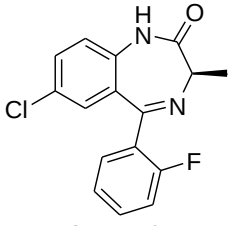

GL-III-52

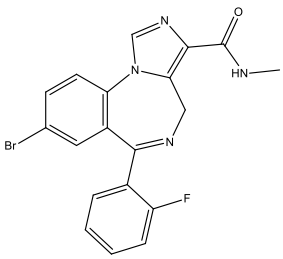

RV-II-04
Chemical Formula: $C_{19}H_{14}BrFN_4O$
Molecular Weight: 413.24

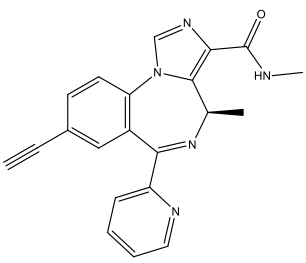

GL-II-31
Chemical Formula: $C_{21}H_{17}N_5O$
Molecular Weight: 355.39

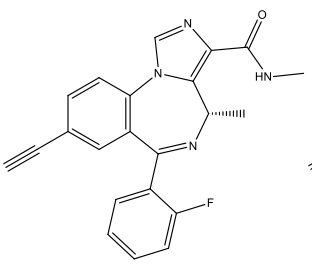

MP-III-023
Chemical Formula: $C_{22}H_{17}FN_4O$
Molecular Weight: 372.39

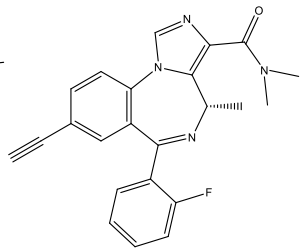

GL-I-54
Chemical Formula: $C_{23}H_{19}FN_4O$
Molecular Weight: 386.42

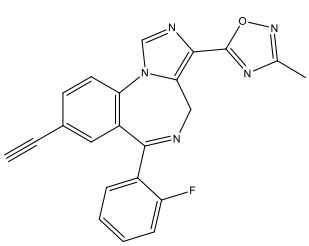

GL-III-23
Chemical Formula: $C_{22}H_{14}FN_5O$
Molecular Weight: 383.38

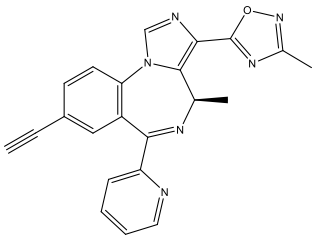

GL-II-33
Chemical Formula: $C_{22}H_{16}N_6O$
Molecular Weight: 380.40

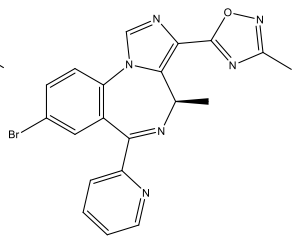

GL-II-54
Chemical Formula: $C_{20}H_{15}BrN_6O$
Molecular Weight: 435.28

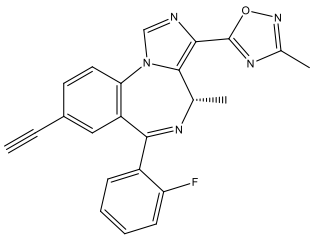

GL-I-65
Chemical Formula: $C_{23}H_{16}FN_5O$
Molecular Weight: 397.40

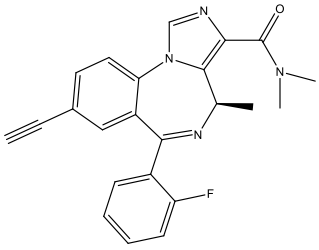

GL-II-73
Molecular Weight: 386.42

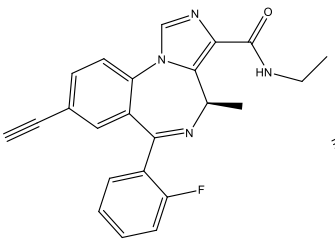

GL-II-74
Molecular Weight: 386.42

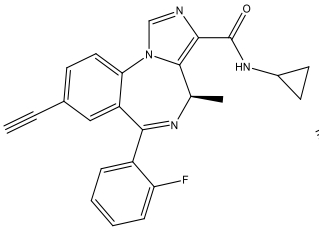

GL-II-75
Molecular Weight: 398.43

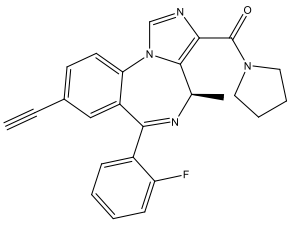

GL-II-76
Molecular Weight: 412.46

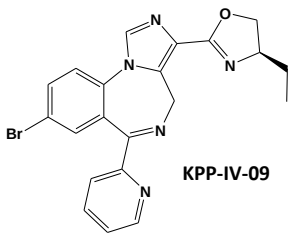

KPP-IV-09

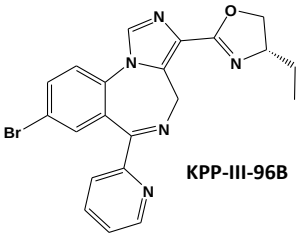

KPP-III-96B

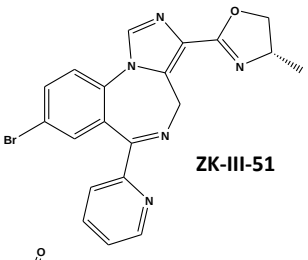

ZK-III-51

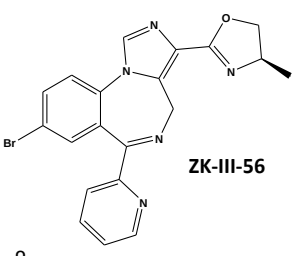

ZK-III-56

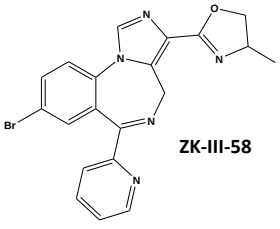

ZK-III-58

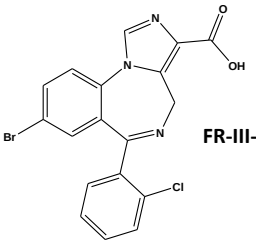

FR-III-45

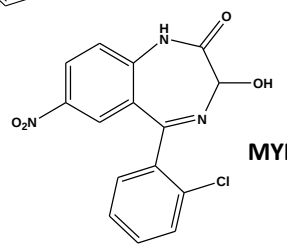

MYM-III-10

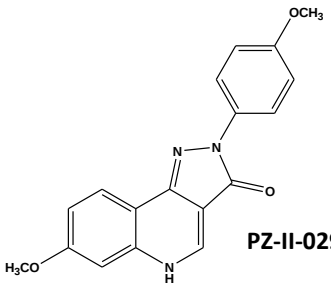

PZ-II-029

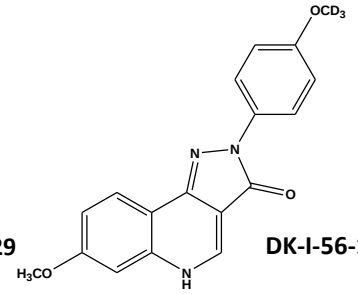

DK-I-56-1

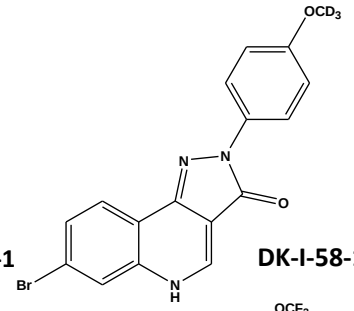

DK-I-58-1

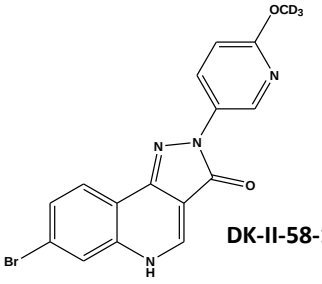

DK-II-58-1

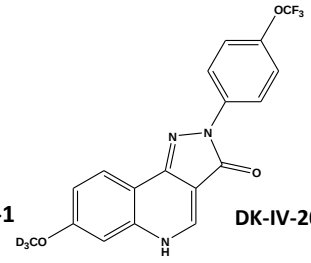

DK-IV-20-1

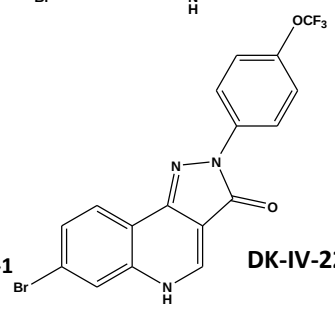

DK-IV-22-1

Appendix C – RotaRod Graphs

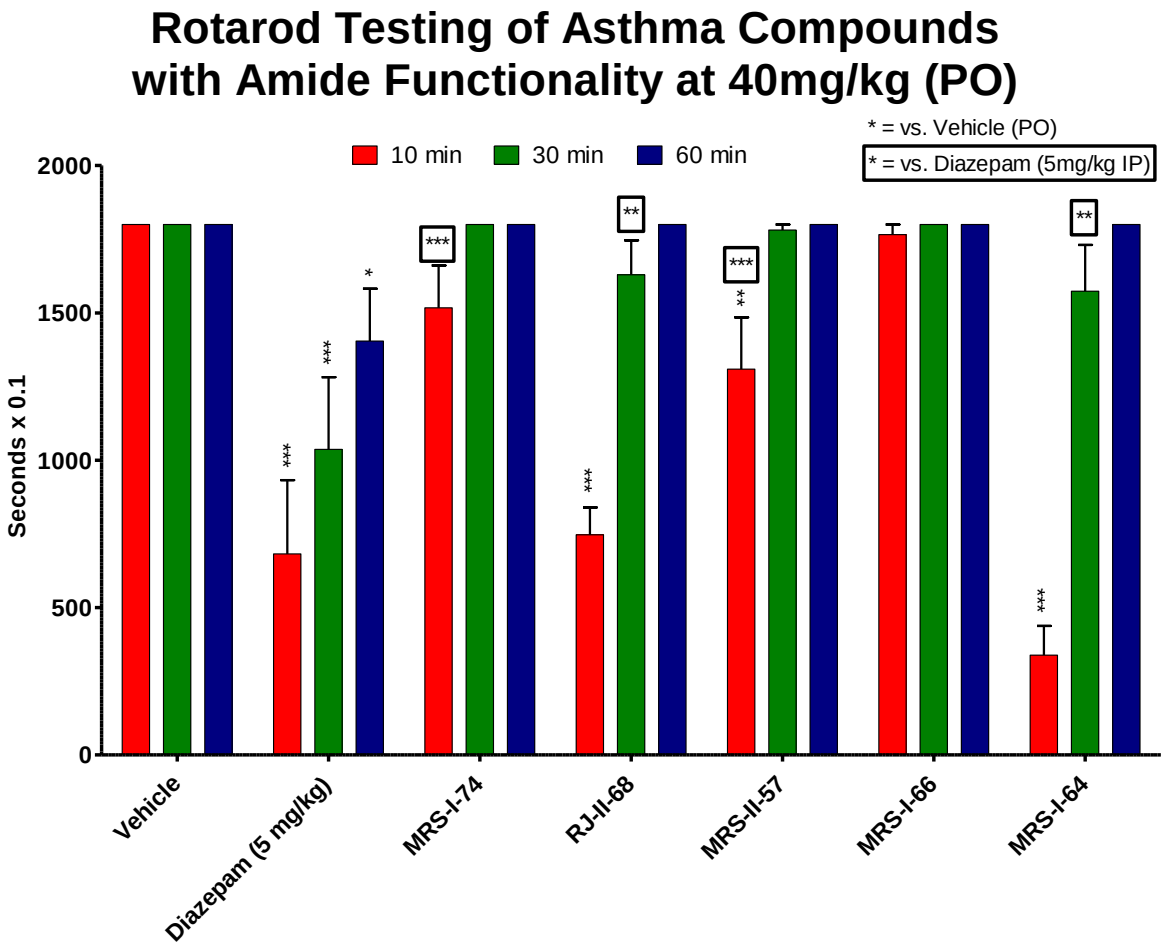

Figure 7. RotaRod Study of Asthma Compounds with Amide Functionality. *Trained female CFW mice (N≥10) were placed on the RotaRod at 10, 30, and 60 min after compound administration. The Rotarod was set at a constant speed of 18 rpm. Compounds were administered 40mg/kg PO and compared to vehicle as negative control and diazepam as positive control*.

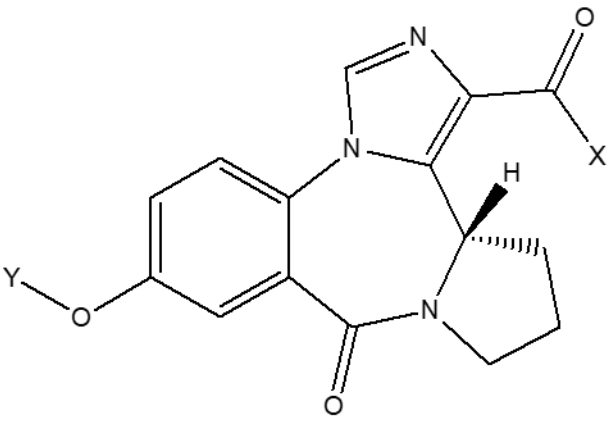

	X	Y
MRS-01-74	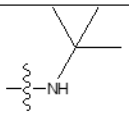	CH_3
RJ-02-68	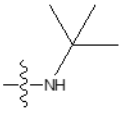	CD_3
MRS-02-57	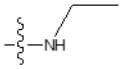	CH_3
MRS-01-66	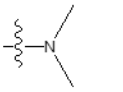	CH_3
MRS-01-64	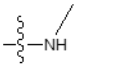	CH_3

Figure 8. Asthma Compounds with Amide Functionality. *Table shows X and Y groups corresponding to respective functionality. Compounds were synthesized according to Jahan et al.[9]*

Compounds in **Figure 8** were synthesized by Rajwana Jahan (RJ) and Michael Rajesh Stephen (MRS).[9] Shown in **Figure 7**, MRS-I-66 demonstrated the least motor impairment across all time points, while the other four amides each were shown to have motor impairment at the 10 mi time points with little to no impairment at the following time points.

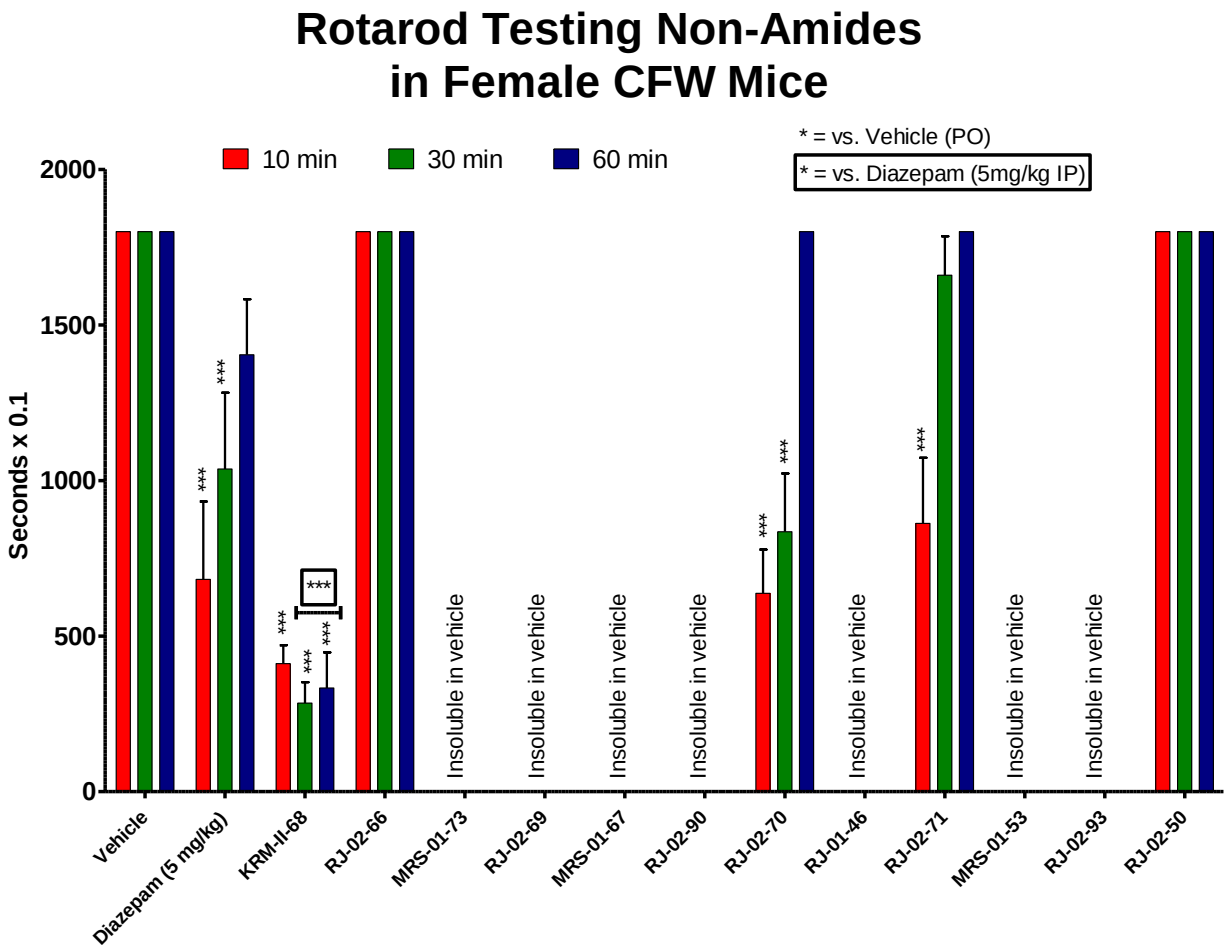

Figure 9. RotaRod Study of Asthma Compounds with Non-Amide Functionality*. Trained female CFW mice (N=10) were placed on the RotaRod at 10, 30, and 60 min after compound administration. The Rotarod was set at a constant speed of 18 rpm. Compounds were administered 40mg/kg PO and compared to vehicle as negative control and diazepam as positive control. Compounds not soluble at 500uM in DMSO were excluded from testing.*

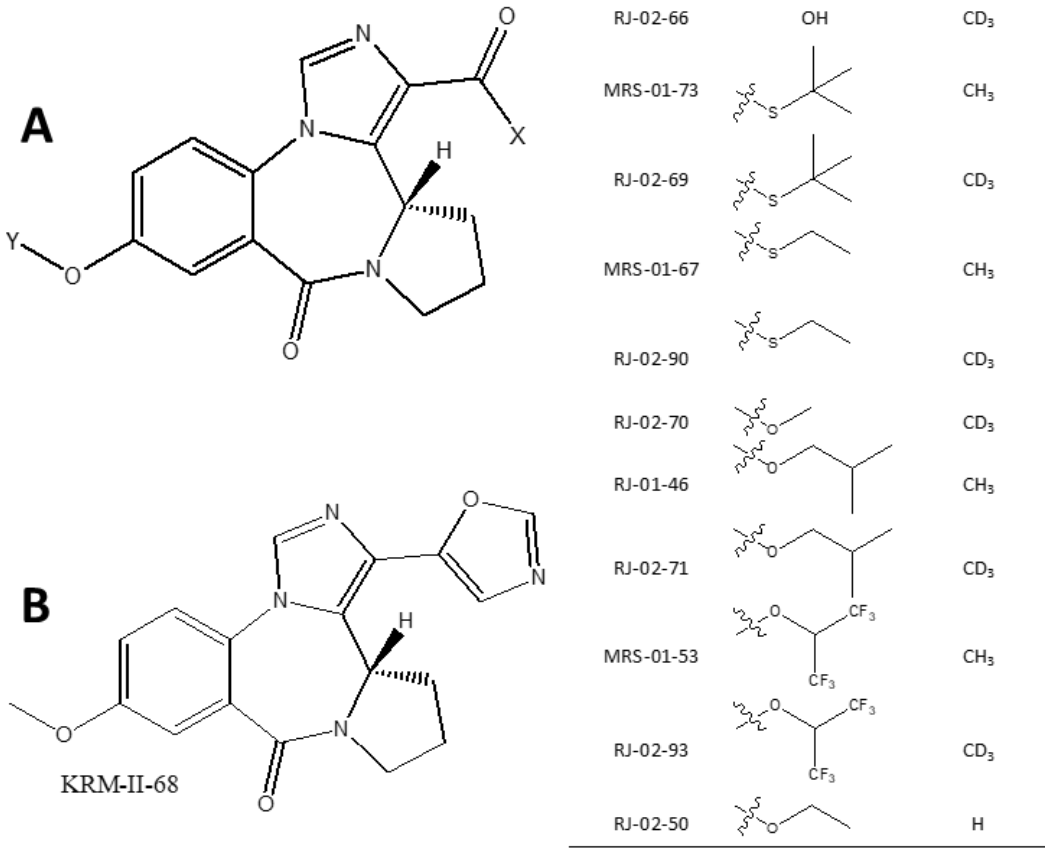

	X	Y
RJ-02-66	OH	CD_3
MRS-01-73		CH_3
RJ-02-69		CD_3
MRS-01-67		CH_3
RJ-02-90		CD_3
RJ-02-70		CD_3
RJ-01-46		CH_3
RJ-02-71		CD_3
MRS-01-53		CH_3
RJ-02-93		CD_3
RJ-02-50		H

Figure 10. Asthma Compounds with Non-Amide Functionality*. Table shows (A) X and Y groups corresponding to respective functionality and (B) compounds KRM-II-68. Compounds were synthesized according to Jahan et al.*[9]

Several of the non-amides in **Figure 10** were insoluble and were not investigated further. **Figure 9** shows compound KRM-II-68 demonstrated severe motor impairment at all time points, while compounds RJ-II-70 and RJ-II-71 had motor impairment at the 10 and 30 min time points. No motor impairment was shown in mice treated with RJ-II-66 and RJ-II-50.

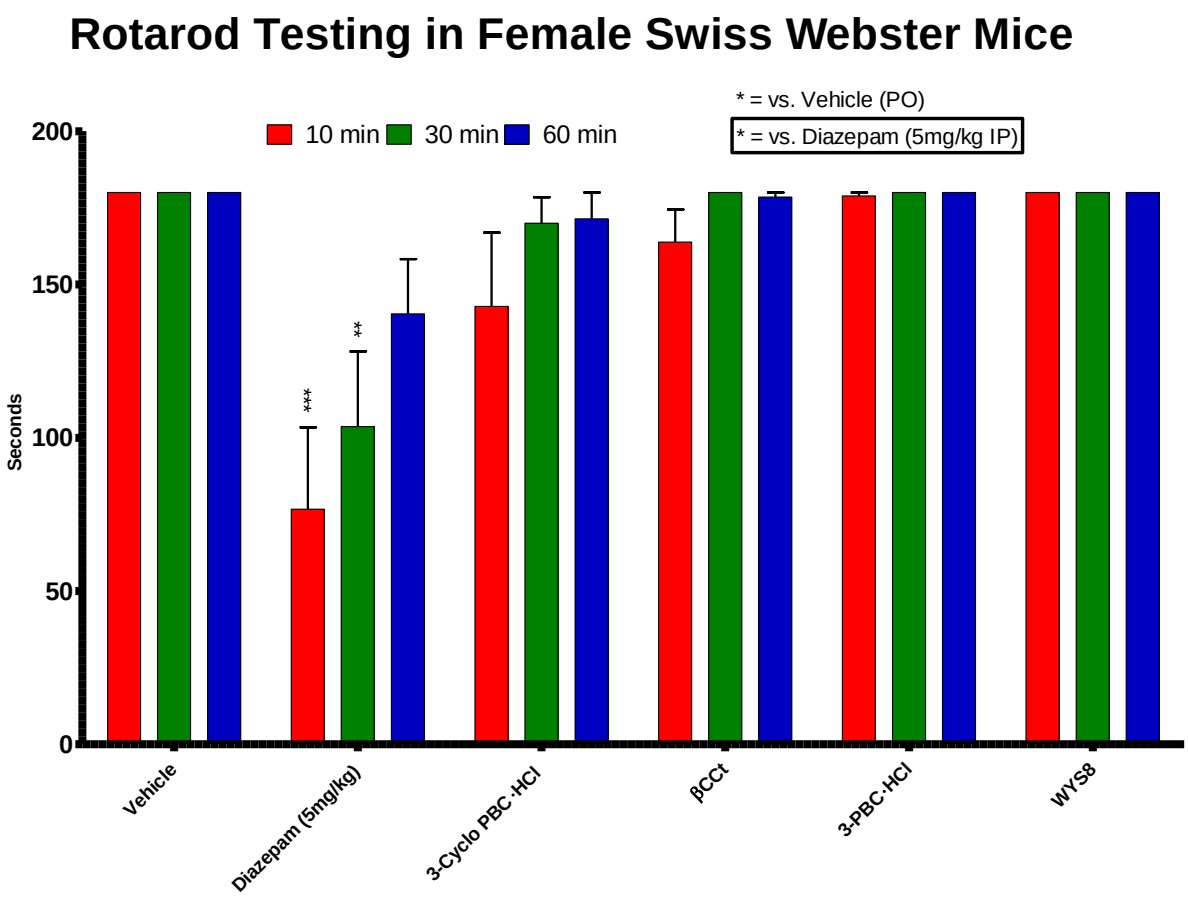

Figure 11. RotaRod Study of Phani Babu Tiruveedhula's Compounds*. Trained female CFW mice (N=10) were placed on the RotaRod at 10, 30, and 60 min after compound administration. The Rotarod was set at a constant speed of 18 rpm. Compounds were administered 40mg/kg IP and compared to vehicle as negative control and diazepam as positive control.*

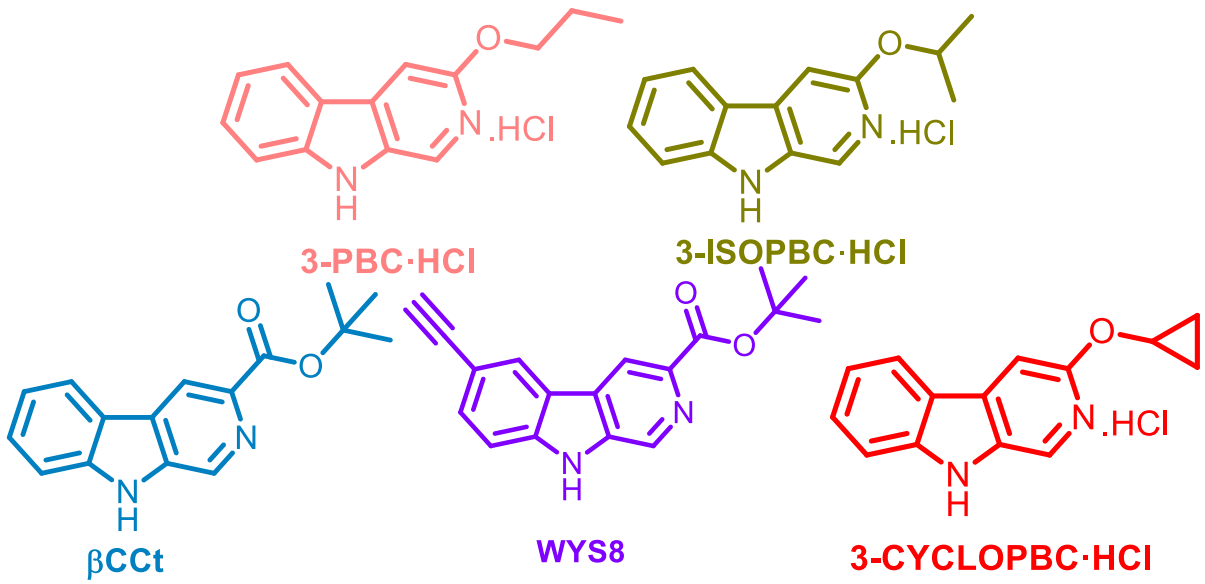

Figure 12. Structures of Phani Babu Tiruveedhula's Compounds*. Compounds were synthesized by Phani Babu Tiruveedhula (Cook Group) and were subsequently administered 40mg/kg IP and compared to vehicle as negative control and diazepam as positive control.*

Lead compounds in **Figure 12** from Phani Babu Tiruveedhula (Cook Group) aimed at treating alcohol-dependency were delivered to mice and tested on the rotarod. **Figure 11** demonstrates a few of the mice delivered 3-CycloPBC•HCl and βCCt were unable to complete the entire time on the rotarod at the 10 and 30 min, however there was no statistical significance in any of the compounds when compared to vehicle-treated mice.

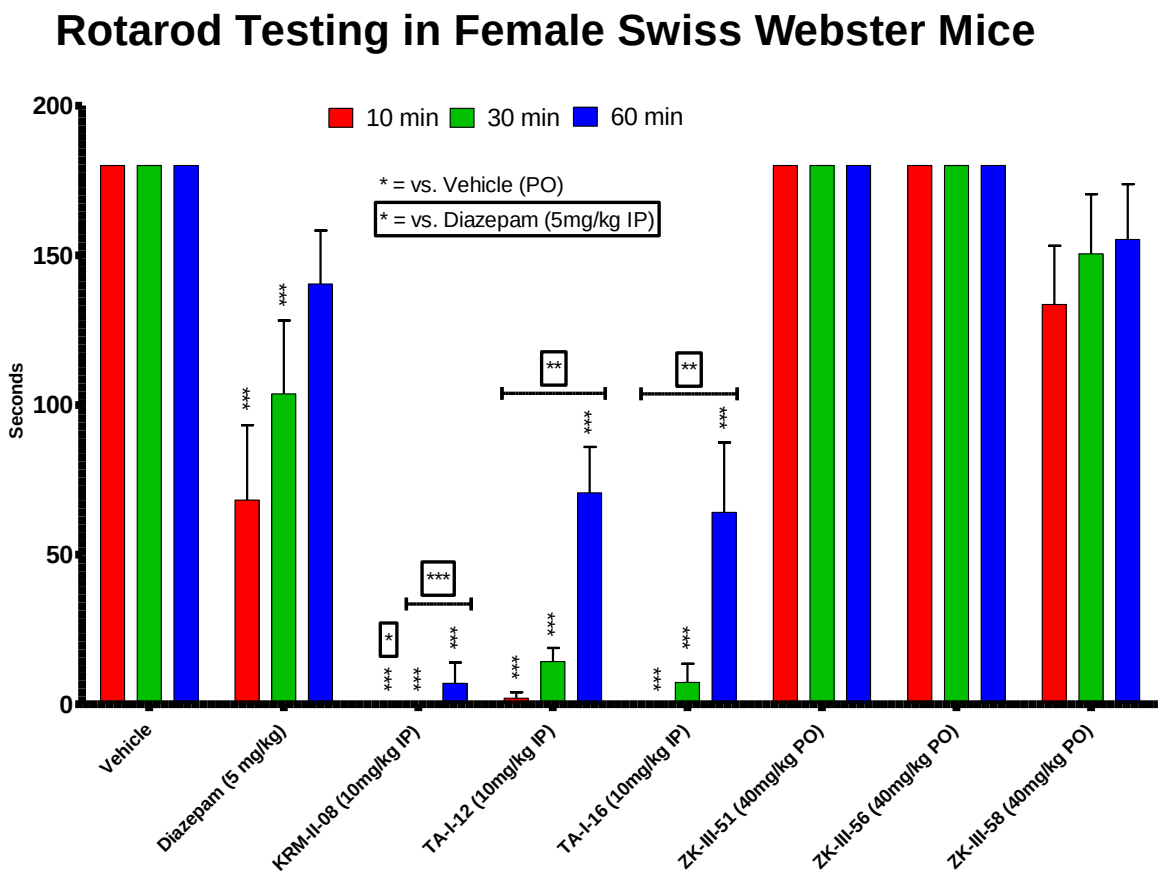

Figure 13. RotaRod Study of Compounds*. Trained female CFW mice (N≥10) were placed on the RotaRod at 10, 30, and 60 min after compound administration. The rotarod was set at a constant rate of 18 rpm. Compounds were administered and compared to vehicle as negative control and diazepam as positive control.*

Compounds synthesized by Taukir Ahmed and Zubair Ahmed Khan (Cook Group) were analyzed for impaired motor coordination on the rotarod apparatus and are disclosed in **Figure 13**. KRM-II-08, TA-I-12, and TA-I-16 at 10mg/kg IP were shown to have severe motor impairment, sedation, and seizures at

all time points. These compounds were immediately rejected as potential drug candidates. ZK-III-51 and ZK-III-56 were shown to have no impaired motor coordination, as well as ZK-III-58 despite not all mice performing the full time on the rotarod.

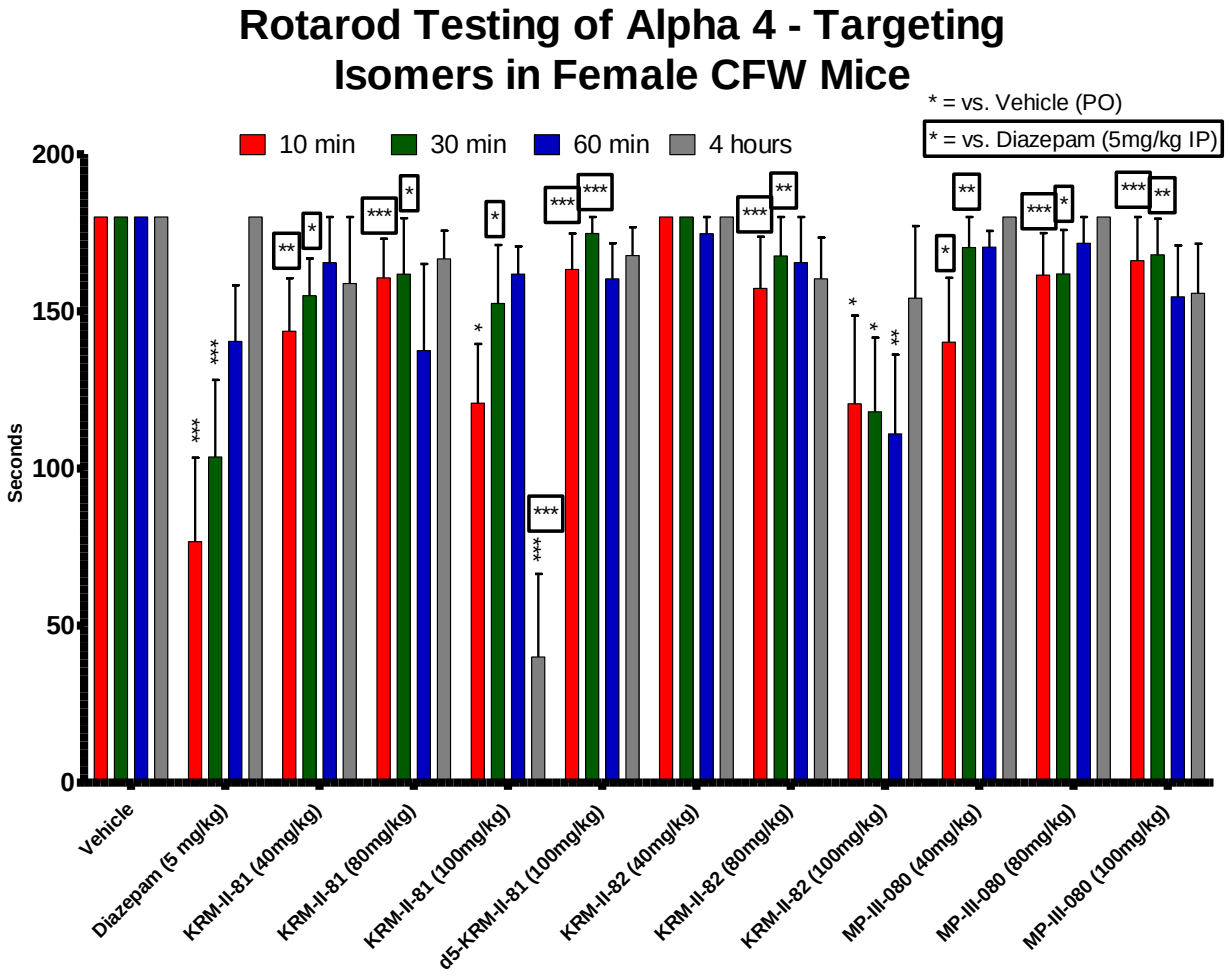

Figure 14. RotaRod Study of Lalit Golani and Kamal Pandey's Pain Compounds*. Trained female CFW mice (N≥10) were placed on the RotaRod at 10, 30, and 60 min after compound administration. The rotarod was set at a constant rate of 18 rpm. Compounds were administered and compared to vehicle as negative control and diazepam as positive control.*

Compounds targeting $GABA_aRs$ containing an α4 subunit were synthesized by Lalit Golani and Kamal Pandey (Cook Group) and tested for motor coordination up to 4 h after compound administration. All four compounds in **Figure 14** had significantly less motor impairment when compared to negative control 5 mg/kg diazepam (IP), but only 100 mg/kg KRM-II-81 and KRM-II-82 (PO) also had significantly more motor impairment when compared to vehicle-treated mice.

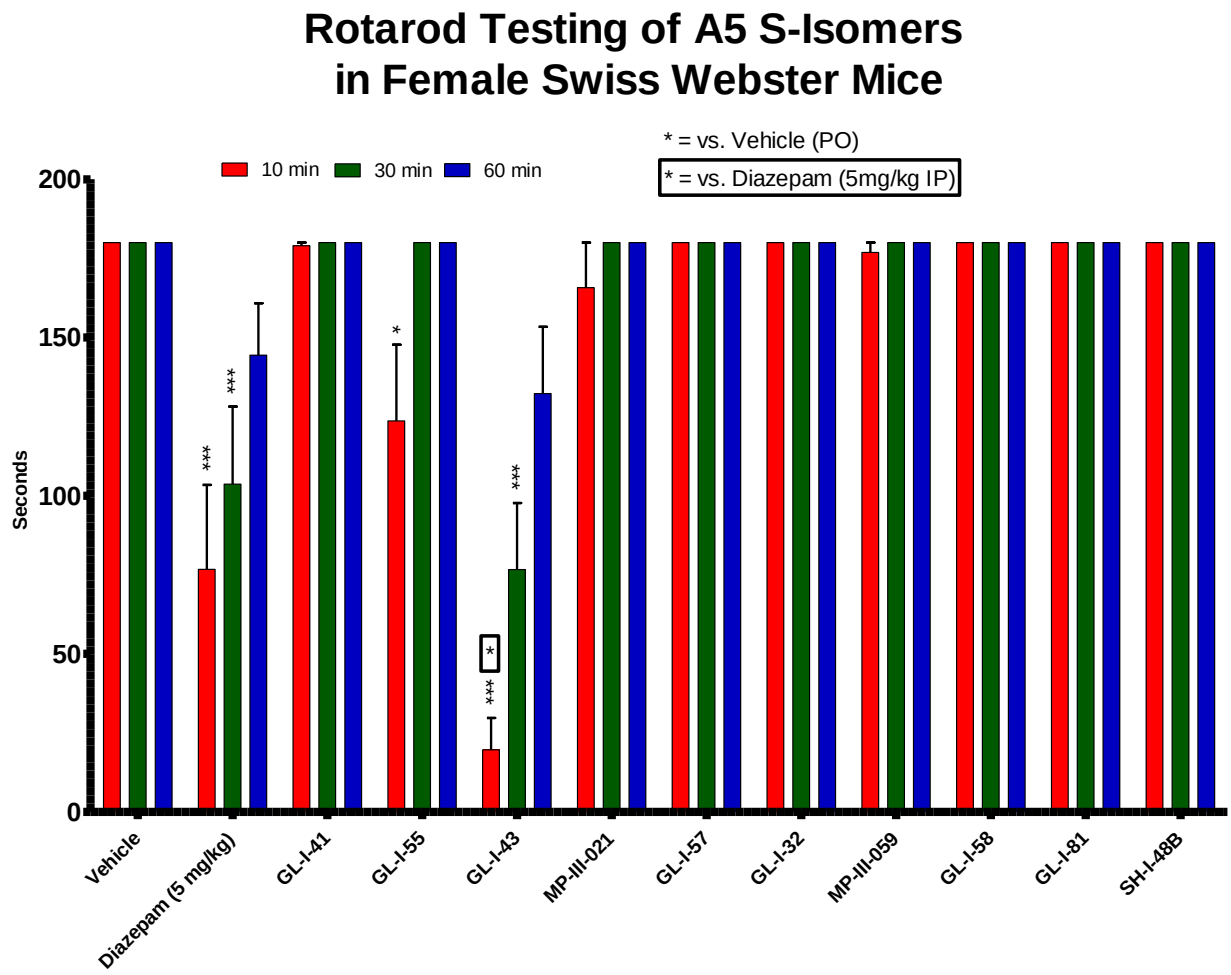

Figure 15. RotaRod Study of Guanguan Lee's Pain Compounds*. Trained female CFW mice (N≥10) were placed on the RotaRod at 10, 30, and 60 min after compound administration. The rotarod was set at a constant rate of 18 rpm. Compounds were administered and compared to vehicle as negative control and diazepam as positive control.*

Imidazodiazepines targeting $GABA_aRs$ containing α5 subunits were synthesized by Guanguan Lee (Cook Group), tested on the rotarod apparatus, and presented in **Figure 15**. All compounds were not significantly different than vehicle-treated mice with the exception of GL-I-55 at 10 min and GL-I-43 at the 10 and 30 min.

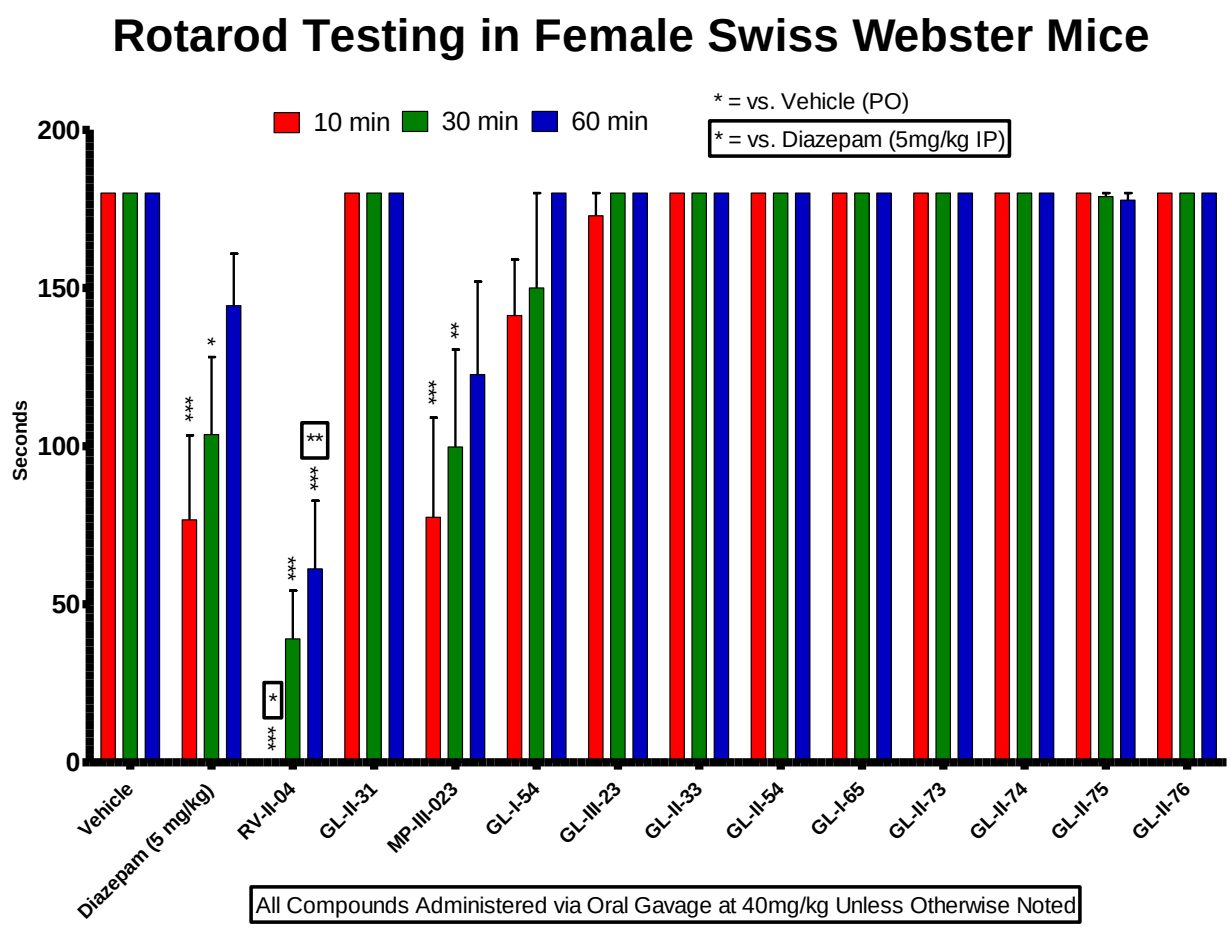

Figure 16. Further RotaRod Testing of Guanguan Lee's Pain Compounds*. Trained female CFW mice (N≥10) were placed on the RotaRod at 10, 30, and 60 min after compound administration. The rotarod was set at a constant rate of 18 rpm. Compounds were administered and compared to vehicle as negative control and diazepam as positive control.*

Additional compounds synthesized by Guanguan Lee (Cook Group) were analyzed on the rotarod. **Figure 16** revealed MP-III-023 as having significantly more motor impairment at 10 and 30 min compared to vehicle. RV-II-04 treated mice performed extremely poorly and experienced tremors up to one h after administration. This compound was not studied further. Compounds in this series that exhibited neither cytotoxicity nor sensorimotor impairment are GL-II-31, GL-II-33, GL-II-54, GL-I-65, GL-I-73, GL-I-74, and GL-I-76.

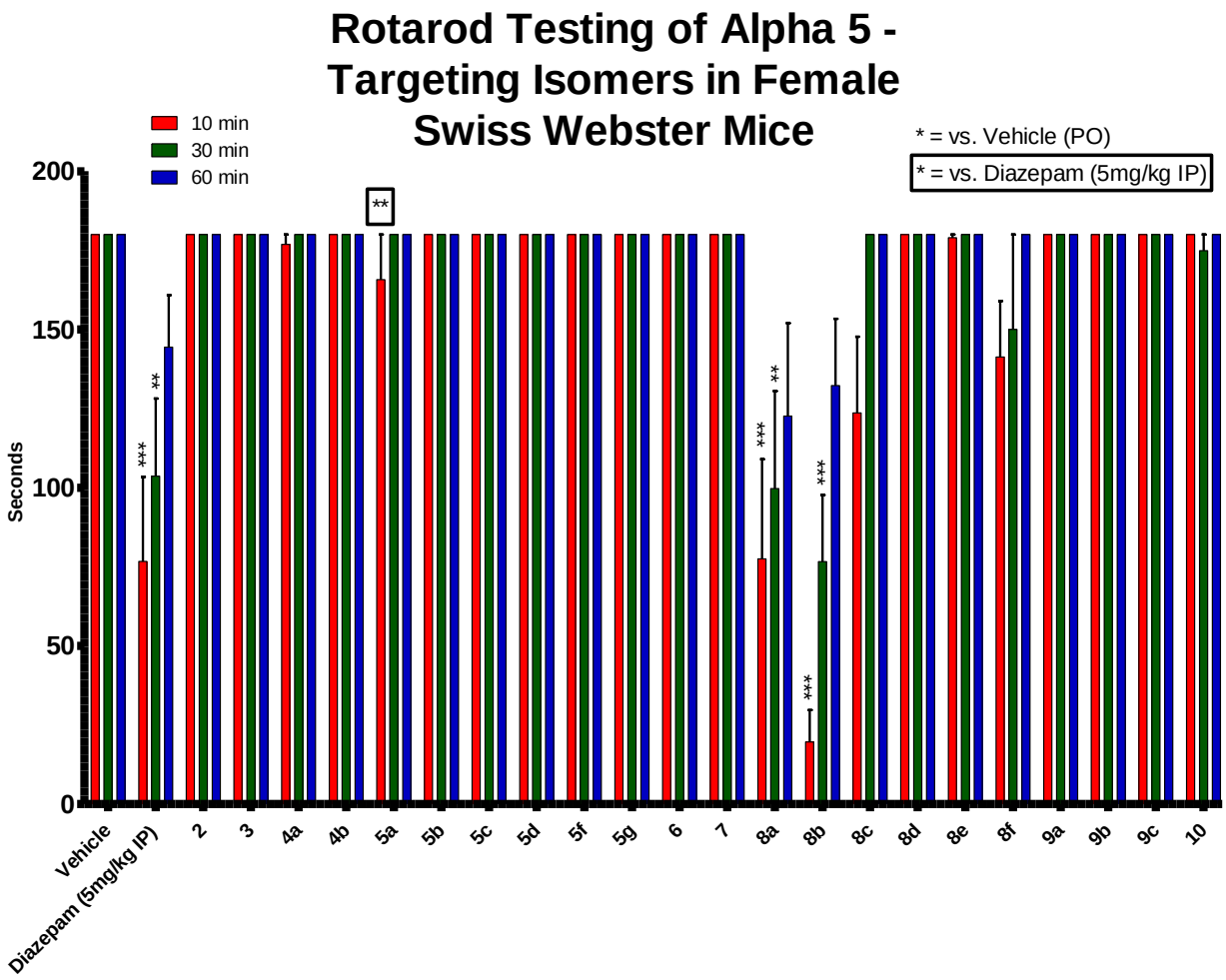

Figure 17. RotaRod Study of Guanguan Lee's* α5-targeting *Compounds*. Trained female CFW mice (N≥10) were placed on the RotaRod at 10, 30, and 60 min after compound administration. The rotarod was set at a constant rate of 18 rpm. Compounds were administered and compared to vehicle as negative control and diazepam as positive control.*

Ligands that selectively bind to the α1 containing $GABA_AR$ subtypes affect motor coordination. **Figure 18** shows α5-selective ligands synthesized by Guanguan Lee (Cook Group). At 40 mg/kg PO, only compounds 8a (methyl amide functionality) and 8b (ethyl amide functionality), were shown to have significantly higher motor impairment than vehicle at the 10 and 30 min time points, while 8f (dimethyl amide functionality) treated mice also had some failures although not significantly different compared to vehicle. **Figure 17** demonstrates good efficacy in terms of motor coordination for this class of compounds with the exception of 8a and 8b.

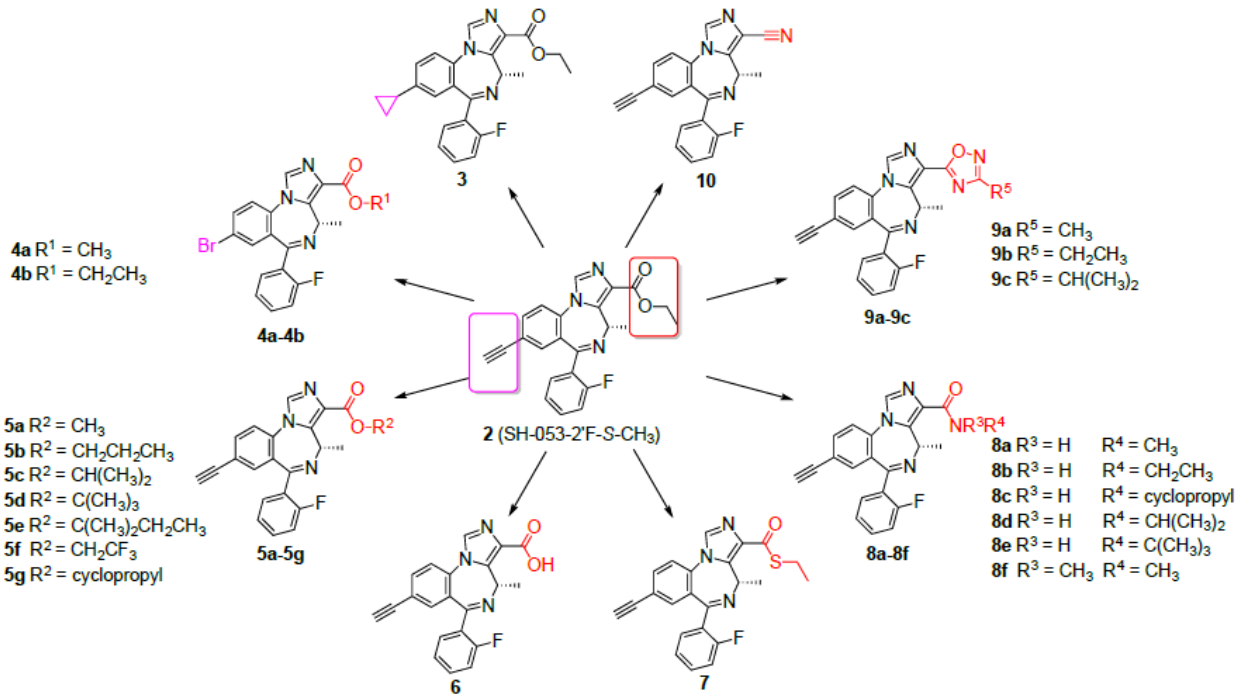

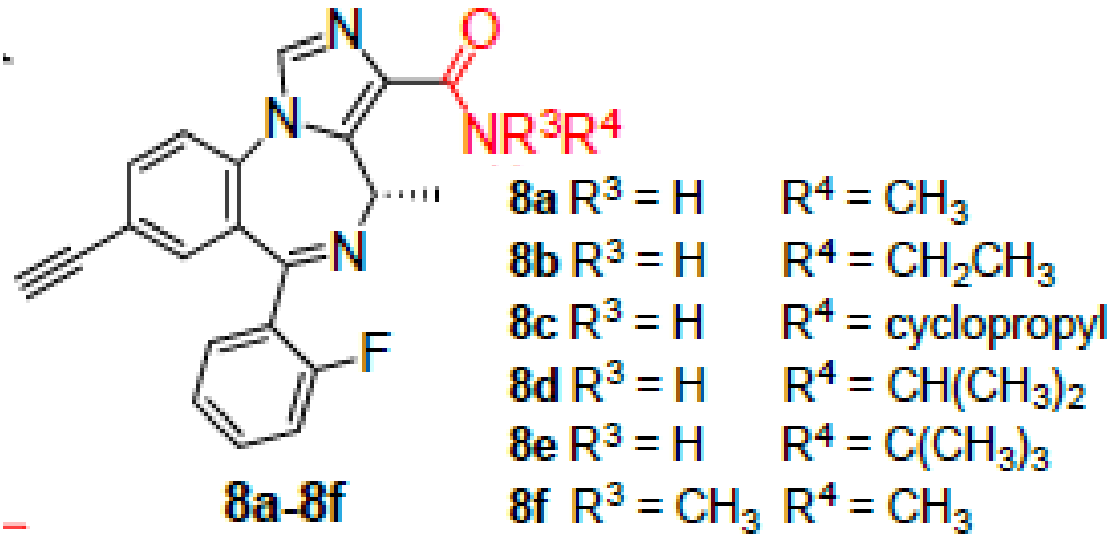

Figure 18. Functionalities of α5-Targeting Compounds Synthesized by Guanguan Lee*. Table shows different functionalities at two locations from parent compound SH-053-2'F-S-CH₃.*

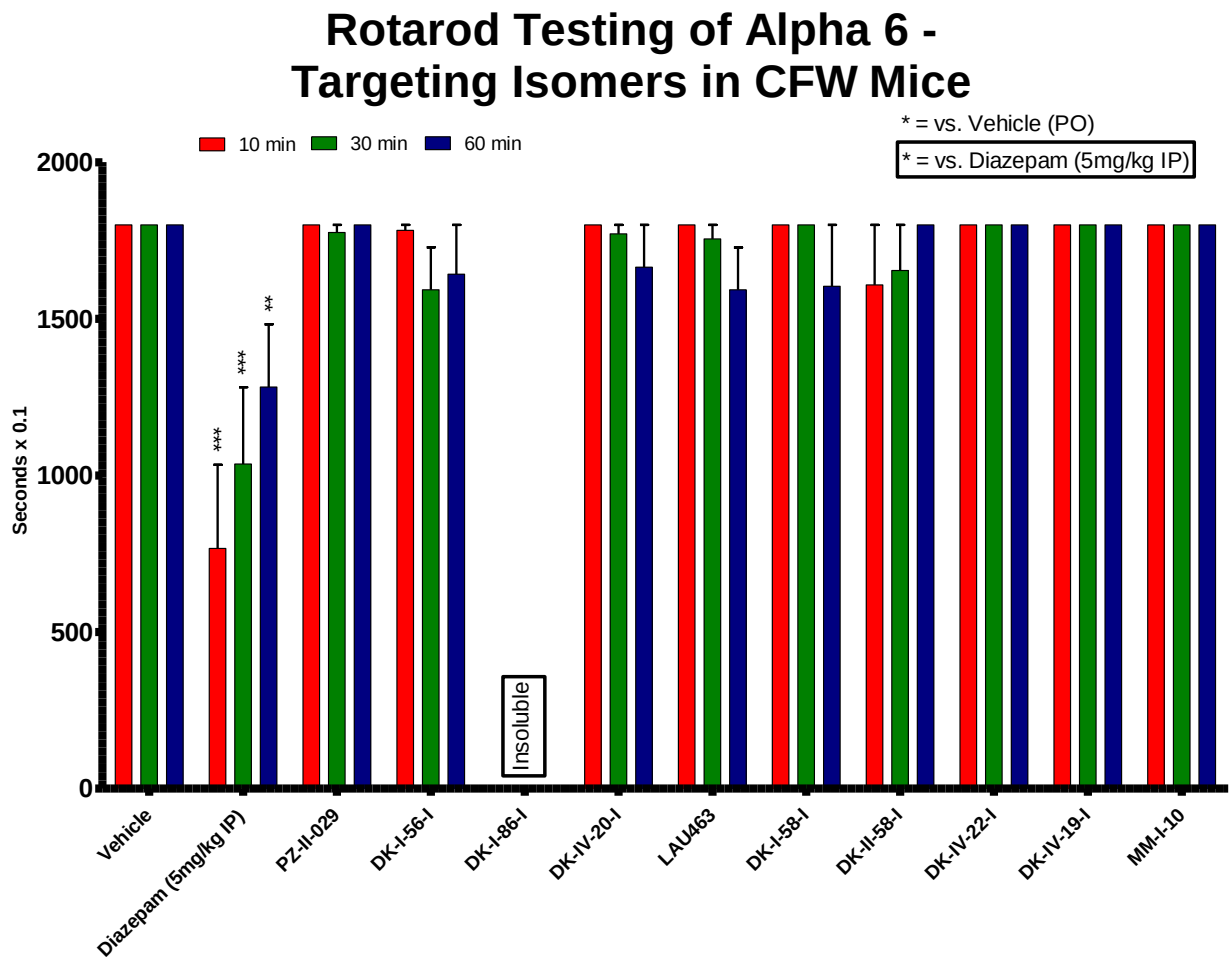

Figure 19. RotaRod Study of Daniel Knutson's α6-targeting Compounds*. Trained female CFW mice (N≥10) were placed on the RotaRod at 10, 30, and 60 min after compound administration. The rotarod was set at a constant rate of 18 rpm. Compounds were administered and compared to vehicle as negative control and diazepam as positive control. Compounds not soluble at 500 μM in DMSO were excluded from testing.*

Compounds targeting α6 containing $GABA_AR$ were synthesized by Daniel Knutson (Cook Group) and analyzed on the rotarod. DK-I-86-I was insoluble at 40 mg/kg PO and was not included in the study. As displayed in **Figure 19**, no compounds were statistically different than vehicle treated mice.

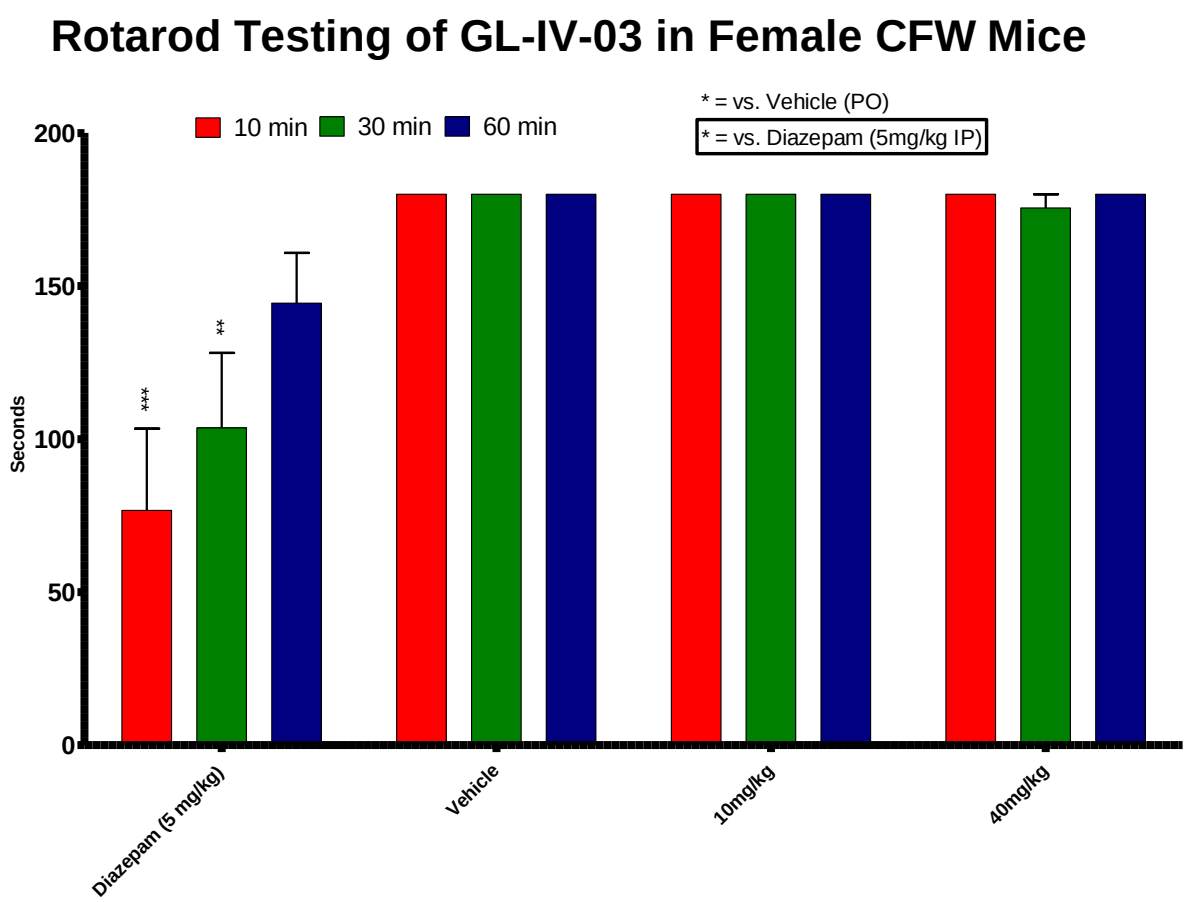

Figure 20. RotaRod Experiment of Guanguan Lee's GL-IV-03 Lead Pain Compound*. Trained female CFW mice (N≥10) were placed on the RotaRod at 10, 30, and 60 min after compound administration. The rotarod was set at a constant rate of 18 rpm. Compounds were administered and compared to vehicle as negative control and diazepam as positive control.*

Compound GL-IV-03 (Guanguan Lee) was chosen as a compound of interest and analyzed on the rotarod at 10 mg/kg and 40 mg/kg PO and displayed in **Figure 20**. No significant difference was reported when compared to vehicle-treated mice.

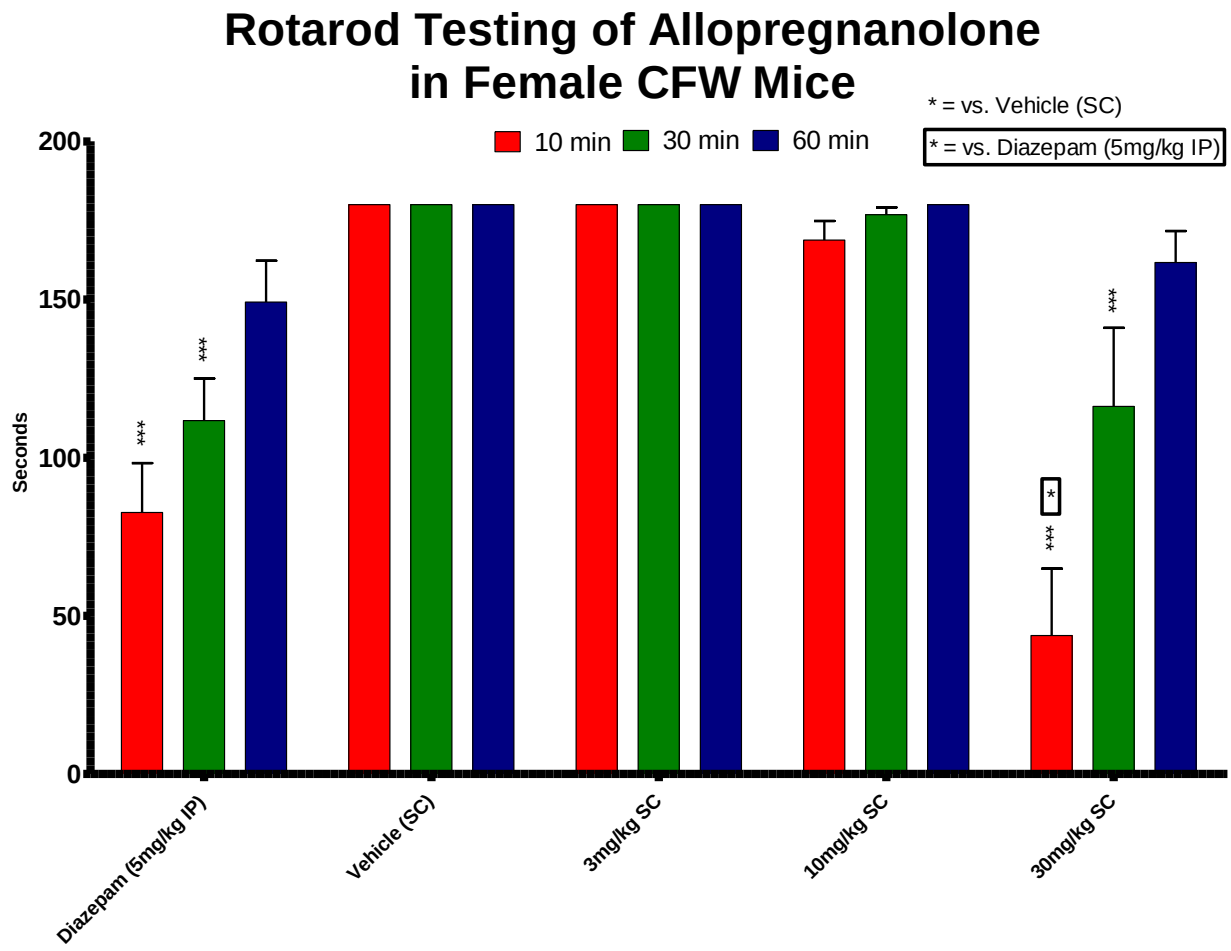

Figure 21. RotaRod Testing of Allopregnanolone*. Trained female CFW mice (N≥10) were placed on the RotaRod at 10, 30, and 60 min after compound administration. The rotarod was set at a constant rate of 18 rpm. Compounds were administered and compared to vehicle as negative control and diazepam as positive control.*

In collaboration with Expansion Therapeutics Inc., allopregnanolone (ALLOP), a positive allosteric modulator of the $GABA_aR$, was delivered to mice to analyze motor coordination. ALLOP showed little to no sedation or impaired motor coordination in female Swiss Webster mice up to 10 mg/kg (SC), however when delivered 30 mg/kg (SC) the motor coordination was severely impaired at the 10 min time point and moderately impaired at the 30 and 60 min time points, as revealed in **Figure 21**.

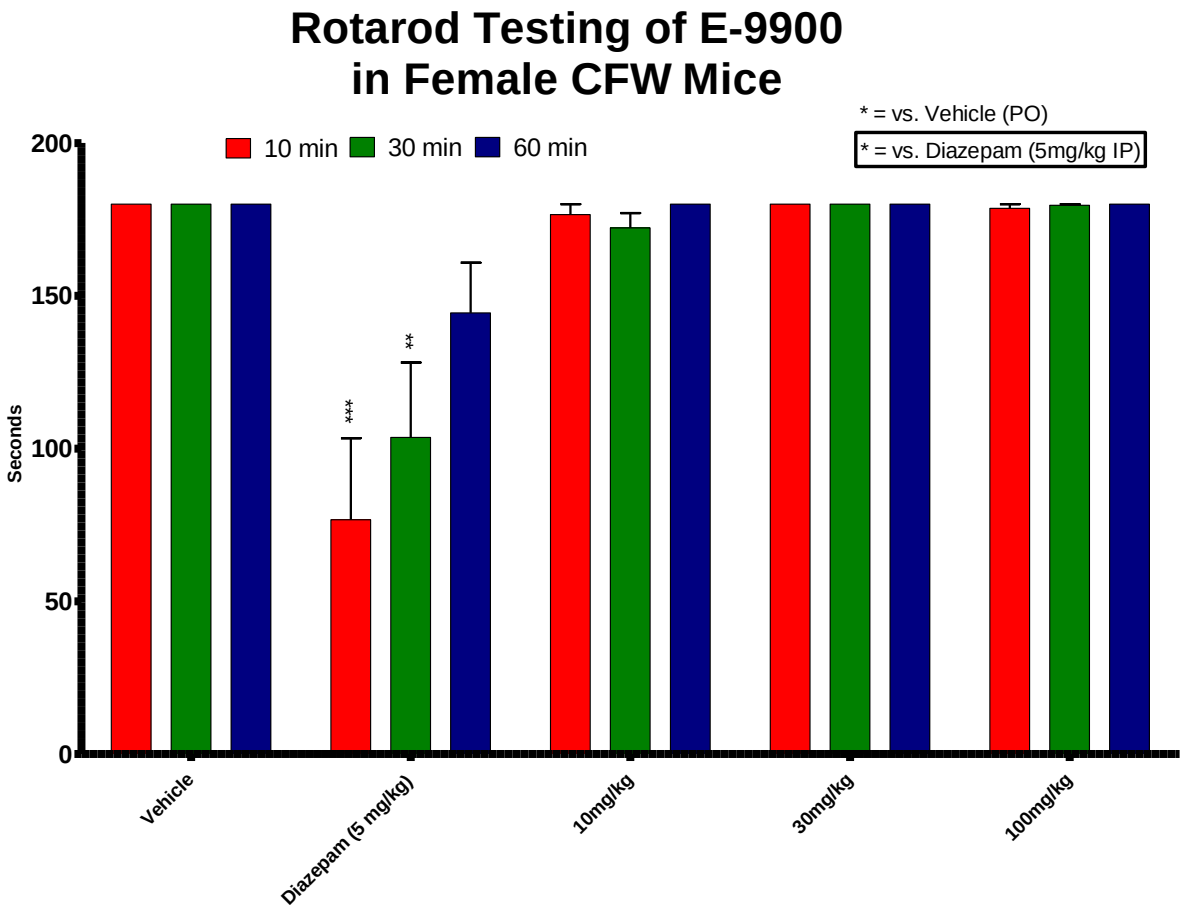

Figure 22. RotaRod Experiment of E-9900 (Expansion Therapeutics Inc.)*. Trained female CFW mice (N≥10) were placed on the RotaRod at 10, 30, and 60 min after compound administration. The rotarod was set at a constant rate of 18 rpm. Compounds were administered and compared to vehicle as negative control and diazepam as positive control.*

Data reported in **Figure 22** shows female Swiss Webster mice delivered compound E-9900 and expressing no sedation with very little impaired motor coordination up to 100mg/kg (PO).

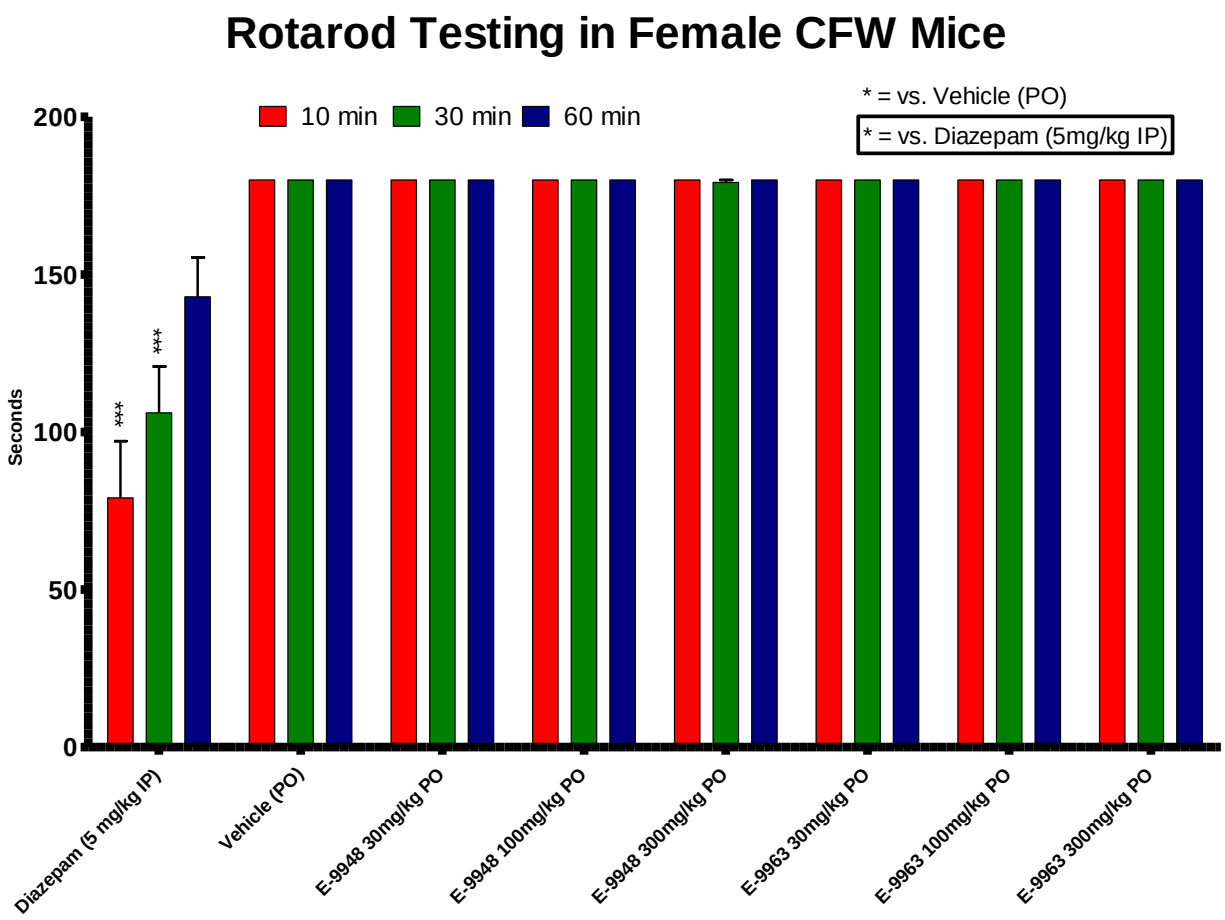

Figure 23. RotaRod Experiment of E-9948 and E-9963 (Expansion Therapeutics Inc.)*. Trained female CFW mice (N≥10) were placed on the RotaRod at 10, 30, and 60 min after compound administration. The rotarod was set at a constant rate of 18 rpm. Compounds were administered and compared to vehicle as negative control and diazepam as positive control.*

When analogs E-9948 and E-9963 (Expansion Therapeutics Inc.) were delivered at concentrations up to 300 mg/kg PO, there was no sedation or impaired motor coordination at any time point. As indicated in **Figure 23**, E-9948 and E-9963 can be used in future co-administration studies to determine site-specific binding in presence of a $GABA_aR$ antagonist.

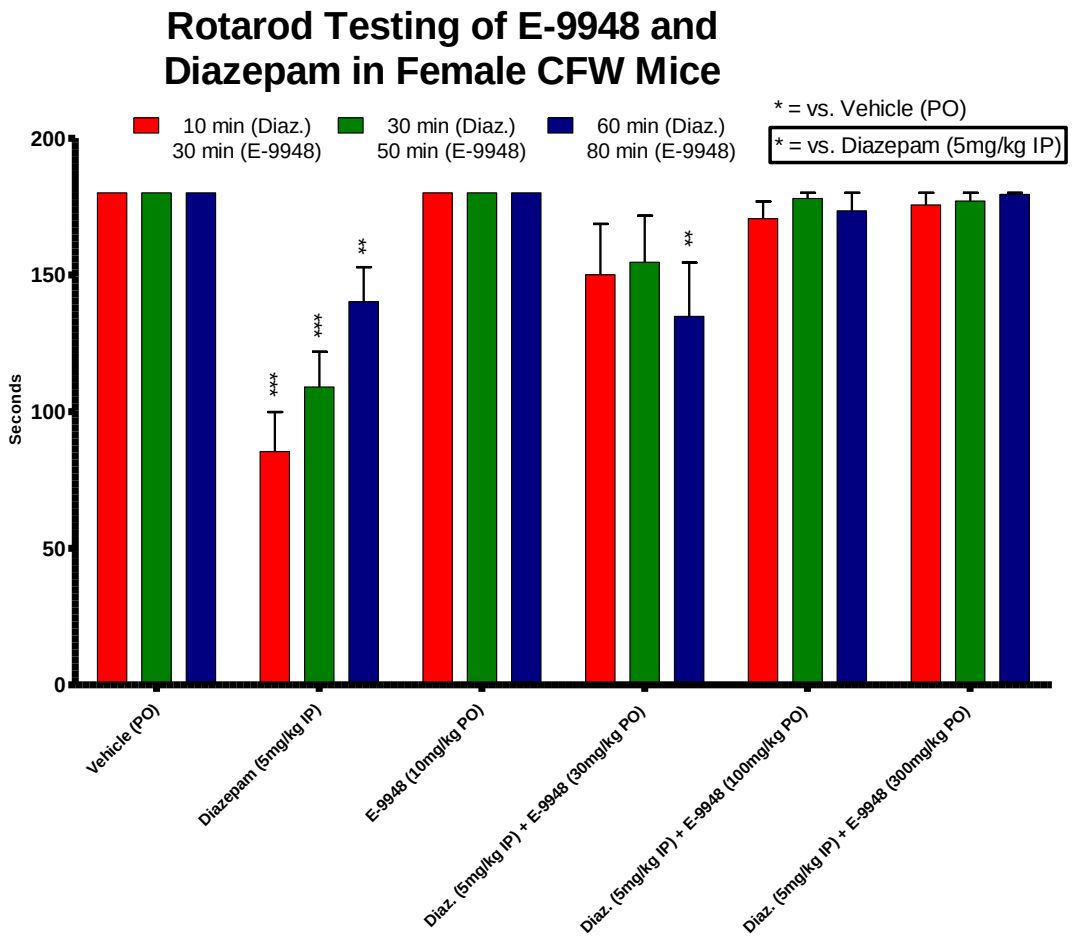

Figure 24. RotaRod Experiment of Single Dose and Co-administration of Diazepam and E-9948 (Expansion Therapeutics Inc.)*. Trained female CFW mice (N≥10) were placed on the RotaRod at 10, 30, and 60 min after Diazepam administration, which corresponds to 30, 50, and 80 min after E-9948 administration. The rotarod was set at a constant rate of 18 rpm. Compounds were administered and compared to vehicle as negative control and diazepam as positive control.*

Positive control diazepam showed sedation and impaired motor coordination at 5 mg/kg IP while compound E-9948 (Expansion Therapeutics Inc.) showed no sedation or impaired motor coordination at 10 mg/kg (PO). Under the same protocol used in **Figure 5**, **Figure 24** confirms co-administration of diazepam at 5 mg/kg (IP) and E-9948 at 30 mg/kg (PO) showing no sedation or impaired motor coordination. E-9948 (PO) was delivered 20 min prior to diazepam (IP) to match T_{max} values. When delivered at concentrations greater than 30 mg/kg, E-9948 was shown to inhibit the sedative and impaired motor function normally observed with 5 mg/kg (IP) diazepam administration. When compared to the

previous study of flumazenil and diazepam co-administration, E-9948 was shown to have similar effect as flumazenil in reducing or completely eliminating the impairing sensorimotor effects of diazepam.

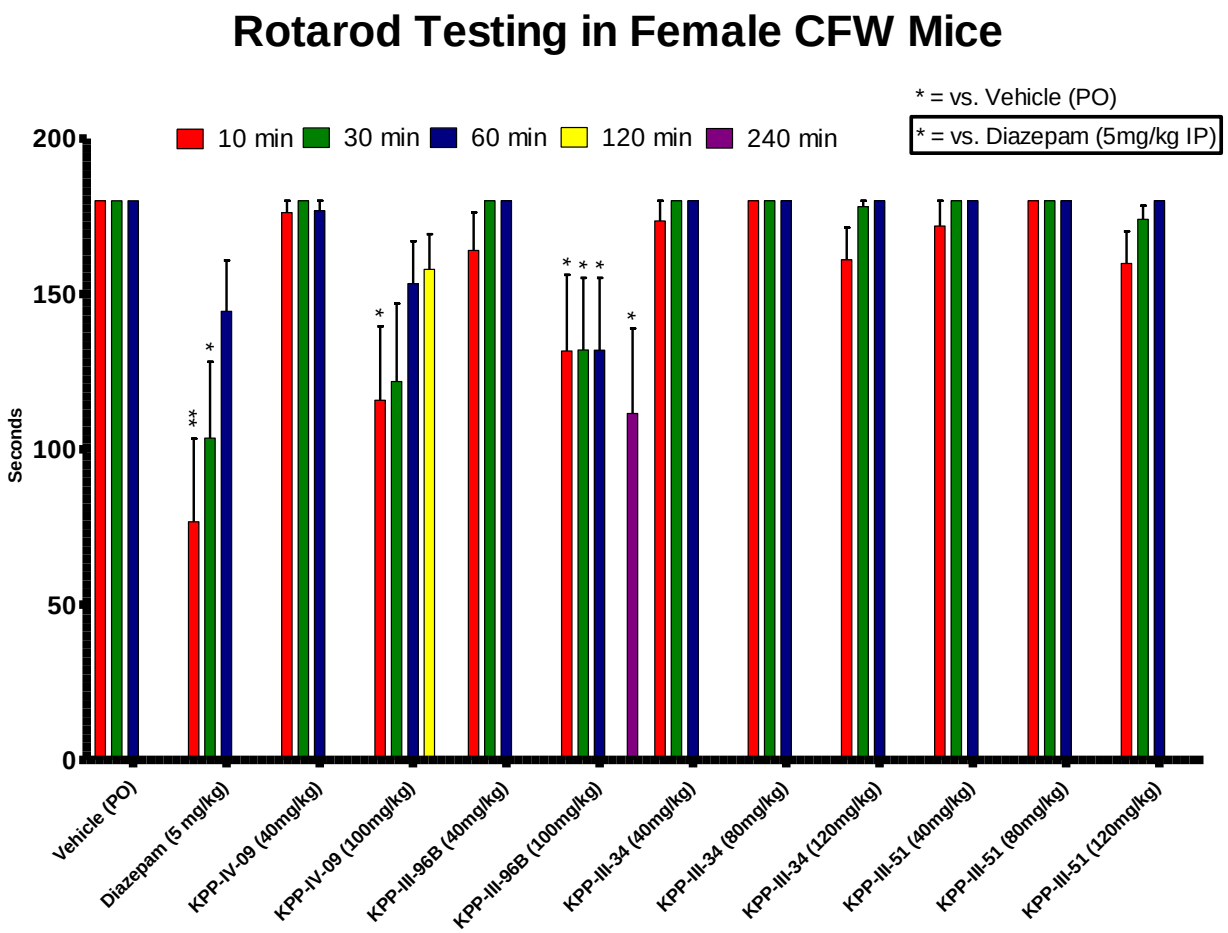

Figure 25. RotaRod Testing of Kamal Pandey's Compounds. *Trained female CFW mice (N≥10) were placed on the RotaRod at 10, 30, and 60 min after compound administration. The rotarod was set at a constant rate of 18 rpm. Compounds were administered and compared to vehicle as negative control and diazepam as positive control.*

Compounds synthesized by Kamal Pandey (Cook Group) were analyzed on the rotarod and presented in **Figure 25**. 100 mg/kg KPP-IV-09 (PO) was shown to have significant impaired motor coordination at 10 min, while 100 mg/kg KPP-III-34 (PO) was shown to have impaired motor coordination up to 4 h after administration.

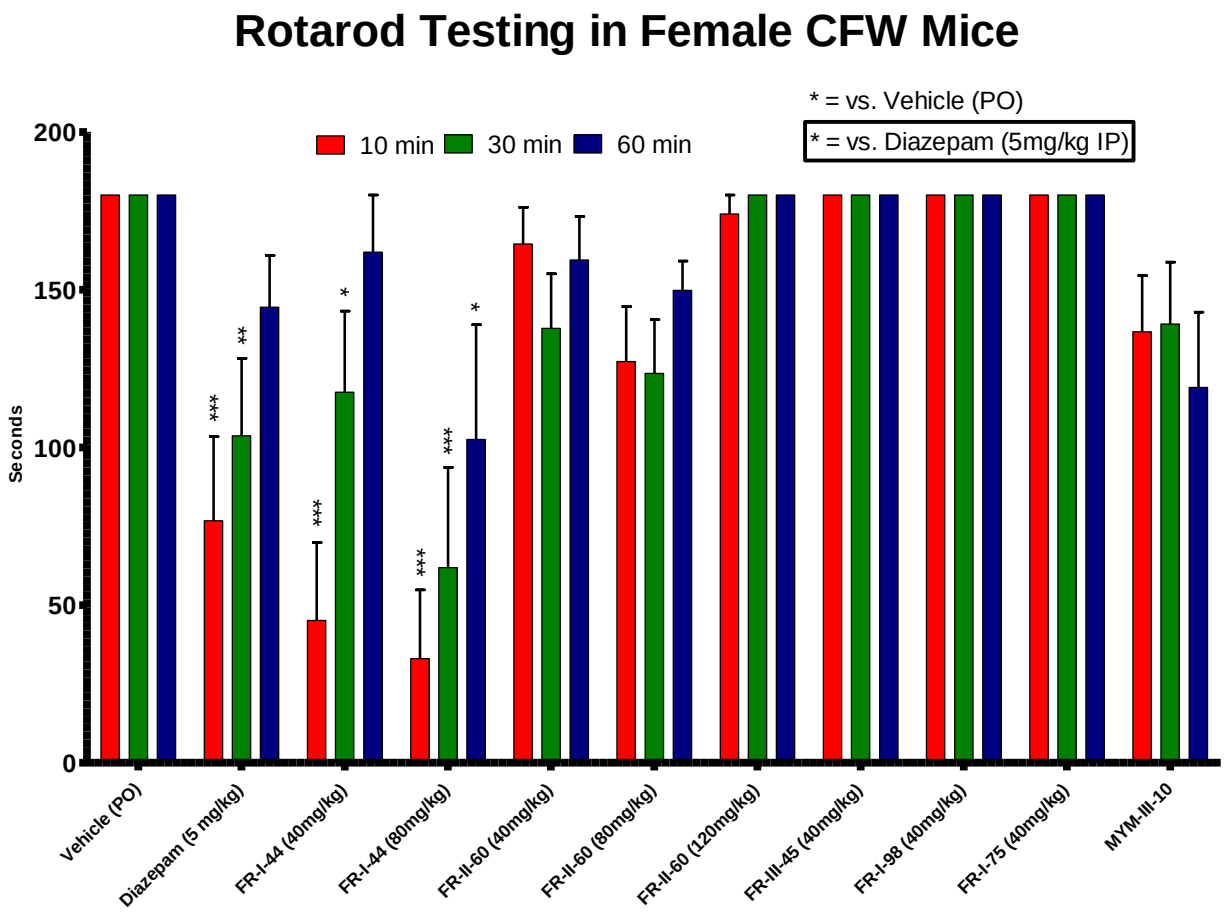

Figure 26. RotaRod Testing Farjana Rashid's Compounds. *Trained female CFW mice (N≥10) were placed on the RotaRod at 10, 30, and 60 min after compound administration. The rotarod was set at a constant rate of 18 rpm. Compounds were administered and compared to vehicle as negative control and diazepam as positive control.*

Ligands synthesized by Farjana Rashid (Cook Group) were investigated for sensorimotor coordination and compared to vehicle-treated mice. **Figure 26** indicates FR-I-44 at 40 mg/kg and 80 mg/kg PO caused severe motor impairment at 10 and 30 min. An 80 mg/kg dose induced impairment for at least one h.

Appendix D – Video Conversion and Compilation for Open Field Test

How to convert and run videos through Ethowatcher:

*Download Version 2.0 VLC (Make sure you set your computer to open these video type as "always" to this version of VCL)]
*Download Ethowatcher (Make sure computer is displaying its resolution at 1920x1080p)
*Download K-lite_Codec_Pack)1526_Full
*Download Xvid-1.3.6.20191204
*Download VirtualDub-1.10.4

Take videos from OneDrive and download/open (videos usually in "MOV" at this step)
> Open videos in Video Editor (defult program in Windows)
> Create video project
> Add all of the project's videos
> Then only one video on storyboard at a time;
> Add each video to the storyboard.
> Rotate each video so longest part of the cage is on the x-axis
> On top right, click the kebab menu
> Change the aspect ratio to 4:3
> Click finish video
> Save at low video quality
> Export to desired location (will be in MP4)
Run video on VCL
> Go to tools
> Effects and filters
> Video Effects
> Set Saturation to 0 and slightly increase contrast (you will only have to do this step once)
> Go to Media
> Convert/Save
> File selection
> Click "add" desired video
- Under "profile" keep the video at H.264 + MP3 (MP4)
- The next button on the right click "MOv/MP4" and with H.264 Save
- Browse and put video in desired folder
- Image properties filter
- Click Start (will have to wait for the time to finish before starting another convert)
Run Xvid MiniConvert
-The source file is the video you just converted. (look at "all file" types)
-Target is where you want this new file to go.
-Press Convert

Run VirtualDub
> File
> Open
> Find your video from the last step
- Press open

- Press OK

If your native video resolution is other than 320 x 240 pixels, you can transform it to this resolution Try the following:

> Go to Video
> Filter
> Add, and select Resize. (It will open a window)
> Under aspect ratio click "disabled" option. In the “new size“, write 320 x 240, and click on OK.
> Add Greyscale filter
> Go to File
> Save as AVI, save your video file. (Will take time to convert.)

Make sure computer is displaying resolution at 1920x1080p (Ethowatcher will not work with higher resolution)

Run Ethowatcher (Between each video you must close and restart Ethowatcher)
> Click "Activity Analysis and Tracking"
> Once clicked, click "Show All Steps"
> Calibration (must do for each video)
> Start
> Under "images"
- Open Video (make sure video has $\leq$ 5 letters)
- Base; pick frame with no animal, then 'capture'
- Animal; pick frame with animal, then 'capture'
- Background; click on picture where it is the darkest
> Under "subtraction"
- Move bar and press subtraction preview until the mouse is the only thing you see.

Skip Erosion
- Under "Proc. Area"
- Click right image, you will see normal video screenshot
- Click 'rectangular'
- Set width and height to overshoot the cage a little (210 by 130-ish)
- Under 'Enter object diameter.. in cm' type "41"
- Under "Finish"
- Click Ok
-Activity Analysis
-Open video (corresponding to previous calibration video)
-"Begin at frame" mark frame that first has mouse in video
-"Finish frame", press forward three times on frame navigation (900 frames), then mark frame.
- Press "process"
- Press "report", (these are CSV files), create a descriptive file name.

Final Conversion:
> Go to the Ethowatcher shared Google Drive (might be possible to use the OneDrive version)

> Once you have all of the CSV files, import them to the google masterfile under "CSV"
> Go to the Master document and on the top middle there is an 'ethowather' tap.
> Click 'import CSV'
-will ask a for email, make sure it's a gmail account.
-name the title, the title to the study
-put '30' in the FPS (this is if you are still using an iPhone 5)

-Open email with the compiled CSV files. Save a copy with the google version and save a copy of an excel version.

-Add Excel file to OneDrive. Save.

Appendix F – Primers

IL-13 Mouse Primers[199]

5’TGAGGAGCTGAGCAACATCACACA 3’/5’TGCGGTTACAGAGGCCATGCAATA3’

Primer pair 1

Sequence (5'->3')	Length	Tm	GC%	Self complementarity	Self 3' complementarity
Forward primer TGAGGAGCTGAGCAACATCACACA	24	64.36	50.00	5.00	2.00
Reverse primer TGCGGTTACAGAGGCCATGCAATA	24	64.78	50.00	4.00	2.00

Products on target templates

>NM_008355.3 Mus musculus interleukin 13 (Il13), mRNA

product length = **176**

Forward primer 1 TGAGGAGCTGAGCAACATCACACA 24

Template 179 202

Reverse primer 1 TGCGGTTACAGAGGCCATGCAATA 24

Template 354 331

GAPDH Mouse Primers[199]

5’TCAACAGCAACTCCCACTCTTCCA 3’/5’ACCCTGTTGCTGTAGCCGTATTCA3’

Primer pair 1

Sequence (5'->3')	Length	Tm	GC%	Self complementarity	Self 3' complementarity
Forward primer TCAACAGCAACTCCCACTCTTCCA	24	64.04	50.00	3.00	0.00
Reverse primer ACCCTGTTGCTGTAGCCGTATTCA	24	64.19	50.00	4.00	2.00

Products on target templates

>XM_017321385.2 PREDICTED: Mus musculus glyceraldehyde-3-phosphate dehydrogenase (Gapdh), transcript variant X1, mRNA

product length = **225**

Forward primer 1 TCAACAGCAACTCCCACTCTTCCA 24

Template 1372 1395

Reverse primer 1 ACCCTGTTGCTGTAGCCGTATTCA 24

Template 1596 1573

IL-13 Primers[200]

(forward, ACAGCTCCCTGGT TCTCTCA; reverse, GCTACTTCGATTTTGGTATCG)

Primer pair 1

Sequence (5'->3')	Length	Tm	GC%	Self complementarity	Self 3' complementarity
Forward primer ACAGCTCCCTGGTTCTCTCA	20	60.18	55.00	4.00	1.00
Reverse primer GCTACTTCGATTTTGGTATCG	21	54.89	42.86	4.00	2.00

Products on target templates

>NM_008355.3 Mus musculus interleukin 13 (Il13), mRNA

product length = **370**

Forward primer 1 ACAGCTCCCTGGTTCTCTCA 20

Template 34 53

Reverse primer 1 GCTACTTCGATTTTGGTATCG 21
Template 403 383

β-Actin Primers[200]
(forward, GATGACGATATCGCTGCGCTG; reverse, GTACGACCAGA GGCATACAGG).
Primer pair 1

Sequence (5'->3')		Length	Tm	GC%	Self complementarity	Self 3' complementarity
Forward primer	GATGACGATATCGCTGCGCTG	21	61.89	57.14	8.00	4.00
Reverse primer	GTACGACCAGAGGCATACAGG	21	59.93	57.14	4.00	2.00

>NM_007393.5 Mus musculus actin, beta (Actb), mRNA

product length = **440**
Forward primer 1 GATGACGATATCGCTGCGCTG 21
Template 113 133

Reverse primer 1 GTACGACCAGAGGCATACAGG 21
Template 552 532

IL-13 Primers[201]
Forward, 5'-GGGTGACTGCAGTCCTGGCT-3' and Reverse, 5'-GCTGGAGACCGTAGTGGG-3'.
Primer pair 1

Sequence (5'->3')		Length	Tm	GC%	Self complementarity	Self 3' complementarity
Forward primer	GGGTGACTGCAGTCCTGGCT	20	64.29	65.00	10.00	3.00
Reverse primer	GCTGGAGACCGTAGTGGG	18	59.11	66.67	3.00	0.00

Products on target templates

>NM_008355.3 Mus musculus interleukin 13 (Il13), mRNA

product length = **299**
Forward primer 1 GGGTGACTGCAGTCCTGGCT 20
Template 79 98

Reverse primer 1 GCTGGAGACCGTAGTGGG 18
Template 377 360

Curriculum Vitae

SUMMARY STATEMENT

I'm a young and energetic scientist with a PhD in biochemistry and seven years' experience in pharmaceutical/medical research with animals in the area of respiratory diseases and pain. I am interested in immunology, especially *in vitro* cell-based assays as well as *in vivo* animal models. I want to pursue a postdoctoral position that will allow me to build and contribute to challenging research studies with career aspirations in the fields of immunology and molecular biology.

RESEARCH EXPERIENCE

University of Wisconsin – Milwaukee, Milwaukee, WI **2018-2022**

Development of New Treatments for Asthma and Neuropathic Pain

Department: Chemistry, PI: Prof. Alexander (Leggy) Arnold

- Maintained multiple mammalian cell lines and cultured primary murine cells
- Performed *in vitro* assays including RNA quantification, RT-qPCR, ELISA, and fluorescence and luminescence - based assays
- Screened compound libraries using high-throughput cell-based assays and animal models
- Performed *in vivo* mouse studies and carried out physiological and behavioral measurements in asthma and pain models
- Experienced in animal handling, injections, small animal surgeries, tissue harvesting, and sample preparation for analysis
- Optimized numerous murine models to achieve better statistics with smaller group sizes
- Utilized Excel, Microsoft Word, PowerPoint, Adobe, ChemDraw, FinePointe, and GraphPad software for analysis, statistics, graphing, and presentations
- Experience in working with interdisciplinary teams
- Mentored graduate and undergraduate students on lab techniques, experimental protocols, statistical analysis, and data presentation

EDUCATION

University of Wisconsin – Milwaukee, Milwaukee, WI **January 2018 - May 2022**

Ph.D. in Biochemistry

Dissertation: Development of New Treatments for Asthma and Neuropathic Pain Based on γ-Aminobutyric Acid A Receptor ($GABA_AR$) Ligands

PI: Prof. Alexander (Leggy) Arnold

B.S. in Biochemistry, Kinesiology **September 2009 - May 2015**

WORK EXPERIENCE

University of Wisconsin – Milwaukee, Milwaukee, WI **2015 – 2018**

Laboratory Technician

- Performed and optimized rotarod, airway hyperresponsiveness, microsomal stability, and pharmacokinetic studies
- Executed IP, IV, SubQ, and PO injections on mice, ran coordination tests, and harvested tissue samples
- Developed proficient pipetting, dilution, homogenization, and extraction techniques
- Created and optimized sample preparation for *in vivo* compound quantification
- Performed statistics, graphed, and presented data to the PI and Department Chair in weekly group meetings
- Provided maintenance, gathered inventory, and placed orders on: gas tank cylinders, liquid nitrogen, nitrogen generators, oil in instrument motors, and general lab supplies

AWARDS

UW-Milwaukee Undergraduate Symposium Poster Award (3rd place)	2015
UW-Milwaukee Distinguished Graduate Student Fellowship	2019-2020
Pantherics Incorporation Fellowship	2021
UW-Milwaukee Distinguished Dissertator Fellowship	2021-2022
Chancellor's Fellowship	2018-2019, 2020

TEACHING EXPERIENCE

University of Wisconsin – Milwaukee, Milwaukee, WI

Teaching Assistant – CHEM 344 (Organic Chemistry Laboratory)	2018
Teaching Assistant – CHEM 105 (General Chemistry for Engineers)	2018-2019, 2020
Teaching Assistant – CHEM 104 (General Chemistry and Qualitative Analysis Laboratory)	2021

PUBLICATIONS

1. Forkuo, G.S.; Guthrie, M.L.; Yuan, N.Y.; Nieman, A.N.; Kodali, R.; Jahan, R.; Stephen, M.R.; Yocum, G.T.; Treven, M.; Poe, M.M.; Li, G.; Yu, O.B.; Hartzler, B.D.; **Zahn, N.M.**; et al. (2016). Development of GABAA Receptor Subtype-Selective Imidazobenzodiazepines as Novel Asthma Treatments. Molecular Pharmaceutics. 13, (6): 2026-2038.
2. Jahan, R.; Stephen, M.R.; Forkuo, G.S.; Kodali, R.; Guthrie, M.L.; Nieman, A.N.; Yuan, N.; **Zahn, N.M.**; et al. (2016). Optimization of substituted imidazobenzodiazepines as novel asthma treatments. European Journal of Medicinal Chemistry. (126): 550-560.
3. Forkuo, G.S.; Nieman, A.N.; Yuan, N. Y.; Yu, O.B.; **Zahn, N.M.**; . . .; Arnold, L.A. (2017). Alleviation of Multiple Asthmatic Pathologic Features with Orally Available and Subtype Selective GABAA Receptor Modulators. Molecular Pharmaceutics. 14, (6): 2088-2098.
4. Knutson, D.E.; Kodali, R.; Divović, B.; Treven, M.; Stephen, M.R.; **Zahn, N.M.**; et al. (2018). Design and Synthesis of Novel Deuterated Ligands Functionally Selective for the γ-Aminobutyric Acid Type A Receptor (GABAAR) α6 Subtype with Improved Metabolic Stability and Enhanced Bioavailability. Journal of Medicinal Chemistry. 61, (6): 2422-2446.
5. Forkuo, G.S.; Nieman, A.N.; **Zahn, N.M.**; et al. (2018). A Novel Orally Available Asthma Drug Candidate That Reduces Smooth Muscle Constriction and Inflammation by Targeting GABAA Receptors in the Lung. Molecular Pharmaceutics. 15, (5): 1766-1777.
6. **Zahn, N.M.**; Huber, A.T.; Mikulsky, B.N.; et al. (2019). MIDD0301 – A first-in-class anti-inflammatory asthma drug targets GABAA receptors without causing systemic immune suppression. Basic & Clinical Pharmacology and Toxicology. 125, (1): 75–84.
7. Prevot, T.D.; Li, G.; Vidojevic, A.; Knutson, D.E.; Stephen, M.R.; Kodali, R.; **Zahn, N.M.**; Arnold, L.A.; et al. (2019). Novel Benzodiazepine-Like Ligands with Various Anxiolytic, Antidepressant, or Pro-Cognitive Profiles. Mol Neuropsychiatry. 5 (2): 84-97.
8. Roni, M.S.R.; Li, G.; Mikulsky, B.N.; Knutson, D.E.; Mian, Md.Y.; **Zahn, N.M.**; et al. (2020). The Effects of pH on the Structure and Bioavailability of Imidazobenzodiazepine-3-Carboxylate MIDD0301. Molecular Pharmacology. 17 (4): 1182-1192.
9. Li, G.; Nieman, A.N.; Mian, M.Y.; **Zahn, N.M.**; Mikulsky, B.N.; Poe, M.M.; Methuku, K.R.; Liu, Y.; Cook, J.M.; Stafford, D.C.; Arnold, L.A. (2020). A Structure-Activity Relationship Comparison of Imidazodiazepines Binding at Kappa, Mu, and Delta Opioid Receptors and the GABAA Receptor. Molecules. (25): 3864.
10. Nieman, A.N.; Li, G.; **Zahn, N.M.**; Md. Yeunus, Mian; Mikulsky, B.N.; Hoffman, D.A.; Wilcox, T.M.; Kehoe, A.S.; Luecke, I.W.; Poe, M.M.; Alvarez-Carbonell, D.; Cook, J.M.; Stafford, D.C.; Arnold, L.A. (2020). Targeting Nitric Oxide Production in Microglia with Novel Imidazodiazepines for Nonsedative Pain Treatment. ACS Chemical Neuroscience. 11, (13): 2019-2030.
11. **Zahn, N.M.**; Mikulsky, B.N.; Roni, M.S.R.; Yocum, G.T.; Mian, Md.Y.; Knutson, D.E.; Cook, J.M.; Emala, C.W.; Stafford, D.C.; Arnold, L.A. (2020). "Nebulized MIDD0301 Reduces Airway Hyperresponsiveness in Moderate and Severe Murine Asthma Models" ACS Pharmacology & Translational Science. 3, (6): 1381-1390.
12. Fan, H.; Zaman, A.; Chen, W.; Ali, T.; Campbell, A.; Zhang, Q.; Setu, N.; Saxon, E.; **Zahn, N.M.**; Benko, A.; Arnold, L.A.; Peng, X. (2021). Assessment of ROS-Activated Phenylboronic Acid Nitrogen Mustards as Potent and Selective Drug Candidates for Triple Negative Breast Cancer. ACS Pharmacol. Transl. Sci. 4, (2): 687-702.
13. Roni, M.S.R.; **Zahn, N.M.**; Mikulsky, B.N.; Webb, .DA.; Mian, Md.Y.; Knutson, D.E.; Guthrie, M.L.; Cook, J.M.; Stafford, D.C.; Arnold, L.A. (2021) Identification and Quantification of MIDD0301 Metabolites. Current Drug Metabolism. 22, (14): 1114-1123.
14. **Zahn, N.M.**; Roni, M.S.R.; Yocum, G.T.; Meyer, M.J.; Webb, D.A.; Mian, Md Yeunus; Cook, J.M.; Emala, C.W.; Stafford, D.D.; Arnold, L.A. (2022) Development of inhaled GABAA receptor modulators to improve airway function in bronchoconstrictive disorders. ACS Pharmacology & Translational Science. 2022, 5, 2, 80–88
15. Roni, M.S.R.; **Zahn, N.M**.; Yocum, G.T.; Webb, D.A.; Mian ,Md. Yeunus; Meyer, M.J.; Tylek, A.S.; Cook, J.M.; Emala, C.W.; Stafford, D.C.; Arnold, L.A. (2022) Comparative pharmacodynamic and pharmacokinetic study of MIDD0301 and its (S) enantiomer. Drug Development Research. doi: 10.1002/ddr.21926.
16. Golani, L.K.; Divovic, B.; Sharmin, D.; Pandey, K.P.; Mian, Md. Y.; Cerne, R.; **Zahn, N.M.**; et al. (2022) Metabolism, pharmacokinetics, and anticonvulsant activity of a deuterated analog of the a2/3-selective GABAkine KRM-II-81. Biopharmaceutics & Drug Disposition. doi: 10.1002 /bdd.2313.

POSTER PRESENTATIONS

Zahn, N.M.; Kodali, R., Guthrie, M.L., Jahan, R., Stephen, MR., Poe, MM., Cook, J., Stafford, D., Arnold, L.A. Metabolic Analysis of Benzodiazepines in Human and Mouse Liver Microsomes. (2016). Presented UWM Undergraduate Research Symposium.
Zahn, N.M.; Kodali, R., Guthrie, M.L., Jahan, Cook, J., Stafford, D., Arnold, L.A., et al. Nervous System Effects & Metabolic Analysis of Imidazobenzodiazepines in Human and Mouse Liver Microsomes. (2016). Presented at Int. Chemistry Biology Society in Madison, WI.
Zahn, N.M.; Kodali, R., Guthrie, M.L., Li, G., Huber, A., Trepanski, M., Jahan, R., Cook, J., Stafford, D., Arnold, L.A., et al. Characterization of a Novel Orally Available $\alpha_5\beta_3\gamma_2$ Subtype-Selective $GABA_a$ Receptor Agonist for the Treatment of Asthma. (2019). Presented at Annual UWM Chemistry Department Symposium.
Zahn, N.M.; Mikulsky, B.N.; M.S. Rashid, Roni; Md. Yeunus, Mian; Knutson, Daniel; Cook, J.; Emala, C.; Stafford, D.; Arnold, L.A. Development of new treatments for asthma and neuropathic pain. (2021). Presented at ACS Annual Symposium.
Zahn, N.M.; Mikulsky, B.N.; M.S. Rashid, Roni; Md. Yeunus, Mian; Knutson, D.E.; Cook, J.; Emala, C.W.; Stafford, D.C.; Arnold, L.A. Nebulized MIDD0301 Recues Airway Hyperresponsiveness and Bronchoconstriction in Murine Models. (2021). Presented at Annual UWM Chemistry Department Symposium.